Residual and Unspecified Elements in Steel

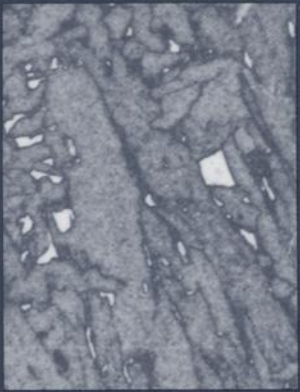

Melilli/Nisbett,
editors

ASTM

STP 1042

STP 1042

Residual and Unspecified Elements in Steel

Albert S. Melilli and Edward G. Nisbett, editors

ASTM
1916 Race Street
Philadelphia, PA 19103

Library of Congress Cataloging-in-Publication Data

Residual and unspecified elements in steel/Albert S. Melilli and
Edward G. Nisbett, editors.
(Special technical publication; STP 1042)
"ASTM publication code number (PCN) 04-010420-02."
Papers presented at the Symposium on Residual and Unspecified
Elements in Steel, sponsored by ASTM Committee A-1 on Steel,
Stainless Steel, and Related Alloys.
Includes bibliographies and index.
ISBN 0-8031-1259-9
1. Steel—Inclusions—Congresses. 2. Steel—Refining—Congresses.
I. Melilli, Albert S. II. Nisbett, Edward G. III. Symposium on
Residual and Unspecified Elements in Steel (1987: Bal Harbour, Fl.)
IV. American Society for Testing and Materials. Committee A-1 on
Steel, Stainless Steel, and Related Alloys. V. Series: ASTM special
technical publication; 1042.
TN693.I7R47 1989 89-32224
669'.142—dc20 CIP

Peer Review Policy

Each paper published in this volume was evaluated by three peer reviewers. The authors addressed all of the reviewers' comments to the satisfaction of both the technical editor(s) and the ASTM Committee on Publications.

The quality of the papers in this publication reflects not only the obvious efforts of the authors and the technical editor(s), but also the work of these peer reviewers. The ASTM Committee on Publications acknowledges with appreciation their dedication and contribution of time and effort on behalf of ASTM.

Printed in Baltimore, MD
July 1989

Foreword

The Symposium on Residual and Unspecified Elements in Steel was held on 11-13 Nov. 1987 at Bal Harbour, FL. The symposium was sponsored by ASTM Committee A-1 on Steel, Stainless Steel, and Related Alloys. Albert S. Melilli, Raytheon Company, and Edward G. Nisbett, Consultant, served as chairmen of the symposium and are editors of the resulting publication.

Contents

KEYNOTE ADDRESS

STEEL MELTING

SOLIDIFICATION AND SUBSEQUENT PROCESSING

HEAT TREATMENT, MICROSTRUCTURE, AND INCLUSION MORPHOLOGY

PROPERTIES

WELDING, PREHEATING, AND POSTWELD HEAT TREATING

Overview

It has been generally accepted practice when writing material specifications to indicate limits or ranges, or both, of individual elements in the tables of chemical compositions. Normally, only those elements pertinent to a particular alloy designation or grade of material were listed with appropriate limitations.

There existed a general understanding among knowledgeable producers and users of steel products that there would always be present some minute levels of trace, residual, or unspecified elements orginating from the basic ores during melting and from additions during the subsequent metal refining processes. ASTM Methods, Practices, and Definitions for Chemical Analysis of Steel Products (A 751) addressed the permissive reporting analyses of these elements as well as the impracticality of establishing limits for all possible elements.

ASTM held its first symposium on the subject of residual elements in 1966. *Effects of Residual Elements on the Properties of Austenitic Stainless Steel* (Special Technical Publication [STP] 418) contains the papers presented at the symposium. There were a combination of influencing factors taking place in the steel industry resulting in an increasing interest in the subject of residual and unspecified elements at this time. First, there was the proliferation of steel alloys, grades and specifications. Not only were these new alloys being specified in standards writing bodies, but also, corporate and government specifications were equally being developed. Second, within these new specifications were narrower and more restrictive limitations on certain elements to satisfy the end product-oriented needs of the user. Third, steelmaking changes were taking place not only aimed at satisfying the new requirements but also aimed at improving efficiency of operations brought on by competitive pressures.

One of the first technical subcommittees of ASTM Committee A-1 on Steel, Stainless Steel, and Related Alloys to address the subject of residual and unspecified elements originating in 1968 was Steel Forgings. When it was brought to the attention of the subcommittee, certain ASTM standards have tables of chemical composition wherein not all the elements have limitations specified, it may be construed that those unspecified elements may be present in any amount or they are neither permitted nor prohibited. This was certainly not the intent since the specification addressed only those elements pertinent to the grade of steel. Other technical subcommittees soon initiated task groups to discuss residual and unspecified elements, for example, Steel Castings, Pressure Vessel Plates, Valves, Fittings and Bolting, Pipe and Tubular Products, Bar, Stainless Steel and Structural Steel.

Acknowledgment of the contribution by Mr. Vernon W. Butler, who deceased during the preparation of this volume, is particularly noted for his leadership on residual and unspecified elements as Subcommittee Chairman of Boiler and Pressure Vessel Steel Plates.

As the interest in residual and unspecified elements in steel grew among the various technical subcommittee, so did an interest in Committee A-1 to sponsor a symposium to address the concerns of those producing, specifying, designing, manufacturing, testing, examining, joining and evaluating the properties of steel products.

In this volume of the papers presented at the symposium, are technical examples of the broad range of interest in the subject of residual and unspecified elements in steel. Raw materials used in steelmaking were covered by the scrap metal industry indicating how that industry has taken steps to segregate raw materials for the steel producers to improve their chemical composition requirements. Steel producers presented papers detailing the progress that has been made in their internal manufacturing processes for controlling residual and unspecified elements not only to meet specification requirements but also for economic advantages. How the steelmaking industry has responded to the challenges of controlling residual and unspecified elements is well exemplified by these papers.

Not only were the controls for residual and unspecified elements covered, but also papers in this volume addressed very low, or ultra-low, levels of certain elements. Steel manufacturing technology, mechanical property effects, and metal joining characteristics of steels with extremely low levels of certain elements have been included.

Machinability of steels as affected by individual and combined effects of certain residual and unspecified elements was also addressed by authors in this volume. Microstructural constituents and inclusion morphology examples were presented.

There were quite a few papers presented by authors interested in the effects of residual and unspecified elements on specific material behavior characteristics. Covered in this volume are properties, such as temper embrittlement, corrosion resistance, elevated temperature creep-rupture strengths, fracture toughness, and room-temperature tensile strengths. Some of the papers dealt with steels in nuclear applications.

Welding processes and post-weld heat treatments affected by residual and unspecified elements were discussed by several authors. Not only were the base materials of concern but also the welding consumables.

In summary, this volume treats the broad spectrum of residual and unspecified elements in steel from the raw materials used for steelmaking through machining and welding to the long-term effects on properties. Very specific technical data are included for future reference by those concerned from all phases of the steel industry.

ASTM Committee A-1 has already reflected many of the issues presented in this volume through its published books of standards. Residual and unspecified elements in steel is a dynamic subject and will continue to be evaluated by the ASTM technical committees as the need arises.

Albert S. Melilli

Raytheon Company; Lowell, MA 01853; symposium chairman and editor.

Keynote Address

George J. Schnabel[1]

Service Experience Related to Unspecified Elements

REFERENCE: Schnabel, G. J., "**Service Experience Related to Unspecified Elements,**" *Residual and Unspecified Elements in Steel, ASTM STP 1042,* A. S. Melilli and E. G. Nisbett, Eds., American Society for Testing and Materials, Philadelphia, 1989, pp. 5-25.

ABSTRACT: Over the past 50 years the anomalous behavior of steels has not always been consistent. Part of the inconsistency can be attributed to transient or other conditions that exceeded design conditions. Another part can be attributed to unspecified elements. Conversely, some steels have proven exceptionally capable to withstand their service conditions. Some of the more generic problems were serious enough to generate cooperative group actions to resolve them. Graphitization, weldability, low creep resistance, stress corrosion, caustic embrittlement, poor fracture toughness, shifting nil-ductility transition temperatures, and low upper shelf impact resistance have been some of the more notorious problems.

Until recently there was little attention given to the buildup of residuals (or unspecified elements) in steels where scrap steels were recycled into new product forms. Copper, chromium, cobalt, zinc, tin, nickel, and nitrogen have all influenced the behavior of steels. In some cases they could be beneficial. However, without a clear understanding of their synergistic behavior, it is difficult to predict their service behavior. If our industry potential is to remain strong in its world position, it will be necessary to develop more specific information on materials. We look forward to the successful implementation of the National Materials Properties Data Network (NMPD) to provide the data base from which the generation of new or more specific data will provide more confidence for the least cost.

KEY WORDS: steels, unspecified elements, graphitization, weldability stress corrosion, caustic embrittlement

Over the past 50 years the anomalous behavior of materials used in Power Plant operation has been inconsistent. Since all failures are directly related to materials, it is imperative that an understanding, or at least an appreciation, of the causes of anomalous behavior be pursued. It can be generalized that there are three major contributors to failures. These are best represented by a Venn type diagram, more recognizable as the Ballentine logo, in which three intersecting circles depict the three conditions for failure. One circle represents force, which we term as stress, a second represents the environment to which the material is subjected, and a third represents the condition of the material. The area of intersection portrays the severity or the probability of failure.

It is natural for the control responsibility for one of these factors, that is, stress, environment, or material condition, to be more dominant than the other two. However, it has been well documented that all three usually have a part in the failure mode.

Time will not permit disclosure of the myriad of isolated failures that have occurred, but there are sufficient generic problems to illustrate that unspecified elements can and do contribute significantly to anomalous behavior in service. Some of the more serious problems have generated group actions to resolve or mitigate future faults. Typical of these are caustic embrittle-

---

[1] Consulting mechanical engineer, retired from Public Service Electric and Gas Company, 80 Park Place, Newark, NJ 07102.

ment, hydrogen embrittlement, graphitization, sigmatization, poor weldability, low creep resistance, low fatigue resistance, corrosion, stress corrosion, inadequate fracture toughness, high nil ductility transition temperatures, and low upper shelf impact resistance.

As noted before, failures are usually caused by a combination of conditions and most post mortem analyses are hampered by difficulty in ascertaining the initiating condition leading to eventual failure. Furthermore, the multitudinous activities between production, forming, fabrication, erection, and operation of these materials can all be suspect. We are suspicious that the buildup of residuals or unspecified elements are becoming more influential in their effect on materials when recycled into new product forms via the scrap route.

Many years ago caustic embrittlement was a real concern for the drum steels in low-pressure boilers. Initially it was found that variable sensitivity appeared to be associated with an unspecified copper content in carbon steels, that is, the higher the copper content the less serious the attack. This caustic cracking problem was eventually mitigated by establishing a more specific feedwater chemistry control. Similarly, when graphitization of carbon and carbon molybdenum piping was a serious problem with the weld heat affected zones and cold bends of piping, it was found that materials with up to 0.25% chromium exhibited a significant resistance to graphitization. This problem was subsequently mitigated by establishing proper heat treatments after bending or welding.

When austenitic Type 347 stainless steel became popular for high temperature steam service, it was necessary to add or maintain some ferrite to perform hot working or welding to minimize fissuring. Too much ferrite accelerated the formation of the Sigma phase, which increased hardness and reduced ductility. This challenged the ductility desired to accommodate thermal and pressure shocks. Close compositional control of ferrite and austenite formers reduced this tendency, but control was difficult to maintain. Another problem with the austenitic Type 347 and 321 stainless steels was the variability in hot shortness, which made sound casting and welding nearly impossible to predict. Efforts to establish proper ratios of specified elements did not produce consistent results. Reduction of unspecified elements, such as boron, tantalum, copper, tin, and so forth, as well as reducing phosphorus, silicon, and sulfur did not produce the desired results either.

A concerted effort was made to provide suitable specifications for heavy walled piping by introducing ASTM A376 and A430 for Central Station high temperature steam piping. Included in these specifications was a supplementary test called The Hot Ductility Test to predetermine the materials behavior during a welding cycle. Unfortunately, it could only be used for informational purposes and was never pursued to determine how to assure weldability with good hot ductility. Subsequently, heavy walled Type 347 and 321 stainless steels were outlawed for high-temperature service use because of unpredictable weldability. Recently both the German and Japanese steel producers have indicated a willingness to supply these materials with warranted hot ductility properties.

Type 316 was used to replace 321 and 347. As more service experience accrued, this material also exhibited poor weldability but not as serious as the previous grades. It was also found that the unstabilized Type 316 suffered a loss in ductility and structural stability by a carbide precipitation mechanism which occurred at the 1100°F (593°C) operating temperatures.

For operating temperatures at 1000 to 1050°F (538 to 566°C) the use of Type 304 for heavy wall main steam piping was made possible by the increased American Society of Mechanical Engineers (ASME) Boiler and Pressure Vessel Code allowable stresses for this material. There was no real change in the specifications, which supported the higher allowable stresses for Type 304, other than more recent test data that indicated that it was justified. This disturbed the utilities since the premature creep-rupture failures in the fine grained type 321 superheater tubes had been costly to rectify. Subsequent laboratory investigations of new and old heats of Type 304 uncovered a marked increase in nitrogen (unspecified) content, which was a result of the notable increase in manganese content from less than 1.00% to an average of about 1.30% thereby increasing the affinity for nitrogen during the melting process.

Efforts to establish a nitrogen requirement for the "H" grades in the ASTM standards were not successful, and the utilities had to write this requirement into their own specifications.

During production of materials with specific nitrogen additions, remarkable improvements in strength were noted with no other apparent problems. Hence, the introduction of a new "N" Grade of Austenitic materials. This grade has been used for nuclear grade piping in lightwater reactors that operate at temperatures below 600°F (565°C). This has been a particularly important consideration because of sensitization of austenitic stainless steels at the weld-heat affected zones promoting the onset of intergranular stress corrosion cracking. Hence the introduction of another new nitrogen enhanced extra-low carbon grade (ELC) grade with nitrogen added to maintain the desired strengths. However, strict control is needed to avoid fissuring and nitriding.

Pursuit of successful operation necessitates control of the environment to which the material will be subjected. Consequently a significant effort has been exerted to provide a rigorous water chemistry control as well as matching materials to the service conditions. This includes an in-depth understanding of the specified and the unspecified elements.

Successful operation of pressurized water reactors mandates strict control of materials and water chemistry. Corrosion and wastage of tubes and supports in steam generators has made it necessary to reduce the ionic form of copper and nickel as much as possible. Both the boiling water reactor (BWR) and pressurized water reactor (PWR) operation requires the lowest achievable oxygen to inhibit corrosion. The elimination of copper alloys and the introduction of hydrogen to scavenge oxygen in the feedwater circuit are corrective actions that have been instituted to accommodate material behavior in existing nuclear power plants. Eventually it will be necessary to develop alloys that will be more tolerant of the nuclear system environment.

Fracture toughness has now become much more important to assure safety and reliability of nuclear power plant operation. Copper in carbon and low alloy steels has a marked effect on the fracture toughness of reactor pressure vessel steels when subjected to a high neutron fluence. The upward shift of the nil-ductility transition temperature and the lowering of the upper shelf Charpy impact values have been associated with increasing copper contents in reactor pressure vessel steels and their weldments. This is of particular concern for pressurized thermal shock. It is also of concern for water hammer.

Not new but of increasing importance is the resistance of carbon steels to the erosion-corrosion of these materials in the feedwater, extraction steam, and main steam piping for power plants. Investigations have shown that small amounts of chromium, and to a lesser extent copper, have provided significant resistance to erosion-corrosion in feedwater and wet steam piping systems where high fluid velocities have reduced wall thicknesses to the point of failure. It has been well documented since 1948 that chromium can increase the resistance of carbon steels dramatically with additions of $>0.25\%$.

Recently a relatively new problem called microbial corrosion has become a dominant factor in the service life of piping and pressure vessel components of cooling water systems for power plants. This appears to be associated with a reactivation of marine life and the lack of suitable chemical control of algae and marine organisms that attack the inner surfaces of these systems with subsequent failures. This will also demand corrective actions with more emphasis on the control of unspecified elements in materials.

Service experience cannot be related to static components only. There has been and continues to be a need to understand the high cycle fatigue characteristics and the recognition of what controls it. Rotating machinery, such as fans, motors, pumps, and turbines, have all been subject to sudden and complete failures because of crack initiation, growth, and eventual loss of mechanical stability. Efforts to produce improved steels for rotors, discs, retaining rings and blades must be increased as well as methods to inspect and categorize flaws. These flaws, occasioned by surface or subsurface separations can grow by creep-fatigue or pure fatigue because of cyclic stresses in operation. Here again the level of impurities or unspecified elements appear to be a dominant factor in the service behavior of these materials.

Improvements in inspection equipment and analytical capability have increased our knowledge and recognition of the condition of the faults. However, increased awareness must be generated to reduce the initiation of faults. Better steel production methods and more attention to unspecified elements in steel will be needed if we are to move forward.

Last but not least is the current activity of life extension for current power plants. Increasing the useful life of fossil fueled power plants from 25 to 50 years and from 30 to 60 years for nuclear power plants is an ambitious goal. It is necessary and has been economically justified because of the rapid increase in capital costs and the lack of environmentally suitable sites for new plants. However, investigations of the suitability for materials to be used safely and reliably must include careful considerations of the existing properties. Knowledge of unspecified elements will be an important part of these investigations.

There is no doubt that we have learned a lot about materials in the past 50 years. We have also found that we need to learn a lot more. As difficult as it is to account for all of the variables contributing to premature failures, we must apply our energy toward producing materials that will withstand the intended service conditions with the recognition and allowances for the dynamics that will occur during transients.

If our industrial potential is to remain strong in its world position, it will be necessary to develop more specific information on materials. This should also include the study of materials removed from service. Furthermore we must increase the accessibility to this information. The successful implementation of the National Materials Properties Data Network (MPDN) should provide the base from which the generation of new or more specific data will provide more confidence for the least cost.

Steel Melting

Daniel A. Pflaum[1]

Residual Problems and the Scrap Industry

REFERENCE: Pflaum, D. A., "**Residual Problems and the Scrap Industry,**" *Residual and Unspecified Elements in Steel, ASTM STP 1042,* A. S. Melilli and E. G. Nisbett, Eds., American Society for Testing and Materials, Philadelphia, 1989, pp. 11–25.

ABSTRACT: Purchased scrap is generally accepted as a major source of residual and unspecified elements in steel. Current trends in the steel industry will precipitate a more important role for scrap as a raw material. A principal factor in minimizing residual elements is the monitoring and control of this nonhomogeneous, nonmanufactured product by scrap processors and steel producers. By examining the variation in scrap grades through computer analysis and by integrating various techniques such as material segregation, inspection, and statistical process control procedures, more predictable and potentially lower residual levels can be achieved.

KEY WORDS: purchased scrap, nonhomogeneous, nonmanufactured, steel producers, scrap suppliers, examined variations, control procedures, more predictable, lower residuals

Trends in the Steel Industry

In 1970, 30 tons (27.23 metric tons) of scrap were purchased for every 100 tons (90.78 metric tons) of steel produced. In 1986, that ratio increased to 48 tons (43.57 metric tons) of scrap for every 100 tons (90.78 metric tons) of steel. Moreover, many factors currently affecting the steel industry indicate that the ratio of scrap melted to ton of steel produced should continue to increase in the future (Fig. 1).

Some of the key technological shifts contributing to scrap's expanded role in steelmaking are as follows.

Electric Furnace Steel Production

In the United States, the percentage of steel produced by electric furnaces grew from approximately 6% of total production in 1954 to roughly 15% in 1970. A steeper growth curve followed with electric furnaces supplying 36.4% in 1986 (Fig. 2).

Continuous Casting

The growth of continuous casting in the U.S. steel industry has been astronomical. Continuous casting has risen from less than 7% of steel produced during the industry's record production year, 1973, to 54% in 1986 and has increased to more than 60% in 1987. According to estimates, three-quarters of the steel made in this country will be continuous cast by 1990 (Fig. 3).

A direct result of the conversion to continuous casting has been a sharp reduction in internally generated scrap, which, in turn, has decreased the amount of home scrap available for melting (Fig. 4).

---

[1] Quality manager, David J. Joseph Company, 300 Pike St., Cincinnati, OH 45202.

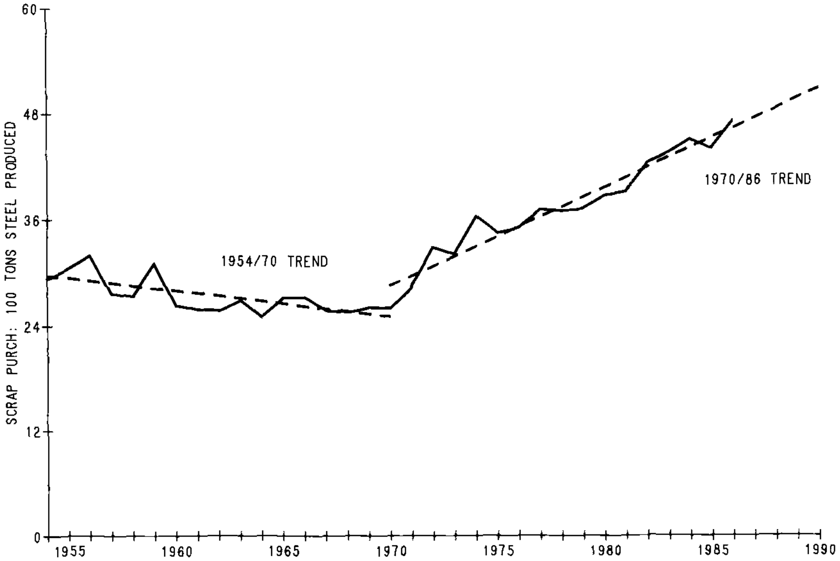

FIG. 1—*Ratio of scrap purchased to steel produced.*

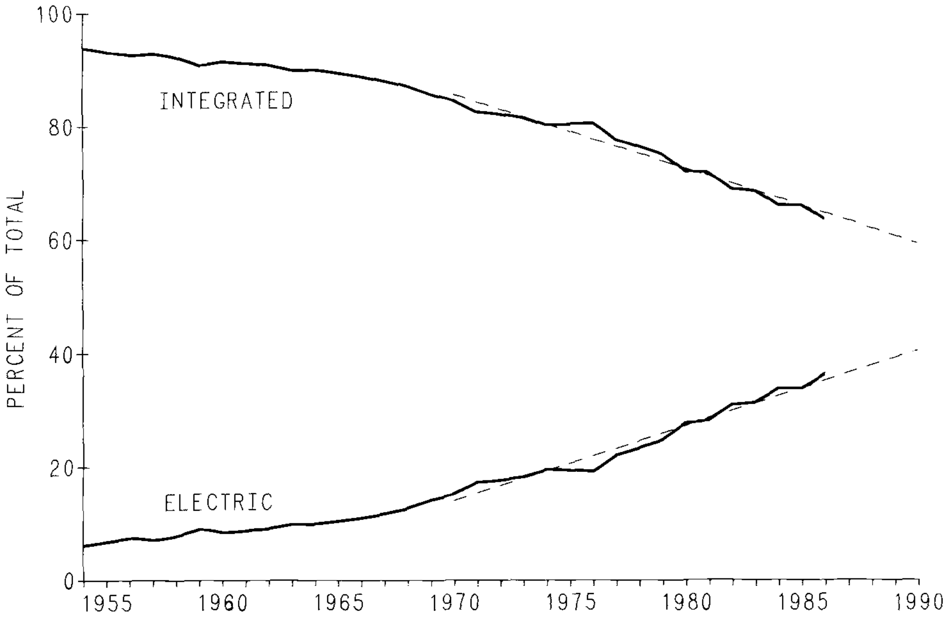

FIG. 2—*U.S. steelmaking mix, 1954–1990.*

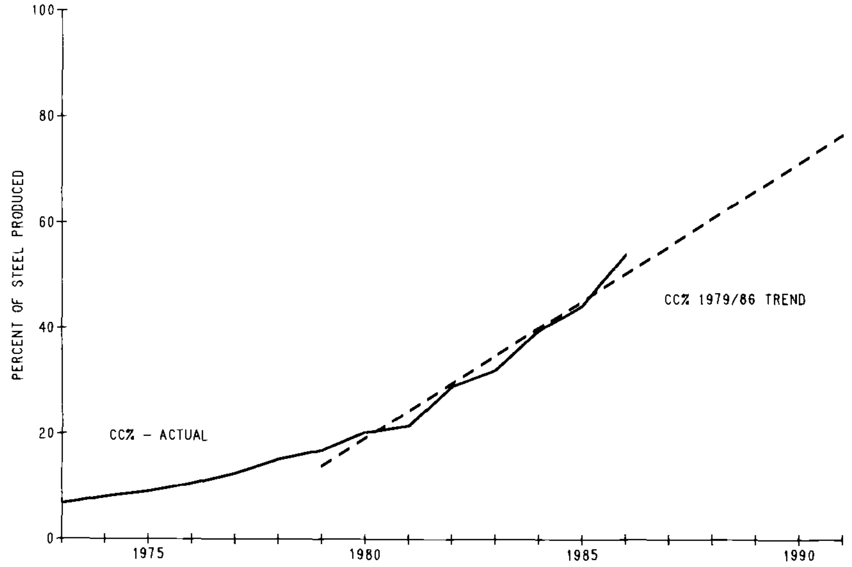

FIG. 3—*Continuous casting percent of steel produced.*

FIG. 4—*Home scrap production as a percent of scrap consumption (all consumers).*

Advanced Furnace Procedures

Numerous technological advances in the last 30 years have increased the capacity of basic oxygen furnace (BOF) vessels to melt additional tons of scrap and boosted the productivity of scrap-based electric furnace shops. Ladle metallurgy, oxy-fuel burners, scrap preheating, and other rapid melting techniques have increased the tons/h of arc furnaces. Post combustion, hydrocarbon fuels, and new blowing techniques have led to an alphabet soup of BOF variations, Q-BOP, K-OBM, LBE, KMS, KS, and so on, which are intended to homogenize the melt, maximize a mill's supply of hot metal, and, in many cases, increase cold scrap charges.

Scrap will, therefore, continue to be a vital raw material in iron and steel production.

Sources of Scrap

In any discussion concerning the ferrous scrap industry, a key principle to establish is that scrap is an involuntary product. Scrap is either a by-product of manufacturing processes or a result of obsolescence. The approximate breakdown of scrap purchased by steel mills and foundries is (1) 40% industrial scrap, a by-product of stamping, drilling, and other manufacturing processes; (2) 20% generated from the 7 to 9 million cars and trucks scrapped in the United States each year; (3) 5% from the 65 to 70 000 railroad cars retired annually; and (4) the remaining 35% from obsolete iron and steel products, such as structural steel, farm and construction tractors, water pipes, and kitchen sinks.

Scrap from these various sources finds its way into processing yards, of which there are approximately 3000 in the United States, where it is sorted, sheared, shredded, and prepared for sale and shipment to melting facilities. Therefore, scrap often exhibits significant variations from region to region, depending on the characteristics of each processor's operation, metalworking facilities, geographic location, and requirements of each scrap consumer. The Institute of Scrap Recycling Industries publishes approximately 40 specifications for non-alloy steel scrap grades and about 20 specifications for iron scrap grades. Scrap material actually shipped under a certain grade specification can vary extensively from one processor to another.

The Challenge

The paradox to resolve is how best to use this increasingly important raw material that is not homogeneous and control the residual and unspecified elements in the steel produced. The inherent variability of scrap requires that several methods be employed to regulate accurately its quality. The critical quality parameters that can affect the residual elements in steelmaking are given below.

Melting Yield

Melting yield is largely dependent on nonmetallic content, for example, wood, rubber, and so on, and oxidation losses due to the melting operation or initial rust. Low yields can affect the melt chemistry by altering heat weights, and, consequently, the corresponding percentages of the nonvolatized residual elements. For example, with no change in the quantity of each element charged, a 3% reduction in yield can equate to a 0.01% increase in the melt-in copper, nickel, and molybdenum percentages.

Size and Density

The specified size and density are functions of handling practices, type and size of furnace, and melt rates. Locating scrap with the proper chemistry that is too large or lacks the density to make the melting operation practical is of little benefit. Also, material with a high surface area to volume ratio, that is, small pieces or light gauge, will have a lower yield due to higher oxidation rates during melting.

Chemistry

The acceptable chemistry of each grade is dictated by the charge mix designed to achieve the desired final melt chemistry. Determining the representative chemistry for each grade, supplier, or both is the most important and difficult segment of the program.

Scrap Versus Other Raw Materials

In analyzing the problems associated with scrap, reviewing other raw materials that steel producers have successfully controlled with regard to cost and quality is helpful. Examples are refractories, ferroalloys, and electrodes. Vital factors in achieving quality control of these items are:

(1) An accurate, applicable specification that defines the necessary requirements of the product, for example, 24 in. (60 cm) electrodes, 70% alumina ladle brick 9.5 by 9.5 by 12 in. (24 × 24 × 30 cm);

(2) Supplier or source identification; as these materials are put into service, melt shops know which electrode supplier they are using, which ladle or furnace brick supplier is in production, and so on; and

(3) Methods of monitoring material performance by supplier are established, for example, Supplier A's electrodes 10.5 lb/ton, Supplier B's electrodes 9.7 lb/ton, or Supplier X's bricks 70 heats/ladle, Supplier Y's bricks 63 heats/ladle.

Using these techniques, steel producers can monitor the performance of each supplier's product, accurately assess its value, qualify suppliers, and improve control of the effect on the manufacturing process. Drastically simplified, these methods, that is, specifications, supplier identification, and a monitoring system, can effectively be applied to scrap with similar results. The following is a review of how scrap consumers can and are dealing with this problem of scrap quality.

Specifications

Scrap specifications for each purchased grade must be designed to address the four parameters most often considered measures of scrap quality: melting yield, density, size, and chemistry. Emphasis should be placed on determining the role of each grade in the scrap mix, consequently writing the specification to achieve this objective and incorporating consistency within each item. In designing a specification, specifying what is not acceptable in each grade is often valid, for example, rebar, pipe, and chain are not acceptable in plate and structural. This specifying is practical information that the scrap processor can use. Writing specifications is an important first step, but monitoring conformance and maintaining supplier identity are key elements in a quality program.

Inspection

Visual inspection, although the oldest method of control, is still a valuable tool in evaluating scrap cleanliness, nonmetallics content, and size. However, this procedure should be taken a step further by establishing a quantitative rating system for size, nonmetallic material, nonferrous material, and consistency. Calculating bulk densities, using car and truck weights and volumes, adds an objective measure of scrap quality and consistency. Table 1 shows a typical daily inspection report used in a rating system. In this example, scrap is rated on a scale of 0 for rejectable, 1 for acceptable, 2 for good, or 3 for very good, for each of the indicated categories.

Table 2 describes the ratings within each category of Table 1. The ratings are accumulated, averaged, and recorded for each month according to supplier and scrap grade. Armed with this report, scrap consumers can begin to determine not only who the poor quality suppliers are and what problems exist with each, but, just as important, who the higher quality suppliers are.

An intensified inspection program improves the predictability of melting yields by reducing the inclusion of nonferrous, nonmetallic, undersized, and excessively oxidized material in the scrap grades. As previously explained, this factor is important in producing less heat chemistry variation. Also, by detecting the obvious contaminates, for example, electrical motors, aluminum parts, alloy gears, and shafts, this program is capable of reducing off analysis heats due to scrap related residuals.

Scrap Chemistries

One of the most difficult problems in controlling scrap quality is determining how to obtain a representative chemistry for each grade and supplier. For some industrial grades, such as busheling, turnings, borings, and Number 1 bundles, a statistical sampling program based on purchase volumes can be very effective in establishing chemical profiles. However, less homogeneous grades require multiple linear regression analyses of melt chemistries versus charge mixes to produce useful information by grade or supplier or both.

To achieve the regression analysis, scrap must be identified and recorded during the charging operation. Scrap taken directly from incoming railroad cars is tied to a specific supplier, whereas scrap from outside inventory or material trucked directly into the charging aisle maintains only grade identity. The melt-in chemistry and any alloys charged into the furnace are also recorded. Linear regression of this data establishes and quantifies the relationship between the weight of each scrap grade and the heat chemistry, and, through this calculation, produces the predicted chemistry of the scrap categories.

Table 3 is an example of the results of a regression analysis of the copper content for one month's melt shop production. The *X* coefficient is the calculated copper content for each grade, for example, Number 1 bundles contain 0.02% copper, busheling contains 0.03% copper, and so on. The standard error of deviation of the coefficient measures the range of the calculated chemistry for each scrap grade. For example, in Table 3, the *X* coefficient of Number 2 steel computed an average of 0.236% copper plus or minus the standard error of 0.115, which indicates a range of 0.121 to 0.351%. This assumes a normal distribution, when in actuality the variability of residuals in scrap is skewed to the high side, that is, 0.121% copper in Number 2 steel is unlikely whereas 0.35% can be expected.

Regression analysis of individual suppliers often yields unreliable data due to the large number of scrap sources involved. However, information similar to the example in Table 3, calculated periodically, is useful in determining residual suspect grades and can be applied to indicate chemistry trends. Once a sufficient data base has been established, scrap consumers can also compare predicted melt chemistries versus the actual analysis for each heat. Reviewing the charging data for those heats outside the predicted or allowable limits may offer clues about the origin of the increased variability. Suppliers that consistently have material in these off analysis heats can be highlighted for more detailed inspection and monitoring. In this fashion, the computer study of the scrap charge can supply the inspector with valuable knowledge of where to concentrate his efforts. Therefore, over a period of time, scrap grades and, eventually, suppliers contributing to residual problems can be determined and corrective action taken accordingly.

TABLE 1—*Daily ratings.*

Shipper	Date	Car Truck #	Grade	Size Density	Nonmetallics	Non-Ferrous	Alloy	Hazard	Total
Supplier A	1/01/87	TR 1111	Shred	1	3	2	1	3	2.0
Supplier B	1/01/87	BN 36841	#1HM	2	3	2	2	3	2.4
Supplier C	1/01/87	CO 1235	#1HM	0	1	1	2	3	1.4
Supplier D	1/01/87	SBD 8753	#1 Bundles	3	3	3	3	3	3.0
Supplier E	1/01/87	TR 1112	Dies	0	2	0	0	3	1.0
Supplier F	1/01/87	NW 46579	Bushelings	3	1	2	3	3	2.4
Supplier A	1/01/87	TR 1113	Shred	3	1	2	1	3	2.0
Supplier C	1/01/87	BN 68752	#1HM	3	1	3	2	3	2.4
Supplier B	1/01/87	TR 1114	#1HM	2.0	2.0	1.0	0.0	0.0	1.0
	Total 1/01/87			1.9	1.9	1.8	1.6	2.7	2.0

TABLE 2—*Grade: plate and structural.*

Category & Specifications	Rejectable	Acceptable	Good	Very Good
Size:				
$3/10''$[a] min thickness $8''$ max thickness cut to $5' \times 2'$[b] maximum	Sufficient material exceeding these maximums, that is, approximately 1000 lb[c]/car	Material cut to size maximums	10-50% of material cut to $3' \times 2'$	Over 50% of the material cut to $3' \times 2'$
		55 GT/car (62 lb/ft^3)[d]	60 GT/car (67 lb/ft^3)	65 GT/car (73 lb/ft^3)
Nonmetallics:				
None	Over 100 lb visible per car	100-50 lb visible per car	0-50 lb visible per car	No nonmetallics visible in car
Non-ferrous:				
None	Over 50 lb visible per car	25-50 lb visible per car	0-25 lb visible per car	No nonferrous material visible
Out of Spec Material:				
No unsplit pipes No galvanized or other coatings	In excess of 500 lb of unsplit pipe, galvanized or other coated material, or alloy steel	500-200 lb of unsplit pipe, galvanized or other coated material, or alloy steel	1000-200 lb of unsplit pipe galvanized or other coated material, or alloy steel	Less than 100 lb of unsplit pipe, galvanized or other coated material, or alloy steel
	In excess of 15% of the material heavily rusted.	5-15% heavily rusted material.	Only light surface rust visible.	No visible rust.
Hazardous:				
No closed cylinders or radioactive or lead containing material	Any closed cylinders with no visible holes, radioactive or lead containing material	Closed cylinders with visible holes		No material considered to be closed cylinders

[a] 1 in. = 25.4 mm.
[b] 1 ft = 0.305 m.
[c] 1 lb = 0.454 kg.
[d] 1 lb/ft^3 = 16 kg/m^3.

TABLE 3—*Regression output: Copper content.*

Constant	0
Standard Error of Y Est	40.9816711
R Squared	0.7981965
No. of Observations	124
Degrees of Freedom	117

Parameter	#1 Bundles	Bushelings	#2 Stl	#1 Stl	Turn	Pit	Home
X Coefficient(s)	0.021772	0.032023	0.236009	0.117396	0.063043	0.073536	0.070654
Standard Error of Coefficient	0.011609	0.013608	0.115005	0.005389	0.057209	0.071130	0.008735

Material Segregation

Once a quantitative rating program and regression and off grade chemistry analyses are generating information about the quality level of various suppliers, material segregation can be implemented to improve control of residual elements. The goals of material segregation are to increase supplier accountability and optimize the use of certain grades or suppliers or both to reduce the variability of the melt chemistries. For example, very low residual busheling segregated from the normal busheling material can be applied to the more critical heats. More predictable chemistries and lower scrap costs can be achieved as demonstrated in Table 4 versus Table 5. In this example, use of identified low residual busheling and shredded resulted in $2.00/ton savings and reduced copper, chromium, and nickel by 0.006, 0.02, and 0.02%, respectively. Figure 5 shows a substantial decrease in off analysis melts at a steel mill by separating busheling sources.

Achieving source separation of large volume grades may not be practical due to the number of suppliers and amount of material involved. In this situation, a statistical sampling program may be feasible where, on a random basis, an individual supplier's scrap is inventoried separately for a period of time and examined. Efforts are made to charge this scrap with known analysis material to check the chemistry and yield by back calculations. Use of low cost scrap grades such as Number 2 heavy melt, turnings, and Number 2 bundles can drastically lower material charge costs. These grades also have higher variability in quality, particularly chemistry. Some high quality steel producers efficiently consume limited quantities of these grades by segregating each by source. Supplier identity is maintained throughout inspection procedures, statistical sampling, and charging resulting in improved traceability, and also consistent, predictable material. Which scrap grades are segregated is a function of finished product specifications, scrap availability, and melt shop logistics. Yet, the practice of material separation is an integral part of a scrap quality program.

Results

Standard *X* and *R* statistical process control charts plotting melt chemistries are largely used to monitor residual levels. These charts demonstrate that steel producers obtain better residual level control through inspection, material segregation, quantitative rating systems, statistical sampling, and regression analysis. Figures 6 and 7 show one mill's reduction in melt copper and missed heats using these techniques. Similarly, the decreases in the average copper values of purchased scrap grades at a mill are shown in Table 6.

TABLE 4—*Scrap, without segregation, low residual heat.*

Code	Name	Weight, lb[a]
BND1 I	#1 Bundles	80000.0
BUSH I	Bushelings	100000.0
HOME I	Home Scrap	20000.0
SHRD I	Shredded	20000.0
Total Weight Charged		220000.0
Total Weight Recovered		203200.0
Scrap Cost		$130.00/NT

Element	Predicted Chemistry Lb[a]	Predicted Chemistry %	Max
Cu	152.8	0.0752	0.0800
Cr	146.4	0.0721	0.0800
Ni	126.2	0.0621	0.0800
Mo	20.1	0.0099	0.0100
Sn	14.7	0.0073	0.0100
P	42.0	0.0207	0.0250
S	49.6	0.0244	0.0250

[a] 1 lb = 0.454 kg.

TABLE 5—*Scrap, with segregation, low residual heat.*

Code	Name	Weight, lb[a]
BND1 I	#1 Bundles	50000.0
LRBU I	Low Residual Bushelings	100000.0
LRSD I	Low Residual Shredded	50000.0
HOME I	Home Scrap	20000.0
Total Weight Charged		220000.0
Total Weight Recovered		202300.0
Scrap Cost		$128.00/NT

Element	Predicted Chemistry Lb[a]	Predicted Chemistry %	Max
Cu	139.1	0.0688	0.0800
Cr	100.4	0.0496	0.0800
Ni	87.1	0.0431	0.0800
Mo	19.2	0.0095	0.0100
Sn	18.7	0.0093	0.0100
P	26.2	0.0130	0.0250
S	41.0	0.0203	0.0250

[a] 1 lb = 0.454 kg.

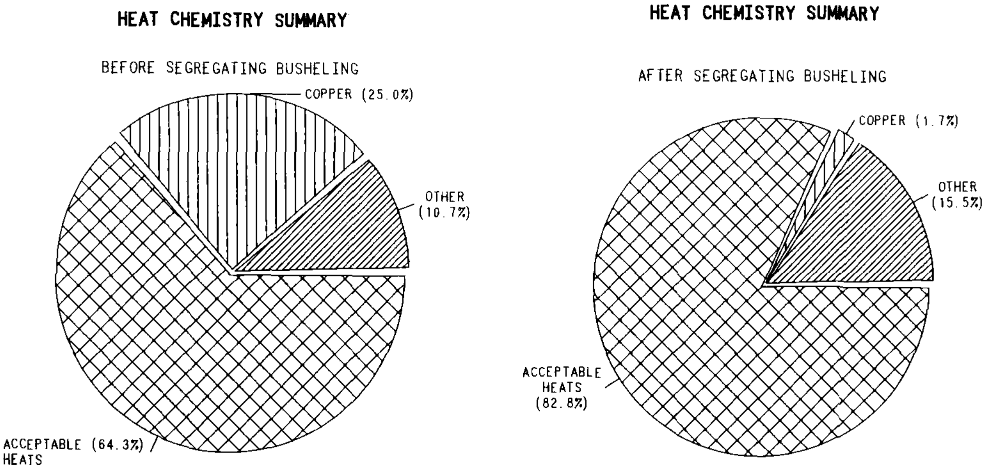

FIG. 5—*Heat chemistry summary, before segregating busheling and after segregating busheling.*

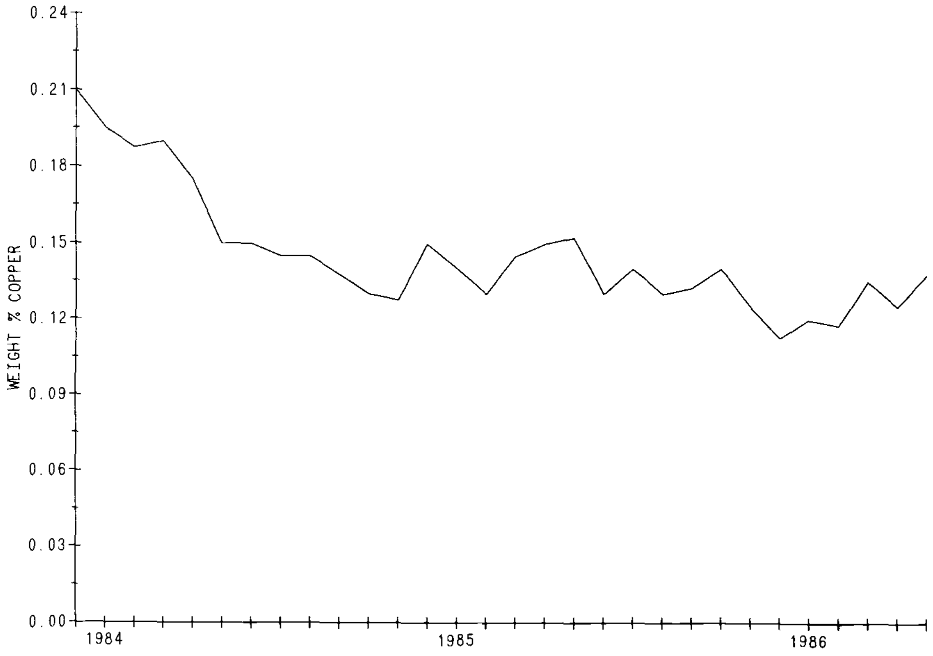

FIG. 6—*Average monthly residual for copper.*

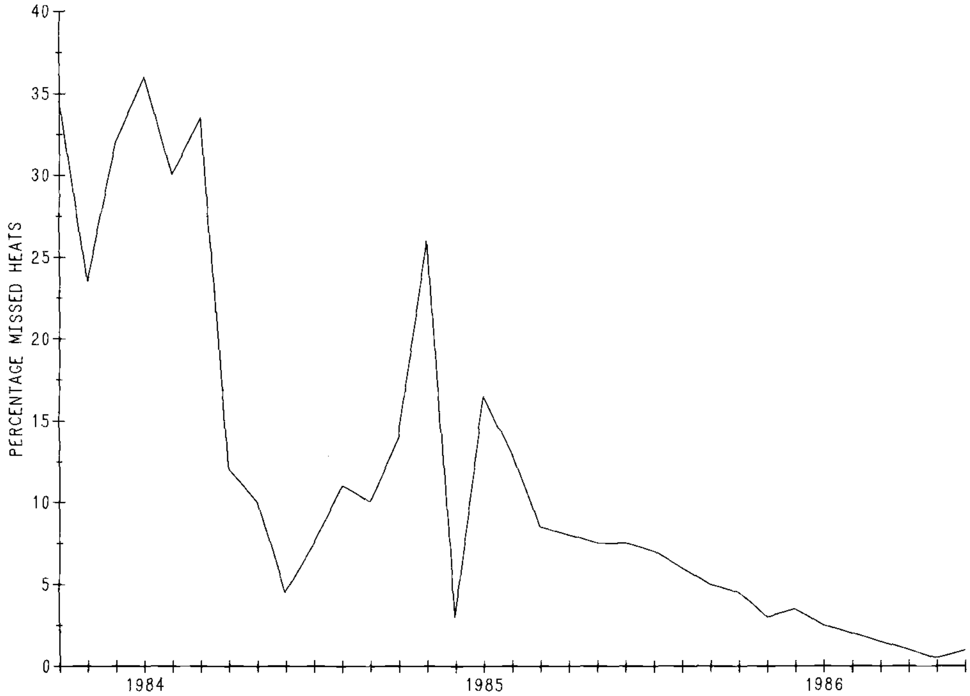

FIG. 7—*Percentage of heats exceeding residual specification.*

TABLE 6—*Decreases in average copper values of purchased scrap grades.*

Grade	% Cu
Prior to Scrap Quality Program	
Shredded	0.23
#1 Heavy Melt	0.24
#2 Heavy Melt	0.46
Turnings	0.29
#2 Bundles	0.51
After Scrap Quality Program	
Shredded	0.16
#1 Heavy Melt	0.19
#2 Heavy Melt	0.37
Turnings	0.18
#2 Bundles	0.42

Scrap Suppliers

As these types of controls are implemented at the consumer level, the downstream effect is that suppliers are beginning to be more conscious of the material's quality that they are shipping. These changes are occurring in the scrap industry as statistical process control methods and other improvements are being employed at scrap processor facilities.

At a Joseph Company shredder operation, the density, nonmetallics, and copper content are

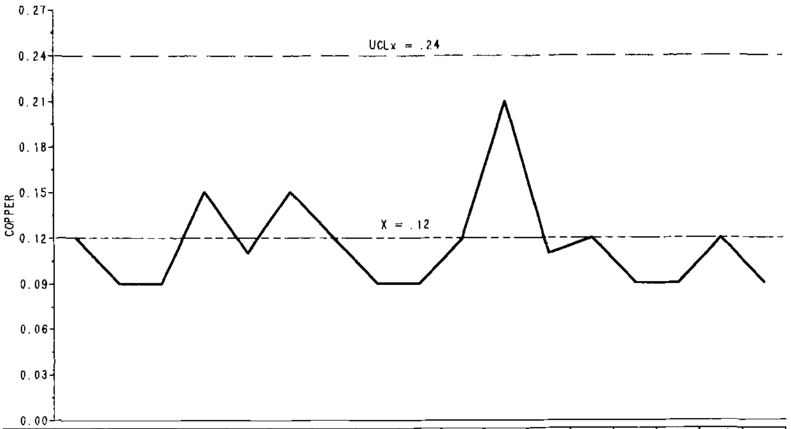

R =	.12	.09	.09	.15	.11	.15	.12	.09	.09	.12	.21	.11	.12	.09	.09	.12	.09
DATE	6/1	6/2	6/3	6/5	6/10	6/11	6/12	6/15	6/16	6/17	6/18	6/22	6/23	6/24	6/25	6/26	6/29

FIG. 8—*Control chart for copper of shredded scrap (X chart).*

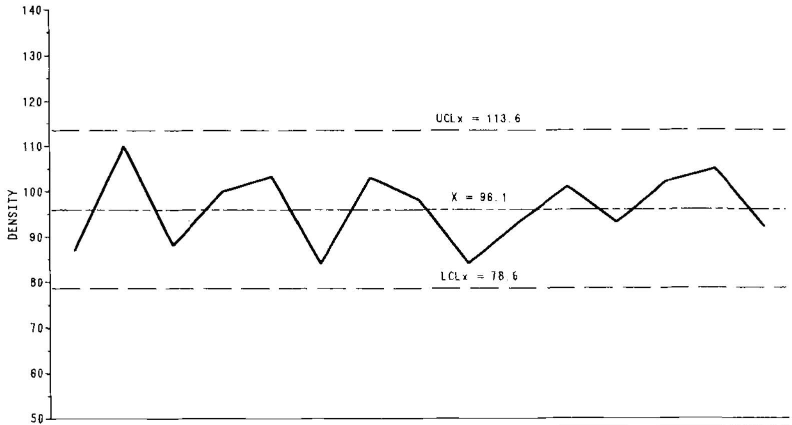

X	87.0	110.0	88.0	100.0	103.3	84.0	103.0	98.0	84.0	93.0	101.0	93.0	102.0	105.0	92.0
DATE	5/1	5/4	5/5	5/6	5/7	5/8	5/11	5/12	5/14	5/15	5/18	5/19	5/20	5/21	5/26

FIG. 9—*Control chart for density of shredded scrap (X chart).*

checked on a daily basis and plotted on X and R charts as shown in Figs. 8 and 9. Copper levels have been reduced from 0.23% to an average of 0.13%. The density has improved from 70 to an average of 90 lb/ft^3 (1121 to 1441 kg/m^3). This change has improved the predictability and productivity and reduced the cost of melt shop operations.

Scrap suppliers are beginning to segregate and control material from a chemistry standpoint in other grades, such as busheling and turnings. Recently, the Joseph Company has undertaken a program to analyze various scrap sources, storing this information on a computer file so that material can be applied more accurately and efficiently based on customers' specifications. Grade segregation in railroad scrap is also being implemented where the high residual railroad car sides are being separated from the cleaner, denser railroad wheels, trucks, and axles. This type of segregation once again improves a melt shop's predictability.

Summary

As this type of work continues, melt shops can take advantage of their own knowledge and supplier's abilities to improve the quality and, in some cases, reduce their scrap costs. This is not to say that items, such as pig iron, direct reduced iron (DRI), and other virgin low residual materials will not play an important role in the future of the steel industry. These grades are not a competitor of scrap, but a complement to this type of quality program.

In conclusion, this paper has demonstrated that scrap quality, and, therefore, residual and unspecified elements can be controlled by using the following procedures:

(1) Designing scrap specifications to set material standards;

(2) Obtaining supplier identity as the scrap is received, maintaining this during the charging operation when practical, and implementing material segregation; and

(3) Establishing an accurate monitoring system with a quantitative rating program, regression analysis of melt data, review of off analysis heats, and statistical sampling.

There is no magic in the scrap industry where one can wave a wand or perform some chemical wizardry to improve the quality and consistency of the scrap grades. What is required is hard work, effective use of manpower, computerization, and ingenuity to take full advantage of the increased control and savings to be realized in scrap.

DISCUSSION

H. V. Makar[1] *(written discussion)*—In a slide to illustrate the importance of specifying to the scrap supplier what is not wanted in the scrap as well as what is wanted, the example given was that galvanized steel and piping were not wanted. This example created some confusion regarding whether these items were not desired at all or just for plate and structural grades of scrap. Some clarification on this might be helpful. Also, can you comment on why galvanized scrap is undesirable?

D. A. Pflaum (author's response)—The inclusion of galvanized material in any grade of scrap is a function of the scrap consumer's specifications. The ability to use galvanized material largely depends on the product specification and melting method at the foundry or steel mill. Therefore, it is important for scrap consumers to specify the acceptability of galvanized material in each of their scrap grades.

G. P. Simkins[2] *(discussion question)*—With improved scrap processing techniques, the residual level of high residual scrap will tend to increase rapidly. Are there sufficient customers for this material, or will some material become contaminated beyond use?

D. A. Pflaum (author's response)—To date, sufficient customers have been found for most higher residual scrap, and, in some cases, scrap melters can benefit from the alloy content of this type of material.

---

[1] U.S. Department of the Interior, Bureau of Mines, 2401 E St., NW, Washington, DC 20241.

[2] Westinghouse Plant Apparatus Division, P.O. Box 425, Pittsburgh, PA 15234.

F. M. Harris[3] (*written discussion*)—The Department of Defense now has identified a serious problem with counterfeit bolts. There has been much publicity about the counterfeit Grade 8 bolts problem. After legal retention of stocks are satisfied, the Defense Logistics Agency will sell as scrap several tons of bolts with head markings showing Grade 8, per the Society of Automotive Engineers specification, that are made from the boron steel required for Grade 8.2 bolts. The bolts will be sold only to scrap melters with a requirement for government witness of material being loaded into furnaces. Congress has virtually mandated we sell only to scrap melters and witness melting. My questions are as follows.

1. Should we continue with current plans to maintain segregated scrap sales offerings?
2. What are realistic limits for the maximum scrap weights that we can expect a scrap melter to handle at one time?
3. Will someone in ASTM provide answers or point me to the right area for assistance?

D. A. Pflaum (author's response)—I am not familiar with the specific circumstances concerning the counterfeit Grade 8 bolts. However, I would suggest that scrap segregation be maintained so that better chemistry control of the melt and verification of melting can be established. The maximum scrap weights that can be melted at one time may vary significantly for each melting operation, and therefore, it is best to discuss this with the scrap consumers on an individual basis.

---

[3] Chief, Engineering Programs Division, Defense Logistics Agency, Technical and Logistics Directorate, Cameron Station, Alexandria, VA 22304-6100.

Barry M. Glasgal[1]

Some Practical and Economic Aspects of Residual Element Control in Engineered Bar Products

REFERENCE: Glasgal, B. M., "**Some Practical and Economic Aspects of Residual Element Control in Engineered Bar Products,**" *Residual and Unspecified Elements in Steel, ASTM STP 1042,* A. S. Melilli and E. G. Nisbett, Eds., American Society for Testing and Materials, Philadelphia, 1989, pp. 26-37.

ABSTRACT: With the increasing use of electric arc furnaces (EAF) for the production of carbon and alloy special quality engineering bar steels, controlling and restricting residual elements have become an increasingly significant economic component of steelmaking. This paper reviews the trend in EAF production and discusses the various types of scrap used in EAF steelmaking and the formulation of scrap charges to achieve residual control. Reasons for specifying residual restrictions and some rational alternatives are presented.

KEY WORDS: residual elements, electric furnaces, continuous casting, scrap, copper, hot shortness, formability, hardenability

Controlling residual elements in engineered bar products essentially means, to the producer, controlling the copper, nickel, chromium, and molybdenum content of his product. Since these elements are for all practical purposes not removable from steel during melt, controlling their levels of occurrence relies on the ability of the producer to control the raw materials of steelmaking. Ideally, this could be accomplished by knowing the residual content of all raw materials and selecting them accordingly. While this method may have been a practice and a practical solution at one time, it is now neither a practical nor economical reality to do so. In order to understand the reasons driving this change one must necessarily understand some of the significant transitions that have occurred in the steel industry in recent years.

In the last ten years there have been substantial changes in the industry in terms of composition, capacity, and productivity of the producers, and the increasing adaptation and application of technology to steel processing. This discussion will show how these changes have impacted the ability of producers to control residual elements, and the economic interdependency that has been created because of the various aspects of change that have occurred.

The Advent of Electric Furnace Steelmaking

To appreciate fully the issue of residual control in engineered bar products it is necessary to review some of the transitions that have taken place in the steel industry as a whole. To begin with, raw steel production capability in the United States over the last ten years has declined from approximately 160 million tons to less than 135 million tons (Fig. 1) [*1*]. At the same time, the method of melting this steel has undergone a substantial change as well. In 1976, electric

---

[1] Manager of product development, LTV Steel Bar Division, LTV Steel Company, 410 Oberlin Ave., S.W., Massillon, OH 44646.

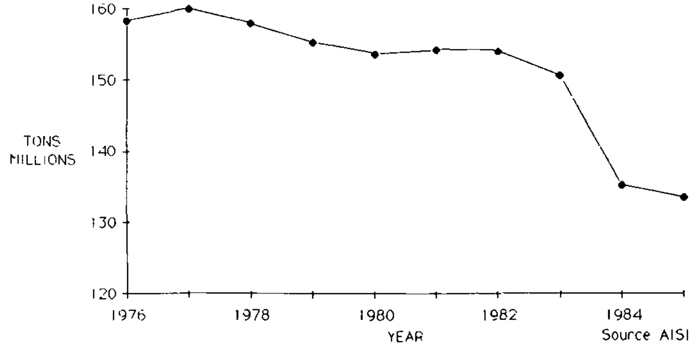

FIG. 1—*U.S. raw steel capability.*

furnace steelmaking represented less than 20% of total steel production. As shown in Fig. 2 [*1,2*], during this same time, electric furnace steelmaking has nearly doubled. The significance of this transition relative to residual element control is that a much more substantial percentage of steel is now being produced by electric furnace melting, a scrap intensive process, and scrap is the principal source of residual elements.

While these figures (Figs. 1 and 2) from the American Iron and Steel Institute accurately portray the change in the steel industry as a whole, the transition is even more pronounced when viewed from the perspective of engineered bar products alone. Today, while electric furnace melt accounts for approximately 36% of total steel production, it accounts for an extraordinary estimated 79% of the melt devoted to the production of engineered bar products. The importance of this last statement is that iron ore based low residual products are not widely available, and residual element control in nearly 80% of the bar products produced in the United States is dependent on the consistency, quality, and management of the primary raw material of electric furnace steelmaking—scrap.

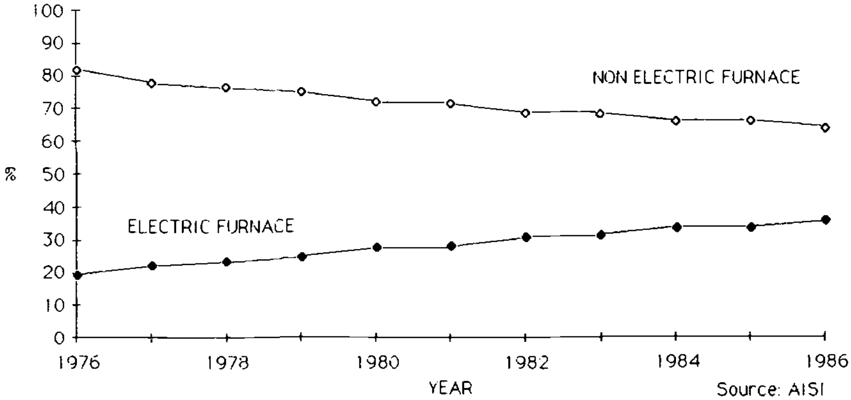

FIG. 2—*Percent of U.S. production by furnace type.*

The Growth of Continuous Casting

Just as increased electric furnace steelmaking created increased usage and demand for scrap on the part of steel producers, the advent of continuous casting, curiously enough, had a similar effect. As can be seen in Fig. 3 [*1*], over the same time during which electric furnace production doubled, continuous casting increased four fold. The influence of continuous casting on scrap consumption and scrap availability is somewhat less apparent than that caused by electric furnace production.

Continuous casting is a more efficient process than the ingot casting process that it replaces. As such there is a higher yield of usable product from molten metal and therefore less primary scrap produced for recycling in the melt facility. In addition, continuous cast product is generally higher in quality than ingot cast product. This manifests itself in less in-process steel plant scrap generation during subsequent processing to final product, as well as less in-process scrap generation as a result of material quality failures in customer manufacturing operations. The "loss" of scrap generated internally creates increased external replacement demand from the melt facility, while the "loss" of scrap in the manufacturing sector decreases its availability.

Increased use of the continuous casting process has not only affected scrap availability, but also scrap quality available to bar producers. The predominant growth of continuous casting has occurred in flat rolled production and in that segment of the industry scrap replacement demand has been created. Since flat rolled product is the principal source of low residual high quality scrap, flat rolled producers are also the principal consumers of low residual high quality scrap. Due to the enormous volume of flat rolled production compared to bar production, the vast majority of available low residual scrap is being consumed in flat rolled operations, thus creating a shortage for bar producers.

So, as is apparent, the increased use of continuous casting as a method of manufacturing has had a dramatic effect on both scrap quality and availability.

Scrap—The Variable Constant

Familiarization with scrap, its characteristics, sources, uses, and ramifications for steel production has been reserved for a relatively limited audience for a variety of reasons, not the least

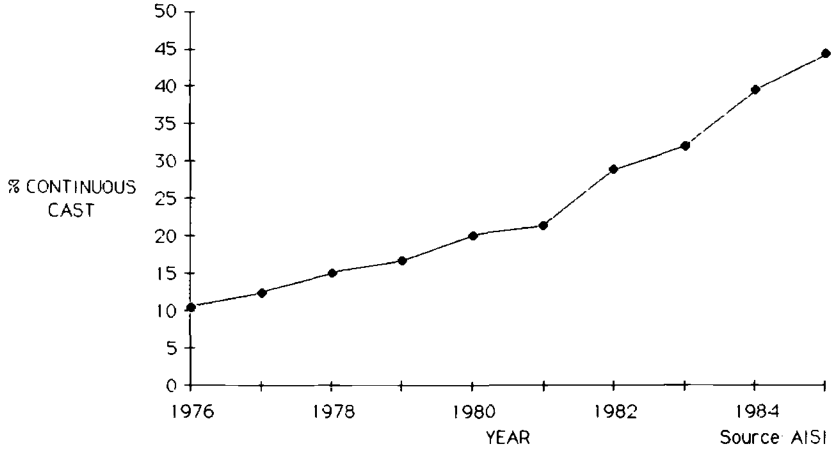

FIG. 3—*Percent of U.S. production as continuous cast.*

of which perhaps is that the subject is not particularly glamorous. Therefore, a little background information and a brief primer is probably in order.

Scrap, as it is used in steelmaking, is thought of in two general categories, revert scrap and purchased scrap. Revert scrap, as the name implies, is a by-product of the steel production process and includes such things as rolling mill discards as well as in-process rejects. When properly managed scrap can be fairly well characterized in accordance with alloy content. Purchased scrap, on the other hand, is more diverse.

Purchased scrap has a revert scrap counterpart called prompt industrial scrap, which, as the name implies, is the by-product of industrial manufacturing much the same as revert scrap is the by-product of steel production. Prompt industrial scrap is comprised principally of No. 1 bundles and busheling, which, similar to revert, can also be fairly well characterized by (low) alloy content. Most other No. 1 scrap cannot be characterized by alloy content due to the variable sources from which it is derived and the general inability of suppliers to reliably segregate it into separable entities.

The other classification of purchased scrap generally used in steel production is called obsolete scrap. The composition of obsolete scrap is lesser known or controlled, and its sources include such familiar origins as old automobiles, appliances, and components of demolished buildings.

In addition to origin, purchased scrap is also classified in accordance with composition, size, and shape, all of which bear on productivity and manufacturing costs in the melting facility. The variability and complexity of purchased scrap can be best appreciated by referring to Table 1, which lists and describes 30 different types of steelmaking scrap classified by the Institute of Scrap Iron and Steel.

Of importance to this discussion of purchased scrap, in addition to its diversity, is residual alloy content control through either specification or selection.

For specification purposes, scrap is considered by the Institute of Scrap Iron and Steel [*3*] to be "free of alloys" when the residual alloying elements do not exceed the following percentages:

(1) Nickel 0.45%;
(2) Chromium 0.20%;
(3) Molybdenum 0.10%; and
(4) Manganese 1.65%.

Notably absent from the list above is copper.

For comparative purposes, commercially produced engineered bar products are generally produced to the following maximum levels of residual content when not otherwise restricted by the consumer:

(1) Nickel 0.25%;
(2) Chromium 0.20%;
(3) Molybdenum 0.06%; and
(4) Copper 0.35%.

Since, as previously stated, these residual elements are essentially not removable from steel during melt, scrap that is to be purchased as "free of alloys" must often be diluted with scrap of known low residual content to ensure compliance with the above maximum levels. This is exactly the type of scrap, No. 1 bundles and busheling, that the increased use of electric furnace melting and continuous casting has caused to be both in short supply and of premium price. The proper selection of scrap for the purpose of controlling residual elements by accurately predicting residual levels and thus reducing the need to dilute scrap charges with expensive No. 1 bundles and busheling, has therefore become one of the most important economic aspects of steelmaking and melt shop management.

TABLE 1—*Various scrap types used in making carbon and alloy steels: basic open hearth, basic oxygen, electric furnace, and blast furnace grades.*

	ISIS[a] Code No.
No. 1 heavy melting steel. Wrought iron and/or steel scrap $1/4$ in.[b] and over in thickness. Individual pieces not over 60 × 24 in. (charging box size) prepared in a manner to ensure compact charging.	200
No. 1 heavy melting steel 3 ft[c] × 18 in. Wrought iron and/or steel scrap $1/4$ inch and over in thickness. Individual pieces not over 36 × 18 in. (charging box size) prepared in a manner to ensure compact charging.	201
No. 1 heavy melting steel 5 ft × 18 in. Wrought iron and/or steel scrap $1/4$ inch and over in thickness. Individual pieces not over 60 × 18 in. (charging box size) prepared in a manner to ensure compact charging.	202
No. 2 heavy melting steel.[d] Wrought iron and steel scrap, black and galvanized, $1/8$ in. and over in thickness, charging box size to include material not suitable as No. 1 heavy melting steel. Prepared in a manner to ensure compact charging.	203
No. 2 heavy melting steel.[d] Wrought iron and steel scrap, black and galvanized, maximum size 36 × 18 in. *May include all automobile scrap properly prepared.*	204
No. 1 bundles. New black steel sheet scrap, clippings or skeleton scrap, compressed or hand bundled, to charging box size, and weighing not less than 75 lb/ft^3[e]. (Hand bundles are tightly secured for handling with a magnet.) May include Stanley balls or mandrel wound bundles or skeleton reels, tightly secured. May include chemically detinned material. May not include old auto body or fender stock. Free of metal coated, limed, vitreous enameled, and electrical sheet containing over 0.5% silicon.	208
No. 2 bundles. Old black and galvanized steel sheet scrap, hydraulically compressed to charging box size and weighing not less than 75 lb/ft^3. May not include tin or lead-coated material or vitreous enameled material.	209
Shredded Scrap. Homogeneous iron and steel scrap, magnetically separated, originating from automobiles, unprepared No. 1 and No. 2 steel, miscellaneous baling and sheet scrap. Average density 50 lb per cubic foot.	210
Shredded Scrap. Homogeneous iron and steel scrap magnetically separated, originating from automobiles, unprepared No. 1 and No. 2 steel, miscella-	211
tightly secured for handling with a magnet.) May include Stanley balls or mandrel wound bundles or skeleton reels, tightly secured.	
Bundled No. 1 steel. Wrought iron and/or steel scrap $1/8$ in. or over in thickness, compressed to charging box size and weighing not less than 75 lb/ft^3. Free of all metal coated material.	217
Bundled No. 2 steel. Wrought iron or steel scrap, black or galvanized, $1/8$ in. and over in thickness, compressed to charging box size and weighing not less than 75 lb/ft^3. Auto body and fender stock, burnt or hand stripped, may constitute a maximum of 60% by weight. (This percent based on makeup of auto body, chassis, driveshafts, and bumpers.) Free of all coated material, except as found on automobiles.	218
Machine shop turnings. Clean steel or wrought iron turnings, free of iron borings, nonferrous metals in a free state, scale, or excessive oil. May not include badly rusted or corroded stock.	219
Machine shop turnings and Iron borings. Same as machine shop turnings but including iron borings.	220

No. 2 heavy melting steel 3 ft × 18 in. Wrought iron and steel scrap, black and galvanized, maximum size 36 × 18 in. May include automobile scrap, properly prepared, however, to be free of sheet iron or thin gauged material.	205
No. 2 heavy melting steel 5 ft × 18 in. Wrought iron and steel scrap, black and galvanized, maximum size 60 × 18 in. May include automobile scrap, properly prepared, however, to be free of sheet iron or thin gauged material.	206
No. 1 busheling. Clean steel scrap, not exceeding 12 in. in any dimensions, including new factory busheling (for example, sheet clippings, stampings, etc.). May not include old auto body and fender stock. Free of metal coated, limed, vitreous enameled, and electrical sheet containing over 0.5% silicon.	207
New Black Sheet Clippings. For direct charging, maximum size 8 ft by 18 in., free of old automobile body and fender stock, metal coated, lined, vitreous enameled and electrical sheet containing over 0.5% silicon, must lay reasonably flat in car.	207A
neous baling and sheet scrap. Average density 70 lb/ft^3.	
Shredded Clippings. Shredded 1000 series carbon steel clippings or sheets. Material should have an average density of 60 lb/ft^3.	212
Shredded Tin Cans for Remelting. Shredded steel cans, tin coated or tin free, may include aluminum tops but must be free of aluminum cans, nonferrous metals except those used in can construction, and nonmetallics of any kind.	213
No. 3 bundles. Old sheet steel, compressed to charging box size and weighing not less than 75 lb/ft^3. May include all coated ferrous scrap not suitable for inclusion in No. 2 bundles.	214
Incinerator bundles. Tin can scrap, compressed to charging box size and weighing not less than 75 lb/ft^3. Processed through a recognized garbage incinerator.	215
Terne plate bundles. New terne plate sheet scrap, clippings or skeleton scrap, compressed or hand bundled, to charging box size, and weighing not less than 75 lb/ft^3. (Hand bundles are	216
Shoveling turnings. Clean short steel or wrought iron turnings, drillings, or screw cuttings. May include any such material whether resulting from crushing, raking, or other processes. Free of springy, bushy, tangled, or matted material, lumps, iron borings, nonferrous metals in a free state, scale, grindings, or excessive oil.	221
Shoveling turnings and Iron borings. Same as shoveling turnings, but including iron borings.	222
Iron borings. Clean cast iron or malleable iron borings and drillings, free of steel turnings, scale, lumps, and excessive oil.	223
Auto slabs. Clean automobile slabs, cut 3 ft × 18 in. and under.	224
Auto slabs. Clean automobile slabs, cut 2 ft × 18 in. and under.	225
Briquetted iron borings. Analysis and density to consumer's specifications.	226
Briquetted steel turnings. Analysis and density to consumer's specifications.	227
Mill scale. Dark colored, ranging from blue to black, ferromagnetic iron oxide forming on the surface of steel articles during heating and working.	228

---

[a] Institute of Scrap Iron and Steel.

[b] 1 in. = 2.5 cm.

[c] 1 ft = 0.3 m.

[d] The identical designations given for these two classifications are in accordance with established industry practices in specifying the materials desired.

[e] 1 lb = 0.45 kg.

Scrap Management for Residual Control

When dealing with the issue of residual element control, scrap management today is based upon using the lowest cost mix of scrap to achieve the desired residual level. Considering the number of combinations of scrap types and options available this is not a simple task. The task is further complicated by the limited predictability of the residual levels of the various scrap types with the possible exception of No. 1 bundles. While this scrap is the most dependable and consistent type of low residual scrap, it is also the most expensive, and as shown in Fig. 4, is currently escalating in price at an unprecedented rate.[2] Unwarranted use of this type of scrap will impose an economic burden for the producer that is unsustainable.

Residual control begins with formulating standard charges of various scrap types, which are based upon historical data and updated on an ongoing basis. Figure 5 shows the composition of three such scrap charges used to produce carbon steels with various maximum residual levels. Twelve different types of scrap are used to formulate these charges; some are dictated by operational and productivity criteria, others based on residual control. Figure 6 shows the relative cost of these three charges using the conventional residual charge as the base. One sees that the cost of restricting residuals from a conventional level to a restricted level can be quite substantial, in these cases approximately 15%.

Restriction of residuals has not solely been confined to carbon steels. Restricting one or more residual elements in alloy steels can also be very expensive. First, if the restriction is severe, the steelmaker will be required to use a carbon steel based scrap charge to avoid exceeding the specified element level. As demonstrated above this goal can only be accomplished using expensive No. 1 bundles and busheling. Second, in doing so the recapture of alloy content normally found in alloy scrap is prevented. This alloy deficiency must then be made up by adding expensive virgin alloys to the melt. Figure 7, based on scrap charges similar to those shown previously for carbon steels, shows the relative additional scrap cost incurred when the residual content of alloy steels is restricted from conventional levels. The economic penalty is on the order of 20 to 25% depending upon the level of restriction. These figures do not include the expense of adding virgin alloys to make the required analysis.

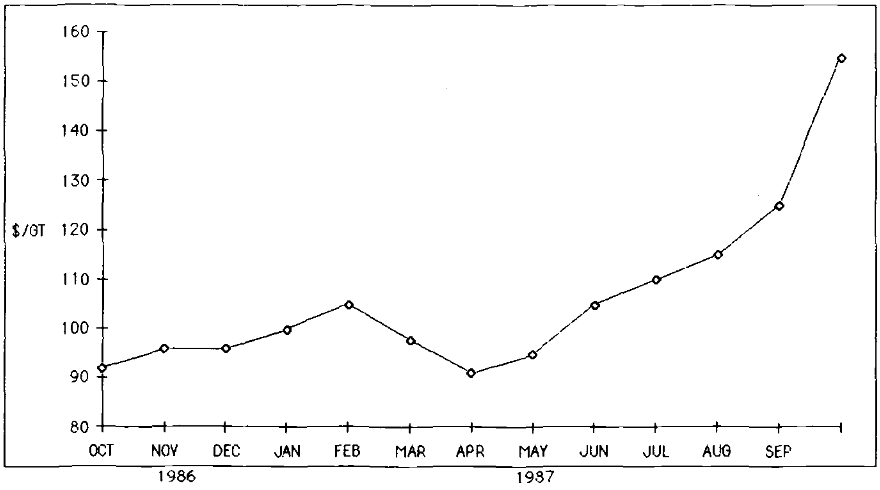

FIG. 4—*No. 1 bundle price trend.*

---

[2] Ebner, R. W., LTV Steel, personal communication.

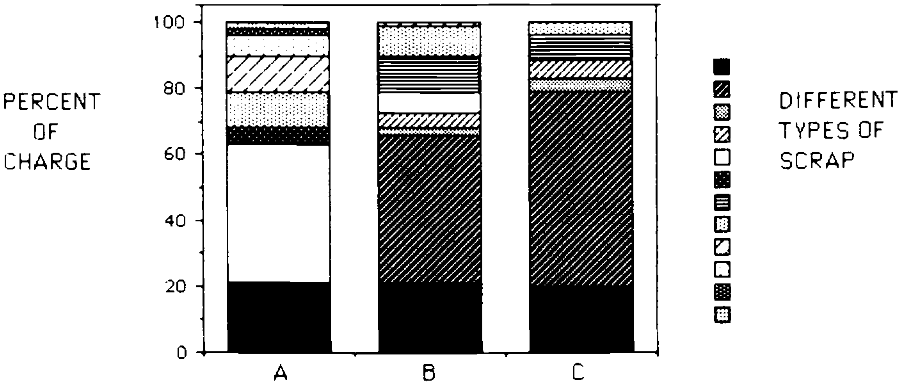

	MAXIMUM RESIDUAL LEVEL		
	A	B	C
CU	35	15	10
NI	25	12	10
CR	20	15	10
MO	06	04	02

FIG. 5—*Typical scrap charges used to produce indicated maximum levels of residuals.*

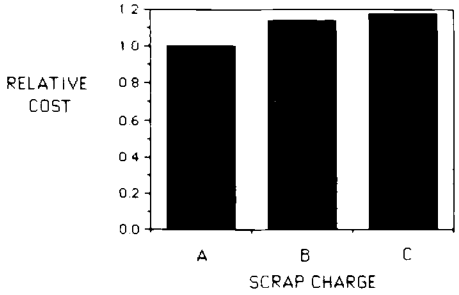

FIG. 6—*Relative cost to control residual levels to the maximums shown in Fig. 5.*

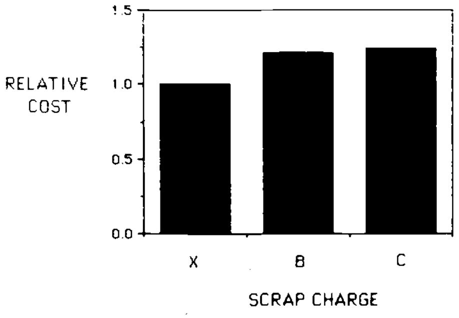

FIG. 7—*Relative cost of restricting residual levels in alloy steel to the levels shown in Fig. 5 (X is unrestricted alloy scrap base charge).*

Why Restrict Residuals?

Having thus demonstrated the economic penalties associated with the restriction of residual elements, for those faced with the high cost and limited availability of low residual scrap reviewing some of the reasons given for restricting residual elements and reassess the efficacy of doing so seems prudent. While discussing all of the reasons for restricting residuals is not possible, an attempt will be made to review some of the more common ones.

Restricting Copper to Avoid Hot Shortness?

Perhaps the element most frequently restricted in steel is copper. When restrictions of copper residuals are subject to close examination they are frequently found to stem from some general misunderstanding of copper's effect on steel and from some historically derived "truths" that have been passed down over the years. The most frequently cited reason for restricting copper is that it causes hot shortness in steel. In a pure sense copper can cause hot shortness, but the mechanisms of this effect, while well understood and controllable, are apparently less well known.

Copper in iron or steel forms a solid solution with ferrite in amounts up to about 0.8% [4]. When a relatively pure iron-copper alloy is exposed to the atmosphere at hot working temperatures for extended periods of time, the iron oxidizes preferentially to form scale, leaving a very thin and imperceptible layer of liquid copper on the surface between the scale and the metal substrate. The liquid copper film attacks the grain boundaries of the underlying metal and, through the mechanism of liquid metal embrittlement, leads to intergranular cracking, commonly referred to as hot shortness [5].

While this phenomenon is observed in a relatively pure iron-copper alloy, it is conspicuously absent when the nickel-copper ratio in the steel is 1:3 or more. In this case, when the surface of the steel is oxidized during heating, the nickel-copper solid solution, which has a higher melting point than pure copper, remains as a solid component of the scale along with the iron oxide and the mechanism of liquid metal embrittlement is avoided [5].

At this juncture, remember that the maximum nickel-copper ratio of unrestricted engineered bar steels at 25:35 is well in excess of the 1:3 ratio required to assure good hot workability. Furthermore, the nickel-copper ratio of steel is known at the time the steel is in the molten state and, should an unfavorable ratio be encountered, the corrective action of adding a small quantity of nickel or changing to an alternate grade with a favorable nickel-copper ratio is a relatively simple matter. Avoiding unfavorable situations such as this for the consumer is part of the value provided by an engineered bar producer.

Therefore, as shown in Table 2, with reasonable care copper related hot shortness can be easily avoided. The causes are rather straightforward and relatively easy to avoid or control without great difficulty or economic penalty. It might be recalled that there are entire families of weathering resistant steels [ASTM Specification for High-Strength Low-Alloy Structural Steel with 50 ksi (345 MPa) Minimum Yield Point to 4 in. thick (A 588) and ASTM Specification for High-Strength Low-Alloy Structural Steel (A 242)], to which about 0.50% copper is intentionally added and which are widely produced and fabricated on a regular basis without incident.

TABLE 2—*Factors favorably affecting hot workability of copper containing steels.*

- Fast heating rates
- Reduced time at temperature
- Limited scale formation
- Nickel: copper ratio greater than 1:3

Copper in steel, when properly managed, is not necessarily a negative. But unduly restricting its occurrence causes the steel producer added expense without adding value. The practice of restricting copper should be reviewed.

Restricting Residuals to Enhance Cold Formability?

Another reason frequently given for restricting residuals in carbon steels is that they negatively effect cold formability. This is another "truth" worth exploring a little deeper. There has been a lot of experimental work done over the years to evaluate the effects of alloy content on cold formability. Several references are given at the end of the text [*6–9*]. The net result of this work has been an advance in the state of the art and understanding of cold forming, culminating in a large number of double and triple alloy steel parts being made by cold forming processes today. These steels contain alloy levels far in excess of the conventional residual levels encountered in unrestricted carbon steels. From this work one could reasonably conclude that carbon steels with normal residual levels are indeed cold formable. Reason not withstanding, some quantification of residual alloy effect is probably worth recording.

One of the most important factors to the cold former is forming pressure. In addition to the mechanical factors of die configuration and lubrication, material strength is also a component of the forming pressure equation. This component has been quantified by several investigators relative to the alloy content of the material. The following equations summarize the alloy content related aspects of some of their findings:

$$\begin{aligned}\text{Backward extrusion pressure (tons/in.}^2\text{)} &= 46.52 + 2.73(\%\text{Mn}) + 16.14(\%\text{Si})\\ &\quad + 0.95(\%\text{Cr}) + 6.0(\%\text{Mo})\\ &\quad + 3.52(\%\text{Ni} + \%\text{Cu}) + 0.33(\%\text{pearlite})\\ &\quad + 0.26(\text{ferrite grain size})^{-1/2}\\ &\quad + 0.018\,(\text{mean free ferrite path})^{-1}\ [6]\end{aligned}$$

$$\begin{aligned}\text{Compressive stress at 0.2 strain (ksi)} &= 47.8 + 70.0(\%\text{C}) + 30.5(\%\text{Si})\\ &\quad + 16.2(\%\text{Mn}) + 11.2(\%\text{Mo}) + 8.1(\%\text{Cr})\\ &\quad + 6.5(\%\text{Ni} + \%\text{Cu}^{*})\ [7]\end{aligned}$$

Focusing on the residual elements of copper, nickel, chromium, and molybdenum, within their range of occurrence as residuals, their coefficients of effect are relatively small when compared to those of other elements and other equation components. For example, in the extrusion pressure equation, decreasing the copper content from 0.35% to 0.15%, the nickel from 0.25% to 0.15%, and the chromium from 0.20% to 0.10% will reduce the extrusion pressure by 15.2 kPa (2.2 ksi) out of 896 kPa (130 ksi) on the average for the materials evaluated. This difference is well within the range of normal variation experienced between die sets or material lots, but as demonstrated earlier would increase by 15 to 25% the cost of the scrap charge required to achieve this reduction. If indeed necessary the same result could be achieved, for example, by reducing the silicon content by 0.07%, at essentially no cost—a far more practical solution.

A similar case can be made using the compressive stress equation. Here, the effect of reducing the residual elements on the compressive strength at 0.2 strain is less than 21 kPa (3 ksi). Once again, both are well within the range of normal variation and of limited significance relative to improving formability.

Another material based factor that often comes to the forefront when discussing cold form-

---

*Modified from original investigator's finding to include copper.

ability is the strain hardening exponent. No correlation has been shown between the strain hardening exponent and composition [*8*].

There appears to be very little evidence, empirical or otherwise, to warrant unduly restricting residual alloy content as a means of improving cold formability. In fact, one could argue that there is evidence to the contrary. More facile solutions such as principal element control, hardness, or thermal treatment control should be considered.

Restricting Residuals for Hardenability Control?

Just as modern steelmaking has caused changes in prime scrap availability and residual element profiles, it has also made possible substantial improvements in hardenability control. Historical practices of hardenability control need to be re-examined to capitalize on this change and once again avoid unnecessary costs.

Since as early as 1935 and before, engineers and metallurgists have been attempting to predict the hardenability of steel from its composition. In 1942, Grossman [*10*] proposed a method of hardenability calculation (D_I) that was based upon carbon content, grain size, and a series of multiplying factors that represented each element's contribution at a specific level toward increasing hardenability. During the period 1942 through 1946, many investigators [*11*] modified and improved on the accuracy and predictability of his concept, and as an engineering concept it is still widely accepted today.

In 1938, Jominy and Boegehold [*12*] introduced the end quench hardenability test, which is familiarly known as the Jominy test after one of its inventors. This test, which correlates cooling rates in a test sample with cooling rates in various size steel bars, has been adopted as what might reasonably be called the "standard" way of measuring and specifying hardenability and is in fact used throughout the world.

As might be expected, considering the ingenuity of the technical mind, over a period of time many investigators developed correlations between the calculated D_I and the measured Jominy test, and prediction of Jominy test results became plausible. Within certain constraints these methods of hardenability specification can be used interchangeably [*11*]. In other words, knowing the D_I makes possible calculating or specifying the Jominy hardenability or knowing the Jominy hardenability makes possible calculating the D_I.

In our current era, with the availability of computers and the ability to manipulate and analyze large volumes of data through regression analyses and other methods, these correlations are not only plausible but much more accurate [*11*]. Their accuracy has been largely achieved through the enhanced ability to compute the multiplying factors associated with each element of composition used to calculate the D_I. One series of D_I calculations is contained in ASTM Method for End-Quench Test for Hardenability of Steel [A 255-67 (1979)].

In carbon steels, hardenability control is frequently given as the reason for restricting residual elements. If hardenability control is the sought-after end point, it stands to reason that hardenability limits might be a more appropriate point of control. The question, however, frequently arises as to how to specify the hardenability. The answer has been provided by Grossman and his successors.

The predominant influence on hardenability is exerted by the predominant elements in carbon steel, carbon and manganese, and these should be the main elements of concern. But, since hardenability is influenced, as discussed above, by the total chemical content, all elements must be taken into consideration. The D_I concept accomplishes this. With D_I control in the offing allowing the steelmaker the option of total chemistry control rather than just residual control seems appropriate.

There is a dividend here for the consumer, which is brought into play by technology. Steelmakers today, through the use of modern steelmaking methods and ladle metallurgy, have the ability to control accurately the additive elements of carbon, manganese, and silicon within relatively narrow ranges. This ability offers exceptional assurance that the hardenability control desired, which is readily calculated from the ladle analysis, will be met on a repetitive and consistent basis without unnecessarily or uneconomically restricting residual elements.

Summary

The changing profile of the steel industry has resulted in a substantial increase in the cost of making steel to standards that were developed based on entirely different methods of manufacture than those existing today. Just as open hearth furnaces replaced the bessemer converter, and the basic oxygen process replaced the open hearths, the character of the steel produced in electric furnaces is different than that of its predecessors. For the health of our manufacturing sector we absolutely must re-examine the reasons for restricting residual elements and the costs of doing so. We must assure ourselves that these restrictions are functional necessities and not just characterization of products of an era gone by. The price to be paid by our society to preserve that era without proper cause and justification may potentially result in curtailing our industrial base by rendering our products non-competitive in world markets. That certainly is not in our best interest and any factors hinging on that possibility need to be reviewed. Restriction of residuals is one such factor.

This review is of necessity brief and could well encompass the content of several volumes; it is intended as food for thought and to foster a re-examination of specifications and ordering practices in light of changing technology and economic realities.

References

[*1*] "Annual Statistical Report," *American Iron and Steel Industry Statistical Review*, AISI, Washington, DC.

[*2*] *Iron and Steelmaker*, Iron & Steel Society, AIME, March 1987, p. 6.

[*3*] *Institute of Scrap Iron and Steel Handbook*, ISIS, Washington, DC, October 1979, pp. 6-9.

[*4*] Clark, D. S. and Varney, W. R., *Physical Metallurgy for Engineers*, D. Van Nostrand Co., New York, 1955, p. 144.

[*5*] McNicol, J. A., "Some Aspects of the Effect of Copper in Cast Iron and Steel," *The Australasian Engineer*, October 7, 1953, pp. 54-60.

[*6*] Cooksey, R. J., "The Cold Extrusion Pressures of Low-Alloy Steels," *Metal Forming*, April 1968, pp. 98-111.

[*7*] Hurley, J. L., Kitchin, A. L., and Crawford, R. R., "Cold Forging of Alloy Steels," *Metals Engineering Quarterly*, Aug. 1971, pp. 36-43.

[*8*] Crawford, J. D., Dunn, R. G., and Humphrey, J. H., "The Influence of Alloying Elements On the Cold Deformation of Steel," *Metals Engineering Quarterly*, November 1964, pp. 1-7.

[*9*] "Prediction of Cold-Extrusion Pressure and Extruded-product Strength," Report, Bethlehem Steel, Bethlehem, PA.

[*10*] Grossman, M. A., "Hardenability Calculated From Chemical Composition," *Transactions of AIME*, Vol. 150, 1942, pp. 227-255.

[*11*] Siebert, C. A., Doane, D. V., and Breen, D. H., "The Hardenability of Steels," *American Society for Metals*, Metals Park, OH, 1977, pp. 64, 203.

[*12*] Jominy, W. E. and Boegehold, A. L., "Hardenability Test For Carburizing Steels," *Transactions of the American Society for Metals*, Vol. 26, 1938, p. 574.

Wilfried Meyer,[1] *Adolf Kucharz,*[2] *and Günter Hochörtler*[3]

Production of Super Clean Steels—Deoxidation Mechanism During Ladle Refining

REFERENCE: Meyer, W., Kucharz, A., and Hochörtler, G., "Production of Super Clean Steels—Deoxidation Mechanism During Ladle Refining," *Residual and Unspecified Elements in Steel, ASTM STP 1042,* A. S. Melilli and E. G. Nisbett, Eds., American Society for Testing and Materials, 1989, pp. 38-47.

ABSTRACT: Investigations carried out by several institutions under Projects RP559, RP2060, RP1403, RP2741 for the Electric Power Research Institute, Palo Alto, CA, resulted in a 3.5% NiCrMoV steel completely free from temper embrittlement as a material for low pressure rotors but also for combination proberty rotors, for example, integral high-pressure low-pressure (HILP) rotors for future steam plants. This steel contains very low percentages of residual elements including sulfur and phosphorus, and its contents of aluminum, silicon, and manganese are also very low.

The main problem in producing such a steel on an industrial scale is gaining a sufficiently low oxygen content as a precondition for successful desulfurization and high cleanliness. This situation is only possible by applying ladle refining techniques. Two model rotors of this "super clean steel" were produced and tested. The tests proved complete resistance to temper embrittlement.

As an approach for further process development and for the economic production of "super clean steels," the mechanism governing the deoxidation was investigated in detail by means of trial heats. The influences of the composition of process slags and the influence of the ladle linings were examined. The deoxidation was found mainly to be based on steel-slag reactions. The minimum oxygen content achievable in the steel is limited by interactions between ladle linings and melt, which create a dissociation of the linings and an oxygen supply to the liquid steel.

KEY WORDS: forging, steam turbine, melting, temper embrittlement, 3,5% NiCrMoV steel, turbine rotor forging, ladle refining, slags, ladle linings, desulfurization, deoxidation

Modern ladle refining processes, using a combination of ladle furnace and vacuum degassing, are a powerful tool to meet steadily increasing requirements for chemical composition and cleanliness of special steels. Therefore, these processes are a field of steady development aiming at an increase in the reproducibility of existing processes and new or improved product properties [*1*], for instance, better mechanical properties, higher cleanliness, or better corrosion resistance.

An example is the development of a process for the production of the so-called "super clean" rotor. To increase the thermal efficiency of steam turbines in the future, increasing the operating temperature of the low pressure rotor from today's 350°C up to 400 to 450°C will be necessary. But, because of isothermal temper embrittlement, conventional 3,5% NiCrMoV steels cannot be used within this temperature range. Investigations recently conducted for the Electric Power Research Insitute (EPRI) by several universities and companies resulted in the develop-

---

[1] Head, Steelmaking Division, Vereinigte Edelstahlwerke AG, Kapfenberg, Austria.

[2] Manager, Melting Shop, Vereinigte Edelstahlwerke AG, Kapfenberg, Austria.

[3] Head, Department for Physical Chemistry and Corrosion Research, Vereinigte Edelstahlwerke AG, Kapfenberg, Austria.

ment of a super clean 3,5% NiCrMoV steel for low pressure rotors free from temper embrittlement. This steel contains very low percentages of aluminum, silicon, manganese, phosphorus, and sulfur [2-6]. Its aim composition is shown in Table 1. To prove the production capability and to verify the laboratory results on a production scale, Vereinigte Edelstahlwerke (VEW) fabricated and tested a 23 metric ton model rotor. The actual composition of this trial rotor is also given in Table 1. An extensive test program was carried out with material from this forging [2, 7]. The results of step cooling and lengthy ductility tests proved a complete resistance to temper embrittlement. In other words, the first 3,5% NiCrMoV rotor without any tendency to temper embrittlement was produced. The fabrication of a second rotor confirmed the applied refining process and the results with respect to temper embrittlement to be reproducible.

Although successful, the melting and refining procedure for the production of the first super clean rotors was mainly developed empirically. The objectives of the work presented in this paper were (1) to understand better the theoretical background of the process, (2) to develop a tool to improve the reproducibility of the results, and (3) to lower the production process cost by shortening refining time.

The main problem in refining such steels is to adjust a sufficiently low oxygen content, on the one hand to have a good precondition for desulfurization, and on the other hand to get a steel with high cleanliness without using silicon, manganese, or aluminum. Therefore, the production of super clean steel for the melting metallurgist is mainly a problem of deoxidation. So, the subject of this research and development work is finally to understand and improve the deoxidation process under the discussed preconditions.

Experiments

All experiments were carried out on production heats. The equipment used and the production step sequence are shown in Fig. 1.

The electric arc furnace has a power supply of 25 to 30 MVA and a capacity of 55 metric tons. The ladle furnace is equipped with a 6-8 MVA power supply. Stirring is done by an electromag-

TABLE 1—*Aim and actual chemical composition of the first super clean prototype rotor.*

Element	Aim, %	Actual, %
C	0.27	0.30
Si	0.02	0.03
Mn	0.02	0.02
P	0.002	0.0024
S	0.001	0.001
Cr	1.65	1.68
Mo	0.45	0.41
Ni	3.50	3.44
Al	<0.005	0.005
As	<0.002	0.0024
Cu	...	<0.05
N	0.0050	0.0044
Sn	<0.002	0.0032
V	0.10	0.09
W	...	<0.01
O	0.0025	0.0027
Sb	<0.002	<0.005
H (ppm)	0.5	0.7

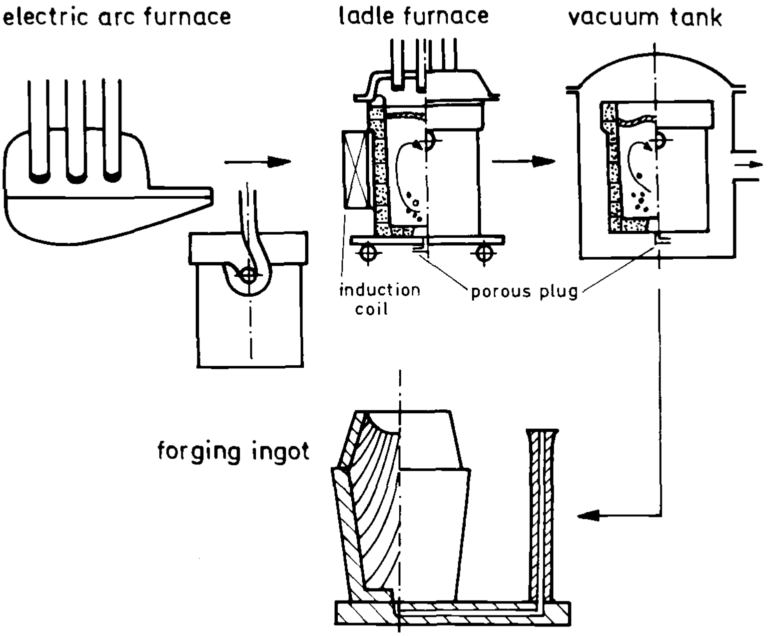

FIG. 1—*Equipment and sequence of procedures used for the production of "superclean steel" heats.*

netic stirrer. Reheating rates of 5°C/min can be achieved. A vacuum tank is used for vacuum treatment of the liquid steel in the ladle. Here the melt is stirred by argon gas introduced through a porous plug in the center of the bottom of the ladle. The minimum pressure that can be achieved in the tank is 10^2 Pa.

The applied procedure consists of melting down and dephosphorization in the electric arc furnace with subsequent tapping and heating in the ladle furnace under a special process slag. During this step, the melt's oxygen activity and the slag's iron oxide content are remarkably reduced. During the second step of the ladle refining procedure, the vacuum treatment, a further decrease of the melt's oxygen activity takes place connected with a desulfurization of about 70% [*8*]. Sometimes an additional heating is necessary, but normally the heat is ready after vacuum treatment.

The results presented in this paper were obtained from 3,5% NiCrMoV steels as well as from similar types of heat treatable steels. All melts used for the trials were started without manganese, silicon, and aluminum additions. After having obtained the desired low sulfur and oxygen contents the melts were normally alloyed and bottom poured.

After tapping the heat from the electric arc furnace several times during ladle heating, before and after vacuum treatment, oxygen activity was determined by means of EMF measurement.[4] Simultaneously, steel and slag samples were taken out of the ladle for chemical analysis. For the trials, both dolomite and alumina lined ladles were used.

---

[4] This measurement is carried out by immerging an EMF probe, fixed on the tip of a lance, in the liquid steel. This probe consists of a solid-state electrolyte with a reference substance (that is, a substance with a defined oxygen potential, in our case a mixture of chromium and chromium oxide) and a molybdenum pin providing an electrical contact to the melt. According to the oxygen activity and temperature of the liquid steel, a voltage between liquid steel and reference substance occurs and is measured by means of a recorder. This way of oxygen determination is state of the art. EMF probes are supplied by several producers.

Results and Discussion

As shown in Table 1 the super clean rotor contains only 0.005% of aluminum. Nevertheless, there exists a theory [*9*] that even this low aluminum content is responsible for the deoxidation of such steels. It is argued that steels, after treatment in the ladle furnace, always contain some calcium so that deoxidation products are not pure alumina, but calcium aluminates. In case of calcium-aluminate formation the equilibrium oxygen-aluminum is shifted towards lower oxygen content in the melt as shown in Fig. 2. This figure shows the deoxidation constant against temperature according to several authors. The full lines are the deoxidation constants measured by several authors for pure alumina formed after deoxidation [*10–13*]. The dashed lines are values for the case that calcium aluminates are formed, evaluated by Schwerdtfeger [*14*] and Turkdogan [*9*]. The deoxidation constant is lowered considerably and, therefore, oxygen activity below the normal aluminum deoxidation equilibrium should be possible. This occurrence is only possible if both the slag and the ladle linings consist of components with sufficiently low alumina activity.

Therefore, the composition of the slag used during the ladle refining process obviously is of outstanding importance. To evaluate this influence of the slag on the refining process, trials with three different slag types according to Table 2 were carried out.

Fig. 3 shows the results of these trials [*15*]. The representation used for this figure has the advantage that it makes possible the comparison of the deoxidation effect in melts even with different aluminum contents. In the as-tapped condition all trial heats had high oxygen activity and low aluminum contents. After the ladle heating period, in most cases the equilibrium line was passed and oxygen activity under the normal aluminum oxygen equilibrium was estab-

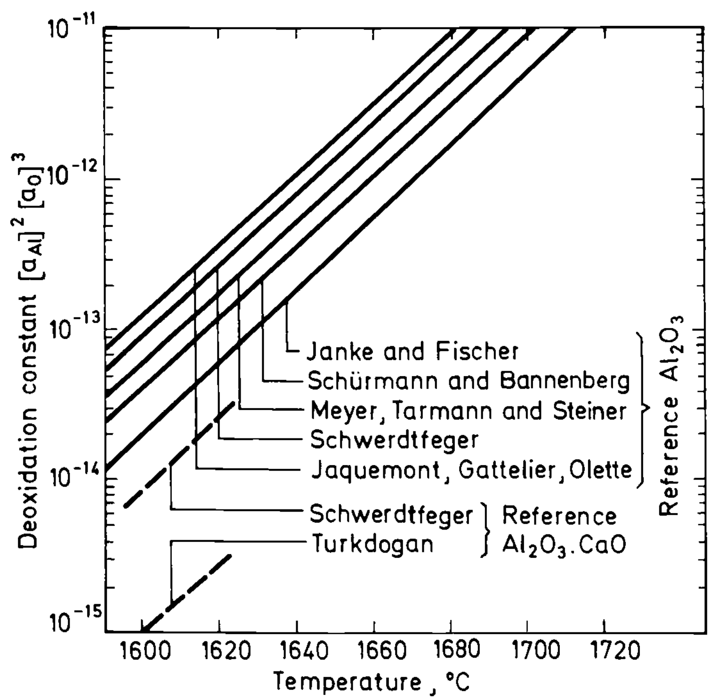

FIG. 2—*Deoxidation constant for aluminum and calcium-aluminum deoxidation according to different authors* [9–14].

TABLE 2—*Chemical composition of applied slag types.*

Slag Type	% CaO	% Al_2O_3	% MgO	% SiO_2	% CaF_2
1	46 to 60	18 to 28	5 to 13	2 to 15	1 to 3
2	49 to 55	7 to 16	7 to 14	7 to 14	6 to 15
3	47 to 54	4 to 7	7 to 10	6 to 16	18 to 27

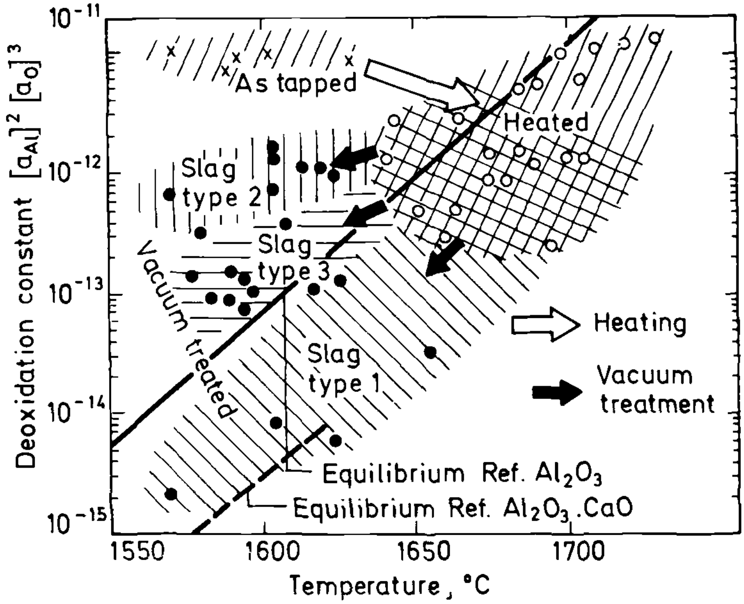

FIG. 3—*Influence of a lime-alumina (Type 1), a lime-alumina-fluorspar (Type 2) and a lime-fluorspar refining slag (Type 3) on the effect of the ladle refining process.*

lished. No significant difference between the three slag types was observed. This changed after the vacuum treatment. Nearly no deoxidation effect took place in melts treated under slag Type 2. A slight deoxidation effect was found in melts treated under pure lime fluorspar slags (Type 3); the most effective deoxidation was observed under calcium aluminate slags (Type 1). According to the theory discussed before [9], in most of these heats oxygen activity below the normal aluminum-oxygen equilibrium was found. Because of these results, all further trials were carried out only with calcium aluminate slags.

If indeed the deoxidation by aluminum is the governing process, lowering the oxygen activity should not be possible after having established a value according to the aluminum-oxygen equilibrium (full line in Fig. 3) when alumina lined ladles are used. Surprisingly, even under such conditions a further decrease of oxygen activity can be obtained by further heating or vacuum treatment, but this decrease always entails an increase of aluminum content in the melt (Table 3).

This increase of the aluminum content can only be caused by dissociation of the alumina in the ladle lining, because such aluminum pickup is not observed in heats refined in dolomite lined ladles under the same slag type. Furthermore, dissociation of the ladle lining also entails a

TABLE 3—*Increase of aluminum content during the refining process in alumina-lined ladles.*

	T, °C	a_o, ppm	Al (actual), %	Al (computed acc. to the equilibrium), %
After tapping	1650	113	<0.003	0.0007
After ladle heating	1690	112	0.003	0.002
After vacuum treatment	1615	22	0.006	0.005

supply of oxygen to the melt as shown schematically in Fig. 4. A precondition for the progress of this reaction is that the oxygen activity of the melt is lowered to or under the oxygen-aluminum equilibrium by another mechanism. This figure also demonstrates that even dolomite linings will dissociate. But in this case, because of the high vapor pressure and the low solubility of calcium and magnesium in liquid iron, only the increase of oxygen and a slight increase of calcium can be detected [*16–18*]. This result happens at lower oxygen content of the liquid steel, to a lesser extent. Therefore, lower oxygen activity in dolomite-lined ladles can be obtained, which can be seen from the results shown in Fig. 5.

These results are of outstanding importance for discussing the mechanism governing the deoxidation. They indicate that a reaction other than a precipitation deoxidation by aluminum, specifically an interaction between steel and slag, is responsible for the oxygen content decrease during the ladle refining process for producing super clean steel.

Figure 4 also indicates the basic reaction of this deoxidation by steel-slag reaction (diffusion

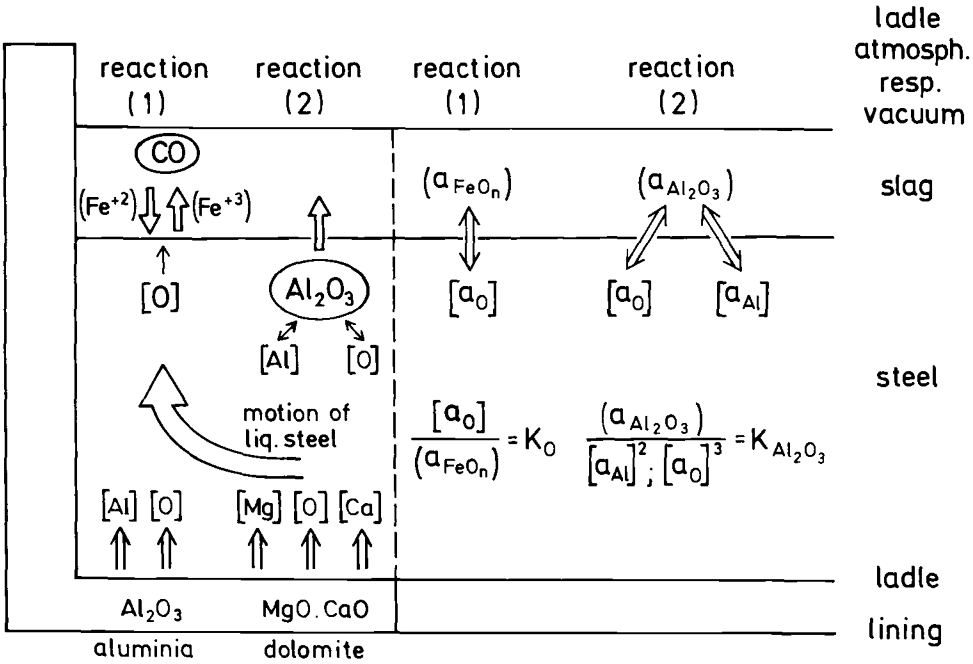

FIG. 4—*Scheme of reactions discussed.*

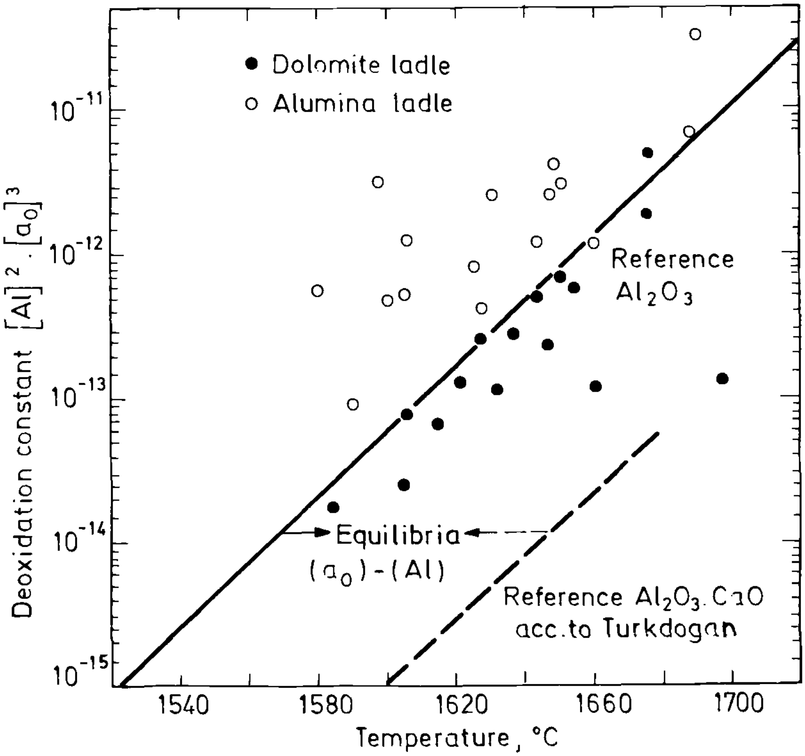

FIG. 5—*The influence of different ladle linings on the effect of deoxidation.*

deoxidation), which is the adjustment of an equilibrium between the iron oxide activity of the slag and oxygen activity in the steel.

The equilibrium constant K_O for this reaction is equal to the saturation oxygen activity in an iron melt under a pure iron-oxide slag. Its value is given by Taylor and Chipman [*19*]

$$\text{Log } [a_{o_{sat}}] = \frac{6320}{T} + 2743 \tag{1}$$

$$[a_{o_{sat}}] = K_O$$

On the assumption that an inert melting pot is used (that is, there are no interactions between linings and liquid steel) and without taking into account kinetic effects, the iron oxide activity a_{FeO_n} of the slag can be computed from Eq 2

$$(a_{FeO_n}) = \frac{[a_o]}{[a_{o_{sat}}]} \tag{2}$$

where a_o is the oxygen activity of the melt.

The iron oxide content of the slag, $\%FeO_n$, can be determined by chemical analysis. It is linked with the iron oxide activity via the activity coefficient f according to Eq 3

$$(a_{\mathrm{FeO}_n}) = f\,(\%\mathrm{FeO}_n) \tag{3}$$

Equation 4 gives the resulting relation between a_o and $\%\mathrm{FeO}_n$

$$[a_o] = [a_{o_{sat}}]\,f\,(\%\mathrm{FeO}_n) \tag{4}$$

For the slag system in question, the value of f was evaluated by Gaye and Coulombet by means of thermodynamic calculations [*20*].

In Fig. 6 the results of our own measurements are compared with the theoretical function according to Eq 4, considering the results of Gaye and Coulombet. For slags with an iron oxide content between 1 and 10%, a rather good correlation between the results of measurements and the theoretical function is evident. But, there is a sudden change if the iron oxide content in the slag is lowered under 1%. As Fig. 6 shows, a further reduction of the slag does not lead to the low oxygen activity that one would expect according to Eq 4. In some cases, even a slight increase can be observed. Apparently the activity coefficient f increases with decreasing iron oxide content in the steel melt. In processes taking place in alumina lined ladles, this increase is more distinct than in those performed in dolomite ladles. In discussing this effect one must necessarily take in consideration (1) the above discussed equilibrium between steel and slag, (2) the interactions between steel and ladle lining, and (3) kinetic aspects of the transportation of oxygen in the slag layer.

As shown above, a decreasing oxygen activity in the melt creates an increasing oxygen supply rate to the steel originating from the dissociation of the linings (Fig. 4). This oxygen supply at

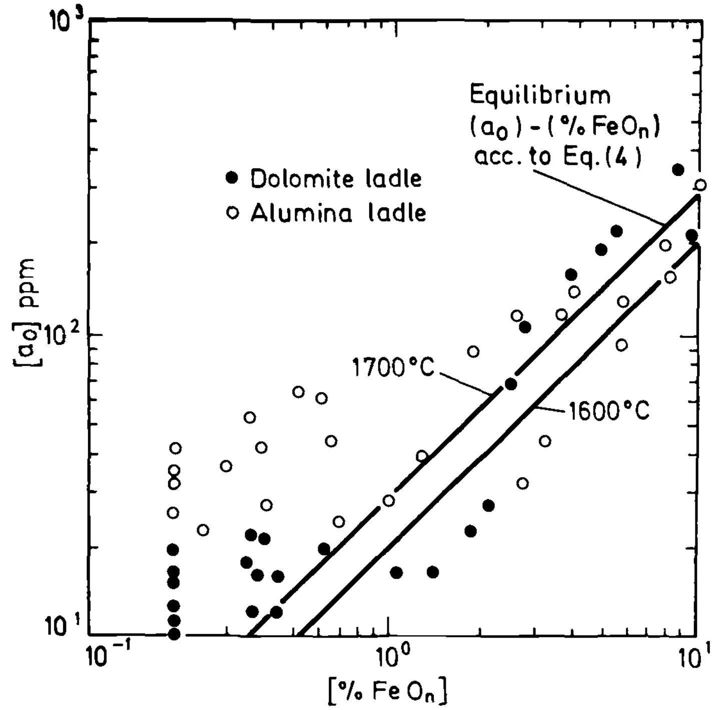

FIG. 6—*Correlation between iron-oxide content in the slag and oxygen activity in the melt.*

least has to be compensated for, but preferably exceeded by, the transportation rate of oxygen from the melt to the slag to achieve or maintain the desired low oxygen activity in the liquid steel.

A model for the oxygen transportation mechanism in the slag was evaluated by Engell [*21*], and Schwerdtfeger and Seshadri [*22*] for the oxidation of the steel in the open hearth furnace, and it is based on the oxidation of bivalent iron ions in the slag to trivalent ones. We propose to apply this model also on the deoxidation of steels by steel-slag reactions as indicated in Fig. 4. This implies that a decreasing amount of iron oxide ions in the slag diminishes the portion of trivalent ions and consequently the rate of oxygen transportation remarkably [*21*]. So there are two opposing reactions: (1) for thermodynamic reasons a low iron-oxide activity in the melt is necessary due to the desired low oxygen activity in the steel, and (2) for kinetic reasons a certain iron-oxide content in the slag is wanted due to a high transportation rate of oxygen ions in the slag layer.

Therefore, under highly reduced slags, an oxygen activity in the melt on a higher level than expected according to Eq 4 is established. For the approach in question, this entails a fictitious increase of the activity coefficient f and a slowing down or stopping or both of the deoxidation process. For steels free from aluminum and silicon, this will take place at an oxygen activity of about 35 ppm in alumina lined ladles and at about 10 to 15 ppm in dolomite lined ladles.

General Conclusion

The deoxidation of super clean 3,5% NiCrMoV steel is based on steel-slag interactions. According to the thermodynamic equilibrium, even very low oxygen activities should be expected under highly reduced slags. In practice, the deoxidation effect is limited by interactions between ladle linings and melt, which create a dissociation of the linings and an oxygen supply to the liquid steel. This oxygen supply has to be exceeded by the transportation rate of oxygen through the slag. The finding that under highly reduced slags only a poor deoxidation effect takes place is explained by the model applied on the transportation of oxygen through the slag. This model is based on the presence of iron-oxide ions in the slag. So the iron-oxide content in the slag has to be carefully adjusted in the range of 0.8 to 1% to meet both the thermodynamic and the kinetic preconditions for a successful deoxidation.

References

[*1*] Meyer, W. and Kühnelt, G., *Conference on Secondary Steelmaking for Product Improvement*, London, October 1984.

[*2*] Jaffee, R. I., Machner, P., Meyer, W., and Steiner, J. E., *Ironmaking and Steelmaking 1986*, Vol. 13, No. 6, pp. 322-326.

[*3*] McMahon, C. J., et al., *Interim Report*, RP1501, Part 1, Electric Power Research Institute, Palo Alto, CA, September 1980.

[*4*] Takeda, Y. and McMahon, C. J., *Met. Trans.*, Vol. 13A, January 1982, p. 111.

[*5*] Watanabe, O. and Ganesh, S., *International Conference on Improved Coal-Fired Power Plants*, November 1986, Palo Alto, CA.

[*6*] Viswanatha, R. and Jaffee, R. I., "I. Eng. Mater. Technology" *Transactions of the American Society of Mechanical Engineers*, Vol. 104, 1982, p. 241.

[*7*] Machner, P., Reisl, E., Meyer, W., and Jaffee, R. I., *International Conference on Improved Coal-Fired Power Plants*, Palo Alto, CA, 1986.

[*8*] Meyer, W., Tarmann, R., and Kühnelt, G., *Proceedings of the 1st European Electric Steel Congress*, September 1983, Aachen.

[*9*] Turkdogan, E. T., *Arch. Eisenhüttenwes*, Vol. 54, No. 1, 1983, pp. 1-9.

[*10*] Jaquemont, A., Gattelier, C., and Olette, M., *Rapport IRSID*, RE 289, 1975.

[*11*] Meyer, W., Tarmann, R., and Steiner, F., *Österreichischer Eisenhüttentag*, Leoben, Austria, May 1979.

[*12*] Jonke, D. and Fischer, W. A., *Stahl und Eisen 96*, No. 8, 1976, pp. 398-401.

[*13*] Schürmann, E. and Bannenberg, N., *Arch. Eisenhüttenwes.* Vol. 55, No. 9, 1984, pp. 409-414.
[*14*] Schwerdtfeger, K., *Arch. Eisenhüttenwes.* Vol. 54, No. 3, 1983, pp. 87-98.
[*15*] Meyer, W., Tarmann, R., and Kucharz, A., *8th ICVM*, September-October 1985, Linz, Austria, pp. 569-581.
[*16*] Fischer, W. A. and Hoffmann, A., *Archiv fur das Eisenhüttenwes*, 30, 1959, pp. 199-204.
[*17*] Chipman, J., *Basic Open Hearth Steelmaking, 2nd ed.*, New York, 1951, p. 638.
[*18*] Meyer, W., Pauker, E., Kucharz, A., and Mayer, A., *International Conference Secondary Metallurgy*, Aachen, West Germany, September 1987, p. 170.
[*19*] Taylor, C. R. and Chipman, J., *Transactions of the American Institute of Mechanical Engineers*, Vol. 154, 1943, pp. 228-247.
[*20*] Gaye, H. and Coulombet, D., *Rapport IRSID*. RE 1064, March 1984.
[*21*] Engell, H. J., *Krupp Techrische Mitteilung 24*, 1966, pp. 1-7.
[22] Seshadri, V. and Schwerdtfeger, K., *Ironmaking and Steelmaking*, No. 1, 1975, pp. 56-60.

DISCUSSION

Harry W. Wolverton[1] *(discussion question)*—What was the process prior to the ladle furnace?

Wilfried Meyer (author's response)—The process was arc furnace.

Harry W. Wolverton (discussion question)—What kind of dolomite ladle lining was used?

Wilfried Meyer (author's response)—A tar bonded with chromium magnesite in the slag line used.

G. S. Hartman[2] *(written discussion)*—The very low levels reported, phosphorus 0.002%, sulfur 0.001%, residuals as tin and arsenic below 0.002%, and low silicon level, must have required extensive ladle deoxidation and refining cycles. Did you remove the phosphorus on the ARC furnace or ladle furnace and by what technique? Did you have to recarburize or how did you pick up the extra carbon content? What was the total ladle furnace time and what was your scrap to hot metal steel yield?

Wilfried Meyer (author's response)—Removal of phosphorus was carried out in the arc furnace by applying conventional dephosphorization practice. As mentioned in the presentation it is necessary to adjust a low level of FeO in the slag. For that reason the slag was deoxidized by means of carbon powder, which finally caused a carbon pick up in the melt. These problems are meanwhile settled. The total ladle furnace treatment takes now about 2 h. The scrap to hot metal yield is about 92%.

---

[1] Quamex—MacSteel, P.O. Box 1101, Jackson, MI 49204.
[2] A. Finkl and Sons Company, Chicago, IL 60614.

Solidification and Subsequent Processing

Hiroshi Yaguchi,[1] *Debanshu Bhattacharya,*[1] *and Masato Yanase*[2]

Effect of Total Residual Content (Cu+Cr+Ni) on the Machinability of AISI 1215 Steel

REFERENCE: Yaguchi, H., Bhattacharya, D., and Yanase, M., **Effect of Total Residual Content (Cu+Cr+Ni) on the Machinability of AISI 1215 Steel,** *Residual and Unspecified Elements in Steel. ASTM STP 1042,* A. S. Melilli and E. G. Nisbett, Eds., American Society for Testing and Materials, Philadelphia, 1989, pp. 51-66.

ABSTRACT: The effect of total residual content (Cu+Cr+Ni) on the machinability of American Iron and Steel Institute (AISI) 1215 (UNS G12150) low carbon resulfurized free-machining steel was investigated jointly between Inland Steel Company in the United States and Nippon Steel Corporation in Japan. Three different machinability tests were used. At Inland, the automatic screw machine test using a modified version of the test method outlined in ASTM Method for Evaluating Machining Performance of Ferrous Metals Using an Automatic Screw/Bar Machine (E 618-81) was used. At Nippon, the automatic screw machine test with its own methodology and the cyclic plunge test were used. Three levels of total residual contents were obtained through addition of copper, chromium, and nickel in ingots. The amounts of these three elements were changed simultaneously to simulate practical conditions. The total residual contents obtained were 0.07, 0.20, and 0.28 wt%. The automatic screw machine test at Inland revealed that rough form tool life, based on part growth, deteriorates slightly when residual content is high. Poor surface finish is occasionally observed in medium and high residual content heats in the automatic screw machine tests carried out both at Inland and Nippon. On the other hand, no deterioration of surface finish was observed in the cyclic plunge test. Overall, the authors conclude the machinability of AISI 1215 steel deteriorates slightly when the total residual content becomes very high; however, it is not affected significantly within the range of normal total residual contents observed in these steels made in the BOF, that is, 0.05 to 0.12%.

KEY WORDS: machinability, free-machining steel, residual elements, chromium, copper, nickel

Residual contents such as copper, chromium, nickel and molybdenum in the American Iron and Steel Institute (AISI) 1200 series free-machining steels are determined by the steelmaking practice, especially by the amount of scrap used. Thus, there is likely to be different residual contents in steels made at different shops such as BOF or electric furnace. This situation indicates the necessity of knowing the effect of residuals on machinability in order to compare, without any ambiguity, the machinability of steels made at different shops and, in particular, to optimize machinability.

There is only a limited number of investigations reported in the literature on the effects of residuals on the machinability of steel, except for some reports on the effect of copper. Unfortunately, however, the effect of copper is not conclusive. Improvement of machinability by adding copper has been reported in AISI 1213 (UNS G12130) steel [*1*], in medium carbon steels [*2,3*]

---

[1] Senior staff engineer and section manager, respectively, Inland Steel Company, Research Laboratories, E. Chicago, IN.

[2] Researcher, Nippon Steel Corporation, Muroran Research and Development Laboratories, Muroran, Hokkaido, Japan.

and in sintered iron [*4*]. On the other hand, there are some reports indicating a negative effect of copper in AISI 12L14 steel [*5*].

The effect of other residual elements such as chromium, nickel, and molybdenum has been generally considered in terms of solid-solution hardening of steel [*6*]. The effect on machinability may be estimated using equivalent carbon content for hardening. Thus, residuals are expected to improve machinability when equivalent carbon content is low but deteriorate when it exceeds the optimum content [*6*]. However, no experimental evidence has been reported on the machinability of low carbon free-machining steel except a short statement indicating a deteriorative effect without showing experimental data [*5*].

In summary, no clear understanding of the effects of residuals on the machinability of low carbon free-machining steels has been obtained yet. Consequently, this investigation was carried out as part of a joint project between the Inland Steel Company in the United States and the Nippon Steel Corporation in Japan.

Residual Levels Investigated

To decide the residual levels to be investigated, the residual levels in recently analyzed production heats were compared. Table 1 summarizes the average contents of copper, chromium, nickel, and molybdenum and the sum of these four contents, standard deviation and number of heats observed. The steels included are those made at the No. 2 BOF shop and those at the No. 1 electric furnace shop, both at Inland, and those at the BOF shop at Nippon's Muroran Works. All residuals in the steels made at the No. 1 electric furnace shop except molybdenum can be seen to be significantly higher than those in the other two. Between the steels made at BOF shops at Inland and Nippon, total content is similar, however, steels made at Nippon have higher chromium and nickel but lower copper than those made at Inland. The differences are statistically significant with more than 95% confidence for the three elements mentioned above. The molybdenum content is constant in all the heats analyzed. At this point, discussing the role of nitrogen is important. While the authors recognize that nitrogen has a significant effect on machinability and that the nitrogen content of steel made in an electric furnace in general are considerably higher than steels made in BOF, this investigation was especially directed at studying the effect of the residuals Cu+Cr+Ni. Hence, nitrogen has not been included as a variable in this investigation.

In this investigation, the authors decided to be pragmatic and study the effect of total residual content rather than the effects of individual elements. The content of each residual element is

TABLE 1—*Residual contents in production heats (wt%).*

Product	Parameter	Cu	Ni	Cr	Mo	Total
Inland BOF	average	0.024	0.015	0.039	0.010	0.088
		0.008	0.005	0.010	0	0.016
	standard deviation number	11	11	11	11	11
Nippon BOF	average	0.011	0.020	0.050	0.010	0.093
		0.003	0	0.013	0	0.013
	standard deviation number	12	14	14	14	12
Inland Electric Furnace	average	0.103	0.049	0.071	0.010	0.228
	standard deviation	0.042	0.008	0.020	0	0.047
	number	5	5	5	5	5

changed simultaneously. Three residual levels are included: the first sample contains the low residual level observed in steels made at the No. 2 BOF shop at Inland; the sample having the highest residual contents contains typical levels in steels made at the No. 1 electric furnace; and the sample with the medium level contains residual contents in between the above two. Since molybdenum does not vary significantly in the mill, it is not varied in this investigation. Nitrogen is not varied for the reason mentioned above.

Experimental Procedure

Three levels of residual contents were obtained at the No. 2 BOF shop at Inland through the addition of chromium, copper, and nickel in ingots from an identical parent heat of AISI 1215 (UNS G12150) steel having low residual contents. Chromium was added in the form of ferrochrome containing 59% chromium. Copper and nickel were added as pure metals. One billet each from a middle ingot cut was hot rolled to 27-mm round bars in coils. The samples were then straightened and cold drawn to 25.4-mm round bars.

Machinability was evaluated by three different tests: two different automatic screw machine tests at Inland and Nippon and a cyclic plunge test at Nippon. The automatic screw machine test methodology used at Inland is a modified form of ASTM E 618-81 as outlined elsewhere [7]. In this test, the rough form tool life based on part growth of 127 μm or catastrophic tool failure was considered to be the major criterion, and finish formed surface finish was the minor criterion. Surface roughness was measured on six pieces, one from each spindle, and the average was calculated. The methodology of the cyclic plunge test developed at Nippon has also been reported [7]. In this test, machinability was evaluated mainly in terms of surface roughness by repeating a 2.8-s cut, followed by a pause of several seconds, repeated 800 times.

The machine used for the automatic screw machine tests at Nippon was a six spindle Mitsubishi-Acme-Gridley machine. The part produced and the tool configurations used are shown in Fig. 1. The machining conditions are summarized in Table 2. Surface roughness on two rough formed surfaces at the first and second positions and two finish formed surfaces at the third and fourth positions were considered the major criterion, and were measured at 250 part intervals.

Results and Discussion

Properties

Table 3 summarizes chemical analysis results. Chromium, copper, and nickel are noted to vary simultaneously as planned. Distribution of these elements was found to be uniform across the whole ingot. Total oxygen content is high and constant among the three heats. Figures 2 and 3 show the effect of the total residual content (Cu+Cr+Ni+Mo) on mechanical properties of as-hot rolled bars. Table 4 shows hardness measurement results in cold drawn bars. Strength and hardness tend to increase slightly, and reduction in area decreases slightly with increasing total residual content.

Four microsamples were made per each heat from cold drawn bars. No significant differences were observed in pearlite structure and grain size among the three heats. Quantitative analysis of manganese sulfide (MnS) inclusions was carried out using an optical automatic image analysis system (OMNICON) in the region 5-mm deep from the surface where a rough form tool in the Inland automatic screw machine cut. The results are shown graphically in Figs. 4 and 5. There is a trend that inclusion size decreases and aspect ratio increases with increasing total residual content.

Oxide inclusions were observed qualitatively in the scanning electron microscope to detect any residual elements. As shown in Fig. 6, chromium is observed occasionally in oxide inclu-

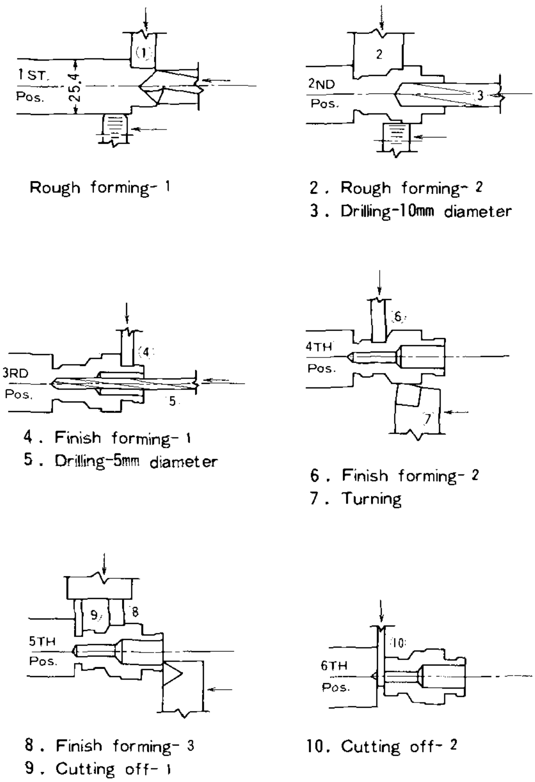

Rough forming- 1

2 . Rough forming- 2
3 . Drilling-10mm diameter

4 . Finish forming- 1
5 . Drilling-5mm diameter

6 . Finish forming- 2
7 . Turning

8 . Finish forming- 3
9 . Cutting off- 1

10. Cutting off- 2

FIG. 1—*Schematic illustration showing the cutting process used for the automatic screw machine test at Nippon Steel.*

sions. On the contrary, copper and nickel are not observed in any oxide inclusions. The presence of chromium in oxide inclusions may indicate some deoxidation by chromium although the total oxygen content is constant among the three heats. Smaller and more elongated inclusions in high residual heats support this argument because MnS inclusions are known to become smaller and more elongated with decreasing oxygen available during solidification [for example, *8-11*]. However, deoxidation effect by chromium, if any, is expected to be small, and the effects on machinability might be more complex because chromium is occasionally observed in sulfide inclusions.

Machinability

Table 5 summarizes the automatic screw machine test results obtained at Inland Steel. Figures 7 and 8 show the effect of total residual content on tool life. At the cutting speed of 1.29 m/s, tool life slightly deteriorates in the high residual content heat, with the other two being essentially equal. On the other hand, at 1.44 m/s the medium residual content heat has the best results, although they are not conclusive due to the limited number of tests. Figures 9 and 10 show the effect on finish formed surface roughness measured at the end of tests. Poor surface finish is occasionally observed in medium and high residual content heats.

Observing tool wear and built-up edge (BUE) on the rake face of the form tools after comple-

TABLE 2—*Machining test conditions.*

	Inland Automatic Screw Machine Test	Cyclic Plunge Test	Nippon Automatic Screw Machine Test
Tool	HSS (AISI-M2)	HSS (JIS—SKH57)	HSS (JIS-SKH57)
Cutting speed, m/s	1.29 and 1.44	1.33	rough (Positions 1 & 2): 1.42 finish (Positions 3 & 4): 0.90
Feed, mm/rev	0.074	0.05	rough: 0.05 finish: 0.03
Cutting fluid	straight oil no additives	straight oil	straight oil Cl: 2.5% S: 2.0% temperature: 25°C±2.5°C
Criteria	(1) Part Growth of 127 μm (2) Surface Roughness, Ra	surface roughness, Rz and tool wear After 800 cycles	Surface Roughness, Rz[a]
Others	ASTM E 618 Part	width: 5 mm cutting time: 2.8 s/cut	

[a] Rz: difference in the third highest peak and the third lowest groove observed within the predetermined length of surface.

tion of each test reveals a very large BUE in one of the tests used for the low residual content heat at the cutting speed of 1.29 m/s, Test 327. A photomicrograph showing the rake face of the rough form tool used for this test and that for the comparison test (No. 326) are shown in Fig. 11. Poor rough formed surface finish in Test 327, Table 5, supports the idea that the large BUE is not an artifact but existed during machining. Although tool life and finish formed surface finish are not affected significantly in this instance, the presence of the large BUE may suggest that this steel is too "gummy," which is detrimental in many instances.

Figures 12 through 15 show surface roughness measurement results obtained from the Nippon automatic screw machine tests. On rough formed surfaces at the first and second positions, surface roughness is not affected by total residual content. However, on finish formed surfaces at the third and fourth positions, elevated residual content heats occasionally show inferior surface finish.

Figure 16 shows the cyclic plunge machinability test results. As can be seen, no effect of total residual content is observed in this test.

From the observations mentioned above, we summarize that within the range of normal residual contents generally observed in the steels made at BOF shops, that is, 0.05 to 0.12% in total content, machinability is not affected significantly. It also appears, however, that the tool life of AISI 1215 steel may be improved slightly with increasing residual contents to approximately 0.2% in total content, although surface finish would deteriorate occasionally. Further increases in total residual contents reduce tool life and occasionally deteriorate surface finish.

There is a possibility that a slight improvement of tool life can be explained in terms of optimum equivalent carbon content as reported by Murphy [6]. This explanation is supported by

TABLE 3—*Chemical analysis (wt%) and roto-bar rejection rate (%).*

Residual Content	Heat	C	Mn	S	P	Si	Ni	Cr	Cu	Mo	N	0 Total	Total Residual Content (Ni, Cr, Cu, Mo)
Low	46754	0.075	0.90	0.32	0.08	0.006	0.02	0.03	0.01	0.01	0.005	0.040	0.07
Medium	46753	0.075	0.90	0.32	0.08	0.006	0.04	0.08	0.07	0.01	0.006	0.043	0.20
High	46755	0.085	0.89	0.32	0.08	0.006	0.05	0.12	0.10	0.01	0.006	0.042	0.28

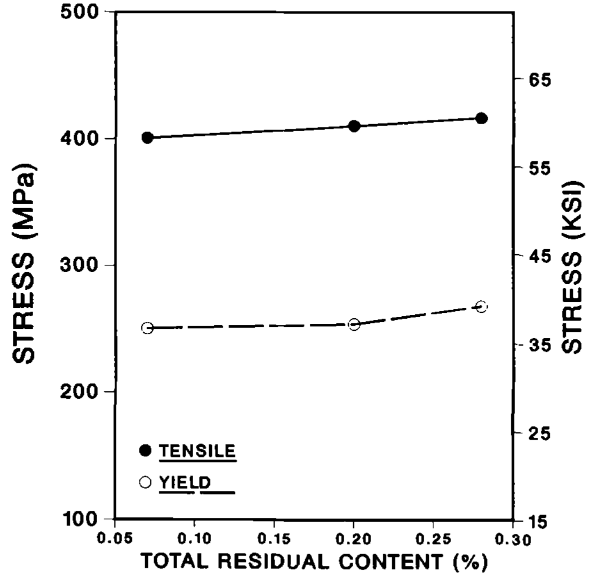

FIG. 2—*Effect of residuals on tensile strength.*

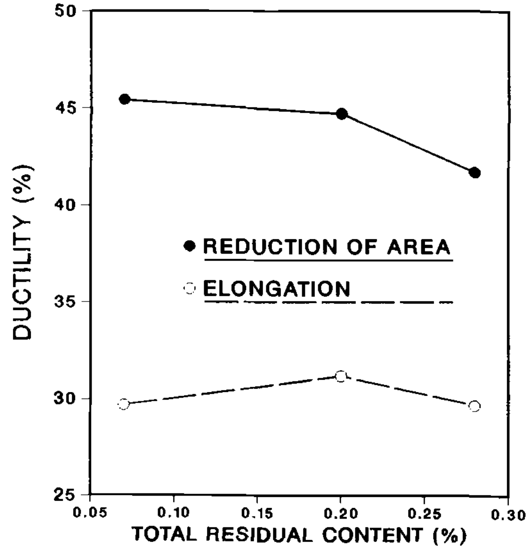

FIG. 3—*Effect of residuals on tensile ductility.*

TABLE 4—*Hardness of samples, HV.*

Distance from edge, mm	1	3	5	7	9	11	Center 12.5	11	9	7	5	3	1	Avg.
Low	185	182	182	185	183	186	178	188	178	185	186	185	185	184
Medium	189	187	187	186	186	186	185	182	183	194	187	187	191	187
High	185	187	183	189	186	188	191	187	179	182	186	189	189	186

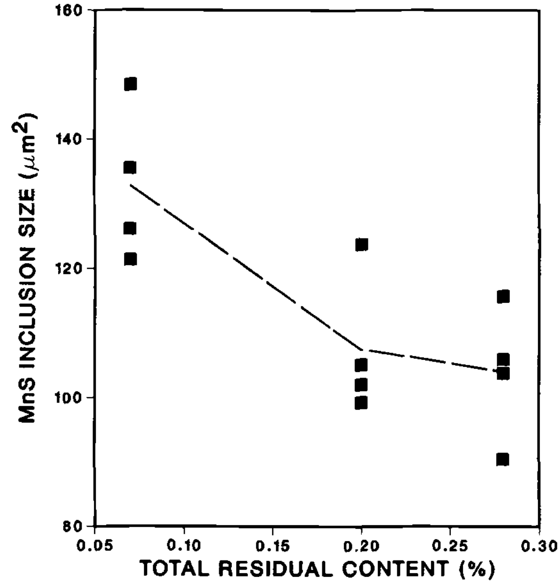

FIG. 4—*Effect of residuals on MnS inclusion size.*

the presence of large BUE in the low residual content heat. As expected from this theory, a further increase in residual content decreases tool life. On the other hand, deterioration of surface finish most likely results from some other factor such as smaller and more elongated sulfide inclusions.

Conclusions

The effects of total residual content (Cu+Cr+Ni) on the machinability of AISI 1215 steel were investigated using three machinability tests. The following conclusions can be obtained as a result of this investigation.

1. The automatic screw machine test revealed that rough form tool life based on part growth deteriorates when residual content is high.
2. Poor surface finish is occasionally observed in medium and high residual content heats in the automatic screw machine tests.

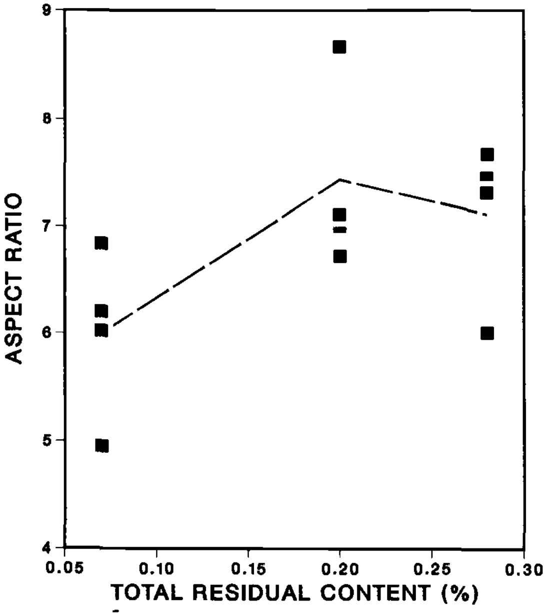

FIG. 5—*Effect of residuals on MnS inclusion aspect ratio.*

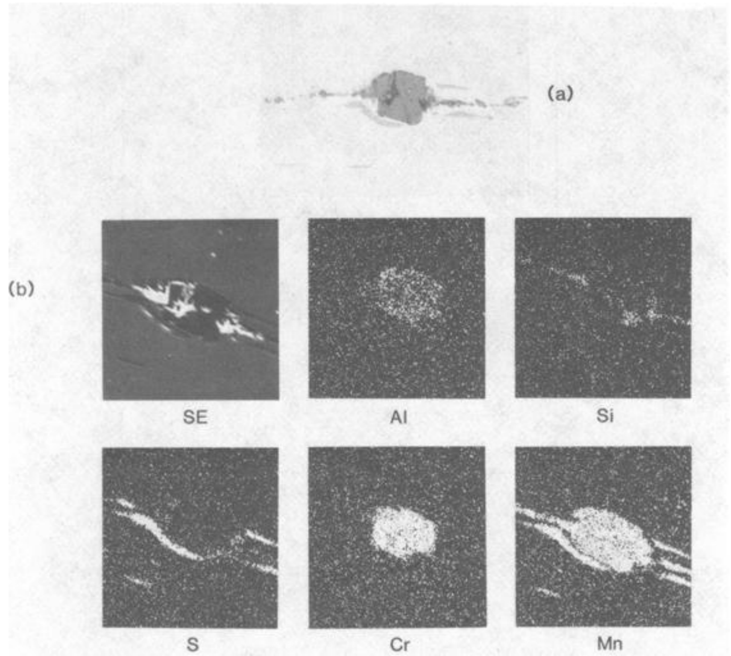

FIG. 6—*Typical oxide inclusion containing chromium in the steel having medium residual content:* (a) *Optical microscopy,* (b) *SEM observation.*

TABLE 5—*Machinability test results.*

Speed m/s	Residual Content	Heat	Test	Rough Form Tool Life Hours	Rough Formed Surface Roughness Ra, μm	Finish Formed Surface Roughness Ra, μm
1.29	Low	46754	327	+8	9.2	2.9
	Low	46754	377	+8	7.4	3.1
	Medium	46753	326	+8	6.9	4.6
	Medium	46753	378	7.9	6.0	4.3
	High	46755	328	5.8	5.5	3.1
	High	46755	376	7.7	6.1	4.6
1.44	Low	46754	380	2.5	5.5	3.1
	Low	46754	400	4.3	4.7	3.1
	Medium	46753	379	7.5	6.0	2.9
	Medium	46753	415	6.0[a]	5.3	4.5
	High	46755	381	5.5	5.7	3.8
	High	46755	401	3.9	5.6	3.3

[a] Estimate (The test was stopped because of being out of material).

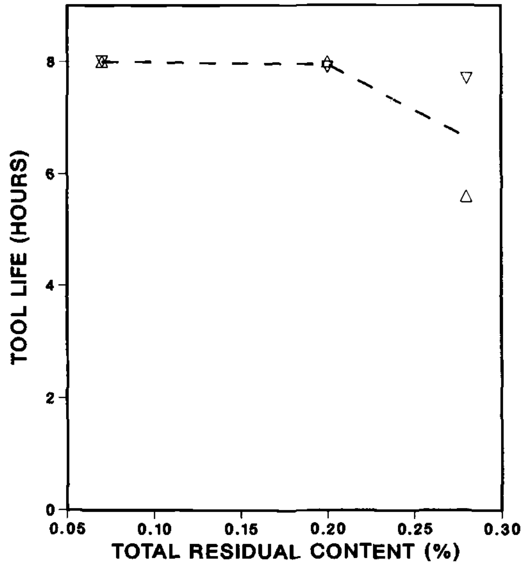

FIG. 7—*Effect of residuals on tool life at the cutting speed of 1.29 m/s (254 sfm) in the automatic screw machine test at Inland Steel.*

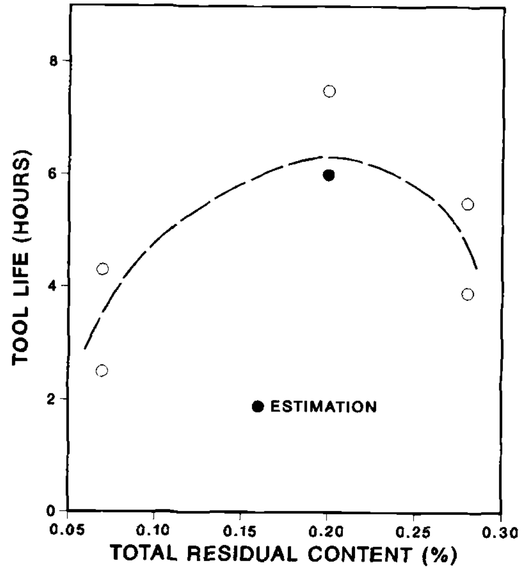

FIG. 8—*Effect of residuals on tool life at the cutting speed of 1.44 m/s (280 sfm) in the automatic screw machine test at Inland Steel.*

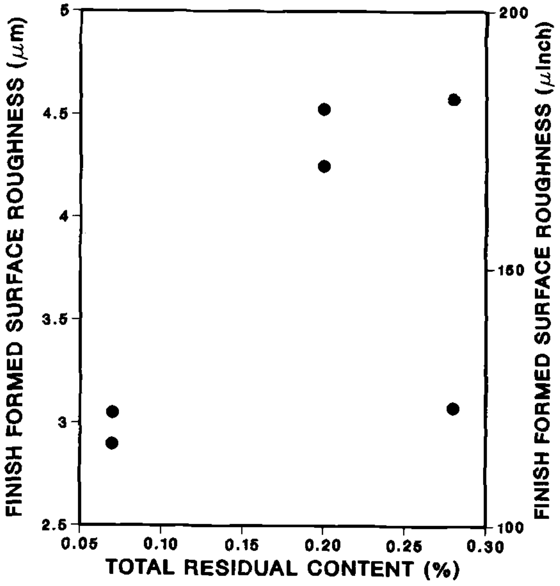

FIG. 9—*Effect of residuals on finish formed surface roughness at the cutting speed of 1.29 m/s (254 sfm) in the automatic screw machine test at Inland Steel.*

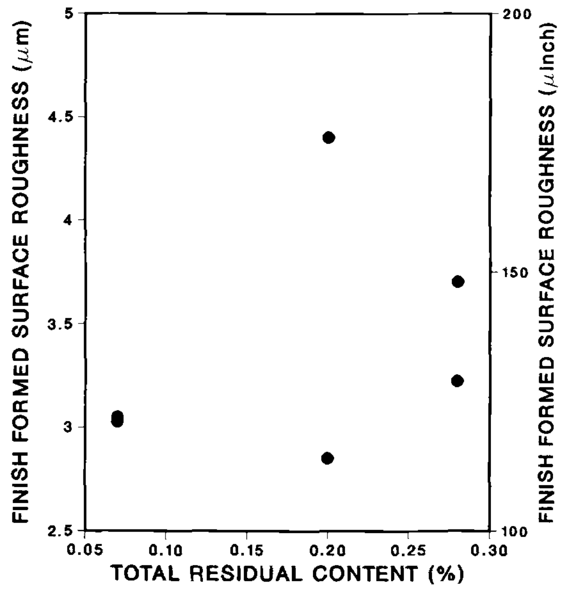

FIG. 10—*Effect of residuals on finish formed surface roughness at the cutting speed of 1.44 m/s (280 sfm) in the automatic screw machine test at Inland Steel.*

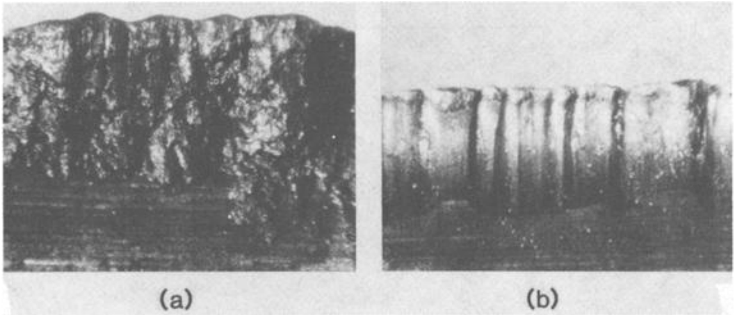

FIG. 11—*Rake face of the rough form tools used for the automatic screw machine test at Inland Steel:* (a) *test 327, note a large built-up edge;* (b) *test 326.*

3. The machinability of AISI 1215 steel is not affected significantly within the range of normal total residual contents observed in the steels made in the BOF.

Acknowledgment

The authors wish to thank many staff members of Inland Steel Company and Nippon Steel Corporation for assisting with sample preparation, carrying out experimental work, and discussions. Thanks are also due both companies for permission to publish this work.

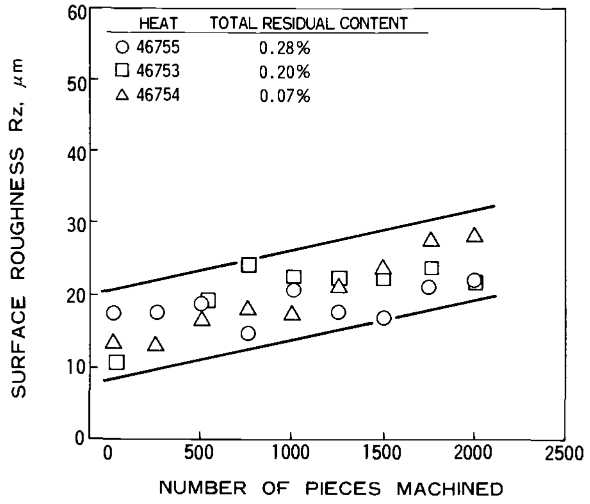

FIG. 12—*Effect of residuals on surface roughness at the first position of the automatic screw machine test at Nippon Steel.*

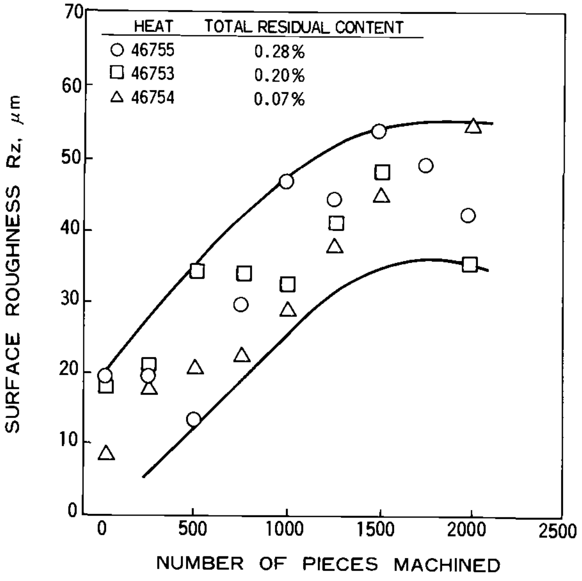

FIG. 13—*Effect of residuals on surface roughness at the second position of the automatic screw machine test at Nippon Steel.*

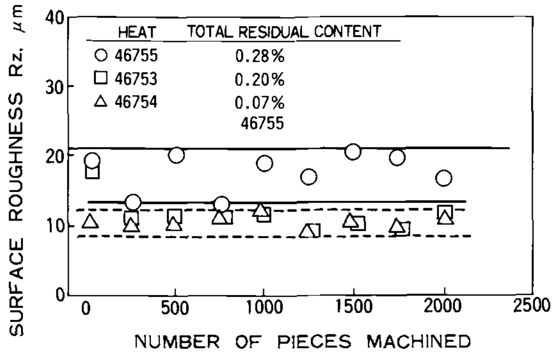

FIG. 14—*Effect of residuals on surface roughness at the third position of the automatic screw machine test at Nippon Steel.*

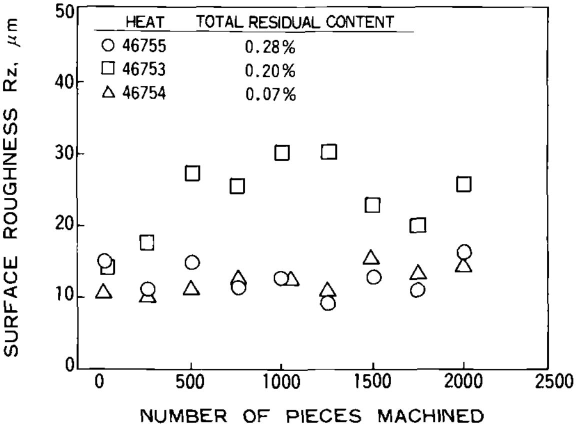

FIG. 15—*Effect of residuals on surface roughness at the fourth position of the automatic screw machine test at Nippon Steel.*

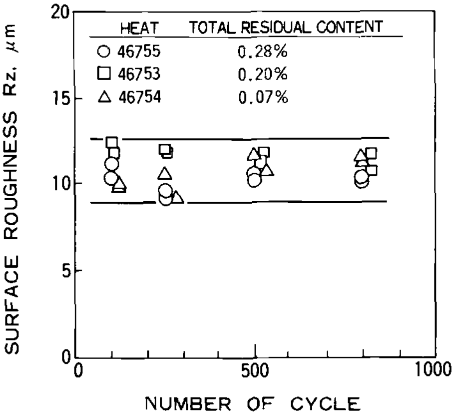

FIG. 16—*Relation between number of machined parts and surface roughness in the plunge machine test at Nippon Steel.*

References

[1] Garvey, T. M. and Tata, H. J., *Mechanical Working of Steel 2.* The Minerals, Metals and Materials Society—American Institute of Mining Metallurgical and Petroleum Engineers, 1964, p. 99.

[2] "Add Copper to Make Steel Bars More Machinable," *Iron Age.* August 22, 1957, p. 112.

[3] Ohnishi, K., *Tetsu-to-Hagane.* Vol. 70, 1984, p. S1284.

[4] Jamison, R. S. and Geijer, E., *Proceedings of the 16th Annual Meeting,* Metal Powders Federation, Princeton, NJ, 1960.

[5] Keane, D. M. and Wannell, P. H., *Mechanical Working and Steel Processing XXII,* Iron and Steel Society—American Institute of Mining, Metallurgical and Petroleum Engineers, 1985, p. 13.

[6] Murphy, D. W., *Iron and Steel Engineer Year Book,* 1967, p. 305.

[7] Ohtani, S., et al., *Journal of Applied Metalworking,* Vol. 4, 1986, p. 245.

[8] Sims, C. E., *Transactions of the Minerals, Metals and Materials Society—American Institute of Mining, Metallurgical and Petroleum Engineers,* Vol. 215, 1959, p. 367.

[9] Yeo, R. B. G., *Journal of Metals,* June 1967, p. 29.

[10] Yeo, R. B. G., *Journal of Metals,* July 1967, p. 23.

DISCUSSION

G. S. Hartman[1] *(discussion questions)*—Does Inland Steel use home scrap as the basic charge for the electric furnace (EF)? If so, is this the reason for the very low residual levels generally experienced there? Are normal EF residual levels using purchased scrap significantly higher?

H. Yaguchi (author's response)—Yes, Inland Steel uses home scrap for at least 75% of charge for the electric furnace, and this is the reason for the low residual contents.

E. L. Murphy[2] *(written discussion)*—In my opinion, residual contents of all those heats are low, although for this study they are designated low, intermediate, and high. EF steels, especially those made mainly with purchased scrap, would probably have much higher total residuals. I believe the study would be more effective if there were more significant differences between the low and high total residual contents.

H. Yaguchi (author's response)—This program was initiated to study the effect of residuals within the range Inland Steel and Nippon Steel generally produce. One of the major objectives was to see whether or not it would be necessary to take into account the difference in residual contents to compare the machinability of steels made at different shops at Inland Steel and Nippon Steel.

G. F. Vander Voort[3] *(written discussion)*—In your initial comparison of BOF and EF steels, why wasn't nitrogen included? The nitrogen content of electric furnaces steels is recognized to be about double of that of BOF steels and, further, that nitrogen has a pronounced influence on machinability, particularly surface finish.

H. Yaguchi (author's response)—The purpose of this investigation was to study the effect of residuals but not to compare BOF and EF steels. The effect of nitrogen is fairly well known but not the effect of residuals. Further, the effect of nitrogen is believed to be quite different from that of residuals. Thus, this investigation was initiated to study the effect of residuals excluding nitrogen.

[1] A. Finkl and Sons Company, Chicago, IL 60614.

[2] Engineering Materials and Processes, 2112 Poppyfield Place, Encinitas, CA 92024.

[3] Carpenter Technology Corporation, Research and Development Center, Reading, PA 19612.

B. M. Glasgal[4] *(discussion questions)*—I have four items to cover; as follows.

1. Whether the EF steel was mechanical and evaluated was unclear. Only the base BOF material and two treated ingots results were discussed.
2. If carbon equivalency (CE) is the control parameter for machinability, what CE value is now used, and are adjustments made during melt to achieve the CE? How? What is the control range? Might there be more important parameters?
3. What is the CE calculation formula? What were the CE of the steel evaluated?
4. The high residual ingot carbon analysis was 0.01% greater than the other two ingots. How do you account for this? How do you predict this occurrence if CE control is required?

H. Yaguchi (author's response)—In response are the following comments.

1. EF steels were used to determine the contents of residuals to be investigated; they were not tested.
2. No attempt is made to control CE. Further, the content of each element is controlled individually. What we have suggested in this paper is that the effect of residuals can be at least partially controlled by CE. However, residual contents generally observed in steels made in a BOF do not affect machinability significantly. Thus, trying to control residual contents in steels made in a BOF is not economical.
3. The same as comment 2.
4. The difference in carbon analysis of 0.01% is believed to be within experimental error.

---

[4] LTV Steel, Massillon, OH 44646.

Heat Treatment, Microstructure, and Inclusion Morphology

J. Saleil,[1] *F. Leroy,*[1] *H. Gaye,*[2] *and C. Gatellier*[2]

Inclusion Control in Calcium Treated Steels

REFERENCE: Saleil, J., Leroy, F., Gaye, H., and Gatellier, C., "**Inclusion Control in Calcium Treated Steels,**" *Residual and Unspecified Elements in Steel, ASTM STP 1042,* A. S. Melilli and E. G. Nisbett, Eds., American Society for Testing and Materials, Philadelphia, 1989, pp. 69-79.

ABSTRACT: Calcium alloys are widely used for controlling the composition and morphology of nonmetallic inclusions (oxides and sulfides). By fine-tuning the calcium treatment, producing very clean steels with good fatigue limits is possible, as is improved machinability steels covering a wide range of machining speeds from carbide tool machining to ceramic tool machining. When producing such steels the steelmaker faces a double problem: adjusting the quantity of calcium to the inclusions to be modified, and forecasting the partition of calcium between oxides and sulfides. To help the steelmaker, two developments were achieved. First was a thermodynamical model predicting the partition of calcium between oxides and sulfides and the compositions of oxides. Second was the analysis of inclusions extracted from steel by nonaqueous electrolyte dissolution to check the model and to provide inclusion ratios like $(Ca/Al)_{oxide}$ and Ca_{sulf} to be correlated with steelmaking practice or a machinability index.

KEY WORDS: calcium, cleanness, inclusion, machinability

Calcium alloys are widely used in steelmaking to control the composition and morphology of nonmetallic inclusions (oxides and sulfides). However, this wide experience with calcium in steelmaking has shown that both thorough comprehension of how calcium acts in the melt and careful and controlled use of calcium bearing alloys are necessary to achieve the aimed metallurgical goals and avoid possible detrimental effects. This paper will deal successively with:

(1) Calcium treatment and clean steel,
(2) Calcium treatment and machinability,
(3) Predictive model of composition of inclusions in calcium treated steel, and
(4) Phase analysis of inclusions containing calcium.

Calcium Treatment and Cleanness

The reputation of calcium in respect to cleanness is not always very good, especially when fatigue life is involved. We intend to show that such a matter should be carefully considered. For a clear understanding of the problem one should probably discriminate, if possible, between the effect of composition of inclusions and the effect of size of inclusions. One should have in mind that occurrence of large globular inclusions is generally the result of an uncontrolled calcium treatment [*1*].

---

[1] Manager of process research development and manager of laboratory machinability, respectively, Ascometal, Saint Etienne, France.

[2] Section manager and researcher, respectively, Intitut de Recherche de la Siderurgie Francaise, voie Romaine-57210, Maizieres-les-Metz, France.

Calcium and Ball Bearing Steels [American Iron and Steel Institute—Society of Automotive Engineers (AISI-SAE 52100 [UNS G52986])]

The phenomenon is well known, that the higher the tensile strength, the more calcium is suspected to be detrimental for fatigue life. This is the case for ball bearing steel with a tensile strength ≥2000 MPa. Figure 1 shows that globular calcium aluminate is very detrimental to fatigue life, which is partly a problem of size. We face here the difficulty of getting very small globular inclusions with calcium in conventional steelmaking. The figure also shows that, even if large calcium aluminates are avoided, fatigue life can be reduced by calcium-manganese sulfides, which are at least as harmful as pure alumina. We meet here, for the first time, a permanent problem of the calcium treatment: the distribution of calcium between sulfides and oxides.

Calcium and Steels for Carbo-Nitriding

Calcium treatment is also suspected to be detrimental to the fatigue life of steels used for gears (Grade 4130 [UNS 641300], for example). The reason is that, after surface treatment, such steels have the same surface hardness as ball bearing steel. However, there is a big difference: in the case of grades like 4130, surface treatment develops compressive residual stresses that can partly balance the effects of inclusions on fatigue life.

According to this consideration, we designed for such grades a steelmaking process including final treatment with calcium. Such a treatment has the following characteristics:

(1) Use of cored wire as calcium inoculator;

(2) Use of low calcium containing alloy in the cored wire; and

(3) Addition of calcium in a melt already as clean as possible, in a quantity proportional to the total oxygen content of the melt.

Table 1 summarizes the characteristics of such a heat and shows a very good ratio for fatigue limit to tensile strength (*σ D/TS*). This ratio is 0.475. If we check the position of the material described in Table 1 on the general diagram [2] giving fatigue limits versus tensile strength (Fig. 2), we find that such heats can be in the upper part of the usual fatigue limits dispersion band. Apparently, calcium treatment can be used for highly stressed gear steels.

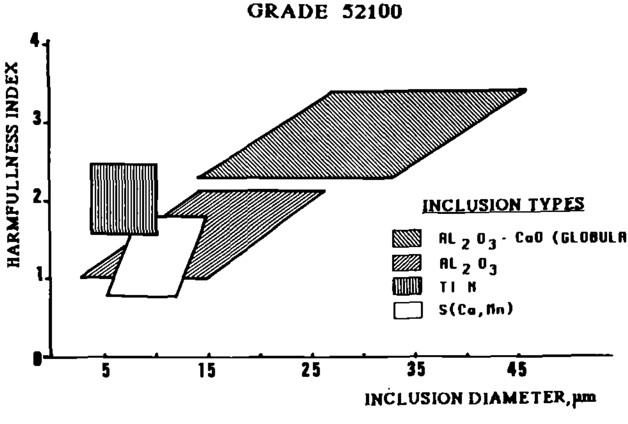

FIG. 1—*Relative harmfulness of various types of inclusions* [3].

TABLE 1—*Fatigue life (rotative bending tests) of 4130 calcium treated steel.*

Analytical characteristics	Ca ppm = 6 S ppm = 300 Al ppm = 200 O_T ppm = 15
Mechanical characteristic } after heat treatment	TS = 1690 MPa YS = 1510 MPa
Fatigue life test (10^7 cycle)	σ_D = 810 MPa $\sigma_{D/TS}$ = 0.475

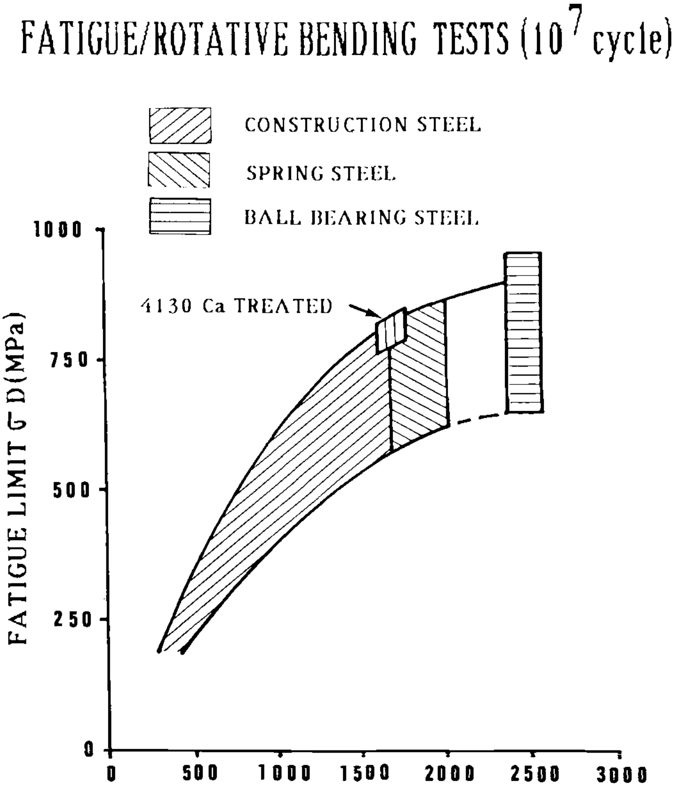

FIG. 2—*Fatigue limit versus tensile strength for various steels* [2].

Calcium and Steel for Cold Upsetting

These steels, mainly AISI-SAE 1010 (UNS G10100ob), have generally high aluminum contents, (0.050 to 0.080%). To present a high capacity of cold deformation they should also have [*4*] extra low sulfur (less than 50 ppm) and high cleanness-they should be free of alumina stringers. A calcium treatment is well suited for such grades to get rid of alumina stringers, provided that large calcium-aluminate inclusions are avoided. This treatment can be done with the same operating practice as above. The above described applications emphasize that clean steel can be produced through calcium treatment, provided a very careful control of the treatment is performed.

Calcium Treatment and Machinability

We shall deal with construction steels containing aluminum for grain size control and a sulfur content of either 0.020 to 0.040% or 0.080 to 0.100%. Machining with carbide tools will be appreciated (with some particular remarks about machining with ceramic tools).

When machining at high speed with carbide tools, the main factor governing machinability is the more or less abrasive nature of inclusions in steel. Alumina stringers are known to be very detrimental to machinability. A calcium treatment transforms alumina inclusions into calcium aluminates with a lower melting point and much less abrasivity, but the treatment should be thoroughly balanced to avoid formation of calcium sulfides or manganese sulfide containing a fairly high amount of calcium, which are nearly as abrasive as alumina.

Figure 3 shows our results for steel having a sulfur content between 0.070 and 0.100%, with machinability depending on total aluminum content and the calcium to oxygen (Ca/O) ratio, where Ca is total calcium, that is, calcium in inclusions and calcium dissolved in steel, and oxygen is total oxygen determined by fusion analysis. With a too low calcium to oxygen ratio and high aluminum, inclusions are mainly alumina with a resulting poor machinability. With a too high calcium to oxygen ratio, oxides are well transformed but manganese sulfides become more substituted with calcium and machinability becomes poor again. With such grades calcium should be carefully adjusted to oxygen and sulfur content. Table 2 gives typical figures of

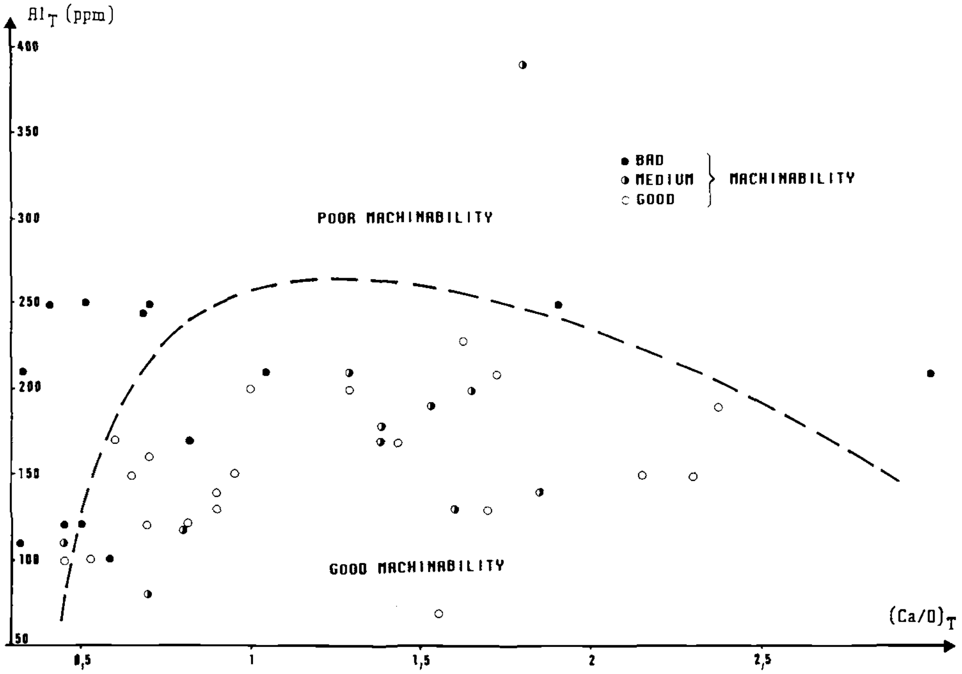

FIG. 3—*Effect of aluminum and calcium to oxygen ratio on machinability (construction steels with a sulfur level of 0.080).*

TABLE 2—*Steel Grade 4140: Sulfur content 0.080% and machinability (carbide tool) according to quality of Ca treatment.*

Poor Ca treatment (excess of CaS)	$V_{20} = 170$ m/min
Poor Ca treatment (insufficient modification of oxides)	$V_{20} = 140$ m/min
Optimum Ca treatment	$V_{20} = 240$ m/min

machinability for Grade 4140 (UNS G41400), according to the quality of calcium treatment. The results given in terms of V_{20}[3] show that differences of up to 70% in machining could result from calcium treatment control.

A more complicated situation occurs when machining with ceramic tools (alumina). The same steel as above (4140 calcium treated with S $\simeq$ 0.080) with an optimum calcium treatment can be machined at a very high speed, up to 600 m/min, with sulfides producing a lubricating layer on the tool. If we select the same kind of steel but with a lower sulfur level (S $\simeq$ 0.030%) and try the same kind of machining with a ceramic tool, we observe even at low speed (250 m/min) a progressive grooving of the tool: the cutting edge of the tool is progressively destroyed. The lower sulfur level probably hinders the formation of the isolating sulfur layer: calcium-aluminate inclusions come in contact with the alumina tool and flux it. With these examples, we have demonstrated that with an adjusted calcium treatment at a sulfur level of 0.080% we can design a highly performing material in a wide range of machining speeds: from carbide tools to ceramic tools (with a lower sulfur level, S $\simeq$ 0.030%, the versatility of material is less with respect to machining speed).

Fundamentals of Inclusion Control in Calcium Treated Steels

We showed previously, with various examples, that a careful adjustment of the calcium addition to the liquid steel was necessary to ensure the proper degree of transformation of primary oxide inclusions, and, in some cases, to avoid side reactions (for example, to avoid the precipitation of calcium sulfide inclusions in resulfurized steels). The main problem was how to predict and check the distribution of calcium between oxides and sulfides. Methods for predictive calculations of composition were developed, together with chemical methods of phases analysis on inclusions extracted from steel samples.

The Predictive Model of Inclusion Composition

These calculations are based on the most recent data obtained at Institut de Recherche de la Siderurjic Fancaise, (IRSID) on solubility products and on a slag model developed to describe the thermodynamic properties (component activities and phase diagram) of complex oxide systems. The first type of calculation is illustrated in Fig. 4, which represents the computed equilibrium diagram for the Fe-Al-Ca-O-S system at 1600°C. The right-hand diagram shows the composition of oxide inclusions as a function of aluminum and calcium activities in the metal. The left-hand diagram shows the conditions for calcium sulfide formation as a function of sulfur activity. Similar diagrams have been drawn for steels containing silicon and manganese, in addition to aluminum and calcium.

A second type of calculation is based on the analysis of a metal sample containing oxide and sulfide inclusions (that is, total contents in aluminum, manganese, silicon, calcium, magne-

[3] V_{20} is the speed of the carbide tool machining, which produces a tool wear of 0.4 mm in 20 min.

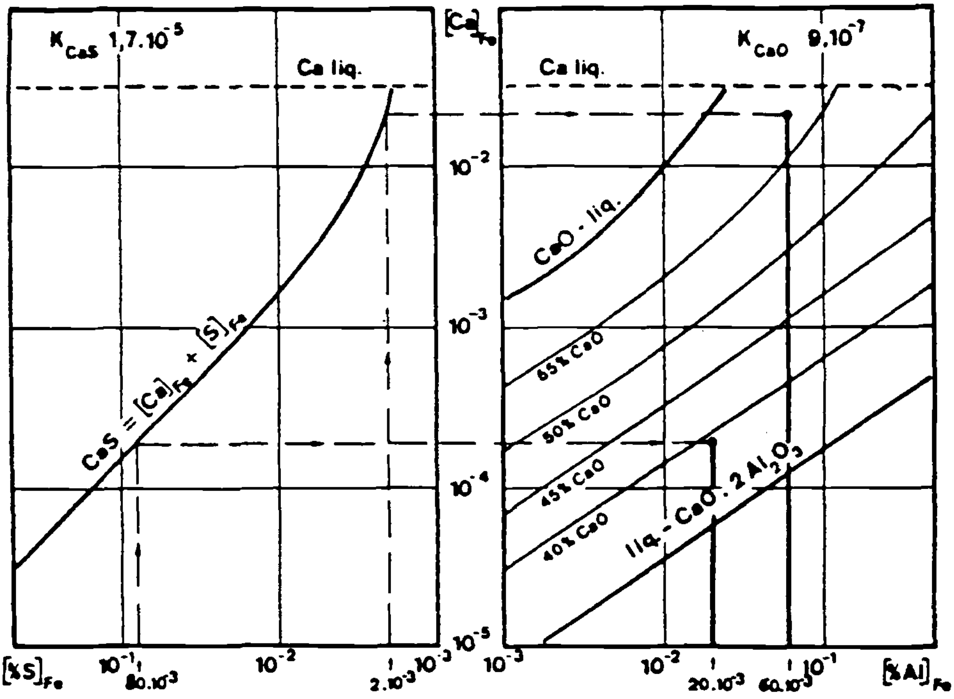

FIG. 4—*Equilibrium diagram for the Fe-Al-Ca-O-S system at 1600°C.*

sium, oxygen, sulfur). The calculation consists of evaluating the composition and amounts of residual inclusions that may have been formed at treatment temperature and during subsequent cooling until the steel starts solidifying. The method makes use of a recurrent procedure for complex equilibria calculation, combining material balances and equilibrium constraints between elements dissolved in liquid steel and liquid or solid oxides and sulfides. Although the method has been used mostly for calcium treated steels, it can be applied in a wide range of situations (for example, for silica-rich inclusions, alumina-silicates).

Figure 5 shows the various steps of the calculation of inclusion composition. Typical results of the calculation for aluminum killed calcium treated steels show that for a given final composition of the steel, the higher the treatment temperature, the higher the calcium oxide content of inclusions. Inclusions formed during calcium treatment have a substantially higher calcium oxide content than the ones precipitated during subsequent cooling from residual dissolved oxygen or reoxidations (assuming that these new inclusions are not reacting with the high temperature ones).

Some of these results are illustrated in Fig. 6, which shows the computed precipitation path of inclusions formed during the calcium treatment and subsequent cooling in a calcium treated 4130 steel containing 0.02% sulfur. In this figure, the left-hand diagram represents the evolution of the distribution, among liquid metal, of the remaining total calcium in oxide and sulfide inclusions, analyzed in the cast product. At this moderate sulfur content, calcium sulfide was precipitated only during the cooling. The right-hand diagram represents the calcium oxide and aluminum oxide contents of the inclusions precipitated at each moment during the treatment and cooling (solid lines), as well as the average contents in the inclusion population (dotted lines). These inclusions contain, in addition, around 9.5% silicon dioxide and 0.1% manganese

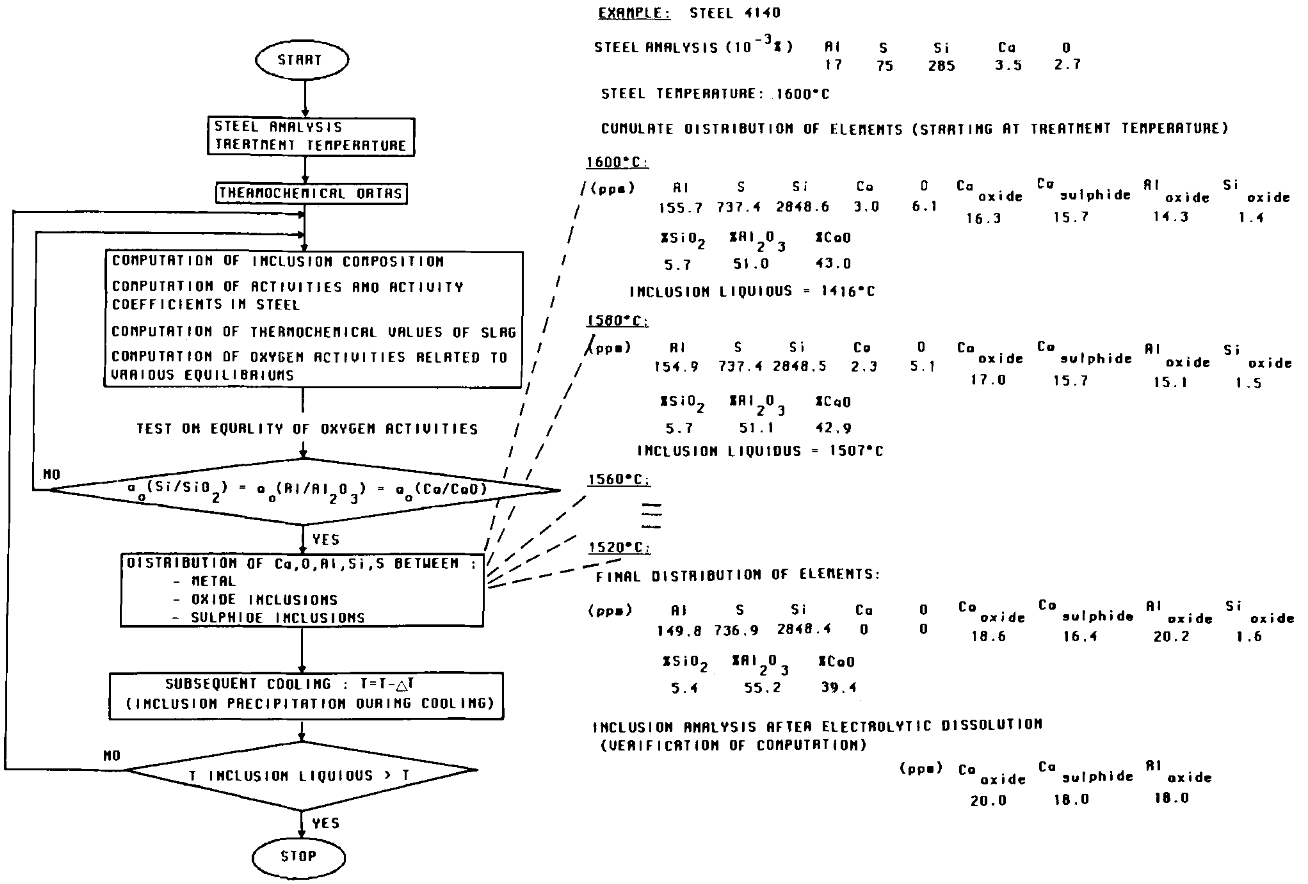

EXAMPLE: STEEL 4140

STEEL ANALYSIS (10^{-3}%)	Al	S	Si	Ca	O
	17	75	285	3.5	2.7

STEEL TEMPERATURE: 1600°C

CUMULATE DISTRIBUTION OF ELEMENTS (STARTING AT TREATMENT TEMPERATURE)

1600°C:

(ppm)	Al	S	Si	Ca	O	Ca_{oxide}	$Ca_{sulphide}$	Al_{oxide}	Si_{oxide}
	155.7	737.4	2848.6	3.0	6.1	16.3	15.7	14.3	1.4

%SiO_2	%Al_2O_3	%CaO
5.7	51.0	43.0

INCLUSION LIQUIDUS = 1416°C

1580°C:

(ppm)	Al	S	Si	Ca	O	Ca_{oxide}	$Ca_{sulphide}$	Al_{oxide}	Si_{oxide}
	154.9	737.4	2848.5	2.3	5.1	17.0	15.7	15.1	1.5

%SiO_2	%Al_2O_3	%CaO
5.7	51.1	42.9

INCLUSION LIQUIDUS = 1507°C

1560°C:

⋮

1520°C:

FINAL DISTRIBUTION OF ELEMENTS:

(ppm)	Al	S	Si	Ca	O	Ca_{oxide}	$Ca_{sulphide}$	Al_{oxide}	Si_{oxide}
	149.8	736.9	2848.4	0	0	18.6	16.4	20.2	1.6

%SiO_2	%Al_2O_3	%CaO
5.4	55.2	39.4

INCLUSION ANALYSIS AFTER ELECTROLYTIC DISSOLUTION
(VERIFICATION OF COMPUTATION)

(ppm)	Ca_{oxide}	$Ca_{sulphide}$	Al_{oxide}
	20.0	18.0	18.0

FIG. 5—*Calculation of inclusion composition.*

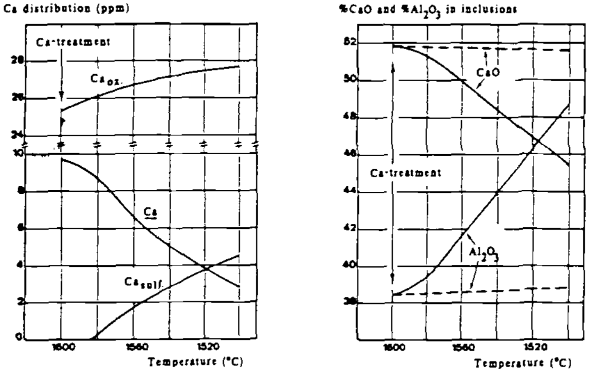

Composition of cast steel : 0.015 % Al - 0.38 % C - 0.75 % Mn - 0.02 % S - 0.25 % Si - 35 ppm Ca - 30 ppm O .

Computed average composition of oxide inclusions : 9.4 % SiO_2 - 38.8 % Al_2O_3 - 51.6 % CaO - 0.1 % MnO

FIG. 6—*Computed precipitation path of inclusions in a calcium treated 4130 steel. Cast steel composition: 0.015% Al-0.38% C-0.75% Mn-0.02% S-0.25% Si-35 ppm Ca-30 ppmO. Computed average composition of oxide inclusions: 9.4% SiO_2-38.8% Al_2O_3-51.6% CaO-0.1% MnO.*

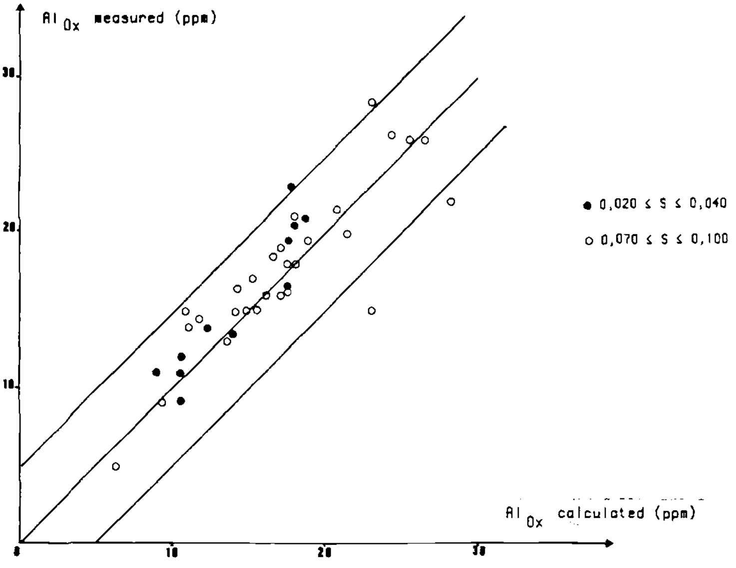

FIG. 7—*Aluminum oxide measured versus calculated.*

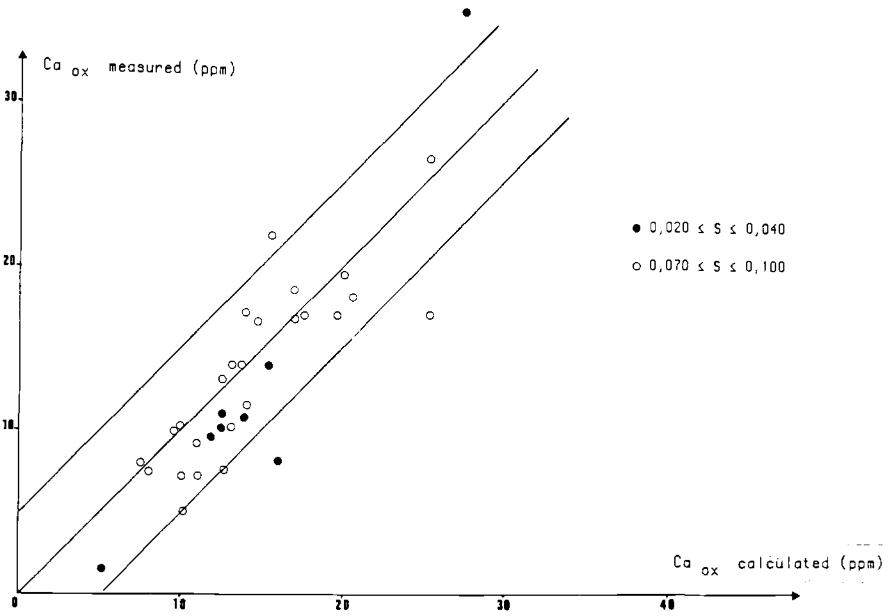

FIG. 8—*Calcium oxide measured versus calculated.*

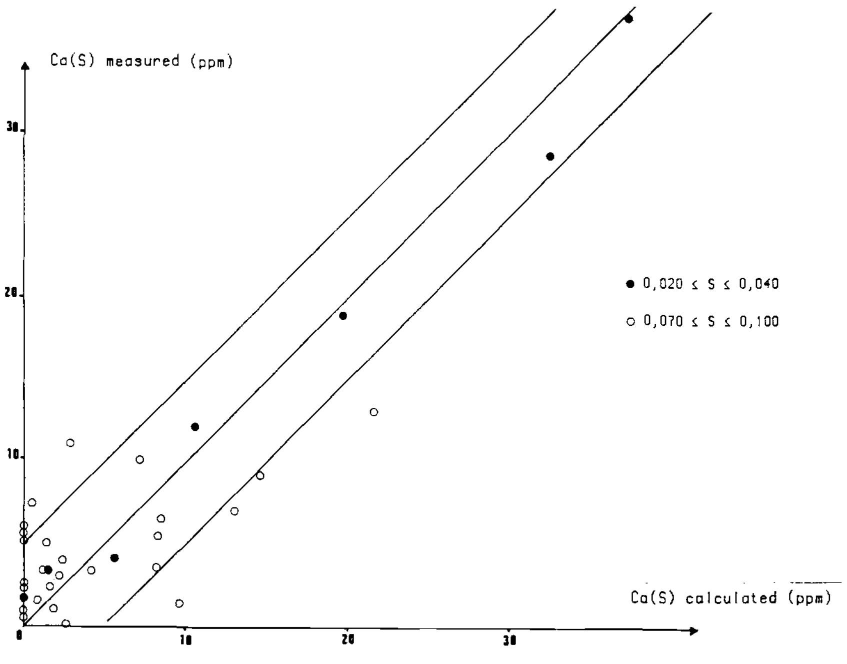

FIG. 9—*Calcium sulfide measured versus calculated.*

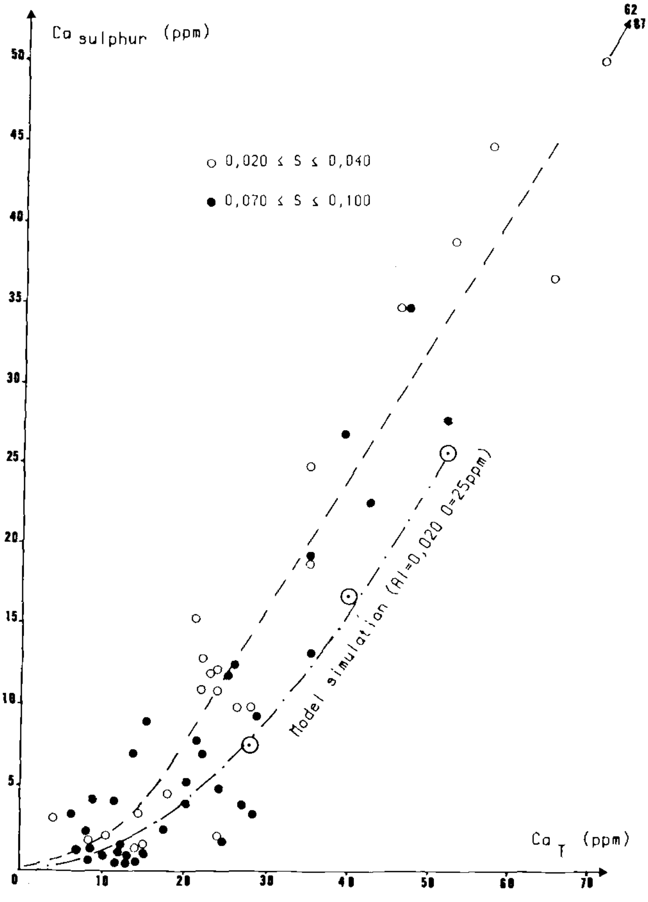

FIG. 10—*Formation of mixed sulfur [S (Ca, Mn)].*

oxide. The remaining dissolved oxygen (1.4 ppm at 1500°C) would react at lower temperatures to form alumina, whereas the remaining dissolved calcium (2.8 ppm) would react to form calcium sulfide or manganese sulfide or both during steel solidification.

Phase Analysis of Inclusions

A method of extraction of inclusions by nonaqueous dissolution of the metal matrix was designed [5,6]. The extraction is followed by selective chemical analysis giving identification and quantification of the various phases: calcium in oxides; calcium in sulfides; silicon dioxide; aluminum in oxides; aluminum in nitrides and so on. The purpose of such a method is twofold. The first purpose is to check the validity of the above computation of inclusions compositions. Figs. 7-9 show a rather good agreement between chemical determinations (after inclusions extraction) and calculation for Al_{oxides}, Ca_{oxides}, and $Ca_{sulfides}$.

The second purpose is to provide some typical inclusion ratios such as $(Ca/Al)_{oxide}$ and $Ca_{sulfide}$ that could be translated in terms of steelmaking practice or machinability. For example, Fig. 10 shows calcium sulfide content depending on Ca_{total} in steel. Such a diagram can be used to design a suitable calcium treatment according to the aimed metallurgical goal.

Conclusions

Calcium treatment is a powerful means to get the right inclusions that will confer high performance on steel. Such a treatment should be accurately designed and performed. The predicting model of inclusions and electrolytic extraction are two valuable means to secure a correct treatment.

References

[1] Gustafsson, S., Mellberg, P. O., and Pettersson, B., "Inclusion Picture and Inclusion Origin in a Calcium Treated Steel," *Swedish Symposium on Nonmetallic Inclusions in Steel.* UDDEHOLM AB, HAGFORS, April 1981.

[2] Wieder, C. and Bellot, J., Internal Report Ascometal, Saint Etienne, France, March 1987.

[3] Cogne, J. Y., Heritier, B., and Monnot, J., "Cleanness and Fatigue Life of Bearing Steels," *Clean Steel,* Balatonfüred, Hungary, June 86.

[4] Boucher, O., Carrot, L., Giroud, G., and Saleil, J., "Inclusions Control and Injection Practices," *ATS Steelmaking Conference,* December 1984.

[5] Henriet, D. and de Gelis, P., "Separation, Identification and Analysis Methods for Inclusions in Steels," Report RE 984, IRSID, 1983.

[6] Gaujac, P. and Hocquaux, H., "Selective Separation of Oxides and Sulphides after Electrolytic Extraction of Inclusions in Steels," *6th International Colloquium of "Cercle d'Etude des Métaux,"* Saint-Etienne, France, Nov. 86.

Properties

P. Andre Coulon[1]

The Role of Trace Elements in a Martensitic 12% Chromium Steel

---

REFERENCE: Coulon, P. A., **"The Role of Trace Elements in a Martensitic 12% Chromium Steel,"** *Residual and Unspecified Elements in Steel. ASTM STP 1042,* A. S. Melilli and E. G. Nisbett, Eds., American Society for Testing and Materials, Philadelphia, 1988, pp. 83–99.

ABSTRACT: The comparison of mechanical properties between a "super-clean" heat of a 12% chromium steel and a heat with an identical chemical analysis, but "industrially" produced, does not yield any definite differences. At most it can be ascertained that the "super-clean" heat displays better ductility and impact strength while keeping a comparable strength to that of the other heats.

The comparisons of structures are more interesting and give better results since the study showed (1) that trace elements, especially antimony, (comparison between castings 7-8 and 91) seem to be responsible for the embrittlement of austenitic intergranular boundaries and (2) that no brittle intergranular fracture has been noticed, which distinguishes this superclean heat from the others. Besides, the following comments may be made on superclean heat: (1) the carbides that are visible under the optical microscope (0.5 to 1 m) are still heterogeneously distributed and (2) few carbides are detected in the platelike crystals of martensite.

The main characteristic of this clean heat is to provide a good impact energy and a low transition temperature. For the more in spite of the very clear and relatively abundant precipitations of carbides and carbonitrides in the grain boundaries, no intergranular rupture as shown up during the scanning electron microscope (SEM) examination of the fracture surfaces. One can deduce from this, that the brittle intergranular ruptures observed in the case of heats 7-8 and similar heats are more as a result of the intergranular segregations of trace elements than that of carbides and carbonitrides derived from contents of carbon, nitrogen, neon, niobium, vanadium, and so forth, since all these steels undergo the same thermal treatments.

But it clearly appears that the relationship between the content and distribution of these various carbides and the mechanical properties measured (creep, impact strength) is of prime interest for future research. This paper does not claim to establish this close relationship. Moreover, it is not absolutely certain that this study would be interesting to the mechanics specialist. A materials specialist might well have an opposed opinion.

KEY WORDS: martensitic steels, steam turbines, turbine rotors, creep resistance, residual elements, carbides

"Super critical" steam turbines with one or several super-heating stages use thermodynamic cycles with temperatures of between 550 and 600°C at the high and intermediate pressure module inlets. The traditional low-alloy, chromium molybdenum-vanadium steel has an insufficient creep resistance at these temperatures. Martensitic 12% chromium steels correspond better to the properties required for high temperature rotors. There are certain grades of such steels available on the market, but it is impossible to draw conclusions on their properties at the core of large forgings (barrel diameter 1400 mm) as such pieces have not yet been manufactured [*1*–*7*].

A research program conducted by Alsthom and Creusot-Loire Industrie [*8*] has made it possible to define a steel specifically intended for very large high and intermediate pressure rotors,

---

[1] Research manager, Alsthom, Steam Turbine Department, Belfort, France.

taking into account the inherent problems of the hardenability of such steels and of their structural transformations; this steel nevertheless has a notable resistance to long-term creep.

The objective of fracture at 100 000 h under a minimum load of 180 MPa at 550°C and of 100 MPa at 600°C [*8, 9*] was achieved in conditions simulating the core of a 1400-mm-diameter rotor.

The steel produced for the manufacture of such pieces, possibly weighing in excess of 30 tonnes, should, in order to display acceptable mechanical properties, be derived from selected scrap so as to minimize residual elements such as sulfur, phosphorous, copper, tin, arsenic, and antimony. The content of such elements in the steel should, however, be "compatible" with industrial know-how and facilities and with economic costs [*10*], the compromise lying in low but not nil residual element contents.

In order to assess the influence of such residual elements a pure heat, that is to say, virtually free from trace elements, was carried out in the laboratory. This paper deals with the comparative properties of a "standard" heat and a "pure" heat for martensitic 12% chromium steel developed by Alsthom and Creusot-Loire Industrie for turbine rotors operating at high temperatures.

General Research Program Objectives

These objectives were as follows [*8*]:

(1) minimum mechanical properties at ambient temperature: tensile strength, elongation, reduction in area, impact strength, transition temperature;

(2) minimum hot instantaneous tensile strength at 550 and 500°C; and

(3) long-term creep and elongation characteristics on smooth and notched test pieces at temperatures ranging from 550 to 600°C.

Table and Fig. 1 show the minimum levels aimed for.

TABLE 1—*Minimum levels aimed for.*

Rotor Barrel Diameter, 1400 mm

1. On periphery of rotor, radial. and tangential directions
   UTS = 870 to 970 MPa
   Yield 0.002 = 670 MPa
   $E > 12\%$
   RA > 32%
   Charpy V 20°C > $20\ \mathrm{J\cdot cm^{-2}}$
   FATT < +50°C
2. Along rotor axis, longitudinal direction
   UTS = 890-950 MPa
   Yield = 650 MPa
   $E > 12\%$
   RA > 32%
   Charpy V 20°C > $17.5\ \mathrm{J\cdot cm^{-2}}$
   FATT < +100°C
3. At 550°C under instantaneous tensile stress
   UTS ≥ 480 MPa
   Yield 0.002 ≥ 400 MPa
4. At 550°C rupture at 100 000 h ≥ 180 MPa
   At 600°C rupture at 100 000 h ≥ 100 MPa

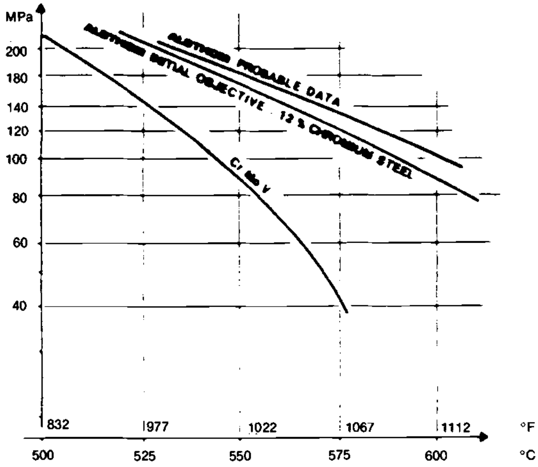

FIG. 1—*Improved 12% chromium steel for rotors, 10⁵-h creep rupture.*

"Pure" Heat Procedure

Table 2 gives the chemical composition of the "pure" or super clean heating (numbered 91) compared to five "standard" heatings (numbered 7, 8, 711, 721, and 731), which fulfill the objectives aimed for in Table 1.

Remarks Concerning the "Super Clean" Heat

The content at alloying elements "aimed for" (carbon, nickel, molybdenum, vanadium, niobium, nitrogen, and boron) corresponds to that of the optimal chemical analysis as defined by the program [*8*].

The content of trace elements "aimed for" (sulfur, phosphorus, copper, arsenic, tin, antimony, and aluminum) corresponds to the manufacturing possibilities of Creusot-Loire, imply who produced the steels.

The silicon and manganese contents were deliberately reduced to very low levels; as for silicium, experience previously acquired had shown that its absence improved creep resistance.

The same experiment had shown that steel containing manganese showed a certain sensitivity to embrittlement; however, manganese had a positive influence on hardenability over a great thickness.

Program Carried Out

The heats were produced by Creusot-Loire Industrie imply the resulting ingots were forged in 2 heating stages at 1200 to 1250°C in bar form. The final coefficient of area reduction was 4, identical to that required for the rotor.

Role of Heat Treatments

Homogenization Treatment

Five treatments were tested (variations in temperature and time parameters) followed by cooling at a controlled rate (different cooling rates were used).

TABLE 2—*Chemical composition of products.*

Elements, % mass		Standard Heats					Super-Clean Heat	
	7	8	711	721	731	Min/Max	91	Aimed for
C	0.191	0.206	0.198	0.186	0.181	0.180-0.205	0.186	0.185
S	0.016	0.014	0.015	0.015	0.015	0.015	0.0052	0.005[a]
P	0.018	0.018	0.010	0.013	0.012	0.015	0.0037	0.005
Si	0.230	0.206	0.243	0.248	0.255	0.200 to 0.250	0.026	0.03
Mn	0.379	0.380	0.384	0.404	0.401	0.380 to 0.420	0.053	0.1
Ni	0.780	0.790	0.778	0.792	0.776	0.75 to 0.80	0.786	0.75 to 0.80
Cr	11.46	11.51	11.30	11.35	11.35	11.2 to 11.5	11.37	11.2 to 11.5
Mo	0.95	0.97	1.09	1.10	1.09	0.90 to 1.10	1.10	0.9 to 1.10
V	0.323	0.310	0.301	0.309	0.307	0.280 to 0.320	0.284	0.290
Cu	0.102	0.102	0.059	0.061	0.060	0.1	0.016	0.050
Sn	0.005	0.005	0.005	0.005	0.005	0.01	0.005	0.005
Al	0.003	0.003	0.005	0.005	0.005	0.005	0.006	0.005[a]
As	0.017	0.017	0.015	0.015	0.015	0.015	0.005	0.005
Sb	0.0034	0.0021	0.0008	0.0003	0.001	0.0015	0.0008	0.0015
W	0.020	0.020	0.070	0.050	0.020	...	0.20	...
Ti	0.005	0.005	0.005	0.005	0.005	...	0.005	...
B	0.0005	0.0034	...	...	...	...	...	...
Co	0.010	0.010	0.10	0.10	0.10	...	0.10	...
Nb	0.131	0.132	0.128	0.200	0.203	0.130 to 0.200	0.128	0.130
N[2]	0.073	0.066	0.1146	0.0786	0.1059	0.07 to 0.115	0.0674	0.07
O[2]	0.0049	0.0054	0.0066	0.0044	0.0048	0.005	0.0045	0.003[a]

[a] Initial objective exceeded.

The tests were concerned with the following:

- structures by micrographical examination;
- the analysis of precipitates and inclusion by examination with a microprobe; the dissolving of vanadium and niobium carbides was quantitatively examined;
- hardness measurements;
- grain size and grain size variations; and
- determination of point A_{C3} generally at a temperature greater than 1000°C.

Quenching Treatment

The following quenching rates were selected:

- fast cooling, 2500°C/h, simulation the outer surface of the rotor and
- slow cooling 25°C/h, air quenching, simulating the rotor core (750 mm deep).

The abundance of carbides and more particularly of pearlite in austenitic grain boundaries has motivated our search for a more efficient quenching process. Spray water quenching has been retained with a minimum cooling rate of 80°C/h at the core.

Tempering Temperature

The tempering procedure (holding for 5 h between 600 and 750°C) with steps of 25°C was established.

The examinations focused on the following:

- hardness measurement and
- structures, using on scanning electron microscope (SEM), with determination of the quantity of pearlite and ferrite formed and appreciation of the role of their own structures: lamella or granular.

Mechanical Tests

The mechanical tests were as follows:

- tension test at 500 to 550°C,
- tension test at room temperature,
- impact test: impact strength transition curve with examination of fractures under the scanning electron microscope, and
- selective creep/elongation tests on combined smooth and notched test pieces aiming for fracture times less than 20 000 h at temperatures of 550, 575, and 600°C.

Comparison of Results Between Standard and Super-Clean Heat Dilatometry

Determination of Ac_1 and Ac_3

The tests were carried out in helium under the following conditions:

- heating at a rate of $150°C \cdot h^{-1}$ up to 1150°C,
- no holding at 1150°C, and
- cooling in air.

Ac_1 and Ac_3 were determined in the usual way.

The results (Table 3) do not show any significant differences between the standard castings and the super-clean casting.

TABLE 3—*Transformation temperatures during heating.*

Heat	Ac_1, °C	Ac_3, °C
7	810	875
8	810	875
711	800	875
721	810	880
731	810	875
91	820	890

Determination of Transformation Temperatures During Quenching Isothermal Transformation Diagram [*11*]

Tests Carried Out

The complete isothermal transformation diagram was plotted from austenitisation of 1 h at AC_3 + 50°C. To assess the effect of austenitisation temperature, two test-pieces were austenitized at a higher temperature: 1 h at 1050°C; one cooled at a rate of $25°C \cdot h^{-1}$, and the other cooled at a rate of $50°C \cdot h^{-1}$.

Dilatometric tests were carried out in helium, and the heating rate V_{700} was approximately $1500°C \cdot h^{-1}$. They were complemented by

- HV 100 N hardness measurements and
- micrographic examination of structure after polishing and etching with CATELLA's reagent.

Austenitization at "Ac_3" + 50°C

The main dilatometric test results are given in Table 4. The four diagrams are comparable. A martensitic transformation takes place for very fast rates at approximately 300 to 350°C; its temperature increases as V_{700} decreases. A transformation into ferrite + carbide takes place for $V_{700} = 10°C \cdot h^{-1}$, the ferrite content is about 10% for Heats 721 and 731 with 0.20% niobium and from 40 to 50% for Heats 711 and 91 with 0.128% niobium. The contents of transformation products become comparable when $V_{700} = 25°C \cdot h^{-1}$.

Hardnesses

The averages of ten measurements taken on each test piece are given in Table 5. For the four castings, hardness decreases slowly when the quenching rate varies from 3 × 10 to $470°C \cdot h^{-1}$. As soon as the transformation into ferrite + carbide starts hardness diminishes suddenly. For Heats 711 and 91 with 0.128% niobium, hardness tends to stabilize when $V_{700} = 25°C \cdot h^{-1}$. For Heats 721 and 731 with 0.20% niobium, hardness continues to decrease with the quenching rate.

The super-clean heat displays both the greatest hardness after fast quenching and the lowest after quenching at a rate of $12.5°C \cdot h^{-1}$.

Structures of the super-clean heat (91) compared with those of the standard heat (711) of comparable chemical composition.

The following structures were found at the respective quenching rates of

- $3 \times 10^5 C \cdot h^{-1}$ martensite (Figs. 2*a* and 3*a*),

TABLE 4—*Dilatometric results after austenitization at Ac_3 + 50° C.*

	Transformation During Cooling											
	At High Temperature, °C				At Low Temperature, °C				HV 100 N			
Quenching Method	711	721	731	91	711	721	731	91	711	721	731	91
							300	300				
Water	...	...	...	...	315	315	315	315	524	496	500	567
Air + refractory steel muffle	...	...	...	...	350	350	340	350	498	485	482	540
Furnace					370	370	360	380	449	447	450	486
Furnace at 100°C · h^{-1}	740	710	725	750	420	410	410	430	373	380	413	328
	640	620	660	650				315				
Furnace at 50°C·h^{-1}	760	740	750	760	450	450	450	450				
	650	630	650	660	160	230	160	320	250	288	300	207
Furnace at 25°C·h^{-1}	770	750	750	800	470	480	470	500				
	665	660	640	700	250	265	230	290	211	203	220	178
Furnace at 12.5°C·h^{-1}	780	780	760	800	550	550	560	550				
	680	700	660	730	315	315	350	290	192	185	194	168

TABLE 5—*Tension test results at 20°C.*

Quenching		V_{700} = 80°C·h^{-1}				V_{700} = 2500°C·h^{-1}			
Heat	Tempering Temperature	UTS, MPa	YS, MPa	*E*, %	RA, %	UTS, MPa	YS, MPa	*E*, %	RA, %
Specified value		850 to 1000	650	12	35	870 to 1000	670	12	35
711	675	988	835	16	45.5	1034	886	16	44
		982	828	16.5	47	1038	888	15	41
		985	832	16.2	46.3	1036	887	15.5	42.5
	710	884	708	20	51	919	756	18.5	47
		876	703	20	51	916	755	18.5	49
		880	705	20	51	918	755	18.5	48
91	675	987	844	17	51	1007	867	17	55
		987	845	16.5	51	1011	869	16.5	54
		987	844	16.7	51	1009	868	16.7	54.5
	710	875	726	19.5	59.5	887	741	20	59
		877	727	21	61	891	742	19	59
		876	726	20.2	60.3	889	741	19.5	59

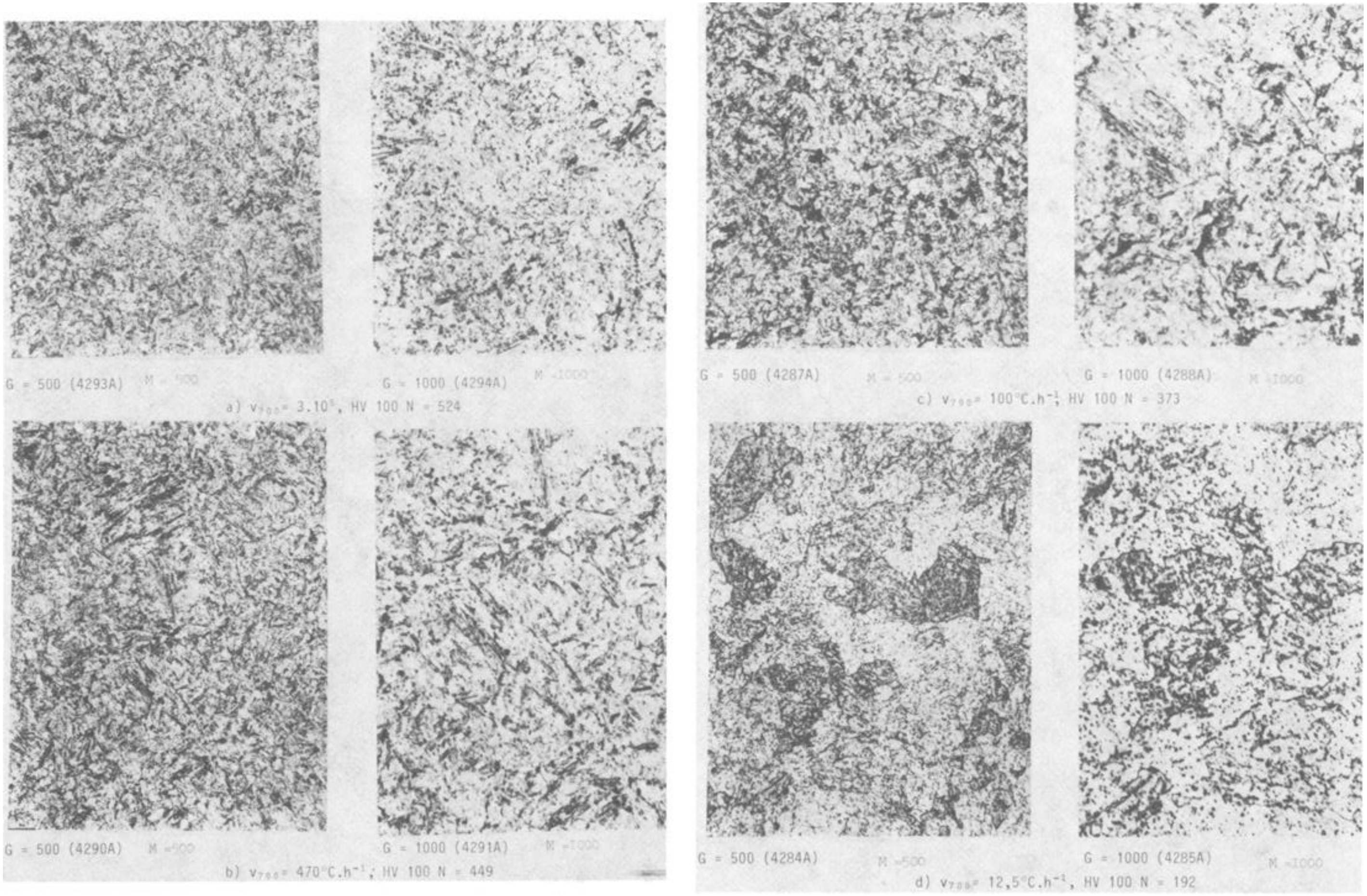

FIG. 2—*Heat 711, influence of cooling rate on the structure.*

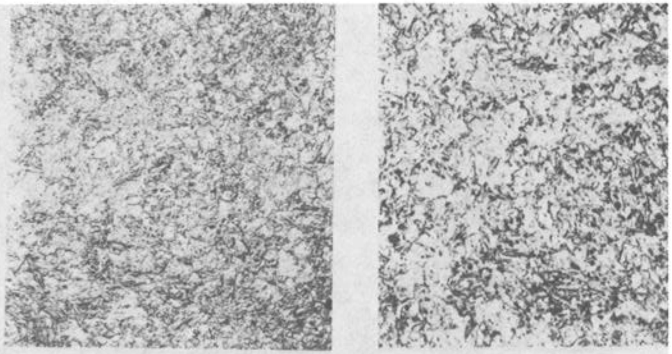

a) v_{700} = 3.10^5 °C.h^{-1}, HV 100 N = 567

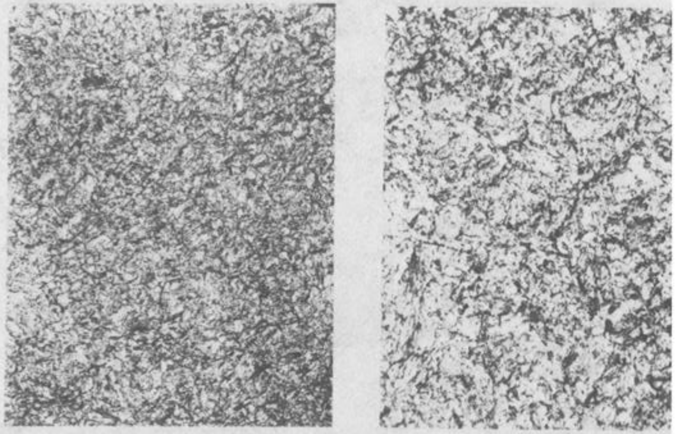

b) v_{700} = 470°C.h^{-1}, HV 100 N = 486

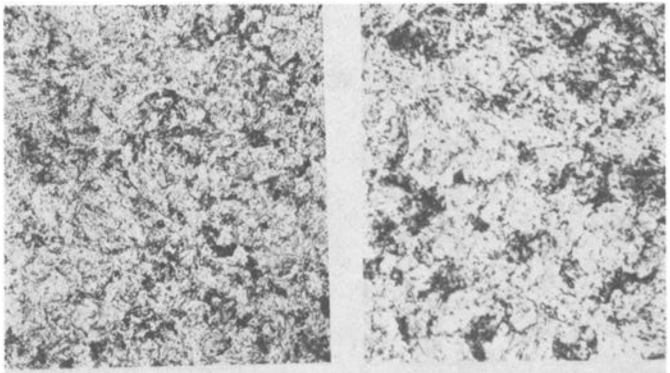

c) v_{700} = 100°C.h^{-1}, HV 100 N = 328

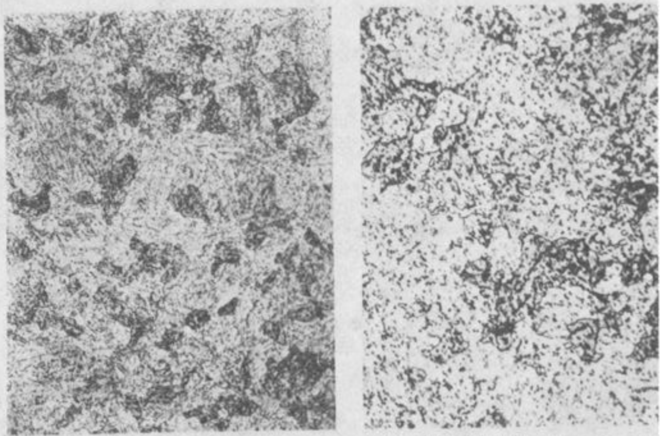

d) v_{700} = 12,5°C.h^{-1}, HV 100 N = 168

FIG. 3—*"Super-clean" heat. influence of cooling rate on the structure.*

- 470°C·h^{-1} martensite or bainite (Figs. 2*b* and 3*b*),
- 100°C·h^{-1} appearance of ferrite + bainite (Figs. 2*c* and 3*c*)
- 12.5°C·h^{-1} ferrite + carbide + bainite (Figs. 2*d* and 3*d*).

All other parameters being equal, the carbonitrides observed in Heats 721 and 731 with a higher niobium content are finer and more abundant than in Heat 711. Moreover, intergranular carbonitrides are observed in Heat 731 with a high niobium and nitrogen content.

The super clean heat (91) differs from the preceding ones by the greater size of niobium and vanadium carbonitrides and the lower relative density of these precipitates at quenching rates of less than 100°C·h^{-1}.

At V_{700} = 100°C·h^{-1}, a fine and more abundant precipitation is observed than for Heat 711. However, at V_{700} = 12.5°C·h^{-1}, the carbonitrides are coarser and denser grained in the super-clean heat than in Heat 711.

Mechanical Properties of Steels After Quenching and Tempering

General

Plates from which the following specimens could be taken have been machined:

- two high-temperature tension test pieces (550°C),
- two 20°C tension test pieces ($Lo = 4d$),
- 24 CV impact strength test pieces of type longitudinal transverse orientation (LT), with length of test-piece parallel to length of bar and notch parallel to transverse length of bar. The notch was made on outer surface side. The specimens were subjected to quenching with a holding time of 5 h at 1050°C and cooling at a rate of either 2500°C·h^{-1}, which simulates quenching at the rotor surface, or 80°C·h^{-1}, which simulates quenching at the rotor core. Then they were tempered for 5 h at either 675 or 710°C (Table 6).

The preceding comment also applies to tension tests at 550°C. Only the reduction in-area is improved by the absence of trace elements. Indeed, this reduction, which is 50% greater than that measured at 20°C, is increased by 10%.

The effect of trace elements is insignificant on ultimate tensile strength (UTS) and yield strength (YS) at 20°C, very low on elongation at fracture, but may be quantified on reduction in-area. Reduction in-area is reduced by approximately 20% in presence of trace elements.

Impact Test Results (Table 7)

The improvement on impact strength is appreciable on the outer surface of the rotor (energy at fracture doubled) for the super-clean heat. Likewise, it can be seen that for the same heat, fracture appearance transient temperature (FATT) or transition temperature decreases by approximately 5 to 10°C. Finally, the temperature at which the lateral expansion (LE) is equal to 0.5 mm on the Charpy V test piece is decreased by 15 to 20°C.

Examination of Fracture Surfaces under a SEM

The fracture surfaces of Heats 711, 721, and 731 display the same features, whatever the tempering temperature may be.

No intergranular fracture was observed on Heating 711 after quenching at a rate of 800°C·h^{-1}, while after quenching at a rate of 2500°C·h^{-1} brittle fracture was observed with cracks propagating intergranularly and transgranularly with cleavage facets.

In the case of the so-called "clean" Heat 91, brittle fracture is systematically transgranular

TABLE 6—*Tension test results at high temperature (550°C).*

Quenching		80°C·h^{-1} (Core)				2500°C·h^{-1} (Periphery)			
Heat	Tempering Temperature	UTS, MPa	YS, MPa	*E*, %	RA, %	UTS, MPa	YS, MPa	*E*, %	RA, %
Specified value		480	400	. . .	. . .	480	400	. . .	. . .
711	675	587	528	22.5	71	617	543	22.5	68.5
		587	528	22.5	68.5	622	543	22.5	68.5
	710	559	492	22.5	73	548	474	23.5	73
		569	490	22.5	68.5	556	474	23.5	68.5
91	675	612	525	20	73	592	559	24	77
		612	560	20	71	592	551	22.5	77
	710	597	467	22.5	77	530	474	25	77
		598	467	20	77	515	474	25	77

TABLE 7—*Impact test results.*

Quenching		80°C·h^{-1} (core)					2500°C·h^{-1} (Periphery)				
Heat	Tempering Temperature, °C	CV at 20°C, J·cm^{-2}	T (°C) CY = 7.5, J·cm^{-2}	T (°C) KCY = 50, J·cm^{-2}	T (°C) 50% Crystal-linity (FATT)	T (°C) LE = 0.5, mm	CY at 20°C J·cm^{-2}	T (°C) CY = 7.5, J·cm^{-2}	T (°C) KCY = 50, J·cm^{-2}	T (°C) 50% Crystal-linity (FATT)	*T* (°C) *E* = 0.5, mm
Specimen A	. . .	17.5	. . .	. . .	+100	. . .	20	. . .	. . .	+80	. . .
711	675	40	−40	+38	+21	+48	34	−40	+30	+22	+42
	710	65	−40	+11	+7	+16	62	−60	+13	+15	+13
91	675	49	−40	+20	+27	+24	63	−40	+10	+17	+22
	710	90	−40	−4	+4	0	133	−60	+13	+4	−8

with cleavage. Ductile fracture is transgranular in all cases. Air inclusions are fine and abundant.

Structural Examination of Impact Test Pieces

The structures obtained for Heats 711, 721, and 731 after quenching at 80 and 2500°C·h^{-1} differ by the abundance of carbides and carbonitrides in and between grains. A more abundant precipitation of fine carbides and carbonitrides occurs in grain boundaries during quenching at 80°C·h^{-1} than during quenching at 2500°C·h^{-1}. However, the matrix of steel quenched at 2500°C·h^{-1} and tempered has a higher content of fine carbides or carbonitrides.

As regards Heat 91, grain boundaries are also marked by the precipitation of carbides and carbonitrides, whatever the quenching rate may be. The precipitate in the matrix has a much lower density than for Heats 711, 721, and 731.

Creep Test Results (Partial)

Three temperatures were retained: 550, 575 and 600°C, with loads ranging between 160 and 350 MPa. Test pieces of "notched and smooth" type, as shown in Fig. 4, were used.

The two Heats anterior to Heats 711, 721, 731, and 91, that is, 7 and 8, which are very similar to Heats 711 and 91, reached a potential of 25 000-test-hours on 3/1/1987. Heats 711, 721, and 91 exceeds 16 000 h.

Extrapolations were performed with the Larson and Miller parameter whose constant was chosen as equal to 25 [*9,12*].

Comparing the numerous test results acquired on Heat 7 and the partial ones obtained on Heat 711 shows great similarity, and it is even impossible to differentiate between the two. The fragmentary results of the "super-clean" Heat 91 seemed slightly greater, 5 to 10%, than those measured on 7 and 711 as shown in Table 8.

Figure 5 reproduces the test results obtained and shows that it is impossible to isolate those relating to test pieces that have broken in the smooth section from those relating to test-pieces

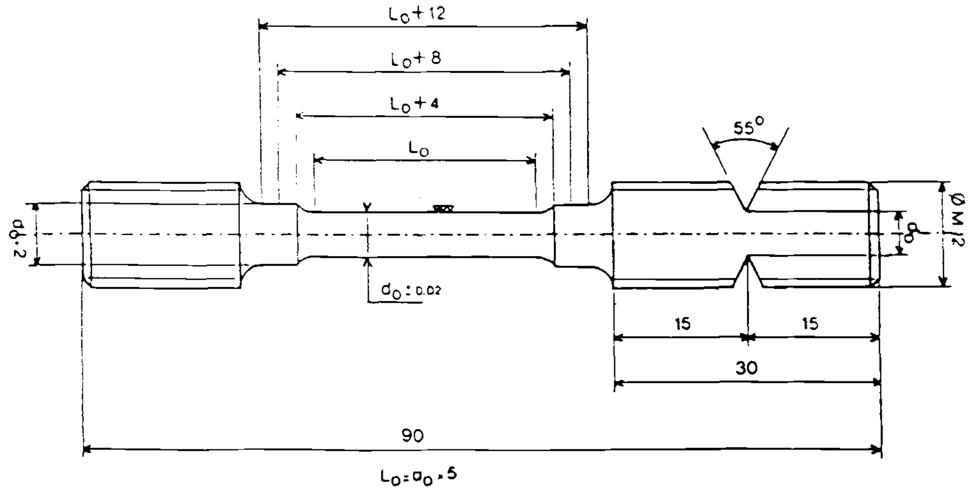

FIG. 4—*Creep test specimen.*

TABLE 8—*Creep resistance: fracture after 10^5 h at 550, 575, and 600°C.*

Heat	Range	550°C, MPa	575°C, MPa	600°C, MPa
7/711	Min	190	140	100
	Max	245	170	130
91	Min	200	145	110
	Max	260	180	140

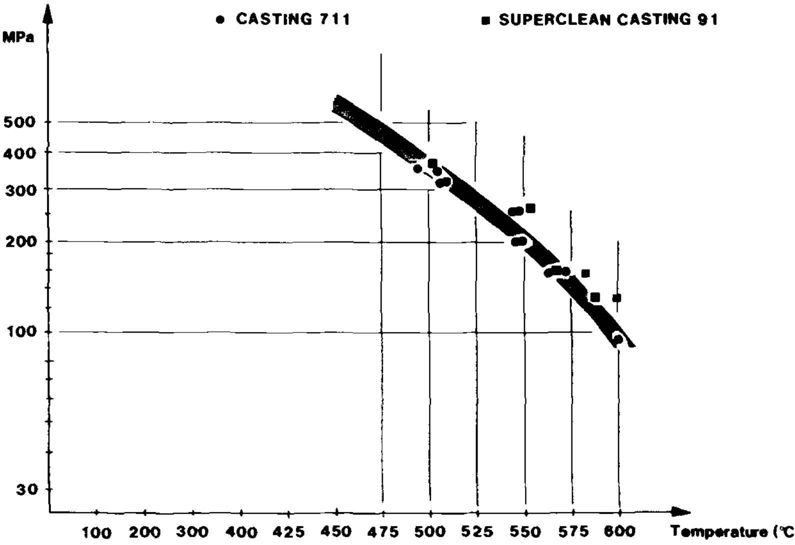

FIG. 5—*Improved 12% chromium steel for rotors, 10^5-h creep rupture. Creep test results after 16 000 h on Heats 711 and 91.*

that have broken in the notch. It is worth noting that for all the test pieces in the program there is a 50% probability of the first fracture occurring in the smooth section (and therefore 50% also of it occurring in the notch), and that the fracture time difference, converted into a temperature difference using the Larson and Miller parameter, does not exceed, under the same load, ±9°C at 10^5h, ±8°C at 10^4h, and ±7°C at 10^3h.

Finally, note the great dispersion of elongation and reduction in area at fracture, these two properties seeming to decrease as temperature or fracture time increases. Moreover, there is no noticeable difference between the values of ductility measured on the reference and on the super-clean heats.

Summary

The comparison of mechanical properties between a "super-clean" heat of a 12% chromium steel and a heat with an identical chemical analysis, but "industrially" produced, does not yield any definite differences. At most it can be ascertained that the "super-clean" heat displays better ductility and impact strength while keeping a comparable strength to that of the other heats.

TABLE 9—*Main carbides analyzed in Heats 711 and 91.*

Main Carbides	Localization	Shape	Size, mm	Chemical Composition				
				Fe	Cr	Mo	V	Nb
Inclusions (thermally stable)	. . .	round	0.5-1	5 to 10 25 to 30	8 to 10 8 to 10	1 1	15 3 to 5	65 to 70 55 to 60
Type I	martensitic matrix martensitic matrix	round . . .	0.02 . . .	10	60 to 65	15 to 20	10 to 15	. . .
Type II	former austenitic grain boundaines	oblong	$L = 1$ to 2 $e = 0.1$	40 to 45	50	5	1 to 2	. . .
Metastable carbides	in the matrix after quenching at 90°C·h^{-1} and tempering at 575°C	. . .	. . .	85	10 to 11	1 to 2	1	1 to 2

The comparisons of structures are more interesting and give better results since the study showed the following:

- that trace elements, especially antimony, are responsible for the embrittlement of austenitic intergranular boundaries and
- that no brittle intergranular fracture has been noticed, which distinguishes this heat from the others.

Moreover, the following comments may be made on Heat 91:

- the carbides that are visible under the optical microscope (0.5 to 1 μm) are still heterogeneously distributed.
- few carbides are detected in the platelike crystals of martensite.
- four types of carbide have been observed under the scanning transmission electron microscope with an X-ray analysis device (Table 9).
- inclusions or carbides with a high niobium content,
- Type-1 carbides with a high chromium content,
- Type-2 carbides, coarser grained, with high iron and chromium contents, and
- metastable carbides, with a high iron content that precipitated during quenching at 100°C$\cdot$h^{-1}, which dissolve by holding above 575°C, and which actually are a cementite alloyed with chromium.

It clearly appears that the relationship between the content and distribution of these various carbides and the mechanical properties measured (creep and impact strength) is of prime interest for future research. This paper does not claim to establish this close relationship. Moreover, it is not absolutely certain that this study would be interesting to the mechanics specialist. A materials specialist might well have an opposed opinion.

References

[*1*] Newhouse, D. L., "Survey by EPRI of 12 Percent Cr Steels," *Proceedings COST-EPRI Workshop Creep Resistant 9-12 % Cr Steels*, Schaffhausen, Switzerland, 13-14 Oct 1986.

[*2*] Ito, F., Mixazaki, M., and Takeda, Y., "Creep Resistant 9-12% Cr Steels," *Improved 12% Cr Rotor Forgings for Advanced Steam Turbines Proceedings COST-EPRI Workshop*, Schaffhausen, Switzerland, 13-14 Oct 1986.

[*3*] Fujifa, T., Nakavayashi, Y., Suzuki, A., and Hizume, A., An Advanced 12 Cr Steel Rotor for EPDC Wakamatsu's Step 1 COST-EPRI Workshop, 13-14 Oct. Schaffhouse, Schweiz, 1986.

[*4*] Briggs, J. Z. and Parker T. D., *The Super 12 % Cr Steels Climax Molybdenum Company*, New York ed., 1980.

[*5*] AMAX Inc Super 12 % Cr Steels, an Update Climax Molybdenum Company Ref M571-7-82 15 M, July 1982.

[*6*] Moore, T. D., Ed., *Structural Alloys Handbook*, Vol. 2, Battele's Columbus Laboratory, Columbus, OH, 1980.

[*7*] *Metals Handbook*, 9th ed., Vol. 3, American Society for Metals, Metals Park, OH, 1980.

[*8*] Coulon, P. A., "An Optimized 12 % Chromium Steel for High Temperature Rotors," *Proceedings of the First International Conference on Improved Coal-Fired Power Plants EPR2*, 19-21 Nov. Palo Alto, 1986.

[*9*] *Source Book on Materials for Elevated Temperature Applications*, Elihu F. Bradley, Consulting Editor, American Society for Metals, Metals Park, OH, 1979.

[*10*] Nowlin, R. E., Nangia, V. K., and Newhouse, D. L., "Electroslag Refined 12 % Chromium Steel for Rotors," *Proceedings, International Forgemasters Meeting*, Terni, Italy, 6-9 May 1970, pp. 739-757.

[*11*] Rickett, R. L., White, W. F., Walton, C. S., and Butler, J. C., "Isothermal Transformation, Hardening and Tempering of 12 % Chromium Steel," TASM 44, 1952, pp. 138/168.

[*12*] Fugita, T., Sato, T., and Takahashi, N., Effect of Mo and W on Long Term Creep Rupture Strength of 12 % Cr Heat-Resisting Steel containing V, Nb, and B, Tetsu-to-Hagane, 61, 1975.

Ali-Asghar Tavassoli,[1] *Pierre Soulat,*[1] *and André Pineau*[2]

Temper Embrittlement Susceptibility and Toughness of A 508 Class 3 Steel

---

REFERENCE: Tavassoli, A. A., Soulat, P., and Pineau, A., "**Temper Embrittlement Susceptibility and Toughness of A 508 Class 3 Steel,**" *Residual and Unspecified Elements in Steel, ASTM STP 1042,* A. S. Melilli and E. G. Nisbett, Eds., American Society for Testing and Materials, Philadelphia, 1989, pp. 100-113.

ABSTRACT: A correlation has been established between the scatter in Charpy and fracture toughness results of an ASTM Specification for Quenched and Tempered Vacuum-Treated Carbon and Alloy Steel Forgings for Pressure Vessels (A 508-84a) Class 3 (UNS K12042) pressure vessel forging steel and the appearance of intergranular facets on the rupture surfaces of specimens tested at low temperatures. Extent of the intergranular rupture has been found to increase with prolonged aging at 500 to 550°C or following an embrittling treatment known as step cooling. Both intergranular rupture and the resultant increase in ductile to brittle transition temperature were reduced or eliminated by a de-embrittling treatment at temperatures ranging from 630 to 660°C, with optimum results obtained at 640°C. Auger analyses carried out on specimens exhibiting cleavage and intergranular rupture have shown segregation of carbon, molybdenum, sulfur, and, in particular, phosphorus at the grain boundaries.

A statistical analysis based on a local rupture criterion is used to describe the probability of intergranular and cleavage failures. Based on the observations made, the main cause of scatter in low temperature results is concluded to be heterogeneous segregation of impurities in thick sections with a corresponding shift in ductile to brittle transition temperature. A slight increase in austenitization and de-embrittling temperatures is suggested in order to reduce segregation and improve toughness.

KEY WORDS: pressure vessel, forging, plate, pressurized water reactor (PWR), A508-Class 3, A533B, temper embrittlement, residual elements, segregation, cleavage, intergranular, Charpy, toughness, axisymmetric specimens, auger spectroscopy

More recent pressurized water reactor (PWR) vessel designs have incorporated extensive use of large manganese-molybdenum-nickel steel ring forgings [ASTM Specification for Quenched and Tempered Vacuum-Treated Carbon and Alloy Steel Forgings for Pressure Vessels (A 508-84a) Class 3 (UNS K12042)] [*1-4*]. This use is due to the fact that such designs offer a number of advantages over the conventional plate [ASTM Specification for Pressure Vessel Plates, Alloy Steel Quenched and Tempered, Manganese-Molybdenum and Manganese-Molybdenum-Nickel (A 533/A 533M-85b), B] designs. Specifically, the designs allow elimination of longitudinal seam welds, which in turn improves structural integrity and ease of service inspection. However, with increased size of the initial ingot (several hundred tons) and the subsequent slow cooling imposed by thick sections, there comes inevitably the risk of micro and macrosegregation of some elements with an associated variation in mechanical properties [*5-10*]. For instance, the steel's susceptibility to temper embrittlement could increase due to local segregation

---

[1] Manager of Scientific Studies and deputy head of a section, respectively Service de Recherches Métallurgiques Appliquées, Departement de Technologie, DMECN, IRDI, CEN-Saclay, Commissariat a l'Energie Atomique, 91191 Gif sur Yvette, France.

[2] Professor, Centre d'Etudes de l'Ecole des Mines.

and buildup of nonmetallic residual impurities such as phosphorus, arsenic, tin, and antimony at the grain boundaries [*5-12*]. As a result, control of minor and residual element concentrations and their distributions has a significant effect on the mechanical behavior of pressure vessels.

In an earlier work we showed that microsegregation of residual elements, especially phosphorus, was at the origin of the reversible temper embrittlement (RTE) susceptibility of ASTM A 508-84a, Class 3 [*5*]. Also, the phenomenon was shown to be more marked in the coarse-grained simulated heat affected zones and that it could be deliberately accentuated through an embrittling treatment known as step cooling. Its main consequences were reported to be a rise in the ductile to brittle transition temperature (DBTT) along with a change in the low temperature fracture mode from cleavage to intergranular. The reversible nature of the phenomenon RTE was demonstrated by reheating above the critical temperature range (>600°C) and rapidly cooling. This treatment produced a decrease in the DBTT, together with a reversion in the low temperature fracture mode from intergranular to cleavage. For more information on RTE and the effect of various parameters involved, including chemical composition and microstructure, the reader is referred to a recent review carried out by Eyre et al. [*9*].

In the present work we have examined the role of residual elements in a forged vessel steel (ASTM A 508-84a, Class 3) exhibiting significant scatter in Charpy and fracture toughness results.[3] We have paid particular attention to the rupture mode and have discussed the fracture toughness results using a statistical analysis in conjunction with a local criterion for rupture [*13-16*].

Materials and Procedures

Materials

The main material investigated is an ASTM A 508-84a, Class 3 type steel taken from a nozzle cutout of a PWR vessel forging (diameter 1420 mm and thickness 270 mm). Also investigated is a commercial ASTM A 533/A 533M-85b, B, plate, which is a similar type of steel. The nominal chemical composition of the two steels is presented in Table 1. Both steels satisfy the corresponding ASTM specifications and have low residual element concentrations. Local variations of chemical composition, as obtained with emission spectrometry analysis carried out on several specimens and also on through thickness samples, are shown in Table 1. Apart from the arsenic concentration, which may be considered high (260-300 ppm), all other values are within the specified limits and do not exhibit a marked variation.

Heat Treatments

The forged steel was tested in several conditions. They are (see also Fig. 1):

(1) Initial state; austenitized at about 875°C after prior heat treatment at 900-950°C, then quenched in water followed by temper at 630 to 650°C for 5 h 30 min;

(2) Step cooled; an embrittling treatment voluntarily applied to intensify the RTE phenomenon: 1 h at 600°C—15 h at 540°C—24 h at 525°C—48 h at 500°C—72 h at 470°C;

(3) Aged state; 2000 h at 500-550°C;

(4) De-embrittled state; about 1 h at 620 to 660°C followed by rapid cooling; and

(5) Reaustenitized at 900°C.

---

[3] This study is part of an AIEA sponsored program in which a large number of commercial PWR vessel nozzle cutouts have been investigated.

TABLE 1—*Nominal chemical compositions of plate and forging steels as well as local variations in the latter.*

Steel	Composition (wt %)[a]													
	C	S	P	Si	Mn	Ni	Cr	Mo	Cu	V	Sb	Sn	As	Al
Plate (A 533B)	0.23	0.002	0.008	0.23	1.46	0.66	0.03	0.51	0.04	0.002	0.005	0.005	0.019	0.028
Forging (A 508 CL3)	0.15	0.009	0.009	0.24	1.36	0.68	0.24	0.46	0.063	0.008	0.01	0.008	0.022	0.031
Specimens taken from the forging														
504	0.15	0.007	0.009	0.26	1.36	0.76	0.26	0.49	0.066	0.012	≤0.002	0.007	0.024	0.033
505	0.15	0.008	0.009	0.26	1.36	0.76	0.26	0.48	0.066	0.011	≤0.002	0.006	0.024	0.032
(1/4)	0.16	0.007	0.010	0.27	1.37	0.78	0.27	0.49	0.068	0.012	≤0.002	0.007	0.026	0.040
(1/2)	0.16	0.009	0.010	0.27	1.38	0.78	0.27	0.49	0.068	0.012	≤0.002	0.006	0.026	0.037
(3/4)	0.16	0.009	0.010	0.28	1.39	0.79	0.28	0.50	0.069	0.013	≤0.002	0.006	0.026	0.037
610	0.18	0.008	0.011	0.29	1.45	0.81	0.29	0.52	0.072	0.014	≤0.002	0.007	0.030	0.037
618	0.18	0.007	0.011	0.30	1.48	0.83	0.29	0.52	0.073	0.015	≤0.002	0.009	0.031	0.034

[a] $N_2 < 0.009$ and $Cu < 0.073$

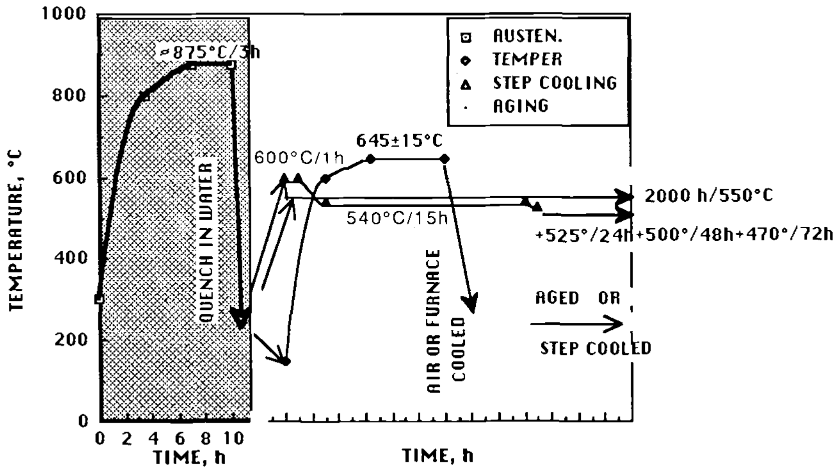

FIG. 1—*Heat treatments applied to A 508 Class 3, except reaustenitization, which was carried out at 900°C.*

The plate material was investigated only in the quenched and step cooled states. The main difference between the two types of product is, apart from their size, a slightly higher austenitization temperature (≈900°C) used for the plate.

Specimens and Mechanical Tests

Two types of specimens were used, standard Charpy V and standard compact tension (CT 25). In addition, a few conventional tensile specimens and axisymmetric notched bars ($\phi = 18$ mm) with different radii (2, 4, and 10 mm) were tested. The main purpose of these tests was to deform plastically a larger volume of the material but also to obtain necessary data used in the local rupture criterion approach. Mechanical tests were carried out at temperatures ranging from +100 to −100°C, but the bulk of tests were performed at −50°C. In general, conventional properties were recorded or calculated after each test. However, instead of K_{IC} we use K_{JC} in order to account for plastic deformation ($P_{max}/P_Q > 1$), of some specimens. K_{JC} was calculated in a similar manner as J.[4]

Fractography

Fractographic observations were carried out using a conventional scanning electron microscope (SEM). Auger electron spectroscopy (AES) analyses were conducted using an ASC 2000 type microscope, Model Riber, operating in differential mode $dN(E)/dE$. The microscope was equipped with a cylindrical mirror analyzer and allowed in situ ion sputtering and high vacuum (2 to 3, 10^{-10} Torr) fracture testing. Primarily, the analysis was restricted to intergranular facets (low toughness specimens), although cleavage facets were also examined for comparison. All the examinations were conducted on small size samples prepared from CT and Charpy specimens and broken inside the microscope, except one Charpy specimen whose fracture surface

---

[4] The terms K_{IC}, K_{JC}, and J are used in fracture mechanics and are usually expressed in MPa$\sqrt{m}$ or KJ/m^2. P_{max} is the maximum (elastic plus plastic) load recorded during tests while P_Q is the maximum elastic load.

was entirely examined as broken in air. In the latter case, about 20 Å of the surface was removed with ion sputtering to eliminate surface contamination.

Results

Figures 2 and 3 show two sets of low temperature Charpy and fracture toughness results obtained with the specimens taken from the forged steel. In both cases the results can be divided into two groups, one that is situated in the normal range and another that is situated in the low toughness range. Fractographic examinations carried out on these specimens revealed that in both situations the low toughness values were associated with appearance of intergranular facets: see for instance Fig. 4. Specimens tested after step cooling also exhibited a scatter in toughness (Fig. 5), but the difference between the two levels was less pronounced. Here also the low values coincided with appearance of intergranular facets. However, the most significant effect of step cooling was a shift of about 20-30°C in DBTT, Fig. 6. Prolonged aging at 550°C also resulted in similar effects, occasionally giving rise to significantly low toughness values ≈ 1,5 *J*.

De-embrittling treatment, carried out before or after step cooling or aging, resulted in restoration of toughness and a net decrease in DBTT (Fig. 6), and in elimination of intergranular facets. Optimum results were obtained after treatment at 640°C, Fig. 7. Furthermore, reaustenitization at 900°C followed by a temper at 640°C gave the forging improved toughness, which remained elevated after step cooling or aging, Table 2. The beneficial effect of reaustenitization at 900°C was such that tempering at a lower temperature (625°C) followed by prolonged aging at 500°C did not induce severe embrittlement as was the case with initial austenitization at 875°C (Table 2).

There was not a significant difference between tensile properties of step cooled and de-embrittled smooth specimens, except a slight increase in yield strength (YS) and ultimate tensile strength (UTS) due to step cooling (Fig. 8). However, some notched specimens exhibited a significant reduction in rupture elongation and average cleavage stress to rupture in the quenched

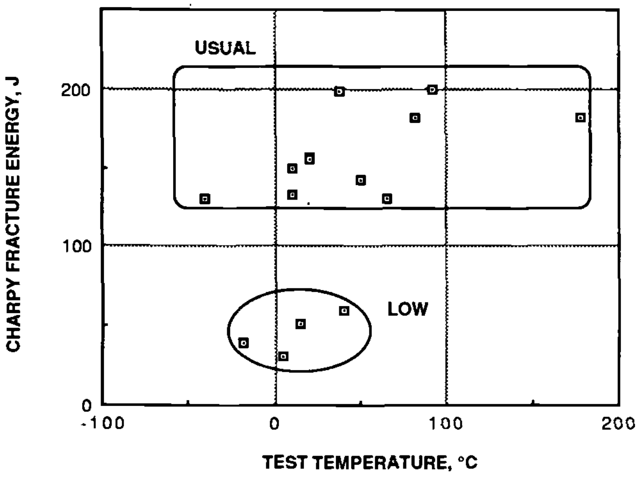

FIG. 2—*Variation of A 508 Class 3 Charpy v notch fracture energy with test temperature showing significant dispersion.*

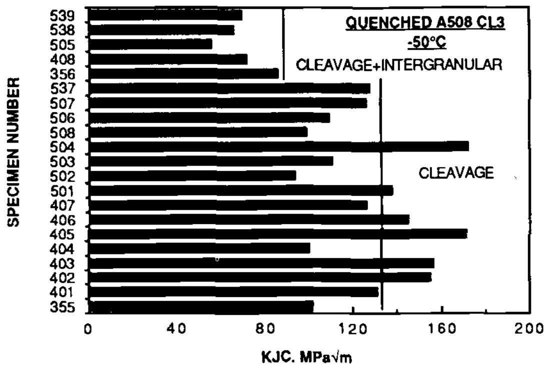

FIG. 3—*Observed scatter in fracture toughness results obtained at* —*50°C.*

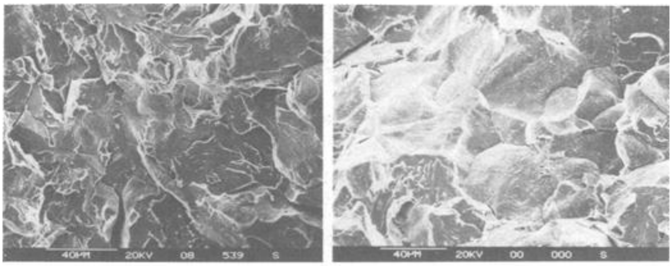

a) As-Received

b) Step-Cooled

FIG. 4—*Fractographic aspects of rupture at* —*50°C, showing* (a) *presence of intergranular facets in a quenched specimen exhibiting low toughness and* (b) *higher density of intergranular facets in a step cooled specimen.*

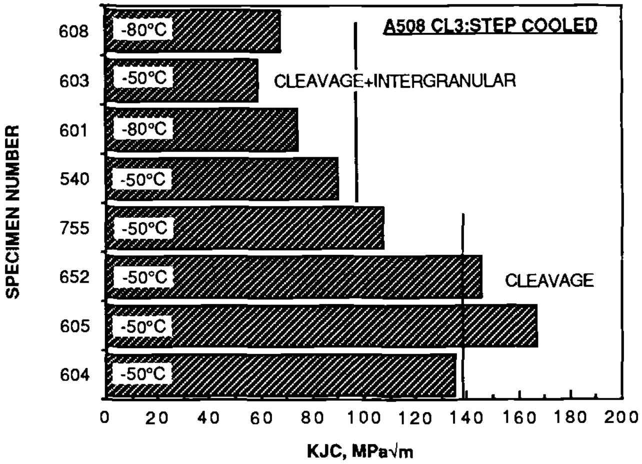

FIG. 5—*Scatter is shown in results following step cooling with low toughness values corresponding to specimens exhibiting intergranular facets.*

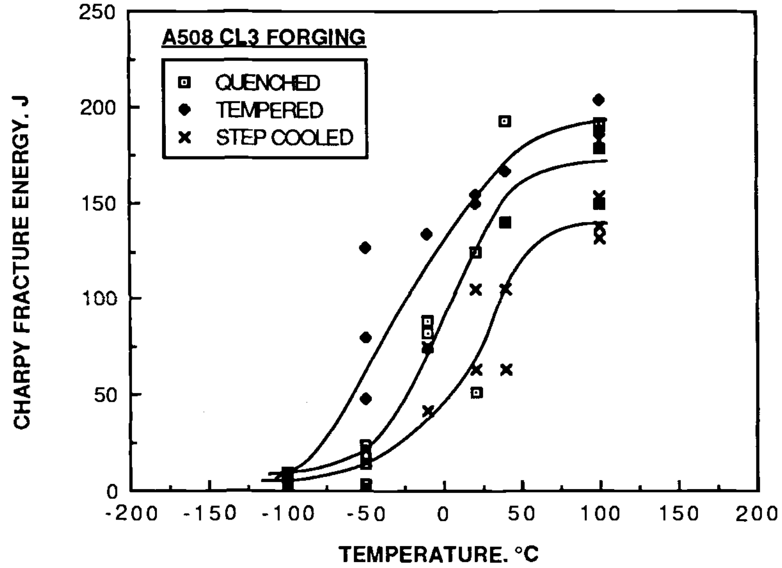

FIG. 6—*Charpy transition curves obtained for A 508 Class 3 specimens tested in the as-received, step cooled and de-embrittled conditions.*

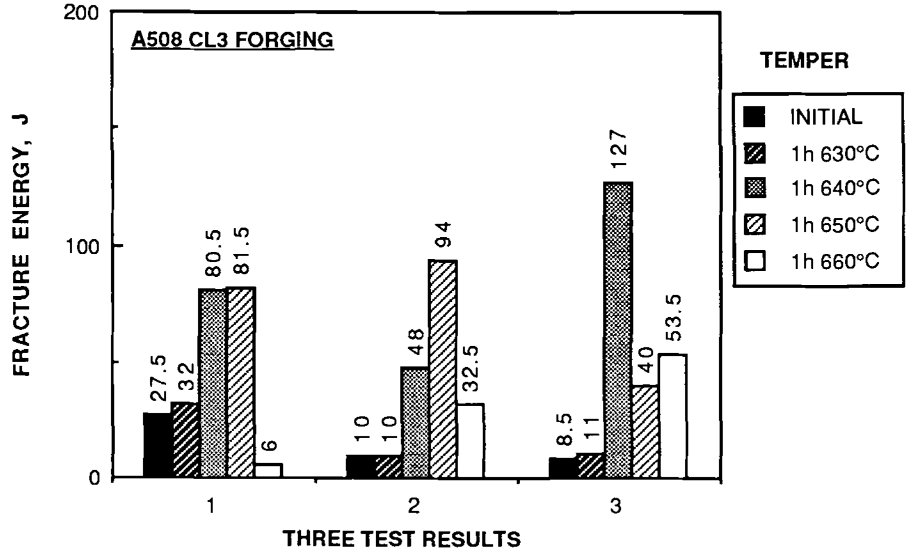

FIG. 7—*Effect of de-embrittling temperature on Charpy toughness of forged steel.*

and embrittled conditions, Table 3. A 533/A 533M-85b, B plate steel in general exhibited a superior toughness at −50°C than A 508-84a, Class 3 forging and was less sensitive to embrittlement, Table 4.

Auger analyses showed traces of carbon, oxygen, chlorine (probably due to contamination), and molybdenum on the fracture surfaces, but most of all they showed a significant segregation

TABLE 2—*Effect of reaustenitization and temper on fracture toughness of A 508-Class 3 forging.*

Specimen	Temperature, °C	K_{JC} (MPa)	Heat Treatment
607	−50	265	reaustenitized at 900°C → quenched in oil → tempered at 640°C → step-cooled.
606	−50	320	
752	−50	127.3	reaustenitized at 900°C → quenched in oil → tempered at 625°C → aged 2000 h at 500°C.
758	−50	139.7	
755	−50	103	
753	−50	130.5	

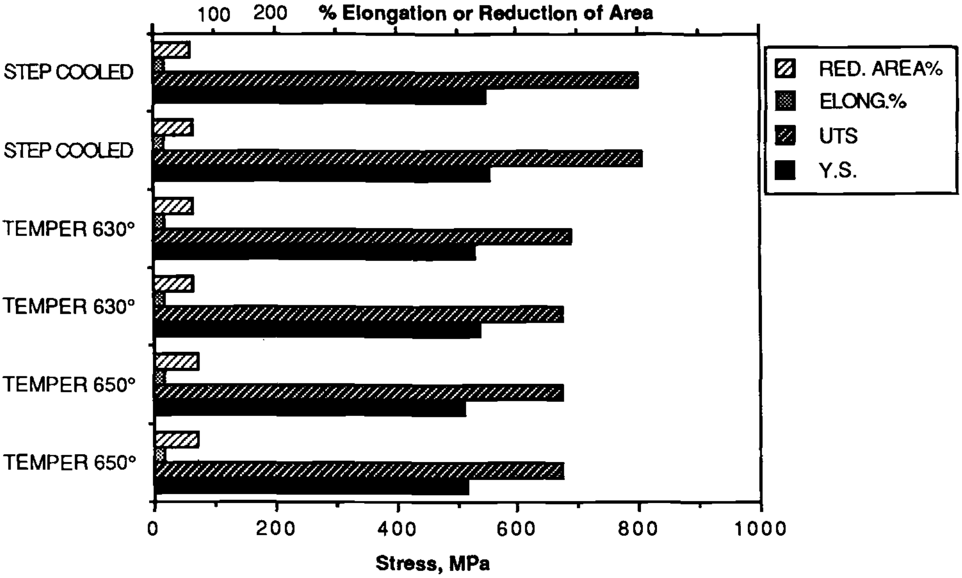

FIG. 8—*Tensile properties in de-embrittled and step cooled conditions.*

of phosphorus in the zones exhibiting intergranular rupture (Fig. 9). Traces of sulfur were also detected on the surface of the specimen broken in air. These traces did not disappear until sputtering was repeated for several hundred Å. In this case also the segregation was more pronounced at the grain boundaries than at the cleavage facets. For instance, the average ratio of S(152 eV)/Fe(631 eV) peak at the grain boundaries were on the order of three times higher than those at the cleavage facets.

Discussion

A simplified explanation to the observed large differences in toughness values of A 508-84a, Class 3 specimens can be given in terms of local variations in transition curves and the changing mode of rupture. Indeed, Charpy specimens taken from regions with more pronounced segregation had a higher DBTT and, therefore, when tested at −50°C broke mainly, if not fully, in fragile mode. This was also confirmed by fracture toughness results where K_{IC} was valid ($K_{IC} \approx K_{JC}$ that is $P_{max}/P_Q \approx 1$). Charpy specimens taken from regions with less segregation had a

TABLE 3—*Effect of step cooling on average stress and strain to rupture, as well as the critical fracture stress, of notched axisymmetrical specimens.*

Notch/Specimen	Temperature, °C	σ_R MPa	Σ%	σ_c MPa	σ_c (corrected) MPa
2 mm (quenched)	−50	1384	41	1633	1330
2 mm/530	−50	1261	27.9	1488	1294
2 mm/528	−50	1156	32.5	1364	1162
4 mm/531	−50	1150	44.3	1426	1142
4 mm/609	−50	1219	28.5	1512	1310
4 mm/611	−50	1210	30.6	1504	1287
4 mm/613	−50	1209	31.1	1499	1284
4 mm/614	−50	1293	16.7	1603	1475
4 mm/612	−50	1235	17.3	1531	1405
4 mm (quenched)	−80	1283	23.1	1591	1418
4 mm (quenched)	−80	1213	14.5	1504	1400
4 mm/536	−80	1281	26.5	1588	1391
4 mm/618	−80	1186	15.8	1470	1358
4 mm/610	−80	1209	21.7	1499	1345

TABLE 4—*Comparison between Charpy V toughness of forged and plate steel at −50°C.*

Condition	Forged (*J*)	Plate (*J*)
As-received (quenched)	27.5	33
	10	24
	8.5	15
Step cooled	24	28
	14	38
	3	46
De-embrittled (1 h at 640°C)	80.5	
	48	
	128	

lower DBTT and therefore when tested at −50°C broke with some plastic deformation. Likewise for these specimens $K_{IC} < K_{JC}$ ($P_{max}/P_Q > 1$). On this basis one may assume that if tests were carried out at higher or lower temperatures than −50°C (more precisely in the upper and in the lower shelves), the above mentioned scatter will disappear.

In practice, some segregation is likely to occur in large ingots and thick sections, although its extent can be reduced by faster cooling, or using slightly higher austenitization and de-embrittling temperatures. Therefore, one would like to predict the probability of brittle fracture independent of its nature, being inter or transgranular. Below we apply Weibull's statistical analysis to our fracture toughness data after a brief review of Beremin's local criterion for failure [*13*].

The notion of critical cleavage stress (see review in [*17*]) was first proposed by Griffith

$$\sigma_c = \sqrt{\frac{2E\gamma}{\pi(1 - \nu^2)l_0}}$$

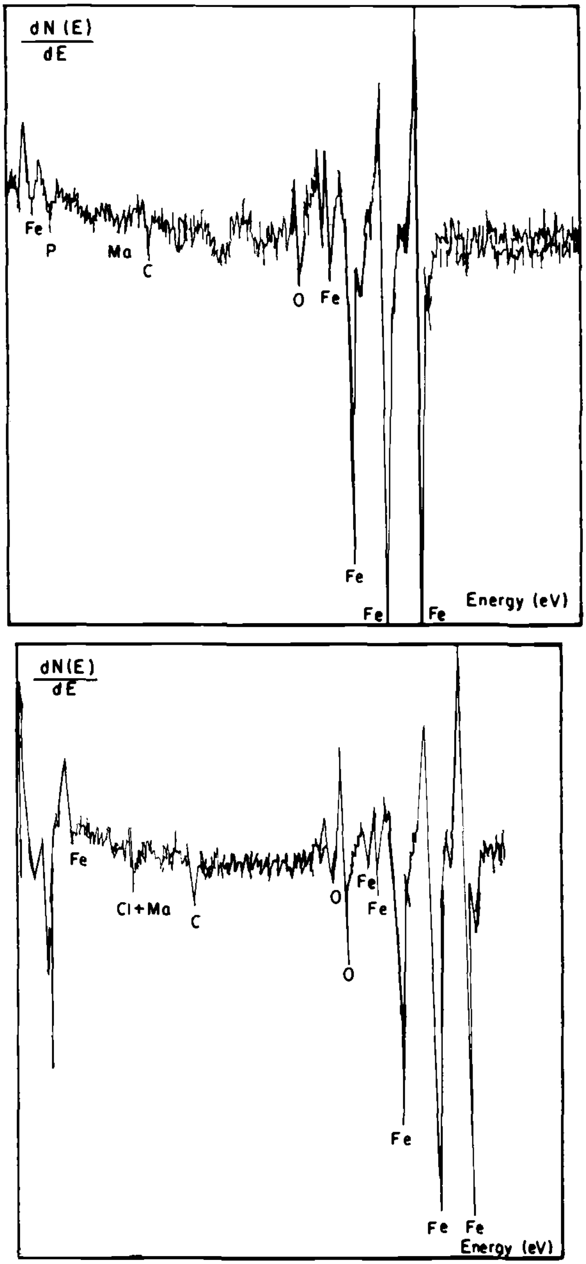

FIG. 9—*Auger electron spectroscopy results showing segregation of* P *at the grain boundaries (above) as compared with cleavage facets (below).*

Here E is Young's modulus, γ surface energy, ν poisson's ratio, and l_0 length of a microcrack, considered to be coherent with metallurgical features (grains or carbides). Later on, Knott [*18*] and Tetelman [*19*] calculated σ_c using the slip line field theory. Ritchie, Knott, and Rice [*20*] subsequently predicted K_{IC} values by assuming that the critical stress is reached at a distance of λ_o from the fissure.

Finally, the local rupture criterion approach was developed in which λ_o was replaced by volume analysis. In this approach the stressed volume of the metal V is divided into smaller volumes V_0, chosen to be on the order of several grains. The probability of failure P_R of the volume V is defined as that of one of the smaller volumes V_0. In its simplified form the expression derived is [*13*]

$$P_R = 1 - \exp - \left[\frac{\sigma_w}{\sigma_u}\right]^m$$

where σ_w is Weibull's stress[5] and σ_u a material constant found to vary with grain size. One can see that the probability of rupture will be = 63% when σ_w reaches σ_u. A similar equation has been proposed by Beremin [*13*] with σ_w and σ_u being replaced by toughness values.

We have used as a first approximation Beremin's proposed equation for cleavage fracture of nuclear pressure vessel steel. The results obtained are presented in Fig. 10. Here, the curve predicting the probability of cleavage fracture (P_R) is given by

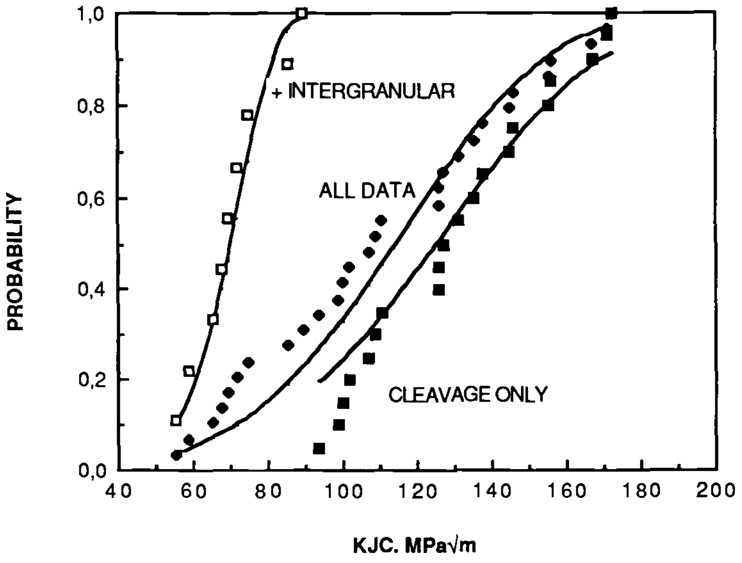

FIG. 10—*Experimental data presented in terms of cumulative probability to failure as a function of* K_{JC} *and compared with predicted curves derived for all data and separated data according to their mode of rupture.*

---

[5] Weibull's stress is calculated through finite element analysis and its main variables are deformation and maximum principal stress in each V_0.

$$P_R = 1 - \exp - \left[\frac{K_{JC}}{K_u}\right]^4$$

where K_u is the material's constant and it depends on the temperature and represents a rupture probability of 63%. Experimental points corresponding to the 29 fracture toughness tests carried out at −50°C are also shown in this figure. The probabilities of these tests are assumed to be 1/29 for the lowest toughness value . . . and 29/29 for highest toughness value.

In the above equation, the K_u value that fit best with the experimental data was found to be 125.3 MPa$\sqrt{m}$. However, as shown in Fig. 10, the theoretical curve obtained provides a good prediction of results in the upper region but fails to follow low K_{JC} values. For this reason we then divided our results into two groups according to their mode of rupture and determined the equation's exponent for each set of data through the least square analysis method [log(1/1 − P_R) versus K_{JC}].

Although the number of tests with intergranular facets are small (nine tests), the results are satisfactorily represented with an exponent of 8 (Fig. 10)

$$P_R^I = 1 - \exp\left(\frac{K_{JC}}{K_{uI}}\right)^8$$

K_{uI} is calculated to be about 73 MPa$\sqrt{m}$. Likewise, the 20 tests with cleavage facets can be represented with an exponent of 4

$$P_R^C = 1 - \exp\left(\frac{K_{JC}}{K_{uC}}\right)^4$$

but with K_{uC} = 137 MPa$\sqrt{m}$. Finally, one may combine the two equations to represent the probability of rupture in all the population

$$P_R = 1 - \left[\lambda_I \exp - \left(\frac{K_{JC}}{K_{uI}}\right)^8 + (1 - \lambda_I)\left(\frac{K_{JC}}{K_{uC}}\right)^4\right]$$

In this equation $\lambda_I = 9/29 = 0.31$. The equation derived is similar to that of Service et al. [*21*], which has been used for analyzing brittle fracture of ceramic materials with two types of defects. However, in our case this assumes that only one of the two modes of rupture, intergranular or cleavage, occurs at one time, while in most cases both modes could occur simultaneously.

Conclusions

Foregoing results clearly demonstrate that the principal cause of the scatter in toughness of the forged steel is local variations in DBTT with a change in low temperature rupture mode from cleavage to intergranular. The mechanism involved is reversible temper embrittlement caused by heterogeneous segregation of residual elements, in particular *P*, at the grain boundaries. A slight increase in the austenitization temperature, from 875 to 900°C, or the de-embrittling temperature, from about 630 to 640°C, or both, can significantly reduce temper embrittlement susceptibility of the steel and consequently reduce variations in toughness.

Acknowledgments

We would like to express our appreciation to P. Juliet, DCAEA-SEA Grenoble, for AES and M. Al Mundheri for the majority of experimental data used in this work.

References

[1] Kawaguchi, S., Tsukada, H., Suzuki, K., Sato, I., and Onodera, S., "Manufacturing of Large and Integral Type Steel Forgings for Nuclear Steam Supply System Components," in *Steel Forgings, ASTM STP 903*, E. G. Nisbett and A. Melilli, Eds., American Society for Testing and Materials, Philadelphia, 1984, p. 398.

[2] Martin, A., Widart, J., and Scailteur, A., *Nuclear Engineering*, Vol. 22, No. 262, 1977, p. 74.

[3] Bocquet, P. G., Saint-Ignan, J-C., and Blondeau, R. P., "Application of New Types of Ingots to the Manufacturing of Heavy Pressure Vessel Forgings," in *Steel Forgings, ASTM STP 903*, E. G. Nisbett and A. Melilli, Eds., American Society for Testing and Materials, Philadelphia, 1984, p. 367.

[4] Bernard, J. L., Houssin, B., and Slama, G., "Validation des Caractéristiques de Calcul des Matériaux Constituant le Circuit Primaire des Réacteurs a Eau Sous Pression," in *Reliability Problems of Reactor Pressure Components*, IAEA-SM-218/13, 1978, p. 251.

[5] Tavassoli, A. A., Bougault, A., and Bisson, A., "The Effect of Residual Impurities on the Temper Embrittlement Susceptibility of Large A508 CL3 Vessel Forging," in *Proceedings of the International Conference on the Effect of Residual, Impurity and Micro-Alloying Elements on Weldability and Weld Properties*. Welding Institute, London, Nov. 1983.

[6] Druce, S. G., Gage, G., and Jordan, G., "The Effect of Long Term Thermal Aging on the Mechanical Properties of ASTM A533B and A508 Steels in the Quenched and Tempered and Simulated Heat Affected Zone Conditions," Report AERE-R 11459, UKAEA Harwell, April 1985.

[7] Druce, S. G., Gage, G., Jordan, G., and Hudson, J. A. "Effect of Thermal Aging on the Mechanical Properties of PWR Pressure Vessel Steels and Weldments," Report AERE-R 11460, UKAEA Harwell, April 1985.

[8] Druce, S. G., "Investigation of the Homogeneity of Chemical Composition and Mechanical Properties in a Large A508 Class 3 Steel Pressure Vessel Forging," Report AERE-R 9581, UKAEA Harwell, September 1979.

[9] Eyre, B. L., Edwards, B. C., and Titchmarsh, J. M., "Physical Metallurgy of Reversible Temper Embrittlement," in *Advances in the Physical Metallurgy and Applications of Steels*, The Metals Society, London, 1982, p. 246.

[10] Al Mundheri, M., "Approches Globale et Locale de la Rupture Fragile et Ductile d'Aciers Faiblement Allieés (16 MND 5), Influence de l'Irradiation," D.E.S. thesis, Université de Paris-Sud, Centre Orsay, France, 1986.

[11] Yu, J. and McMahon, C. J., Jr., *Metallurgical Transactions, A*, Vol. 11A, No. 2, 1980, p. 277.

[12] Guttmann, M., Dumoulin, Ph., and Wagman, M., *Metallurgical Transactions, A*, Vol. 13A, 1982, p. 1693.

[13] Beremin, F. M., *Metallurgical Transactions*, Vol. 14A, 1983, p. 2277.

[14] Al Mundheri, M., Soulat, P., and Pineau, A., "Rupture Fragile et Ductile de l'Acier 16MND5 Effet de l'Irradiation" at *Proceedings of the Seminar International sur l'Approche Locale de la Rupture*, M. Donati, Ed., Carto-Chris, Paris, 1987, p. 243.

[15] Mudry, F., "Local approach to cleavage fracture," *Proceedings of the International sur l'Approche Locale de la Rupture*, M. Donati, Ed., Carto-Chris, Paris, 1987, p. 165.

[16] Weibull, F., *Ing. Vetenskap Akad. Handl.*, Vol. 12, 1939, p. 153.

[17] Pineau, A., *Proceedings of the 5th International Conference on Fracture*, Vol. 2, D. François, Ed., Pergamon Press, Oxford 1982, p. 533.

[18] Knott, J. F., *Journal of Mechanics and Physics of Solids*, Vol. 15, 1967, p. 97.

[19] Wilshaw, T. R., Rau, C. R. and Tetelman, A. S., *Engineering Fracture Mechanics 1*, 1968, p. 147.

[20] Richie, R. O., Knott, J. F. and Rice, J. R., *Journal of Mechanics and Physics of Solids*, Vol. 21, 1973, p. 395.

[21] Service, T. H., Ritter, J. E., Karl Jakus, J. R., and D. Sonderman, *American Ceramic Society Bulletin*, Vol. 64, No. 9, 1985, p. 1276.

DISCUSSION

R. Blondeau[1] *(written discussion)*—I am not sure that your proposal of changing the tempering temperature from 630°C to 640°C will be a good one. The industrial furnaces in which the shells are treated cannot have the precision of a laboratory furnace on all points. And, you show that a 650°C tempering will be detrimental, due possibly to all other embrittling phenomena, which is irreversible, and worse.

A. A. Tavassoli (author's response)—We agree with Mr. Blondeau's remark that temperature control in industrial furnaces is more difficult than in laboratory furnaces. Our proposal is also intended to guide the furnace operator during his temperature setting. For instance, that means that 630°C+ is better than 630°C−.

R. L. Bodnar[2] *(written discussion)*—You indicated that the toughness of A 508-84a Class 3 forgings could be increased by raising the austenitizing temperature from 875 to 900°C, thereby increasing the degree of homogenization (eliminating the microsegregation regions) and suppressing temper embrittlement in the steel. I have an alternative recommendation. I would increase the normalizing temperature or time of the preliminary heat treatment or both to improve homogenization. I would also maintain the lower austenitizing temperature of 875°C to refine the prior austenite grain size, which would be expected to further enhance toughness.

A. A. Tavassoli (author's response)—Mr. Bodnar's suggestion is in line with our findings that improved homogenization reduces the risk of temper embrittlement. We agree that it is preferable, when possible, to achieve this through improved intermediate heat treatment. However, it should be recalled that the actual prior heat treatment temperature used in industry is higher than the final heat treatment (875°C) and is between 900 and 950°C.

W. R. Warke[3] *(written discussion)*—The onset of temper embrittlement susceptibility of 2¼Cr-1Mo pressure vessel steels has been successfully related to a factor attributed to Watanabe

$$J = (\mathrm{Mn} + \mathrm{Si})(\mathrm{P} + \mathrm{Sn}) \times 10^4$$

This factor reflects the observation that manganese promotes phosphorus segregation. In view of the high manganese content of your steels, I wonder if this factor or a similar one, could be used to correlate your data.

A. A. Tavassoli (author's response)—In order to be able to correlate J values with variations in manganese, silicon, and tin contents, a large number of test data obtained from several heats are needed, which we do not have. To answer the question, we can add that the current manganese specification for A 508-84a Class 3 steel is between 1.12 and 1.58% and the steel used in our investigation has about 1.36% manganese. Furthermore, the plate material that is used in our study has 1.46% manganese and is less sensitive to temper embrittlement than the forged material.

[1] Head, Materials Research Center, Creusot-Loire Industrie, Le Creusot F.71202, France.

[2] Bethlehem Steel Corporation, Building G, Homer Research Laboratories, Bethlehem, PA 18016.

[3] Amoco Corporation, P.O. Box 400, Naperville, IL 60566.

Edward G. Nisbett[1]

The Effect of Residual Elements on the Tensile Strength of Heavy Carbon Steel Forgings, Heat Treated for Optimum Notch Toughness

REFERENCE: Nisbett, E. G., **"The Effect of Residual Elements on the Tensile Strength of Heavy Carbon Steel Forgings, Heat Treated for Optimum Notch Toughness,"** *Residual and Unspecified Elements in Steel, ASTM STP 1042,* A. S. Melilli and E. G. Nisbett, Eds., American Society for Testing and Materials, Philadelphia, 1989, pp. 114-123.

ABSTRACT: Residual elements are shown to have influenced the tensile strength of large, heavy section carbon steel forgings that had been heat treated for optimum Charpy V notch properties. The forgings had been made to a specification based on an early revision of ASTM Specification for Forgings, Carbon Steel, for Pressure Vessel Components (A 266-84a, UNS K035 06), but with several provisions of the more modern ASTM Specification for Quenched and Tempered Vacuum-Treated Carbon and Alloy Steel Forgings for Pressure Vessels (A 508-84a, UNS K13502). While not a factor in the particular contract described, the results are also discussed in terms of the use of carbon equivalency in the composition control of forgings for weldability purposes.

KEY WORDS: carbon steel forgings, inter-critical heat treatment, carbon equivalent, negative carbon segregation

A series of large pressure vessel forgings, each consisting of a cylindrical shell with an integral flange, was produced to a proprietary specification, which although originally based on ASTM Specification for Forgings, Carbon Steel, for Pressure Vessel Components (A 266-84a) Class 2 (UNS K03506), actually bore closer relationship to ASTM Specification for Quenched and Tempered Vacuum-Treated Carbon and Alloy Steel Forgings for Pressure Vessels (A 508-84a), Class 1 (UNS K13502), particularly in terms of heat treatment, mechanical test location, and the need for Charpy V notch impact testing, as well as nondestructive examination.

The steel was made by the basic electric furnace process, with vacuum stream degassing. The use of aluminum for grain refining purposes was specifically denied by the specification, but a small maximum level of vanadium was permitted, as shown in Table 1.

The forging size, as machined for heat treatment, is shown in Fig. 1, and had a heat treated weight of 21 273 kg, (46 900 lb). Each forging was upset forged from a big end up forging ingot with a diameter of 2110 mm, (83 in.) and a gross weight of 80 250 kg, (177 000 lb). The mechanical test locations for the flange and shell test areas are shown in Fig. 2.

The melt aim analysis for the steel was intended to optimize the carbon to manganese ratio to improve notch toughness such that a low carbon level would be matched with manganese towards the permitted maximum. Some advantage was also taken of the relatively high maximum limits allowed for nickel, chromium, and molybdenum so that these elements in the first heats could not be described as residuals. As previously mentioned, vanadium was also added within the maximum limit of 0.05% for the product analysis. The melt aim analysis is shown in Table

---

[1] Consultant, 1262 Conewango Ave., Warren, PA 16365.

TABLE 1—*Chemical composition, ordered limits, aim chemistry, and comparable ASTM specifications.*

Specification	C max	Mn	P max	S max	Si	Ni max	Cr max	Mo max	V max	Cu max	UTS, MPa (ksi)	Yield min, MPa (ksi)	%*E* 50 mm (2 in.)	%RA, min	Min Charpy-V Notch, J (ft · lb) @ −12°C (10°F)
Order	0.35	0.40/0.90	0.025	0.025	0.15/0.35	0.45	0.35	0.15	0.05	0.25	485/655 (70/90)	240 (35)	20	38	20 (15) Avg. 13.5 (10) min
Melt Aim	0.25	0.80	0.015	0.015	0.20	0.35	0.25	0.10	0.03	0.10					
ASTM A 266-69	0.35	0.40/0.90	0.040	0.040	0.15/0.35	. . .	. . .	. . .	. . .	. . .	min 485 (70)	240 (35)	20	33	. . .
A 266-85 With S12	0.35	0.40/0.90	0.040	0.400	0.15/0.35	0.25	0.20	0.10	. . .	. . .	485/655 (70/95)	250 (36)	20	33	. . .
A 508/ A 508M-86	0.35	0.40/1.05	0.025	0.025	0.15/0.35	0.40	0.25	0.10	0.05	. . .	485/655 (70/90)	250 (36)	20	38	20 (15) av @ 4.4°C (40°F)

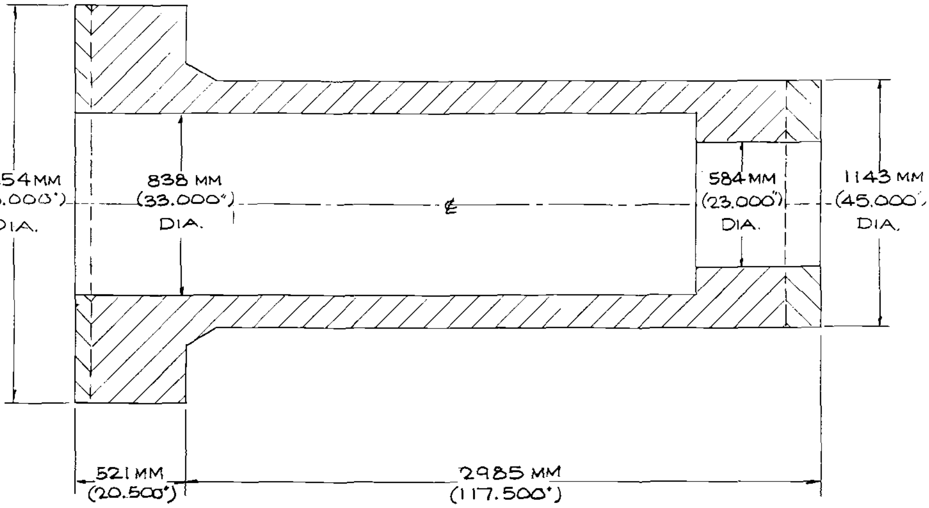

FIG. 1—*Sketch of the heat treatment configuration used for the forgings. Prolongations for mechanical testing were provided at both ends.*

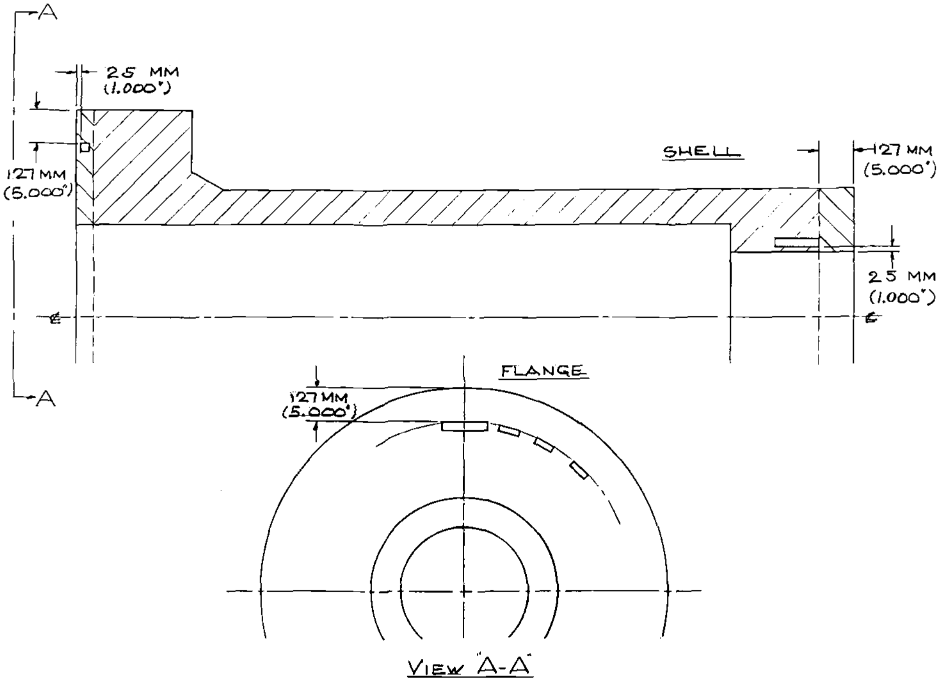

FIG. 2—*Mechanical test specimen locations and orientation in the heat treated forgings. Note the tangential orientation at the flange and axial direction for the shell.*

1, together with the specification ranges, mechanical properties, and, for reference, the composition limits for ASTM A 266-84a, Class 2, and A 508-84a, Class 1.

Heat Treatment

The chosen heat treatment, consisting of normalizing, double quenching, and tempering, followed the inter-critical heat treatment cycle, which had been shown [*1,2*] to enhance the Charpy V Notch absorbed energy by grain refinement. Details of the actual cycle used were as follows:

(1) Normalize, 915°C (1680°F);
(2) Austenitize, 843°C (1550°F);
(3) Water quench;
(4) Austenitize, 793°C (1460°F);
(5) Water quench;
(6) Temper, 638°C (1180°F); and
(7) Air-cool.

The minimum tempering temperature was 593°C (1100°F), and when later in the program some low tensile results were obtained, a reduction in the tempering temperature was tried. No significant improvement in the tension test results were noted in material tempered at 593°C (1100°F) as compared with the results obtained after tempering at 638°C (1180°F).

Mechanical Property Test Results

The mechanical property test results for eight forgings are shown in Table 2, together with the calculated carbon equivalent[2] and the grain size. The heat and product analyses for each forging are given in Table 3. As shown in Fig. 2 the test specimens from the shell end were located 25 mm (1 in.) off the bore, 125 mm (5 in.) from the end face, and oriented in the axial direction. For the flange location the specimens were taken 25 mm (1 in.) from the end face, and 125 mm (5 in.) radially from the outside diameter of the flange. These test specimens were oriented in the tangential direction to the flange. Thus for each test area, the test specimens were oriented parallel to the direction of maximum working during forging.

The effect of carbon content on the ultimate tensile strength of Forgings 1 through 6, inclusive, can be seen in Table 3 through the negative carbon segregation influence at the shell end of each forging. The nickel, chromium, and molybdenum levels for these first six forgings were fairly close to the aim levels. Vanadium, although present, was generally no higher than 0.04%, and probably had little effect on strength.

A cost savings measure was instituted for the next two forgings, 7 and 8, when the intercritical heat treatment cycle was confirmed to be effective in obtaining the required Charpy V notch impact levels. This measure involved removing the lower limits for nickel, chromium, and molybdenum, thus making these elements true residuals. The results of this move were surprising in terms of the low values obtained for these elements, and disturbing for the effect on the tensile strength, which in some tests fell below the minimum of 485 MPa (70 ksi). The Charpy V notch absorbed energy was not noticeably affected by the low levels of these elements.

A final forging, Forging 9, made to higher carbon limits, and with the minimum level restored for the residuals, gave appreciably higher tensile strength with a very slight loss in impact properties.

---

[2] ASTM Specification for General Requirements for Steel Plates for Pressure Vessels (A 20/A 20M-86a), Supplementary Requirement S20. Maximum Carbon Equivalent for Weldability. *Annual Book of ASTM Standards.* Volume 01.04.

TABLE 2—*Tension and impact test results from the prescribed test locations for the flange and shell ends of the forgings, with calculated carbon equivalents based on product analyses from each test prolongation.*

Forging Location	UTS, MPa (ksi)	(.2%) Yield, MPa (ksi)	%E (54 mm)	%RA	Charpy V Notch @ −12°C (10°F), J (Ft · Lb)	C_{eq}, %[a]	Grain Size
Required	485-655 (70-90)	250 min (36 min)	20	33	20 ave min 13.5 min single) (15 ave 10 min single)		ASTM 5 min
1 Flange	517 (75)	362 (52.5)	27	60.1	76 (56); 52 (38); 68 (50)	0.48	10/12
1 Shell	501 (72.7)	356 (51.6)	33.5	72.3	165 (122); 266 (196); 80 (59)	0.43	9/12
2 Flange	508 (73.7)	349 (50.6)	33	66.6	56 (41.5); 68 (50); 125 (92)	0.48	10/12
2 Shell	493 (71.5)	345 (50)	33.5	71.6	155 (114); 130 (96); 180 (133)	0.44	10/12
3 Flange	500 (72.6)	360 (52.2)	30.5	63.4	142 (105); 125 (92); 100 (73)	0.50	10/12
2 Shell	501 (72.7)	352 (51.1)	33	68.4	205 (151); 159 (117); 266 (196)	0.45	10/12
4 Flange	503 (73)	359 (52)	32	67	89 (66); 31 (23); 44 (32.5)	0.43	8/10
4 Shell	484 (70.2)	328 (47.6)	34.5	71.5	140 (103); 174 (128); 159 (117)	0.40	10/12
5 Flange	517 (75)	361 (52.3)	32	69.5	75 (55); 87 (64); 85 (62.5)	0.44	9/11
5 Shell	487 (70.6)	323 (46.9)	28.5	71.3	72 (53); 42 (31); 32 (23.5)	0.41	8/10
6 Flange	507 (73.6)	346 (50.2)	30.5	64.5	77 (57); 35 (25.5); 68 (50)	0.44	8/10
6 Shell	474 (68.8)	325 (47.1)	34	69.2	127 (94); 182 (134); 152 (112)	0.38	8/10
7 Flange	466 (67.6)	304 (44.1)	35.5	70.8	57 (42); 80 (59); 49 (36)	0.39	7/8
7 Shell	452 (65.6)	283 (41)	36.5	73.9	188 (139); 83 (61.5); 54 (40)	0.40	7/8
8 Flange	507 (73.6)	310 (45)	33.5	64	42 (31); 27 (20); 33 (24)	0.47	8/10
8 Shell	465 (67.5)	276 (40)	38.5	72.3	88 (65); 85 (62.5); 77 (57)	0.41	8/10
9 Flange	579 (84)	405 (62.5)	29	65.6	41 (30); 65 (48); 53 (39)	0.55	8/10
9 Shell	534 (77.5)	364 (52.8)	33	67.9	95 (70); 161 (118.5); 106 (78)	0.52	8/10

[a] C_{eq} is Carbon Equivalent.

TABLE 3—*Heat analyses and product analyses from each forging in the study.*

Forging	C	Mn	P	S	Si	Ni	Cr	Mo	V	Cu	C Equivalent[a]
1 Heat	0.25	0.69	0.009	0.012	0.20	0.31	0.15	0.11	0.03	0.09	0.45
1 Shell	0.23	0.68	0.007	0.009	0.20	0.40	0.17	0.10	0.02	0.08	0.43
1 Flange	0.27	0.73	0.009	0.011	0.20	0.38	0.17	0.10	0.01	0.08	0.48
2 Heat	0.25	0.73	0.011	0.006	0.24	0.34	0.27	0.11	0.05	0.07	0.49
2 Shell	0.22	0.69	0.009	0.007	0.22	0.37	0.26	0.09	0.03	0.04	0.44
2 Flange	0.24	0.76	0.011	0.009	0.21	0.41	0.27	0.10	0.02	0.05	0.48
3 Heat	0.24	0.80	0.013	0.012	0.19	0.33	0.27	0.08	0.04	0.06	0.48
3 Shell	0.22	0.78	0.011	0.013	0.17	0.37	0.26	0.08	0.01	0.04	0.45
3 Flange	0.25	0.84	0.011	0.013	0.20	0.36	0.28	0.10	0.02	0.05	0.50
4 Heat	0.25	0.68	0.015	0.014	0.27	0.37	0.22	0.08	0.03	0.08	0.47
4 Shell	0.20	0.70	0.012	0.011	0.28	0.31	0.20	0.09	0.01	0.05	0.40
4 Flange	0.23	0.71	0.013	0.013	0.29	0.33	0.19	0.09	0.01	0.06	0.43
5 Heat	0.25	0.68	0.012	0.014	0.34	0.35	0.25	0.09	0.03	0.09	0.47
5 Shell	0.22	0.66	0.009	0.012	0.30	0.30	0.21	0.07	0.01	0.06	0.41
5 Flange	0.25	0.65	0.010	0.013	0.30	0.30	0.21	0.07	0.01	0.06	0.44
6 Heat	0.26	0.71	0.011	0.012	0.30	0.35	0.24	0.08	0.03	0.13	0.48
6 Shell	0.19	0.64	0.008	0.006	0.25	0.28	0.22	0.06	0.03	0.10	0.38
6 Flange	0.24	0.66	0.009	0.009	0.29	0.33	0.23	0.07	0.01	0.11	0.44
7 Heat	0.25	0.69	0.012	0.014	0.30	0.10	0.12	0.01	0.04	0.07	0.41
7 Shell	0.23	0.79	0.014	0.013	0.26	0.10	0.09	0.03	0.03	0.07	0.40
7 Flange	0.24	0.65	0.014	0.013	0.25	0.11	0.07	0.03	0.04	0.07	0.39
8 Heat	0.29	0.78	0.009	0.013	0.27	0.09	0.09	0.02	0.03	0.07	0.45
8 Shell	0.24	0.82	0.010	0.011	0.27	0.08	0.07	0.03	0.04	0.07	0.41
8 Flange	0.29	0.86	0.011	0.013	0.29	0.09	0.08	0.03	0.04	0.08	0.47
9 Heat	0.31	0.87	0.008	0.012	0.23	0.36	0.29	0.09	0.02	0.07	0.56
9 Shell	0.27	0.87	0.013	0.009	0.20	0.37	0.24	0.10	0.02	0.06	0.52
9 Flange	0.30	0.87	0.013	0.010	0.21	0.38	0.24	0.10	0.02	0.06	0.55

[a] Carbon Equivalent $= \%C + \frac{\%Mn}{6} + \frac{\%Cr + \%Mo + \%V}{5} + \frac{\%Ni + \%Cu}{15}$

To investigate the influence of test specimen location in one of the low tensile strength forgings, an additional series of tests was performed at the shell end test prolongation of Forging 6. These were located near the outer surface, at mid-wall, and at the quarter wall thickness as measured from the bore. Some test specimens were given a simulated stress relief, and others were heat treated. The results are shown in Table 4 together with checks on the carbon and manganese contents at each location. Apart from the lower tensile and yield strength values for the stress relieved 1/4 wall test, the ultimate tensile strength results appeared to be influenced more by carbon variation than by distance from the quenched surfaces.

Carbon Equivalent

A formula commonly used for the calculation of the carbon equivalent for carbon and low alloy steels in some material specifications[2] is as follows

$$C_{eq} = \%C + \frac{Mn}{6} + \frac{\%Cr + \%Mo + \%V}{5} + \frac{\%Ni + \%Cu}{15}$$

Using this formula the carbon equivalents for the heat and product analyses of the individual forgings are shown in Tables 2 and 3, and are plotted in Fig. 3. From the data presented in Table 2, and plotted in Fig. 3, the forging under discussion evidently did not meet the minimum tensile strength when the carbon equivalent was less than 0.42%. This data will be further discussed in connection with the use of the carbon equivalent for composition restriction in carbon and low alloy steel forging specifications.

TABLE 4—*Additional tension test data for Forging 6.*

Location	UTS MPa (ksi)	Yield .2% MPa (ksi)	El% in. 50 mm (2 in.)	RA%	Analysis[a]	
TESTS A: HEAT TREATED AND WITH SIMULATED STRESS RELIEF AT 607°C (1125°F) FOR 18 H.						
					C%	Mn%
Flange 0°	507 (73.6)	346 (50.2)	30.5	64.5	0.24	0.66
Shell 0° 25 mm off Bore	473 (68.6)	325 (47.1)	34	69.2	0.19	0.64
Shell 120° 1/4 Wall off Bore	454 (65.8)	306 (44.4)	33.5	71.1	0.20	0.65
Shell 240° Mid-wall	474 (68.7)	303 (44)	34	70.2	0.22	0.66
Shell 0° 25 mm off O/D	514 (74.5)	352 (51)	31.5	69.5	0.25	0.66
TESTS B: HEAT TREATED ONLY						
Shell 0° 25 mm off Bore	472 (68.5)	310 (45)	33.5	72.9		
Shell 1/4 Wall off Bore	476 (69)	321 (46.5)	31	69		
Shell Mid-wall	481 (69.7)	317 (46)	33	67.8		
Shell 25 mm off O/D	514 (74.6)	360 (52.2)	32	66.4		

[a] See Table 3.

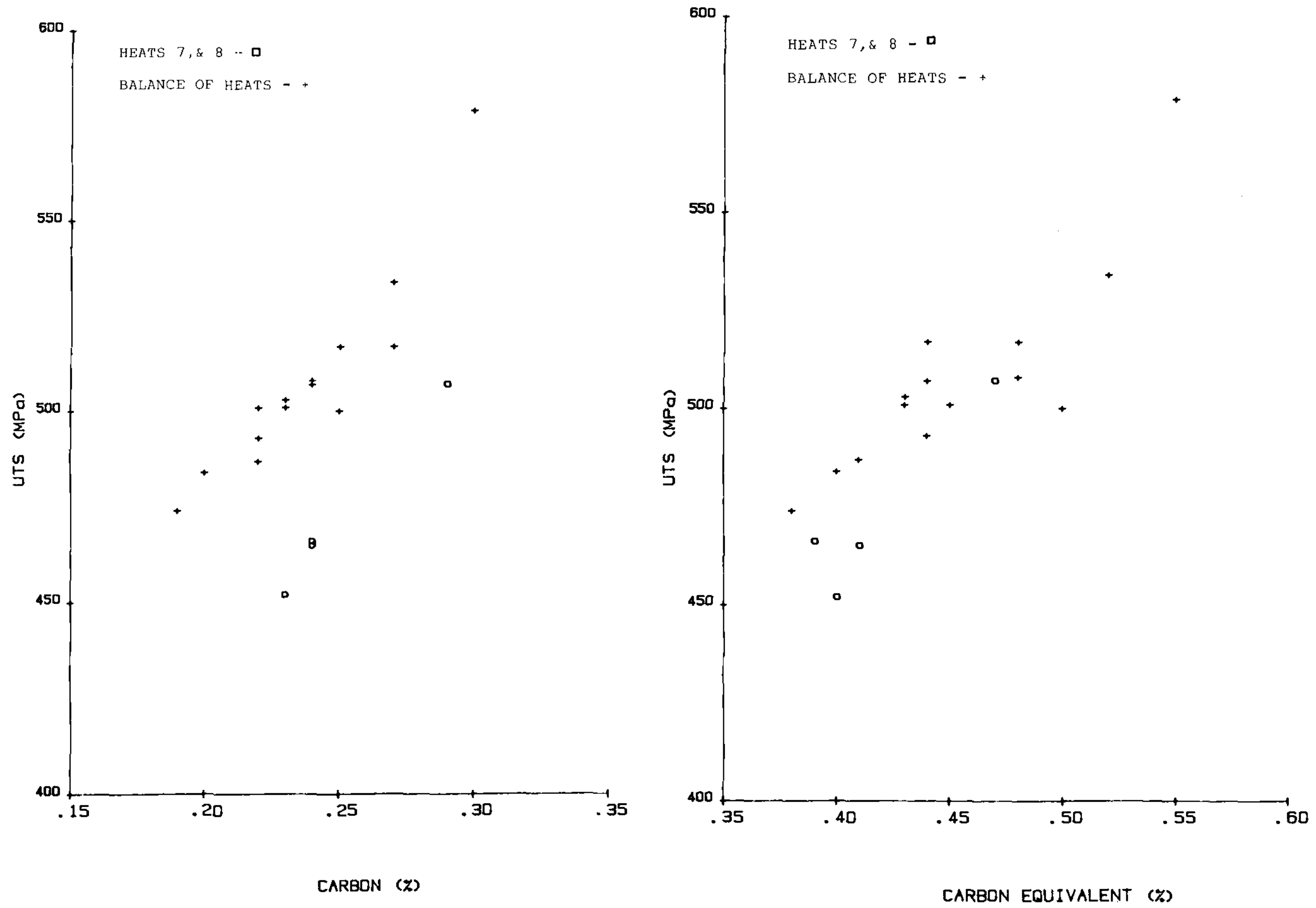

FIG. 3—*Plot of tensile strength against the product analysis carbon content,* (A), *and carbon equivalent,* (B). *The low alloy content heats, 7 and 8, are identified in both cases.*

Chemical Composition

From Table 2 significant negative carbon segregation was clearly present in all of the forgings. The region corresponding to the bottom of the ingot showed lower carbon levels than the flange area, which came from the top of the ingot in each case. The flange composition approximated the heat analysis. The phenomenon of chemical segregation in large ingots has been widely recognized for many years [*3,4*] and constitutes a circumstance that can make composition balance difficult for large forgings.

Discussion

The data presented demonstrates the influence of relatively narrow composition variations on the mechanical properties of large section, heavy carbon-manganese steel pressure vessel forgings, both within the forgings themselves, and from heat to heat. In terms of the specification, the tensile strength was the most seriously affected property since some of the forgings fell below the minimum acceptance limit for ultimate tensile strength. The yield strength, while in parallel with the tensile strength, was always appreciably higher than the minimum requirement.

While shortcomings in the heat treatment process itself would often be suspect in mechanical property variations, this possibility was significantly reduced by the close observation of the heat treatment cycle to document conformance with the written procedure; by the comparison of results from reheat treatments; and by the duplication of the full cycle in other heat treatment facilities.

Given this confirmation of the heat treatment process from forging to forging, the influence of relatively small amounts of the alloying nickel, chromium, and molybdenum on the strength of the forgings is apparent from the tension test results and the product analyses. The sum of these elements did not exceed 0.75%, well below a frequently applied limit of 1.0%.[3] If the flange locations for Forgings 6 and 7, from Tables 2 and 3, are compared, the carbon values were the same for both at 0.24%, and the manganese levels were almost the same at 0.66% for Forging 6, and 0.65% for Forging 7. Due to the variation in the alloying elements nickel, chromium, and molybdenum, the carbon equivalents were 0.44% for the Number 6 flange, and 0.39% for Number 7. While the tensile strength of the Number 6 flange was acceptable at 507 MPa (73.6 ksi), the same property for the Number 7 flange failed at 466 MPa (67.6 ksi). With similar carbon equivalent values, the shell location for Forging 6 had an ultimate tensile strength of the flange of Forging 7.

The layout for the forging operation, which included an upsetting stage, was such that the shell end of the forging was taken from the bottom end of the ingot. The negative carbon segregation at the bottom of the ingot is evident from results in Table 3. The variation in the carbon content through the wall at the shell end, shown in Table 4, is also of interest in the respect that the forging was trepanned after forging.

Although not a part of the original contract for these forgings, carbon equivalency is a frequently used device[4] to curb the composition of carbon and low alloy steel forgings for weldability reasons. The problem that besets the steel producer and forger alike is that there is limited scope to use the composition limits permitted by the specification, bearing in mind that the aim chemistry for the heat must be somewhat less than that which the maximum carbon equivalent permits.

---

[3] ASTM Carbon Steel Fittings for Low Temperature Corrosive Service (A 858/A 858M-86), *Annual Book of ASTM Standards*, Vol. 01.01.

[4] ASTM Specification for Steel Castings, Ferritic and Martensitic, for Pressure-Containing Parts, Suitable for Low-Temperature Service (A 352/A 352M-85), Supplementary Requirement S23. Carbon Equivalent. *Annual Book of ASTM Standards*, Vol. 01.02. ASTM High Strength Butt-Welding Fittings of Wrought High Strength Low Alloy Steel (A 860/A 860M-86), *Annual Book of ASTM Standards*, Vol. 01.01.

While the concept of regarding the composition of a steel from the standpoint of weldability does have some merit, the imposition of an unrealistic value for a carbon equivalent simply to reduce welding costs may tend to result in a general relaxation of welding discipline. For the forgings discussed here, for example, a maximum carbon equivalent of 0.45% would be unacceptable when the required minimum tensile strength would not likely be obtained with a carbon equivalent of 0.42% or less.

The Charpy V notch impact test results were acceptable because of the heat treatment cycle used, and this test was not a factor relative to the composition aspects for these forgings.

Conclusions

The residual alloying elements nickel, chromium, and molybdenum have been shown to affect the tensile strength of large carbon-manganese steel forgings, particularly in the examined aggregate range of 0.2% to 0.75%. The role of the alloy residuals is made more important in the presence of negative carbon segregation in large forging ingots.

The influence of residual amounts of nickel, chromium, and molybdenum on the Charpy V notch properties of large carbon-manganese steel forgings is slight when an inter-critical heat treatment cycle is used, and this test need not have influenced the choice of a low aim carbon content for the modified ASTM A 266-84a, Class 2, material.

Caution should be exercised when imposing carbon equivalency limitations on either carbon or low alloy steel forgings, particularly when large section sizes are involved.

References

[*1*] Nisbett. E. G., Asp, and Morgan, "Improving the Notch Toughness of Nuclear Forgings in Carbon and Low Alloy Steels by Intercritical Heat Treatment," *Proceedings of the Eighth International Forgemasters Meeting,* Kyoto, Japan, Oct. 1977.

[*2*] Nisbett, E. G., "Factors Affecting the Notch Toughness of Carbon and Low Alloy Steel Forgings for Pressure Vessel and Piping Applications," *American Society of Mechanical Engineers Pressure Vessel and Piping Conference.* Montreal. Quebec, Canada. June 1978.

[*3*] "Sixth Report on the Heterogeneity of Steel Ingots," Special Reports Nos. 9 and 9a, Iron and Steel Institute, London, England, 1936.

[*4*] Kim, Pyo, Chang, and Chang, "The Effect of Alloying Elements, and Steel Making Processes on the 'A' Segregation Occurrence in Large Ingots," *Steel Forgings, ASTM STP 903,* E. G. Nisbett and A. Melilli, Eds., American Society for Testing and Materials, Philadelphia.

DISCUSSION

R. L. Bodnar[1] *(discussion questions)*—What was the microstructure in your pressure vessel steels and did the level of residual elements influence microstructure, for example, hardenability, percentage of ferrite? By which strengthening mechanism(s) did the residual nickel, chromium, molybdenum, and vanadium influence tensile strength?

E. G. Nisbett (author's response)—Quantitative analysis of the microstructures obtained in the forgings, after heat treatment was not done, but the structures from the grain size samples were very similar in terms of the relative amounts of ferrite and pearlite. Hardenability studies were not done.

It is believed that solid solution strengthening was the main strengthening effect exerted by the alloy residuals, present in the quantities reported in the paper.

---

[1] Bethlehem Steel Corporation, Bldg. G, Homer Research Laboratories, Bethlehem, PA 18016.

M. L. Hamilton,[1] *G. D. Johnson,*[2] *R. J. Puigh,*[2] *F. A. Garner,*[1]
P. J. Maziasz,[3] *W. J. S. Yang,*[4] *and N. Abraham*[5]

The Effects of Phosphorus and Boron on the Behavior of a Titanium Stabilized Austenitic Stainless Steel Developed for Fast Reactor Service

---

REFERENCE: Hamilton, M. L., Johnson, G. D., Puigh, R. J., Garner, F. A., Maziasz, P. J., Yang, W. J. S., and Abraham, N., **"The Effects of Phosphorus and Boron on the Behavior of a Titanium Stabilized Austenitic Stainless Steel Developed for Fast Reactor Service,"** *Residual and Unspecified Elements in Steel, ASTM STP 1042,* A. S. Melilli and E. G. Nisbett, Eds., American Society for Testing and Materials, Philadelphia, 1989, pp. 124–149.

ABSTRACT: Austenitic stainless steels are used for core component materials in liquid metal cooled reactors (LMRs). To extend the lifetime of LMR fuel assemblies, considerable effort was expended by the U.S. breeder materials program to find ways to minimize radiation induced dimensional changes (swelling and creep) and to maximize the creep rupture strength. After various elements were shown to affect strongly swelling and creep behavior, compositional modifications to a commercial grade austenitic stainless steel (American Iron and Steel Institute 316 UNS S31600) produced an alloy with significant improvement in swelling resistance over the standard 300 series alloys. Changes were primarily in the concentrations of chromium, nickel, silicon, and titanium. ASTM Specification for Austenitic Stainless Steel Tubing for Breeder Reactor Core Components (A 771-83) was approved in 1983 for the new alloy, designated UNS S38660.

Substantial improvement can be produced in the creep rupture behavior of this alloy. Elements such as phosphorus and boron, typically present in trace quantities, have a significant influence on the creep strength of austenitic stainless steels. Several heats of alloy S38660 were made that systematically varied the phosphorus and boron contents. Uniaxial creep tests were conducted at 704°C (1300°F) to evaluate the effects of these elements on the creep rate and the rupture life. The results of these tests were used to guide the production of reactor grade fuel pin cladding for further evaluations. Pressurized tube specimens were tested in the laboratory and also in a fast reactor. Results of these investigations have shown that the elements phosphorus and boron, present in minute but controlled amounts, increase both the in-reactor and ex-reactor rupture life and reduce both in-reactor swelling and creep rate. Microstructural evaluations were also conducted to help ascertain the mechanisms by which the improved properties were obtained.

KEY WORDS: phosphorus, boron, austenitic stainless steel, titanium stabilized stainless steel, swelling, creep, stress rupture, D9, D91

One of the prime objectives in the effort to develop a commercially viable liquid metal reactor (LMR) is the development of an alloy that is resistant to void swelling (radiation induced micro-

---

[1] Senior research scientist and staff scientist, respectively, Pacific Northwest Laboratory, Richland, WA 99352, formerly with Westinghouse Hanford Company, Richland, WA 99352.

[2] Manager of materials engineering and manager of irradiation development, respectively, Westinghouse Hanford Company, Richland, Washington 99352.

[3] Research staff member, Oak Ridge National Laboratory, Oak Ridge, TN 37830.

[4] Knolls Atomic Power Laboratory, Schenectady, NY 12031.

[5] Department of Energy, Washington, DC 20545.

scopic pores that cause a macroscopic volume increase) and has the in-reactor mechanical properties required for fuel cladding or ducts. The fuel cladding is in contact with flowing liquid sodium and has a surface temperature that can vary from 370 to ~650°C (700 to ~1200°F). The duct surrounding each bundle of fuel pins experiences somewhat lower temperatures, ranging from 370 to ~550°C (700 to ~1020°F). These components are also exposed to fast neutron fluxes on the order of 10^{15} n cm^{-2} s^{-1} ($E > 0.1$ MeV). Current goals for the material chosen for cladding and duct applications include the capability of performing adequately to fluences on the order of 2 to 3 $\times$ 10^{23} n cm^{-2} ($E > 0.1$ MeV). For the range of materials of interest, this fluence produces damage levels of 100 to 150 displacements per atom (dpa).

One of the prime initial candidate alloys for commercial LMR fuel cladding and ducts was 20% cold worked American Iron and Steel Institute (AISI) 316 (UNS S31600) steel, a solid solution strengthened austenitic stainless steel further strengthened by cold work [*1–3*]. Current commercial compositional specifications for nuclear grade 316 stainless steel contain only maximum values for impurities such as phosphorus, sulfur, boron, aluminum, niobium, vanadium, tantalum, copper, and cobalt. Typical melting procedures for the alloy involve double vacuum melting of commercial grade starting materials. This practice results in low levels of the aforementioned impurities, which may be 10 to 100 times less than the maximum value allowed by the specification, depending on the particular impurity.

The use of conventional AISI 316 as a cladding or duct material is limited, however, since the alloy undergoes a high degree of void swelling during extended exposure to fast neutron fluxes at LMR operating temperatures. Extensive development efforts aimed at reducing swelling were undertaken successfully [*4–6*], culminating in the definition of a titanium-modified 316 referred to as D9, with a nominal composition of Fe-13.5Cr-15.5Ni-2.0Mo-2.0Mn-0.75Si-0.25Ti-0.04C [*2*]. Specifications within or changes from the usual 316 composition range were primarily in the concentrations of chromium, nickel, silicon, and titanium. ASTM Specification for Austenitic Stainless Steel Tubing for Breeder Reactor Core Components (A 771-83) was approved in 1983 for the new alloy, designated UNS S38660.

The stress rupture behavior of these alloys in fuel pin cladding applications remained, however, as one of the major limitations on fuel pin life. There is significant experimental evidence that controlled additions of boron and phosphorus significantly improve the mechanical properties of austenitic stainless steels at elevated temperatures [*7–19*]. An examination of the ex-reactor rupture data generated on various austenitic alloys during the development of D9 showed that the rupture strength of these alloys exhibited a linear dependence on the combined level of phosphorus, sulfur, and boron (Fig. 1). An experimental program was therefore initiated to investigate systematically the effect of phosphorus and boron on both the swelling and stress rupture resistance of the austenitic stainless steel D9. The program included assessing the individual and synergistic effects of phosphorus and boron on rupture life as well as characterizing the in-reactor swelling and stress rupture behavior of several heats of steel. Although the residual element analysis shown in Fig. 1 considered sulfur, the sulfur content (0.005 to 0.010%) of the experimental heats was not varied since increased sulfur levels are known to cause solidification cracking during welding [*20*].

Experimental Procedures

Nine 50-lb (22.5-kg) experimental heats of double vacuum melted D9 were procured in which the phosphorus and boron concentrations varied as shown in Table 1. Creep rupture specimens were fabricated from 23% cold worked rod stock obtained by cold swaging the as-received bar. Intermediate anneals were conducted at about 1050°C (1920°F) resulting in final grain sizes that ranged from ASTM 7 to 9 (ASTM Methods for Determining Average Grain Size (E 112)). Uniaxial creep rupture tests were conducted in air at 704°C (1300°F) according to ASTM Recommended Practice for Conducting Creep, Creep-Rupture, and Stress-Rupture Tests of Metal-

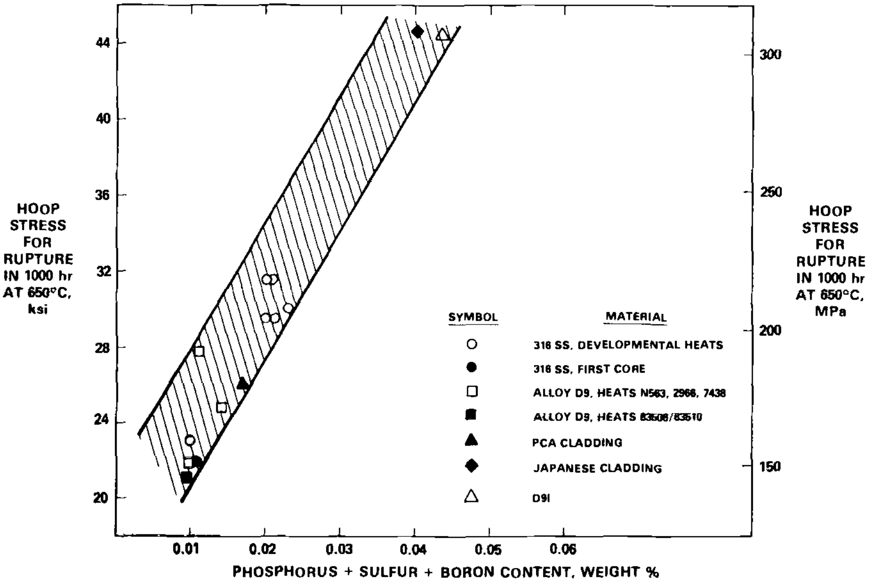

FIG. 1—*Compositional effects on stress rupture.*

TABLE 1—*Nominal phosphorus and boron levels in experimental heats of D9*[a,b] *(uniaxial stress rupture tests).*

Weight Percent Phosphorus	Weight Percent Boron		
	<0.001	0.003	0.008
	HEAT IDENTIFICATION		
<0.01	**C43**[c]	C34	**C35**
0.03	C36	**C38**	C39
0.08[b]	**C37**	C33	**C40**

[a] Base composition: Fe-13.6Cr-15.6Ni-2.2Mn-1.8Mo-0.8Si-0.3Ti-0.05C-0.005S.

[b] All compositions fell within 10% of the nominal value, with the exception of the nominal value of 0.08 phosphorus, which actually ranged from 0.054 to 0.064 phosphorus.

[c] Ruptured specimens of bold-faced heats were given metallographic and microscopic examinations.

lic Materials (E 139-83) at stresses ranging from 210 to 450 MPa (30 to 65 ksi). Creep strains were measured by an extensometer attached to the specimen shoulders.

Three larger double vacuum melted heats were procured from Teledyne Allvac to gain experience in making these heats in typical commercial order quantities. The phosphorus and boron levels of the larger "production" heats were specified identically for each heat at estimated optimum levels. A nominal phosphorus plus sulfur plus boron level of 0.045% was chosen for each heat based on a small experimental welding matrix that had been performed on the experimental heats to indicate susceptibility to weld cracking. Since this matrix had demonstrated that a phosphorus level as high as 0.08% would jeopardize necessary welding operations, the phosphorus level was kept at about 0.03%, the intermediate level of the experimental heats. Compositions of the three heats are provided in Table 2. Heats A093 and A094 were prepared using selected scrap as the feed stock in a manner typical of large orders; only the molybdenum content was varied to determine its optimum level. Heat A095 was prepared from virgin material at the lower (1.8%) molybdenum level to indicate whether continuing the policy of using virgin materials for core component fabrication was necessary. Since these particular heats, and therefore the modified alloy in general, were expected to exhibit improved stress rupture behavior, they were referred to as "improved" D9, or D9I.

Tubing in a 20% cold worked condition was fabricated from each heat of D9I by Carpenter Technology Corporation with interpass anneals at 1070°C (1960°F). Biaxial rupture tests were performed according to ASTM E 139-83 on 76.2-mm (3 in.) long sections of the tubing that measured 5.84 and 5.08 mm (0.230 and 0.200 in.) on the outer and inner diameters, respectively. Specimen loading was accomplished by internal pressurization with argon gas. Machined end caps of 316 stainless steel were TIG (tungsten inert gas) welded to one end of each specimen and a gas inlet tube was similarly welded to the other end. Rupture tests were conducted at constant pressure in static argon at temperatures ranging from 650 to 760°C (1200 to 1400°F) and stresses ranging from 75 to 400 MPa (10 to 60 ksi). The pressure on each specimen was checked daily and adjusted if necessary. Failure was detected by a sudden rise in retort pressure, which actuated a solenoid valve, shutting off a timer.

Optical metallography, scanning electron microscopy, and analytical transmission electron microscopy were used to characterize the microstructure of the as-received tubing and the microstructure and fracture behavior of selected stress rupture specimens. One uniaxially tested specimen from each of five heats was sectioned for microscopy after testing at 704°C (1300°F) and 250 MPa (36.6 ksi). The five heats examined were those with a combination of the highest,

TABLE 2—*Composition of D9I heats used for biaxial stress rupture tests.*

Element	Nominal Composition	Heat Compositions		
		A093	A094	A095
Chromium	13.5	13.74	13.36	13.52
Nickel	15.5	15.11	15.31	14.96
Manganese	2.0	1.89	1.93	1.93
Molybdenum	1.8 to 2.2	1.82	2.24	1.82
Silicon	0.8	0.76	0.81	0.80
Titanium	0.25	0.23	0.26	0.26
Carbon	[a]	0.041	0.046	0.043
Nitrogen	0.005 max	0.0052	0.0052	0.0018
Boron	0.004 to 0.006	0.005	0.005	0.005
Phosphorus	0.025 to 0.040	0.031	0.031	0.030
Sulfur	0.005 to 0.010	0.008	0.009	0.008
Aluminum	0.05 max	0.03	0.04	0.05
Cobalt	0.05 max	0.04	0.04	0.04
Copper	0.04 max	0.02	0.02	0.02
Tantalum	0.02 max	0.04	0.04	0.04
Vanadium	0.05 max	0.04	0.03	0.02
Oxygen	0.01 max	0.003	0.002	0.0012
Zirconium	0.01 max	<0.01	<0.01	<0.01
Iron	Bal	Bal	Bal	Bal

[a] Adjusted for sufficient stabilization such that Ti/(C + N) = 5.

lowest, and intermediate values of phosphorus and boron (Heats C43, C35, C38, C37, and C40 in Table 1).

Pressurized tubes were also used to obtain data on the in-reactor stress rupture behavior of the production heats (Heats A094 and A095). End caps made of D9 were electron beam welded to 25.7-mm (1.01-in.) long sections of the same tubing that was described earlier. Small amounts of unique isotopic mixtures of krypton and xenon gases, referred to as "tag" gases, were used with helium to fill the specimens to the pressures required to produce the desired stresses in the cladding at the intended irradiation temperatures of 400, 490, 550, 605, 670, and 750°C (750, 915, 1020, 1120, 1240, and 1380°F). A different isotopic mixture of tag gas was used for each alloy and irradiation temperature combination to allow the use of an on-line creep rupture detection system based on spectrographic analysis of the tag gas released by rupture [*21*]. Empirical correlations were developed from experimental measurements to relate the fill pressure at room temperature to the pressure at the irradiation temperature. After gas filling, the specimens were sealed by laser welding the fill hole located in one specimen end cap. Weld integrity was then verified using standard helium leak checking techniques. Finally, the specimen preirradiation diameters were measured using a noncontacting laser system prior to being loaded into the irradiation vehicle, designated the Materials Open Test Assembly (MOTA). Irradiation was conducted in the Fast Flux Test Facility located in Richland, WA.

During the course of irradiation the specimen temperatures were actively maintained within 5°C (9°F) of the design temperatures, except for brief periods when the canister temperatures were reduced by more than 75°C (135°F) during the identification of gas releases from other, fueled experiments [*21*]. Spectrographic analysis of gas samples taken when an increased gamma signal was detected in the cover gas confirmed the release of tag gas from the creep rupture specimens and uniquely identified the alloy and irradiation temperature [*22*]. The test matrix contained eight specimens at different stresses for a given irradiation temperature. For a given gas release, the most highly stressed specimen was initially assumed to have failed at the irradiation temperature that had been identified. This assumption was later verified by diametral measurements taken annually during interim examinations of the experiment.

The swelling resistance of D9I and many related alloys was determined primarily by irradiating an extensive matrix of microscopy disks (3-mm diameter by 0.3-mm thick) in the Experimental Breeder Reactor II and comparing pre- and post-irradiation densities. The nominal disk composition was a titanium-modified "high-purity" D9 (Fe-16Cr-14Ni-2.5Mo-2.0Mn-0.8Si-0.2Ti-0.04C-0.01Zr) with controlled additions of up to 0.08 percent phosphorus. Disks were punched from sheet stock in both the annealed and 20% cold worked conditions. They were irradiated in sodium filled subcapsules at temperatures ranging from 425 to 650°C (800 to 1200°F) to maximum displacement levels of about 55 dpa, or a fluence of about 11.0×10^{23} n cm^{-2} ($E > 0.1$ MeV). Density was determined using an automated immersion density technique accurate to ±0.16% swelling. In addition, swelling data on the D9I production heats were obtained from diameter change measurements on unstressed pressurized tube specimens included in the irradiation creep experiment.

Results

Uniaxial Stress Rupture Behavior

Uniaxial rupture tests were conducted at 704°C (1300°F) and 250 MPa (36.6 ksi) on specimens prepared from each of the nine experimental heats. Both phosphorus and boron caused the rupture life of D9 to increase independently, as shown in Figs. 2 and 3. Figure 2 shows that the effect of increasing phosphorus saturated at about 0.03% phosphorus at the lowest boron level, but continued, albeit at a reduced rate, at the higher boron levels. A smaller additional

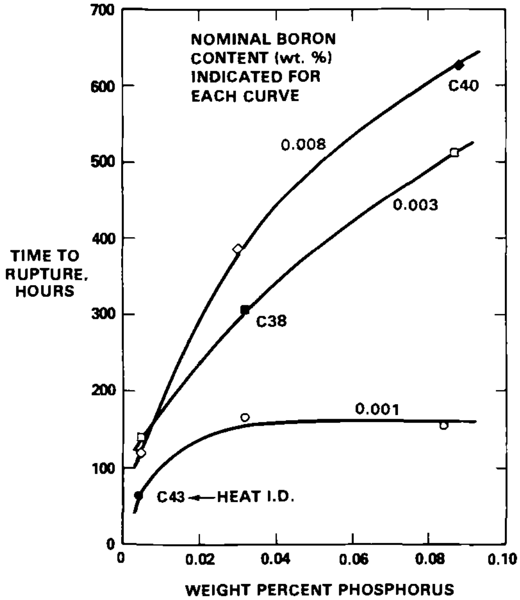

FIG. 2—*Effect of phosphorus on the stress rupture life of D9 at 704°C (1300°F) and 250 MPa (36.6 ksi).*

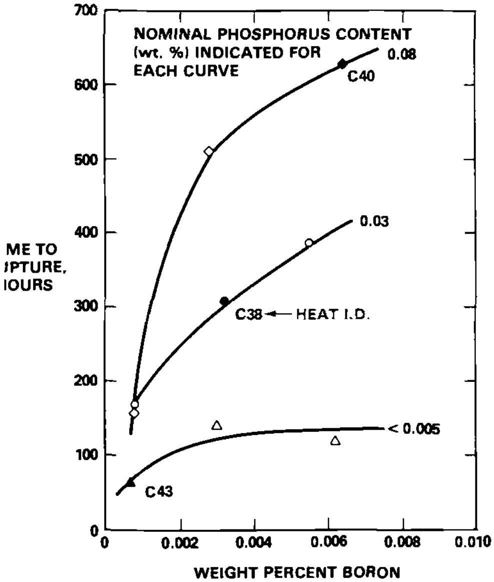

FIG. 3—*Effect of boron on the stress rupture life of D9 at 704°C (1300°F) and 250 MPa (36.6 ksi).*

increment in rupture life was produced by increasing phosphorus from 0.003 to 0.006% than by increasing phosphorus from a trace level to 0.003%.

Figure 3 illustrates a similar dependence on boron level. Saturation was observed by about 0.003% boron in the presence of a low phosphorus level, while the strongest effect of increasing boron level occurred at a high phosphorus level. A large increment in rupture life was produced at the higher boron levels by increasing phosphorus from 0.03 to 0.085%.

The effects of boron and phosphorus on creep strain are shown in Fig. 4 for the uniaxial tests performed at 704°C (1300°F) and 250 MPa (36.6 ksi). The combined effect of the solute modification clearly involves not only delaying the onset of tertiary creep but also decreasing the secondary creep rate.

The effect of boron and phosphorus on total elongation in the uniaxial tests at 704°C (1300°F) and 250 MPa (36.6 ksi) are shown in Figs. 5 and 6. No consistent trends were observed with increasing boron or phosphorus levels, although a simultaneous increase of both phosphorus and boron (solid symbols) resulted in a slight decrease in ductility. While these results are contrary to the generally accepted effect of increased boron levels in austenitic stainless steels [*7,11,12,18*], which is to increase ductility, the ductility levels in question are still in excess of 18%, which is more than adequate for LMR applications.

Figures 7 through 12 show additional data generated in uniaxial tests at 704°C (1300°F) on the nine experimental heats. They show quite clearly that increasing the level of phosphorus is beneficial up to 0.08%, while the beneficial effect of increased boron levels saturates at roughly 0.003%.

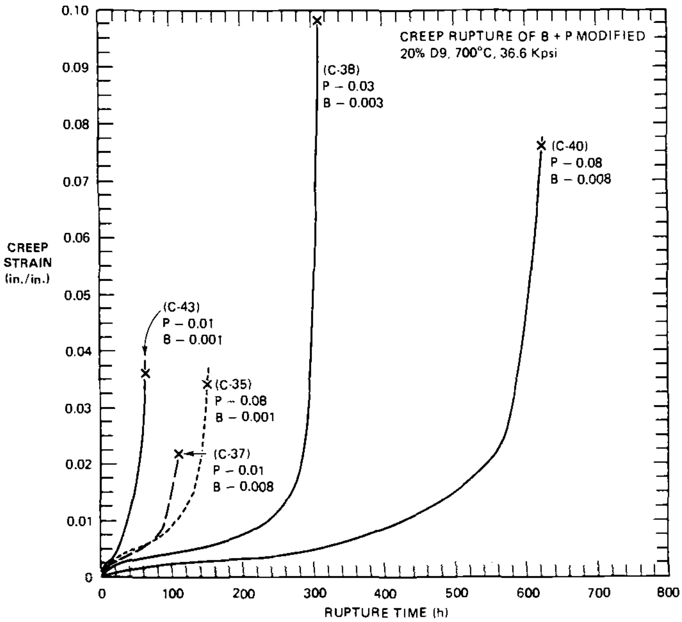

FIG. 4—*Creep curves of D9 modified by additions of boron and phosphorus for tests performed at 704°C (1300°F) and 250 MPa (36.6 ksi).*

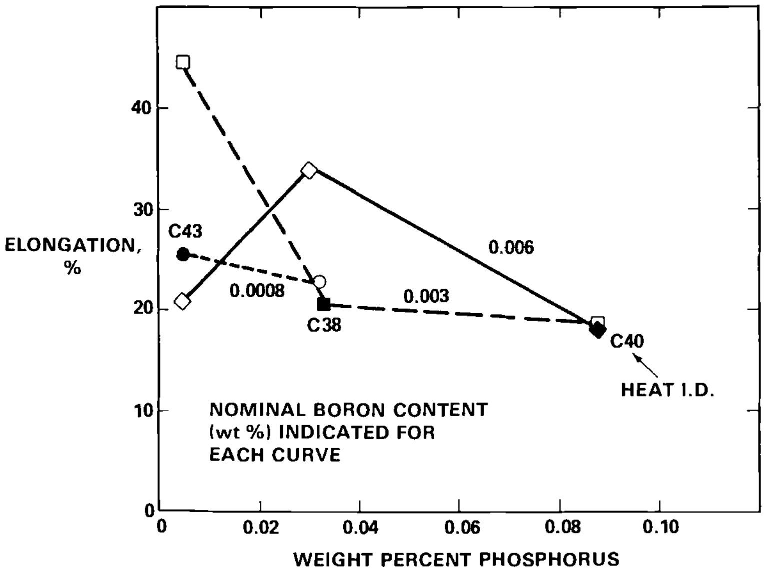

FIG. 5—*Effect of phosphorus on the ductility of D9 at 704°C (1300°F) and 250 MPa (36.6 ksi).*

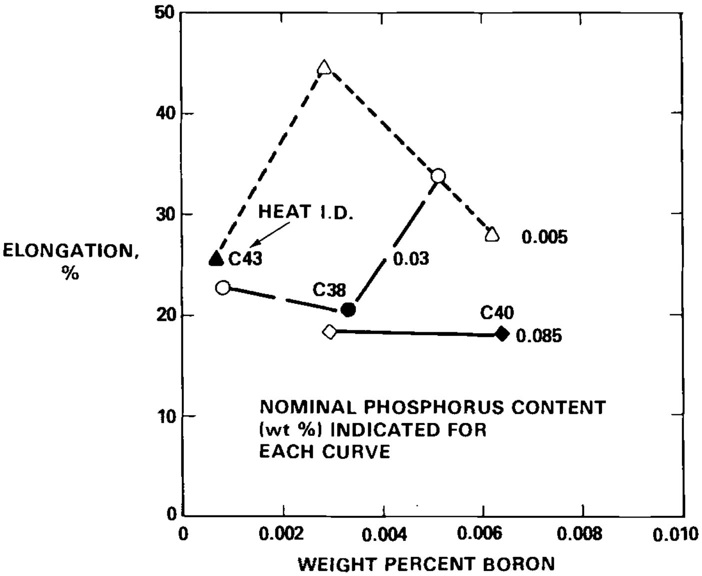

FIG. 6—*Effect of boron on the ductility of D9 at 704°C (1300°F) and 250 MPa (36.6 ksi).*

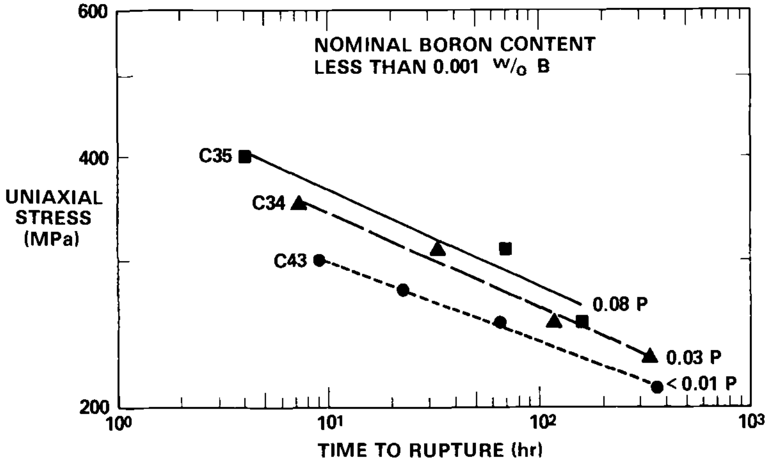

FIG. 7—*Effect of phosphorus on the stress rupture life of D9 containing 0.001% boron at 704°C (1300°F).*

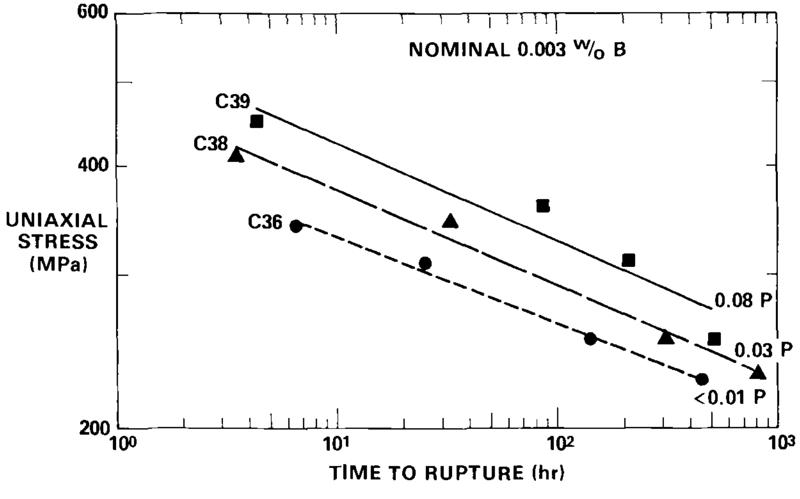

FIG. 8—*Effect of phosphorus on the stress rupture life of D9 containing 0.003% boron at 704°C (1300°F).*

Biaxial Stress Rupture Behavior

At least 15 tests have been completed on each of the three larger production heats of D9I for times as long as 11,000 h. The data are shown in Fig. 13, which shows rupture life as a function of hoop stress and compares the behavior of each heat with that of unmodified D9. It is evident that a significant improvement in stress rupture behavior resulted from the increased phosphorus and boron levels present in D9I.

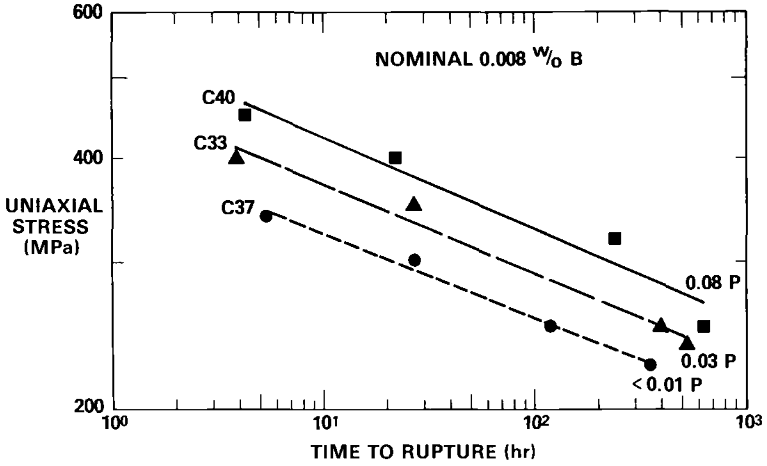

FIG. 9—*Effect of phosphorus on the stress rupture life of D9 containing 0.008% boron at 704°C (1300°F).*

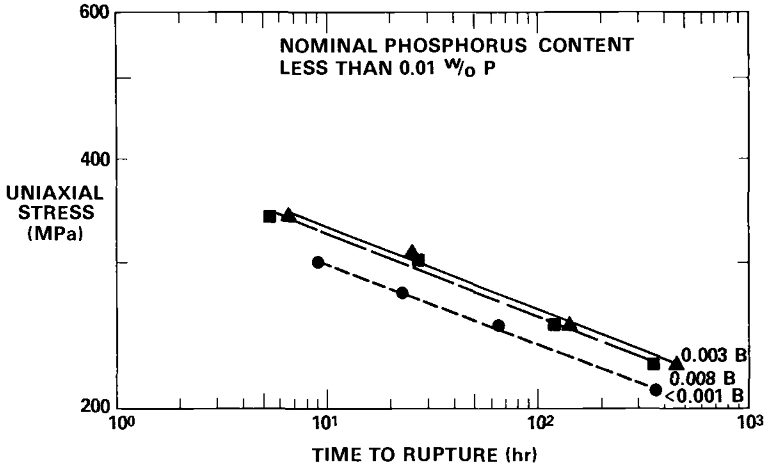

FIG. 10—*Effect of boron on the stress rupture life of D9 containing 0.01% phosphorus at 704°C (1300°F).*

Microscopy Results on Unirradiated D9

Optical photomicrographs are shown in Fig. 14 for specimens prepared from tubing of the three D9I production heats in the as-received condition. The transverse sections reveal a microstructure typical of cold worked titanium-stabilized austenitic stainless steel comprising equiaxed grains, a low density of mechanical twins, a few large blocky particles, and a uniform distribution of smaller particles. Vickers microhardness measurements on the as-received tubing ranged from 255 to 263.

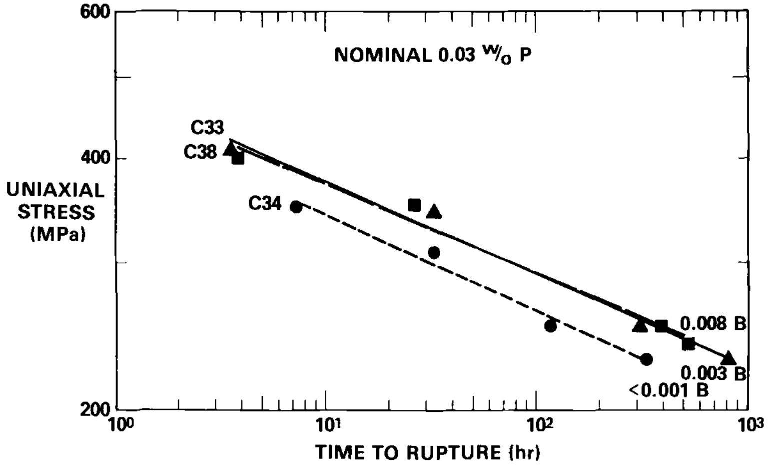

FIG. 11—*Effect of boron on the stress rupture life of D9 containing 0.03% phosphorus at 704°C (1300°F).*

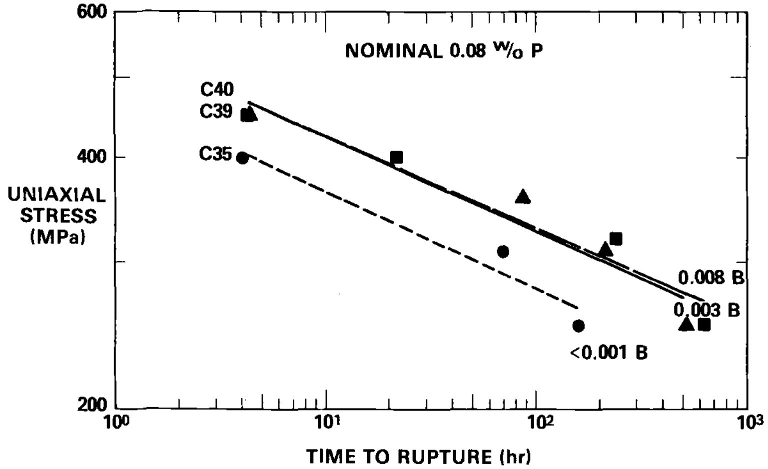

FIG. 12—*Effect of boron on the stress rupture life of D9 containing 0.08% phosphorus at 704°C (1300°F).*

Longitudinally oriented cross sections through the fractured surfaces of the specimens from three of the uniaxial tests are shown in Fig. 15 for tests conducted at 704°C (1300°F) and 250 MPa (36.6 ksi). The three specimens are from heats containing low (C43), intermediate (C38), and high (C40) levels of both phosphorus and boron. As the phosphorus and boron levels increase the degree of grain boundary cavitation also increases, directly reflecting the observed increase in matrix strength and the longer time to rupture. Grain elongation was reduced, consistent with the decrease in elongation obtained with simultaneous increases in phosphorus and boron (Figs. 5 and 6).

These specimens' phase identification was accomplished via X-ray energy dispersion spec-

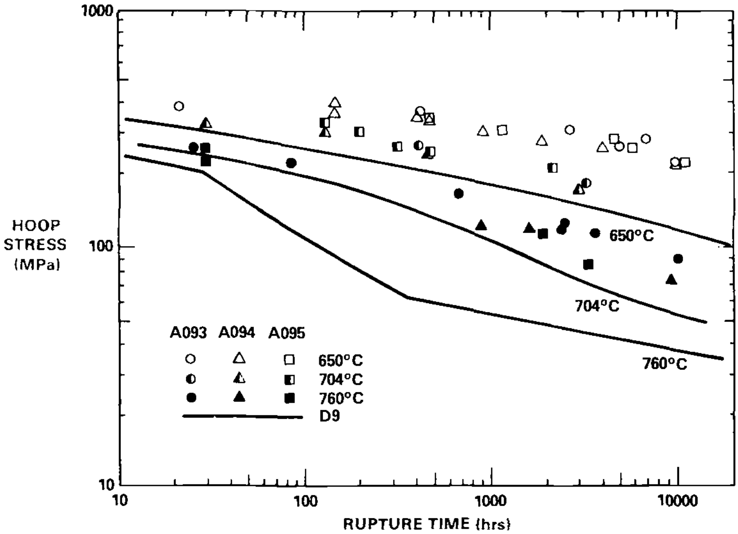

FIG. 13—*Stress rupture behavior of improved D9 heats relative to unmodified D9.*

troscopy on extraction replicas. The relative phase fractions were determined by computer analysis of the X-ray intensities obtained in broad beam analysis. A summary of the observed precipitation behavior in these specimens is provided in Table 3. Quantitative standardless composition determinations, accurate to about 1/2%, were obtained using accepted techniques [*23*].

Increased bulk additions of phosphorus and boron enhance the formation of $M_{23}C_6$ and M_6C at the grain boundaries while the formation of matrix MC on dislocations is progressively suppressed. Laves was found in all five specimens, primarily at grain boundaries. As the more complex carbides developed, however, the relative balance at grain boundaries shifted from Laves toward carbides, such as $M_{23}C_6$ and M_6C, as shown in Fig. 16. Rod-like phosphide formation was promoted in the matrix by increased levels of phosphorus. The phosphides were elongated and were Type M_2P. In the specimen with the highest phosphorus and boron levels (Heat C40), the phosphides had nearly the composition FeTiP, as shown in Fig. 17. The MC composition observed in this specimen is also shown in the figure, but as shown in Table 4, the MC composition was sensitive to increases in the bulk phosphorus and boron levels. The small MC particles ($<$ 10 nm) had surprisingly large levels of molybdenum and phosphorus in addition to the expected high level of titanium. Of particular significance is the incorporation of large amounts of phosphorus into the MC particles as the matrix phosphorus level increased. This incorporation occurred at the expense of titanium and molybdenum in the carbide phase, with a simultaneous increase in iron and nickel levels.

In-Reactor Stress Rupture Behavior

The in-reactor creep behavior of several heats of D9-type alloys is shown in Figs. 18 through 21 for irradiation temperatures of 400, 490, 600, and 670°C (750, 915, 1110, and 1240°F). Shaded areas represent the range of data obtained on various heats tested. Significantly lower creep strains were exhibited by D9I at all temperatures. In-reactor rupture data are shown in Fig. 22 for one heat of D9I (A095) and a very clean heat of unmodified D9 (83508, also referred

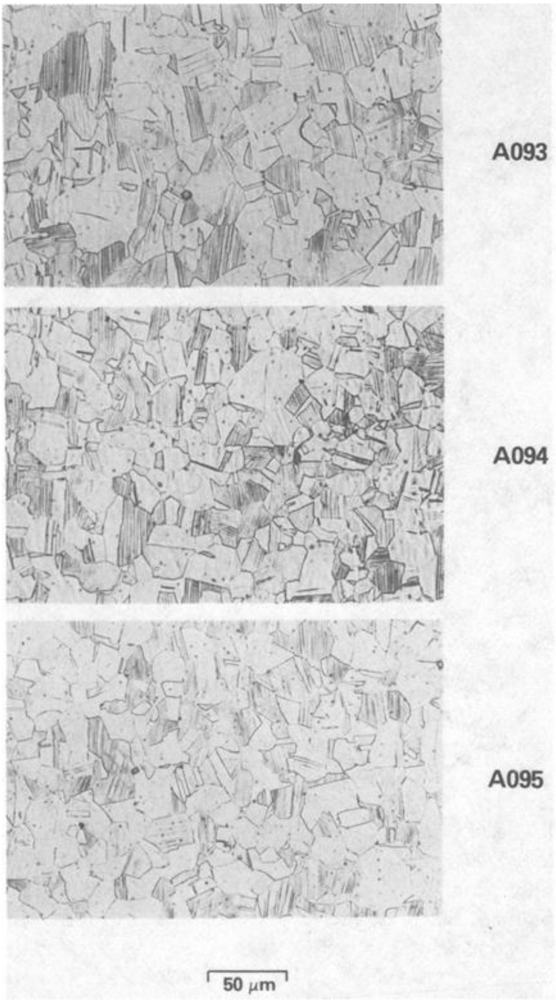

FIG. 14—*As-received condition of transverse sections of tubing from* (a) *Heat A093,* (b) *Heat A094, and* (c) *Heat A095, after etching with glyceregia.*

to as D9C1P). The improvement in creep rupture life observed in out-of-reactor tests by controlled additions of phosphorus and boron is clearly maintained in-reactor for the conditions of interest.

Irradiation-Induced Swelling Behavior

Unstressed Pressurized Tube Specimens—Swelling data were obtained on unstressed pressurized tube specimens from the production heats irradiated to fluences as high as 16×10^{22} n cm^{-2} ($E > 0.1$ MeV). Swelling has been shown many times to yield isotropic strains, and volumetric swelling was, therefore, calculated as three times the measured diametral change for the low swelling levels of interest here. The swelling data shown in Fig. 23 demonstrate that at low temperature, where swelling is typically largest in titanium-modified steels [*4*], the composi-

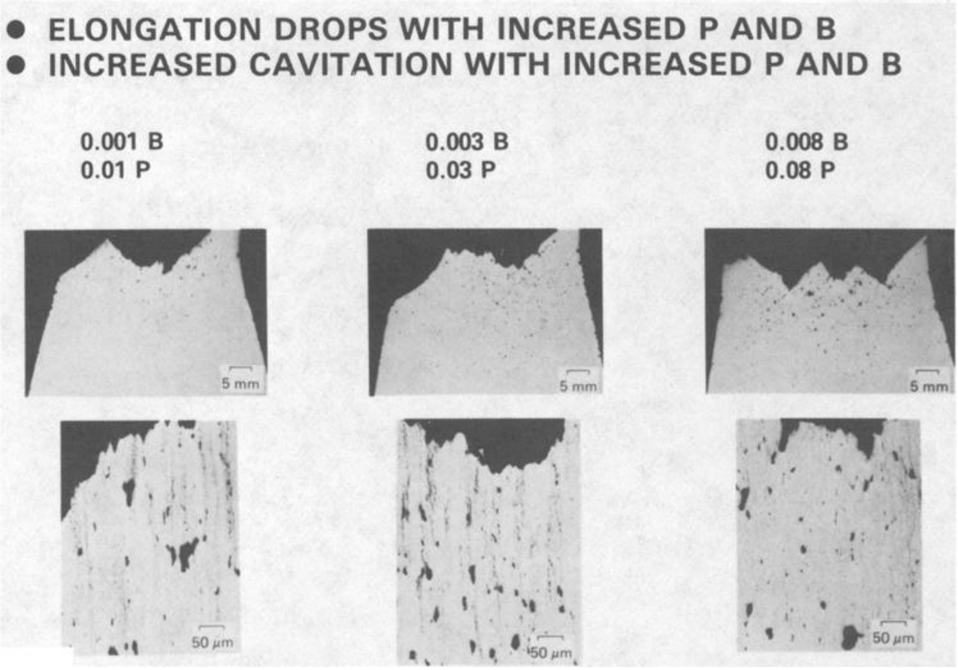

FIG. 15—*Optical sections through three uniaxial stress rupture specimens showing degree of creep cavitation in tests at 250 MPa (36.6 ksi) and 704°C (1300°F).*

TABLE 3—*Phase identification in uniaxial stress rupture specimens tested at 704°C and 250 MPa (1300°F, 36.6 ksi).*

	Phosphorus, wt%		
Boron, wt%	0.01	0.03	0.08
0.001	grain—Laves boundary matrix—fine MC	. . .	grain—Laves boundary—M_6C phosphides matrix—fine MC phosphides
0.003	. . .	grain—Laves boundary matrix—fine MC phosphides	. . .
0.006	grain—Laves boundary matrix—fine MC	. . .	grain—Laves boundary—$M_{23}C_6$, M_6C phosphides matrix—fine MC phosphides

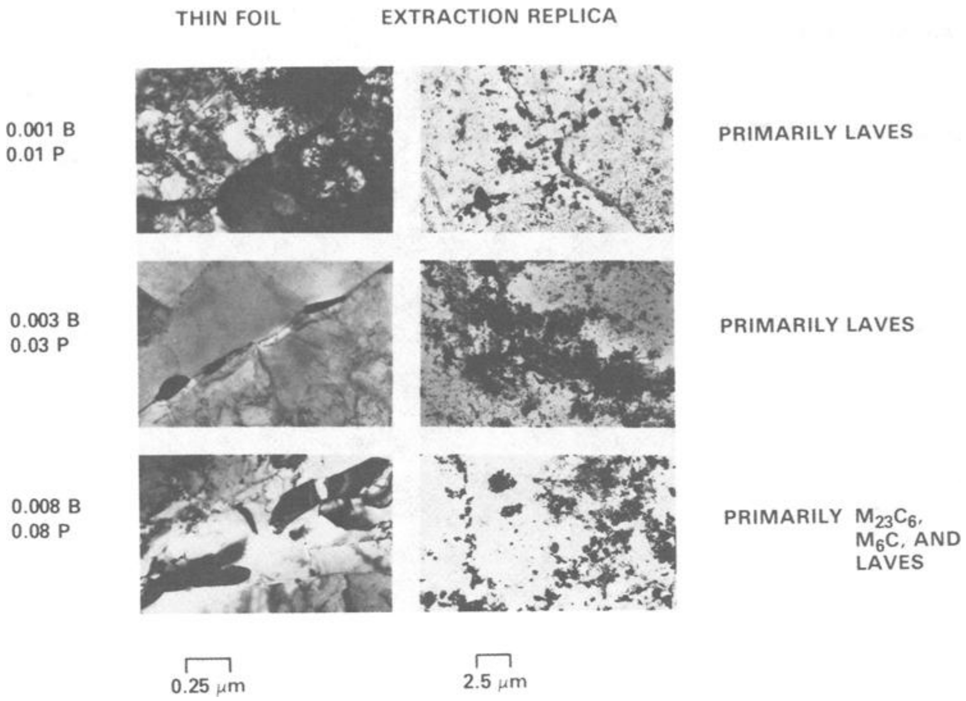

FIG. 16—*Distribution of carbides and Laves in uniaxial stress rupture specimens tested at 704°C (1300°F) and 250 MPa (36.6 ksi).*

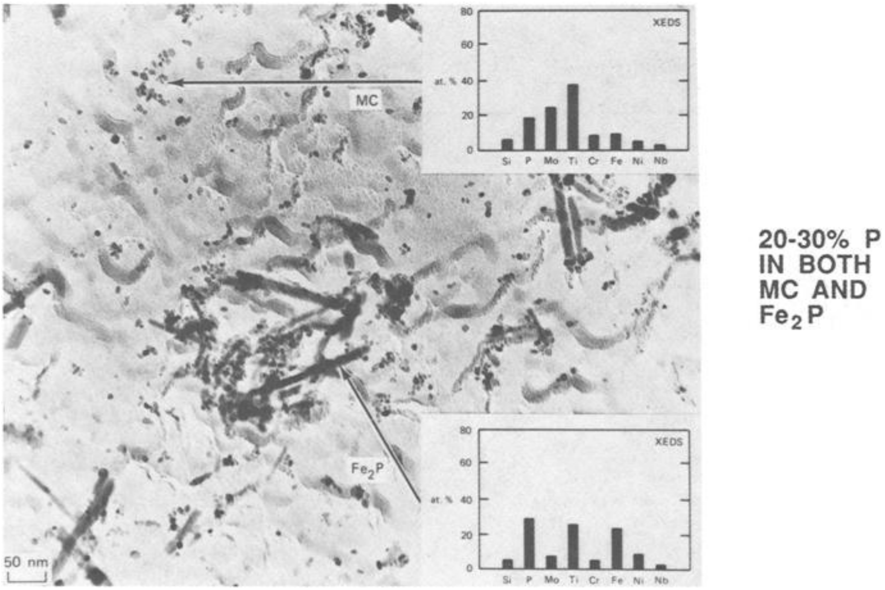

FIG. 17—*Microstructure of high phosphorus-high boron heat (C40) and composition of both phosphide and MC particles.*

TABLE 4—*Composition of MC precipitates in uniaxial stress rupture specimens*[a] *704°C, 250 MPa (1300°F, 36.6 ksi).*

Heat	C43	C38	C40
Element (wt%)	0.001 B 0.01 P	0.003 B 0.03 P	0.008 B 0.08 P
Phosphorus	3.0	3.1	16.0
Iron	0.6	1.3	8.2
Nickel	0.2	0.2	3.9
Niobium	3.9	3.6	1.7
Molybdenum	26.2	27.3	21.6
Titanium	55.2	55.1	35.8
Chromium	6.8	7.0	7.7
Silicon	4.0	2.5	5.2

[a] As determined by X-ray energy dispersion spectroscopy. Note that this technique is not capable of measuring boron levels.

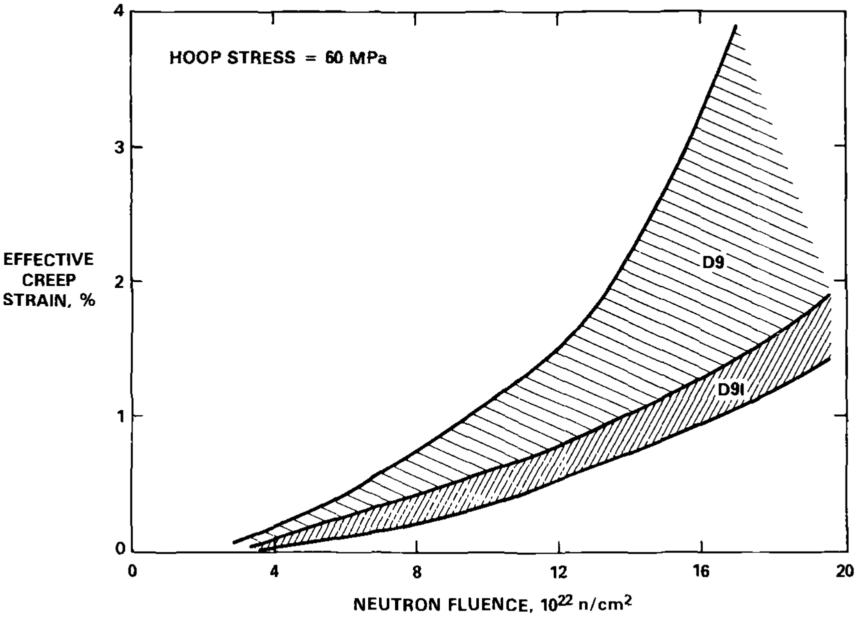

FIG. 18—*In-reactor creep behavior of 20% cold worked D9-type alloys at 400°C (750°F). Effective strains were calculated from diametral strains according to the von Mises criterion.*

tional modification delayed the onset of swelling by roughly 5×10^{22} n cm^{-2} ($E > 0.1$ MeV) compared to D9C1P.

Transmission Electron Microscopy Disks—The influence of phosphorus on swelling and microstructural evolution during neutron or ion irradiation has been studied for a variety of austenitic alloys [*19,24-30*], including an extensive study of improved D9-type alloys [*24,26*]. In

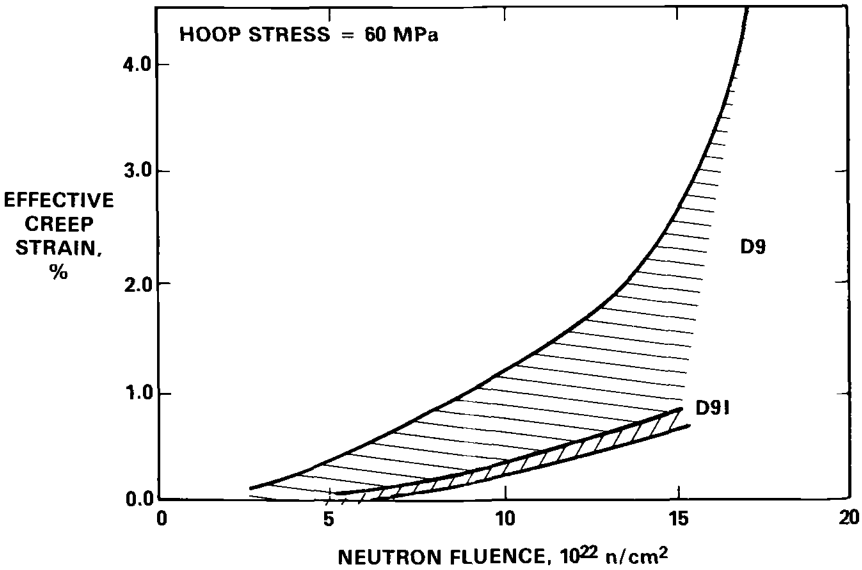

FIG. 19—*In-reactor creep behavior of 20% cold worked D9-type alloys at 490°C (915°F). Effective strains were calculated from diametral strains according to the von Mises criterion.*

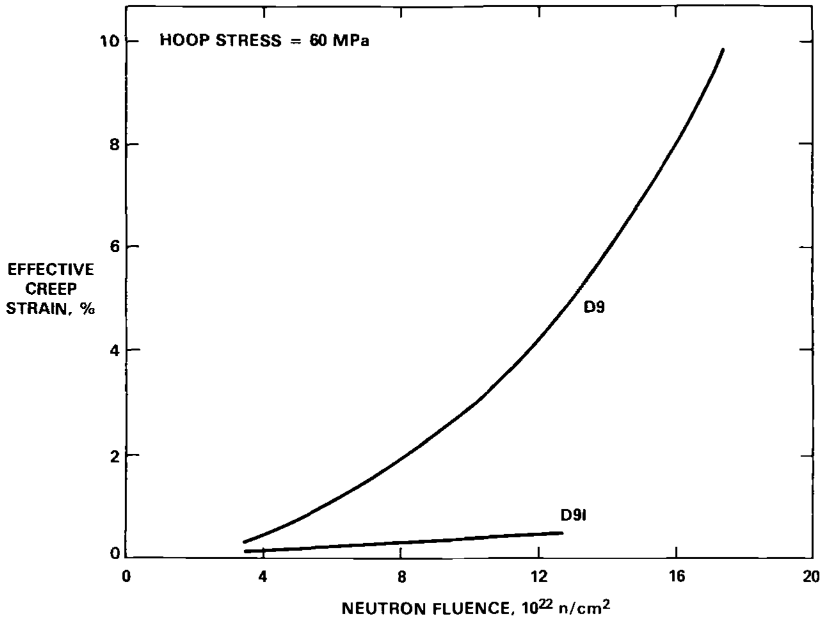

FIG. 20—*In-reactor creep behavior of 20% cold worked D9-type alloys at 600°C (1110°F). Effective strains were calculated from diametral strains according to the von Mises criterion.*

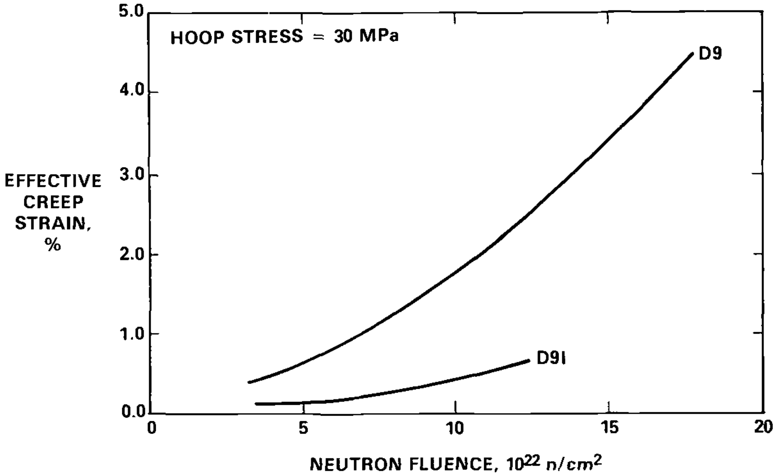

FIG. 21—*In-reactor creep behavior of 20% cold worked D9-type alloys at 670°C (1240°F). Effective strains were calculated from diametral strains according to the von Mises criterion.*

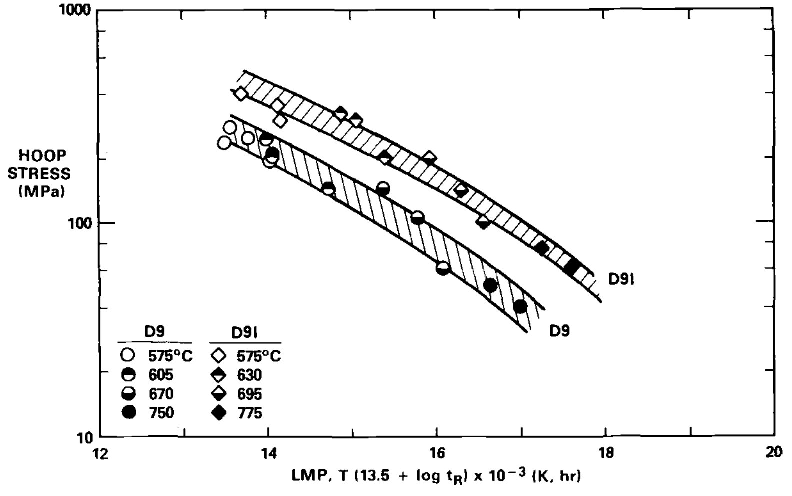

FIG. 22—*Larson Miller Parameter (LMP) representation of in-reactor creep rupture of modified D9, where T is degrees Kelvin and t_R is time to rupture in hours.*

general, the results are very consistent. Except at very low total solute levels, the addition of phosphorus always tends to reduce swelling [*25*]. This reduction occurs due to a progressive phosphorus induced extension of the incubation period that precedes the onset of steady-state swelling. This extension is greatest for higher irradiation temperatures (550 versus 425°C [1020 versus 795°F], for example), and appears to operate on both annealed and cold worked alloys as shown in Figs. 24 and 25. Phosphorus additions also suppress the irradiation creep rate of these same alloys [*24*]. Creep suppression is not surprising since the largest component of the irradiation creep rate is known to be proportional to the instantaneous swelling rate [*31*]. Quite unex-

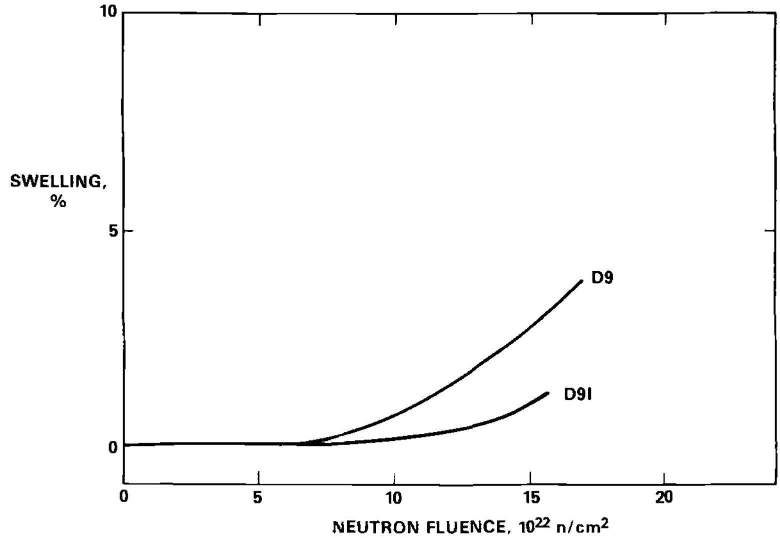

FIG. 23—*Swelling behavior of 20% cold worked D9. D9C1P is a heat with a very low residual content.*

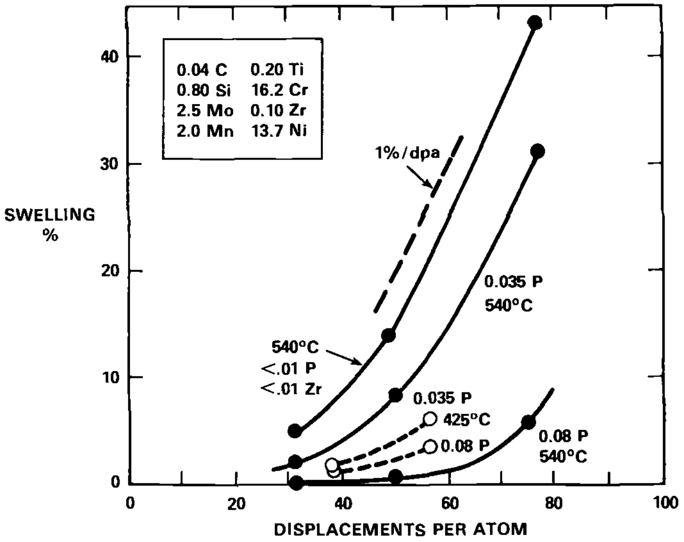

FIG. 24—*The influence of phosphorus and irradiation temperature on the neutron-induced swelling of annealed titanium-modified 316 stainless steel* [23]. *The composition of the alloy is given in the box.*

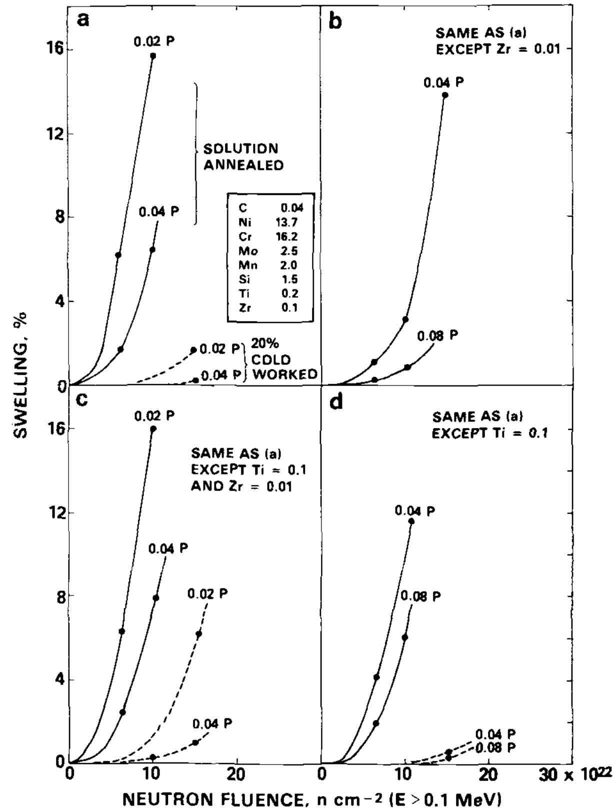

FIG. 25—*The influence of phosphorus and cold work on the neutron-induced swelling of four compositional variants of D9-type steels at 540°C (1005°F)* [25].

pected, however, is the fact that boron exerts only a surprisingly small effect on swelling, with additions of 0.005% causing rather small increases or decreases, depending on the composition of the alloy [*26*].

Discussion

Stress Rupture

The uniaxial rupture data given in Figs. 2 and 3 are shown in Fig. 26 as a function of the product of boron and phosphorus levels. This representation produces a clearer interpretation of the data than that obtained using the approach shown in Fig. 1 (that is, plotting rupture life as a function of the sum of the phosphorus and boron levels). This representation illustrates the synergistic effect of simultaneous boron and phosphorus additions. Rupture life appears to depend exponentially on the product of the boron and phosphorus levels.

The Larson Miller parameter (LMP) is applied in Fig. 27 to the biaxial stress rupture data obtained on the production heats of D9I to illustrate more clearly the significant improvement in stress rupture behavior that resulted from the increased phosphorus and boron levels. The constant in the LMP, 15, was previously selected as the value that best collapsed the extensive

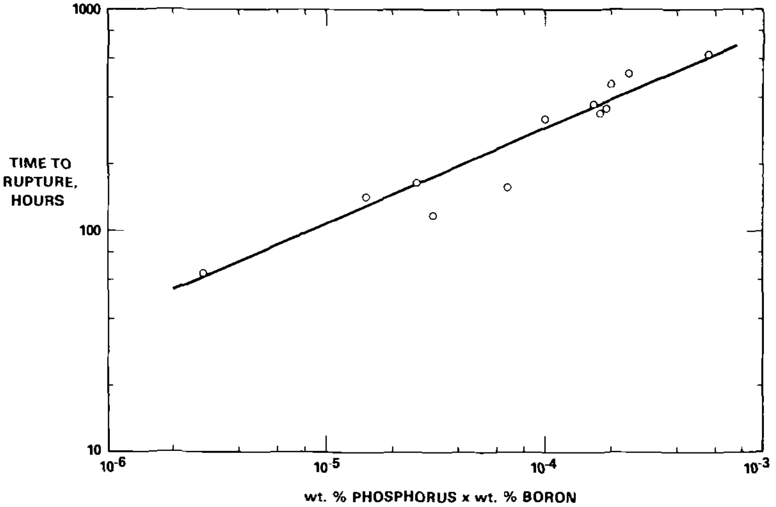

FIG. 26—*Synergistic effect of phosphorus and boron on the rupture life of D9 at 704°C (1300°F) and 250 MPa (36.6 ksi).*

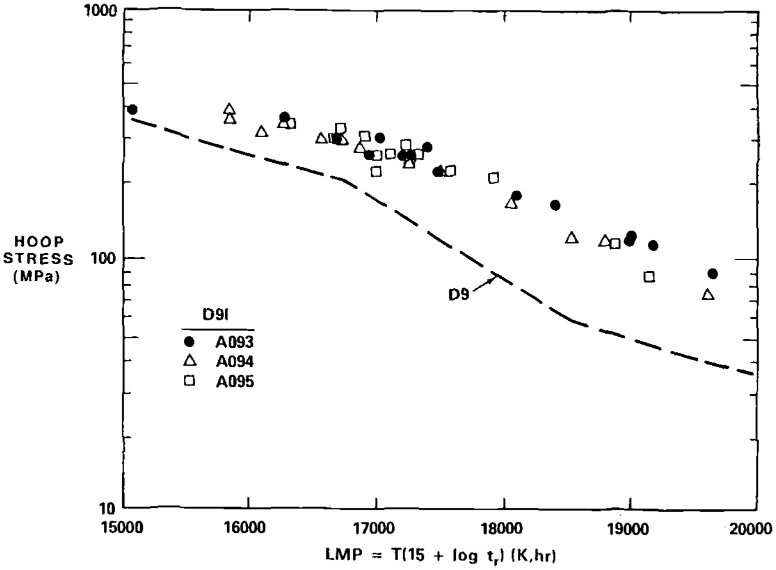

FIG. 27—*Larson Miller Parameter (LMP) representation of stress rupture data on improved heats of D9, where T is temperature in degrees Kelvin and t_R is rupture time in hours.*

D9 data base to a single curve. While the behavior of the three improved heats appears to be comparable at low temperatures or short rupture times, Fig. 27 shows that Heat A093 was stronger at higher temperatures or longer rupture times than either of the other two heats, which exhibited roughly comparable stress rupture behavior. This improvement, shown in Fig. 27 on an LMP basis, corresponds to an improvement of approximately a factor of ten in rupture life for the temperatures of interest. Recall that the strongest heat, A093, was the heat that was made from selected scrap with a lower molybdenum content than the other two heats (1.8 versus 2.2%). Regarding stress rupture behavior, therefore, the data imply that selected scrap should be an adequate feed stock and that a choice of 1.8% molybdenum is superior to that of 2.2% molybdenum. Based on studies of D9-type alloys, this choice of lower molybdenum levels will reduce swelling a small amount [*26*].

In-Reactor Creep

In-reactor creep behavior is determined by the interaction of two components, namely thermally activated and irradiation induced creep. At low temperatures, in-reactor creep is dominated by irradiation induced creep, the largest component of which is directly proportional to the swelling rate [*31*]. Irradiation creep thus displays the parametric sensitivity of swelling as demonstrated by comparing the swelling and creep behavior at 400°C (750°F) in Figs. 19 and 24. At high irradiation temperatures, above ~600°C (~1110°F), in-reactor creep is thought to be dominated by thermally activated creep. The improvement in in-reactor creep behavior shown in Fig. 22 is therefore consistent with the previously demonstrated improvement in ex-reactor stress rupture behavior.

Effect of Phosphorus and Boron

There are several conclusions from these studies that support the supposition that phosphorus and boron exert their influence via separate but sometimes synergistic mechanisms. First, note that boron influences ex-reactor creep behavior but appears to exert no large influence on void swelling. Since the largest component of in-reactor irradiation creep has been found to be proportional to the swelling rate [*31*], boron probably plays no large role in irradiation induced creep. Second, the tendency of boron or phosphorus to extend creep rupture life saturates rapidly when either is added separately, while their synergistic effect does not appear to saturate from the current data. This suggests that one element tends to compensate for the consequences of the other. Third, these and other studies show that the influence of each element is manifested in a different regime of thermal creep. As shown in Fig. 4, boron additions extend the creep rupture life via a delay in the onset of the tertiary stage of creep, rather than through a decrease in the secondary creep rate [*7,12*]. Phosphorus additions, however, exert their primary influence by decreasing the secondary creep rate, as demonstrated in this study (Fig. 4) and that of Reference *12*.

Since boron is a difficult element to detect, the majority of the "hard" results presented were related to the effects of phosphorus. The effect of boron must be ascertained more indirectly. The inferred lack of participation by boron in swelling and irradiation induced creep probably reflects its tendency to precipitate, particularly on grain boundaries. Swelling is a process that occurs in the bulk of the grain and is generally suppressed in the vicinity of grain boundaries, which function as strong sinks for radiation produced point defects. Swelling is sensitive to the presence of gases such as helium, one source of which is $^{10}B(n, \alpha)^{7}Li$ reactions. The cross section for this reaction is rather low in fast reactors, however. Furthermore, the influence of the helium extends only to the range of the alpha particles (~2 μm), leaving most of the grain unaffected since helium has a very low diffusivity [*32-34*].

Boron's relative lack of influence on swelling may also reflect its tendency to segregate to grain boundaries or interfaces and to participate with carbon in the formation of various (boro)carbide precipitates. While the onset of swelling is known to be somewhat sensitive to elements such as carbon, particularly through the compositional modification of the matrix that results from precipitation [*31*], the precipitation kinetics of these steels will most likely be dominated by the relatively high levels of titanium, thus allowing only a small role for boron.

Boron does have a significant effect on thermal creep, however. A wide variety of explanations have been advanced for this, as summarized in Reference *2*. In boron-free stainless steels, tertiary creep is characterized by the growth of grain boundary cavities and fissures leading to intergranular fracture with a relatively small amount of necking. In boron-containing steels, rupture life is increased through a delay in the onset of tertiary creep. Most explanations center on boron's influence on refining the size and distribution of carbide phases formed during heat treatment or early stages of the creep process [*7,12*], although in this work boron had no effect on the already fine distribution of titanium-rich carbide particles. Refinement is also promoted by the high dislocation density characteristic of cold worked steels. Refinement of precipitates in the matrix delays the recovery of the dislocation structure, while refinement of the grain boundary precipitates appears to prevent cavity formation. In stabilized stainless steels, such as those considered in this study, dislocation decoration is further enhanced throughout the matrix, except for well-defined precipitate-free zones at the grain boundaries. Such zones were visible in this study only at higher solute levels, as shown in the scanning electron microscope photographs in Fig. 28. While such decoration strengthens the grains, the precipitate-free zones allow for accommodation of plastic strain near the grain boundary, possibly reducing the formation of vacancy-fed cavity growth on the boundaries.

The suggestion has been made that boron-vacancy interactions play an important role in the transport of boron to grain boundaries and dislocations as well as in the nucleation of carbide-type precipitates [*7*]. In one study, however, boron was observed to have no influence on the equilibrium concentration of vacancies in 316L stainless steel [*35*]. Phosphorus, on the other hand, is relatively soluble in the alloy matrix and has been shown to have a large influence on

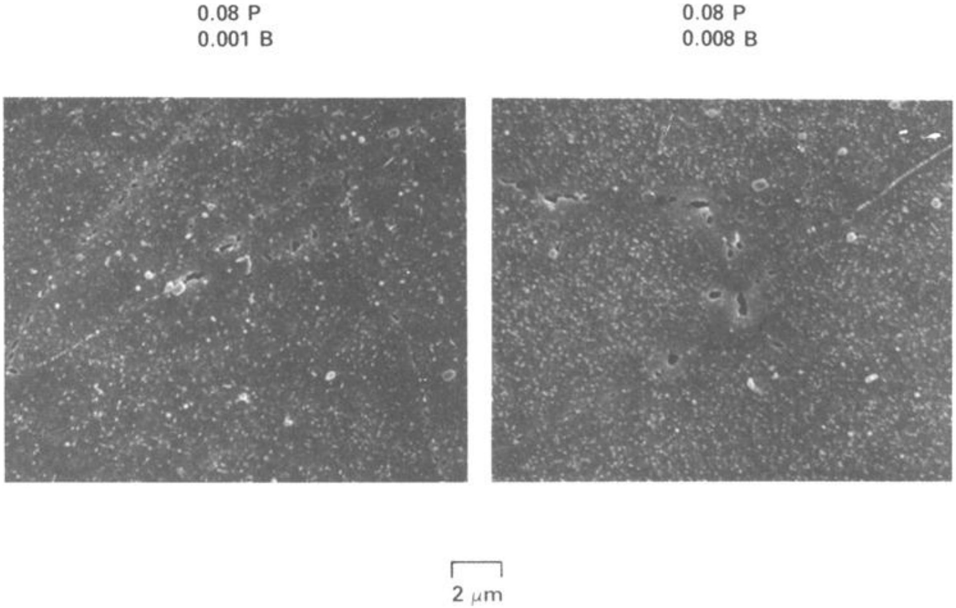

FIG. 28—*Precipitate-free zones observed in the D9 alloy having the highest levels of boron and phosphorus additions.*

the equilibrium concentration of vacancies [*35,36*], exhibiting a very large vacancy binding energy of ~0.4 eV. The effect of phosphorus in increasing the equilibrium vacancy concentration manifests itself in void generation during quenching and aging experiments using phosphorus containing steels [*37-40*]. Such studies confirm that the equilibrium concentration of vacancies is increased by orders of magnitude by small amounts of phosphorus.

The high vacancy concentration is expected to affect precipitation kinetics and distribution of carbide phases and support for this was found in this and other studies. Phosphorus promotes a finer dispersion of carbide phases and above 0.04% also leads to a very high density of needle-like phosphide phases, both of which will impede recovery processes. In addition, the growth of brittle Laves phase on grain boundaries appears to be inhibited by phosphorus.

While one might expect the enhanced vacancy population per se to increase the thermal creep rate it must be remembered that most vacancies are strongly bound and probably do not participate in the creep process. It has been proposed, however, that the enhanced equilibrium vacancy concentration from the phosphorus in solution strongly reduces the supersaturation of vacancies produced during irradiation, thus leading to many orders of magnitude reduction in void nucleation rates and an extension of the transient regime of the swelling [*24,25*]. A reduction in instantaneous swelling rate would also dictate a reduced rate of irradiation creep [*24,31*]. The formation of phosphides also appears to delay not only the recovery process but also the radiation induced formation of nickel and silicon-rich radiation-stable precipitates [*27*], such as G phase and gamma prime. These precipitates may cause void nucleation to increase via removal of particular elements [*25*].

The synergisms exhibited by phosphorus and boron in improving the creep rupture life appear to fall into two categories. Both appear to involve precipitation in the matrix and on grain boundaries. Precipitation in the matrix affects dislocation recovery, which in turn affects the vacancy transport throughout the grain. Precipitation at grain boundaries has a direct effect on cavity formation.

The second type of synergism may rely on the continued hardening of the matrix by the pinning of the high dislocation density by carbides and especially by phosphides. Phosphorus additions and phosphide formation have been noted to delay the radiation induced relaxation of dislocation density [*27*] that is a general feature of fast reactor irradiations of cold worked AISI 316 conducted above ~500°C (~930°F) [*41*]. This shifts the majority of the stress relief process to the grain boundaries, producing stress concentrations that favor the formation of creep cavities. Since boron tends to reduce cavity formation, a synergistic influence of boron and phosphorus results.

Conclusions

Controlled additions of both phosphorus (up to 0.08%) and boron (up to 0.008%) to a titanium stabilized austenitic stainless steel have been shown to lead to a larger improvement in ex-reactor stress rupture behavior than that anticipated from the single addition of either element. The two elements appear to affect stress rupture by different mechanisms. The synergism produced by the combined addition appears to be complex and is not well understood, but the increase in strength can be attributed in part to precipitation on a fine scale in both the matrix and the grain boundaries. The in-reactor creep behavior is also improved by adding phosphorus and boron. Irradiation induced swelling and creep are significantly delayed by the addition of phosphorus, although the full extent of the delay will not be known until additional data are available at higher exposure levels. The improvements in stress rupture, creep, and swelling behavior that result from such compositional modifications have culminated in the definition of an improved and patented D9 alloy referred to as UNS S38660 or D9I, containing 0.002 to 0.008% boron and 0.02 to 0.08% phosphorus. Optimum levels of these elements range from 0.004 to 0.006% boron and from 0.025 to 0.04% phosphorus.

References

[1] Bennett, J. W. and Horton, K. E., *Metallurgical Transactions A*, Vol. 9A, 1978, pp. 143-149.

[2] Korenko, M. K., U.S. Patent 4,407,673 Oct. 1983.

[3] Johnson, G. D. and Powell, R. W., U.S. Patent 4,530,719 July 1985.

[4] Garner, F. A., *Optimizing Materials for Nuclear Applications*. F. A. Garner, D. S. Gelles, and F. W. Wiffin, Eds., The Metallurgical Society of the American Institute of Mechanical Engineers, Warrendale, PA, 1985, pp. 111-139.

[5] Makenas, B. J., *Radiation-Induced Changes in Microstructure: 13th International Symposium (Part I), STP 955*, F. A. Garner, N. H. Packan, and A. S. Kumar, Eds., American Society for Testing and Materials, Philadelphia, 1987, pp. 146-153.

[6] Puigh, R. J. and Garner, F. A., *Radiation-Induced Changes in Microstructure: 13th International Symposium (Part I), ASTM STP 955*, F. A. Garner, N. H. Packan, and A. S. Kumar, Eds., American Society for Testing and Materials, Philadelphia, 1987, pp. 154-160.

[7] Thomas, B. J. and Henry, G., *Boron in Steel: Proceedings of the International Symposium on Boron Steels*, S. K. Banerji and J. E. Morral, Eds., Metallurgical Society of the American Institute of Mechanical Engineers, Warrendale, PA, 1980, pp. 80-105.

[8] Klueh, R. L. and Edmonds, D. P., *Welding Journal*, Vol. 65, 1986, pp. 1s-7s.

[9] Banerjee, B. R., Dulis, E. J., and Hauser, J. J., *Transactions of the American Society for Metals*, Vol. 61, 1968, pp. 103-109.

[10] Varin, R. A. and Tangri, K., *Materials Science and Engineering*, Vol. 72, No. 2, 1985, pp. 177-190.

[11] Sharma, A., Sharma, C. P., and Rajan, T. V., *Tool Alloy Steels*, Vol. 18, 1984, pp. 175-177.

[12] Grover, H. K. and Wickens, A., *Proceedings of the International Conference on the Mechanical Behaviour and Nuclear Applications of Stainless Steel at Elevated Temperatures*, The Metals Society, London, 1981, pp. 81-87.

[13] Park, I. -M. and Fujita, T., *Transactions of ISIJ*, Vol. 22, 1982, pp. 830-837.

[14] Shinoda, T., Tanaka, R., Matsuo, T., Mimino, T., and Kinoshita, K., *Proceedings of the First International Conference on the Mechanical Behavior of Materials*, Institution of Mechanical Engineers, 1972, pp. 181-190.

[15] Monma, Y., Yokoi, S., and Shin-ya, N., *Proceedings of the First International Conference on the Mechanical Behavior of Materials*, Institution of Mechanical Engineers, 1972, pp. 105-113.

[16] Kondo, Y., Yukitoshi, T., Yoshikawa, K., Nagai, N., Ohta, S., and Fujiwara, M., *Proceedings of the International Conference on Radiation Effects on Breeder Reactor Structural Materials*, M. L. Bleiberg and J. W. Bennet, Eds., The Metallurgical Society of the American Institute of Mechanical Engineers, New York, 1977, pp. 253-267.

[17] Hosoi, Y. and Wade, N., *Japan-France Seminar on Fundamental Aspects of Mechanical Properties and Microstructure Evolution of Stainless Steels at High Temperature*, N. Igata and J. de Fouquet, Eds., University of Tokyo, 1984, pp. 55-62.

[18] Williams, T. M., Harries, D. R., and Furnival, J., *Journal of the Iron and Steel Institute*, Vol. 210, 1972, pp. 351-358.

[19] Fujiwara, M., Uchida, H., Ohta, S., Yuhara, S., Tani, S., and Sato, Y., *Radiation-Induced Changes in Microstructure: 13th International Symposium (Part I), ASTM STP 955*, F. A. Garner, N. H. Packan, and A. S. Kumar, Eds., American Society for Testing and Materials, Philadelphia, 1987, pp. 127-145.

[20] "Welding, Brazing and Soldering," *Metals Handbook*, Vol. 6, 9th ed., E. F. Nippes, Coordinator, American Society for Metals, Metals Park, OH, 1983.

[21] Bechtold, R. A., "Fuel Failure Monitoring at the Fast Flux Test Facility," Report WHC-SA-0013, Westinghouse Hanford Company, Richland, WA, July 1987.

[22] Puigh, R. J. and Schenter, R. E., *Effects of Radiation on Materials: Twelfth International Symposium, ASTM STP 870*, F. A. Garner and J. S. Perrin, Eds., American Society for Testing and Materials, Philadelphia, 1985, pp. 795-802,

[23] Zaluzec, N. J., *Introduction to Analytic Electron Microscopy*, J. J. Hren, J. I. Goldstein, and D. C. Joy, Eds., Plenum Press, 1979, p. 121.

[24] Garner, F. A. and Brager, H. R., *Journal of Nuclear Materials*, Vols. 133 and 134, 1985, pp. 511-514.

[25] Garner, F. A. and Kumar, A. S., *Radiation-Induced Changes in Microstructure: 13th International Symposium (Part I), ASTM STP 955*, F. A. Garner, N. H. Packan, and A. S. Kumar, Eds., American Society for Testing and Materials, Philadelphia, 1987, pp. 289-314.

[26] Garner, F. A. and Brager, H. R., *Journal of Nuclear Materials*, Vols. 155-157, Part B, Oct. 1987, pp. 833-837.

[27] Itoh, M., Onose, S., and Yuhara, S., *Radiation-Induced Changes in Microstructure: 13th International Symposium (Part I), ASTM STP 955*, F. A. Garner, N. H. Packan, and A. S. Kumar, Eds., American Society for Testing and Materials, Philadelphia, 1987, pp. 114-126.
[28] Yang, W. J. S., *Radiation-Induced Changes in Microstructure: 13th International Symposium (Part I), ASTM STP 955*, F. A. Garner, N. H. Packan, and A. S. Kumar, Eds., American Society for Testing and Materials, Philadelphia, 1987, pp. 628-646.
[29] Lee, E. H., Mansur, L. K., and Rowcliffe, A. F., *Journal of Nuclear Materials*, Vols. 122 and 123, 1984, pp. 299-304.
[30] Mansur, L. K., Haynes, M. H., and Lee, E. H., *Phase Stability During Irradiation*, J. R. Holland, L. K. Mansur, and D. I. Potter, Eds., The Metallurgical Society of the American Institute of Mechanical Engineers, Warrendale, PA, 1981, pp. 359-382.
[31] Garner, F. A., *Journal of Nuclear Materials*, Vols. 122 and 123, 1984, pp. 459-471.
[32] Gelles, D. S. and Garner, F. A., *Journal of Nuclear Materials*, Vols. 85 and 86, 1979, pp. 687-693.
[33] Garner, F. A., *Radiation Effects*, Vol. 66, 1982, pp. 211-216.
[34] Kumar, A. S. and Garner, F. A., *Radiation Effects*, Vol. 82, 1984, pp. 61-72.
[35] Azarian, A. and Kheloufi, K., *Journal of Nuclear Materials*, Vol. 97, 1981, pp. 25-28.
[36] Azarian, A., "Contribution a l'Etude des Defauts Ponctuels dans les Aciers Inoxydables," CEA-R-4617, Ph.D. Thesis, University of Paris, Paris, France, 1974.
[37] Rowcliffe, A. F. and Nicholson, R. B., *Acta Metallurgica*, Vol. 20, 1972, pp. 143-155.
[38] Rowcliffe, A. F. and Eyre, B. L., *J. Phys. F*, Vol. 1, 1971, pp. 771-777.
[39] Boulanger, L., *Scripta Metallurgica*, Vol. 14, 1980, pp. 67-69.
[40] Azarian, A., DaCunha Belo, M., and Leteutre, J., *Scripta Metallurgica*, Vol. 9, 1975, pp. 185-189.
[41] Garner, F. A., Hamilton, M. L., Panayotou, N. F., and Johnson, G. D., *Journal of Nuclear Materials*, Vols. 103 and 104, 1981, pp. 803-807.

J. R. Kearns,[1] *M. J. Johnson,*[1] *G. Aggen,*[1] *and W. D. Edsall*[2]

The Effect of Boron, Copper, and Molybdenum Residuals on the Corrosion Resistance of Type 304 Stainless Steel

---

REFERENCE: Kearns, J. R., Johnson, M. J., Aggen, G., and Edsall, W. D., "**The Effect of Boron, Copper, and Molybdenum Residuals on the Corrosion Resistance of Type 304 Stainless Steel,**" *Residual and Unspecified Elements in Steel, ASTM STP 1042.* A. S. Melilli, and E. G. Nisbett, Eds., American Society for Testing and Materials, Philadelphia, 1989, pp. 150–165.

ABSTRACT: Systematic variations in the chromium, nickel, copper, molybdenum, and boron and B contents of American Iron and Steel Institute (AISI) Type 304 stainless steel (UNS S30400) were evaluated by electrochemical and immersion corrosion tests in oxidizing, reducing, and chloride solutions. In one series of tests, the chromium and nickel alloy contents were maintained within the flat rolled product tolerance range (17.8 to 18.0 wt% chromium, 7.8 to 8.0 wt% nickel) while the copper and molybdenum alloy contents were increased from a residual level (<0.5 wt%) to a range from 0.6 to 0.7 wt%. Strip specimens with such compositions performed as well as others that had chromium and nickel contents within the specified analytical limits for tubular products (18.0–20.0 wt% chromium; 8.0–11.0 wt% nickel) and copper and molybdenum contents below 0.5 wt%. The results of an ASTM A01.17 committee interlaboratory program (twelve industrial labs testing per ASTM Practices for Detecting Susceptibility to Intergranular Attack in Austenitic Stainless Steels (A 262-85a), Practice C, did not reveal any significant difference in the intergranular corrosion resistance of the said compositions. None of the compositional modifications resulted in increased susceptibility to sensitization as caused by welding or heat treating.

The effect of residual boron on the carbide precipitation kinetics and intergranular corrosion resistance of mill and laboratory produced Type 304 stainless was also evaluated. The corrosion rates for fully annealed samples in boiling nitric, phosphoric, acetic, oxalic, and lactic acids were not related to alloy boron contents in the range 0.0003 to 0.0056 wt%. The rate of corrosion for sensitized (815°C for 24 h) samples in boiling 65 wt% nitric acid declined rapidly with increasing boron contents in the range from 0.0004 to 0.0011 wt%. The corrosion rates for sensitized samples containing 0.0011 to 0.0056 wt% boron were constant and, on average, 0.6 mm/y (0.002 ipm) higher than those for samples in a fully annealed condition.

KEY WORDS: stainless steel, residual elements, corrosion resistance, sensitization, carbides, AISI Type 304, copper, molybdenum, boron

The quality of a conventional stainless steel is usually evaluated relative to specifications that have been established by internationally recognized technical organizations, for example, the American Society for Testing and Materials (ASTM) and the American Society of Mechanical Engineers (ASME). Such specifications are further refined by metal producers, fabricators, and end users. The latter two groups tend to restrict specified ranges according to the requirements of a particular application or product form. Such restrictions often prohibit the metal producer from optimizing raw material and production costs. For instance, the ASTM general requirements for flat rolled products [ASTM Specification for General Requirements for Flat-

---

[1] Senior corrosion engineer, research specialist, and manager, respectively, Allegheny Ludlum Steel Division of Allegheny Ludlum Corporation, Technical Center, Brackenridge, PA 15014-1597.

[2] Director of Quality Assurance and Services, Allegheny Ludlum Steel Division of Allegheny Ludlum Corporation, Brackenridge, PA 15014-1597.

Rolled Stainless and Heat-Resisting Steel Plate, Sheet, and Strip (A 480/A 480 M-84a)] have permitted the use of product analysis tolerances while the ASTM general requirements for tubular products [ASTM Specification for General Requirements for Specialized Carbon and Alloy Steel Pipe (A 530/A 530M-85b) and ASTM Specification for General Requirements for Carbon, Ferritic Alloy, and Austenitic Alloy Steel Tubes (A 450/A 450M-86a)] have not (Table 1). Consequently, certain strip that is acceptable within the broader flat rolled specification cannot be fabricated into tubing. A major concern about resolving the discrepancy between the two specifications has been that reducing the proportions of the major alloying elements, chromium and nickel, might compromise the corrosion performance of the final product, particularly for compositions containing high levels of residual elements. In the first phase of the present study, a typical American Iron and Steel Institute (AISI) Type 304 stainless steel (UNS 530400) strip composition was modified by increasing the copper and molybdenum residual levels (typically 0.2 to 0.5 wt%) to within the range 0.6 to 0.7 wt% and decreasing the chromium and nickel contents toward the minimum of the specified tolerance allowed by the flat rolled product specification (that is, 17.8 to 18.0 wt% chromium; 7.8 to 8.0 wt% nickel).

The second phase of the present study was concerned with the effect of boron at levels less than 0.01 wt% in Type 304. Small amounts of boron as measured by bulk chemical analysis can significantly affect mechanical and corrosion properties. Nevertheless, boron remains an unspecified element in most specifications, including ASTM Specification for Heat-Resisting Chromium and Chromium-Nickel Stainless Steel Plate, Sheet, and Strip for Pressure Vessels (A 240-85) and ASTM Specification for Seamless and Welded Austenitic Stainless Steel Tubing for General Service (A 269-85). The principal reason for unspecified boron is that, except for certain nuclear applications, the control of alloy boron content is most crucial to the metal producer to minimize cracking during hot working operations.The relation of alloy boron content to grain boundary precipitates and intergranular corrosion resistance was evaluated in the present study.

Influence of Copper and Molybdenum

The copper and molybdenum present in the scrap metal in a typical argon oxygen decarburization (AOD) charge are retained to a large extent in continuous or ingot cast austenitic stainless steel slabs. The range for copper and molybdenum in Type 304 stainless can typically vary from 0.05 to 0.5 wt%. Residual levels of copper have been observed to enhance passivity in

TABLE 1—*ASTM compositional specifications for various Type 304 stainless product forms* (wt%).

	A 269/A 450 (Tubing)	A 312/A 530 (Pipe)	A 240/A 480 (Plate, Sheet, Strip)	
Component	Min/Max	Min/Max	Min/Max	Tolerance
C	/0.08	/0.08	/0.08	0.01
Mn	/2.0	/2.0	/0.20	0.04
P	/0.040	/0.040	/0.040	0.005
S	/0.030	/0.030	/0.030	0.005
Si	/0.75	/0.75	/0.75	0.05
Cr	18.0/20.0	18.0/20.0	18.0/20.0	0.20
Ni	8.0/11.0	8.0/13.0	8.0/10.5	0.10
Mo	. . .	. . .	. . .	. . .
Cu	. . .	. . .	. . .	. . .
N	. . .	. . .	. . .	. . .

reducing acids [*1*] while the principal benefit of molybdenum alloying is enhanced resistance to localized corrosion as induced by chlorides. However, associated reductions in weight loss have only been observed when copper and molybdenum contents are an order of magnitude or more above the residual level [*1,2*]. Kiefer and Renshaw [*3*] significantly increased the resistance of AISI Type 316 (UNS 531600) (2.44 wt% molybdenum) to sulfuric acid with an alloy addition of 2.15 wt% copper. Pruger et al. [*2*] have proposed that the austenitizing power of copper be exploited by partially substituting copper for nickel: increasing residual copper to 0.75 wt% would permit a decrease of 0.5 wt% nickel. A similar increase in molybdenum residuals was also advocated, since no adverse effects on physical properties had been observed. In oxidizing acids, copper does not seem to affect corrosion performance while larger amounts of molybdenum have been related to increased rates of corrosion [*1*].

Influence of Boron

The solubility limit of boron in an unstabilized Fe-Cr-Ni stainless steel decreases rapidly from 0.001 wt% (100 ppm) at the eutectic temperature (approximately 1150°C) [*4*]. Workers at Allegheny Ludlum Steel [*2,5*] did not observe any precipitates in an austenitic stainless with normal residual boron contents: 0.0005 to 0.0006 wt% boron. Higher annealing temperatures and faster cooling rates were required to produce precipitate free grain boundaries in stainless with boron contents of 0.001 wt% and greater [*2,5*]. Above 0.004 wt% boron, the segregation of boron to grain boundaries during cooling not only reduces the total quantity of grain boundary precipitation but also replaces chromium carbides with a more corrosion resistant boron-rich precipitate. Boron tends to precipitate preferentially at grain boundaries as a boride (M_2B) and, to a lesser extent, as a borocarbide [$M_{23}(C,B)_6$; where M = (Cr,Fe, lesser Ni)] compound; depending on the alloy boron and carbon contents as well as the heat treatment [*4*]. These changes in the quantity and composition of the grain boundary precipitates during thermal exposure have been related to reduced intergranular corrosion rates.

Several workers [*5-8*] have found that boron had either no influence or was beneficial to intergranular corrosion resistance. Others [*2*] have concluded that the presence of 0.001 wt% boron or more is detrimental to the corrosion resistance of an austenitic stainless steel even in the mill annealed condition. Farrell and Rosenthal [*8*] have found that the corrosion rate for sensitized Type 304 in boiling nitric acid decreases with boron contents from 0 to 0.0007 wt% and increases (by 0.6 mm/y or 0.002 ipm) from 0.0007 to 0.0037 wt% boron, but concluded that boron contents of up to 0.0080 wt% had no significant effect on intergranular corrosion resistance. At levels above 0.0030 wt% boron and up to 0.0100 wt% boron, carbide precipitation was found to be suppressed during sensitizing treatments [*8*]. Boron-rich precipitates would not be expected to form until levels of 0.0030 wt% boron or more were present in the steel. Voeltzel and Henry [*9*] demonstrated that the effect a given amount of boron had on the intergranular corrosion resistance of 18Cr-10Ni type stainless depended on the temperature and duration of an anneal as well as the titanium and molybdenum contents. These authors noted that corrosion rates increased with alloy boron contents above 0.006 wt% and decreased when below this figure. Boron contents above 0.01 wt% are generally accepted as reducing resistance to corrosion in hot nitric acid solutions.

Experimental Procedure

Materials

Three groups of specimens were obtained from laboratory and commercial production. Final cold rolled, annealed, and descaled (CRAD) strip from seven commercial heats that had been continuously cast from a 90 600 kg (100 ton) AOD vessel was used in two cases. One of the commercial heats that was chosen represented a Type 304 chemistry with typical levels of residual and unspecified elements (Table 2). The other six heats were selected for boron contents that varied from 0.0003 to 0.0015 wt%.

Strip from the heat with the typical composition was remelted in a vacuum induction melting (VIM) furnace. Carbon, nitrogen, and manganese additions were made to compensate for estimated losses incurred during remelting. Molybdenum or copper or both were intentionally added to the VIM charge for three of the five remelted heats. The chromium and nickel aims of four heats were designed to be below the A269-85 specified minimums but still within the specification tolerance range for A480/A480M-84a. The VIM heats were cast into 23 kg ingots.

For the boron alloy study, electrolytic chromium, iron, manganese, and nickel and high purity iron silicon (FeSi) went into one master VIM heat (in wt%: 0.038 carbon, 1.78 manganese, 0.015 phosphorus, 0.003 sulfur, 0.41 silicon, 18.60 chromium, 8.65 nickel, 0.010 titanium, 0.0035 nitrogen, 0.0004 boron). Sections of the master ingot were remelted with various boron additions to obtain eleven different boron contents from 0.0004 to 0.0057 wt%. The remelted material suffered minor tungsten (0.005 wt% tungsten) and carbon (0.002 to 0.004 wt% carbon) contamination.

All of the VIM cast ingots were conditioned, reheated to 1200°C, forged to slab, ground, reheated to 1175°C, hot rolled, annealed at 1065°C, water quenched, pickled, hydroblasted,

TABLE 2—*Chemical compositions of modified Type 304 stainless steel.*

	Chemistries (wt%) of Cited Alloy Designations					
Component	Mill Product (AOD)	Lab Control (VIM)	Lean Cr Lean Ni	Lean Cr Lean Ni + Cu	Lean Cr Lean Ni + Mo	Lean Cr Lean Ni + Cu + Mo
C	0.060	0.065	0.060	0.066	0.061	0.061
Mn	1.83	1.87	1.85	1.87	1.85	1.84
P	0.036	0.033	0.034	0.037	0.034	0.034
S	0.008	0.009	0.012	0.010	0.008	0.008
Si	0.57	0.56	0.55	0.53	0.56	0.55
Cr	18.38	18.44	17.80	17.85	17.86	17.85
Ni	8.14	8.13	7.90	7.96	7.99	8.02
Mo	0.24	0.24	0.24	0.24	0.65	0.66
Cu	0.25	0.25	0.23	0.65	0.25	0.67
N	0.063	0.063	0.061	0.063	0.062	0.063
	CORROSION CALCULATIONS BASED ON WILDE AND GREEN [*10,11*]					
Active Corrosion Current Density (μa/cm^2)	442	450	1266	520	573	49
	CORROSION CALCULATIONS BASED ON MORRIS AND SCARBERRY [*12*]					
Graphic Corrosion Current (μa/cm^2)	0.3	0.3	0.4	0.3	0.4	
Calculated Corrosion Rate (mm/y)	0.004	0.004	0.005	0.004	0.005	

cold rolled to a thickness of approximately 0.2 cm, final annealed in an inert gas atmosphere at 1095°C for 15 min and water quenched. A portion of each group of specimens was welded in a gas tungsten arc welding (GTAW) process. The GTA welds were made without a filler metal (that is, autogenously) and with pure argon shield and backup gases. Sensitizing heat treatments were performed for either 1 h at 677°C (1250°F) or 24 h at 815°C (1500°F). The former treatment was performed in a gas fired furnace followed by an air cool and the entire cycle of heating and cooling for the latter treatment occurred in argon atmospheres. The faces of the welded and heat treated specimens were wire brushed, acid cleaned, and degreased prior to immersion and polarization testing. The faces of the VIM specimens used in the boron alloy study were ground to a depth of 0.025 cm to remove deboronized surface layers. The edges of all blanks were machined to obtain a final specimen size of 2.5 by 5 cm.

Corrosion Testing

Specimens in both welded and CRAD conditions were evaluated in the following immersion tests:

(1) Oxalic acid etch test [ASTM Practices for Detecting Susceptibility to Intergranular Attack in Austenitic Stainless Steels (A 262-85a), Practice A]; electrolytic 10 wt% oxalic acid solution at room temperature;

(2) Streicher test (ASTM A 262-85a, Practice B); boiling ferric sulfate-sulfuric acid solution;

(3) Huey test (ASTM A 262-85a, Practice C); boiling 65 wt% nitric acid;

(4) Pitting test {ASTM Test Method for Pitting and Crevice Corrosion Resistance of Stainless Steels and Related Alloys by the Use of Ferric Chloride Solution [G 48-76 (1980), Practice A]}; 6 wt% ferric chloride (10% ferric chloride hexahydrate: 10% $FeCl_3 \cdot 6H_2O$) solution at 23°C; and

(5) Crevice corrosion test [ASTM G 48-76 (1980) Practice B]; 6 wt% ferric chloride solution at 23°C with creviced samples. Immersion tests were also performed according to ASTM Recommended Practice for Laboratory Immersion Corrosion Testing of Metals [G 31-72 (1985)] in the following environments:

(1) Boiling 10 wt% sulfuric acid solution;

(2) 1 $\bar{N}$ sulfuric solution at room temperature; and

(3) 10 wt% phosphoric acid, glacial acetic acid, 10 wt% oxalic acid and 50 wt% lactic acid: all of the solutions were boiling.

Potentiodynamic anodic polarization tests were also conducted per ASTM Practice for Standard Reference Method for Making Potentiostatic and Potentiodynamic Anodic Polarization Measurements (G 5-82) using 1 $\bar{N}$ sulfuric acid and 1000 ppm sodium chloride electrolytes at room temperature. A Petrolite Potentiodyne® M4100 Analyzer was used in conjunction with the electrochemical cell described by Johnson [*10*]. Measurements were made by automatically increasing the applied potential from −1.0 to +1.0 V, relative to a saturated calomel electrode (SCE), at a rate of 6.0 V/h.

Results and Discussion

Influence of Copper and Molybdenum on Lean Type 304

A preliminary assessment of the effects of minor compositional modifications on the corrosion resistance of Type 304 was made based on an empirical relation developed by Greene and

Wilde [11,12]. The equation relates alloy composition to a parameter obtained from anodic polarization tests in 1N sulfuric acid at 30°C

$$I_c = 351 + 373(\mathrm{Mn}) - 1240(\mathrm{Cu}) - 750(\mathrm{Mo})$$
$$+ 76000(\mathrm{S}) - 6500(\mathrm{C}) - 840(\mathrm{Cr} - 18)$$

I_c is the critical anodic current density expressed in $\mu A/cm^2$ and the chemical elements are given in wt%. Of particular relevance to this study was the finding that small decreases in copper, molybdenum, and chromium would increase I_c. The I_c value is inversely related to the passivating tendency of an alloy in weakly oxidizing media. Steels with I_c values below 100 $\mu A/cm^2$ have been found to be resistant to aerated, dilute sulfuric acid and those with values above 1000 $\mu A/cm^2$ pitted severely in 4% sodium chloride solution at 90°C [12]. The calculated I_c values appear in Table 2. Reducing the alloy chromium and nickel content to the minimum of the flat rolled product tolerance range (referred to as "low Cr-Ni") increased the I_c value by an order of magnitude. Additions of copper and molybdenum each reduced the I_c values for the low Cr-Ni composition to approximately that for the mill product. The combination of copper and molybdenum reduced the calculated I_c values even further.

The measured electrochemical parameters for all of the modified compositions were typical of the commercial Type 304 product in 1 N sulfuric acid at 23°C and a scan rate of 6 V/h (Fig. 1):

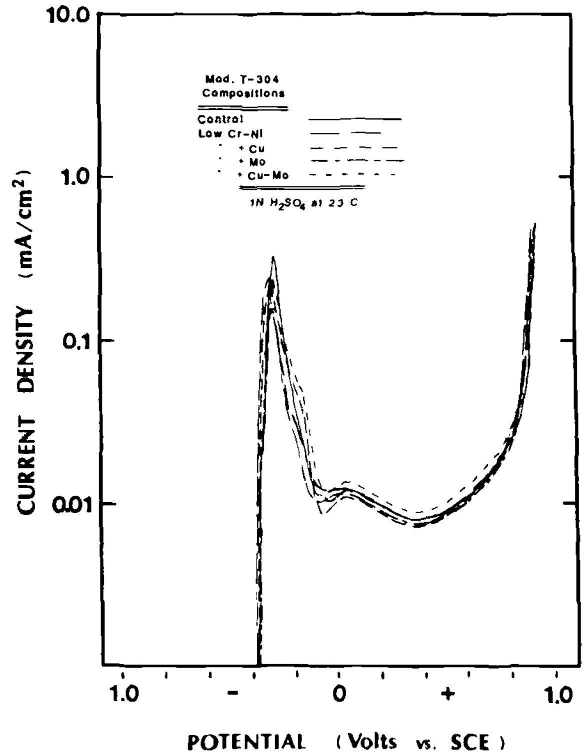

FIG. 1—*Potentiodynamic anodic polarization curves for modified Type 304 stainless compositions in 1N sulfuric acid electrolyte at 23°C.*

1. The peaks of the active loops (that is, I_c values) occurred near −0.32 V(1) with associated primary passive potentials (E_{pp}) in the 0.15 to 0.35 mA/cm^2 range.
2. The passive range of potentials was from −0.8 to 0.6 V.
3. The current density for the passive range of potentials varied from 0.007 to 0.013 mA/cm^2.
4. Signs of pitting were not evident, rather, a smooth transition from passive to transpassive conditions began at applied potentials more electropositive than 0.4 V.
5. The reverse scan line (not shown in Fig. 1) did not cross the forward scan line in the passive range of potentials. The current density rapidly dropped three orders of magnitude with a 0.15 V decrease from the 1.0 V maximum.

The I_c values for each composition were reproducible to within ±9% of a mean for duplicate tests. The current densities were consistent to 5%. Potentials corresponding to various points on a given curve were reproducible to within 0.04 V in both solutions.

Corrosion rates were calculated from the polarization curves (Table 2) by converting graphically extrapolated corrosion current values, as per the methodology of Morris and Scarberry [*13*]. The calculated rates correlated well with the results of immersion tests in 1 $\bar{\mathrm{N}}$ sulfuric acid at 30°C for 100 h (Table 3). The rates in boiling 10 wt% sulfuric acid were four orders of magnitude higher than the rates in 1 N sulfuric acid (Table 3), which is typical of the Type 304 product. In all three cases involving sulfuric acid, no significant difference in the corrosion resistance of the five compositions was evident.

The active peaks that were distinctly present in the scans involving sulfuric acid were absent from scans of samples in the 1000 ppm sodium chloride solution (Fig. 2). The primary passive

TABLE 3—*Corrosion test results for modified type 304 stainless steel.*

		Total Average Corrosion Rate, mm/y, for Cited Alloy Designations				
Corrosion Test	Sample Condition	Lab Control (VIM)	Lean Cr Lean Ni	Lean Cr Lean Ni + Cu	Lean Cr Lean Ni + Mo	Lean Cr Lean Ni + Cu + Mo
ASTM A 262	CRAD	0.590	0.690	0.642	0.653	0.660
Practice B[a]	Welded	0.598	0.689	0.673	0.643	0.628
ASTM A 262	CRAD	0.231	0.268	0.240	0.303	0.277
Practice C[b]	Welded	0.241	0.267	0.256	0.286	0.267
10% H_2SO_4[c]	CRAD	14.440	18.472	15.812	18.900	17.427
	Welded	14.629	19.268	16.034	20.118	17.304
1 $\bar{\mathrm{N}}$ H_2SO_4[d]	CRAD	0.002	0.001	0.002	0.001	0.002
		Total Average Weight Loss (g/cm^2)				
ASTM G 48	CRAD	0.023	0.027	0.027	0.023	0.027
Practice A[e]	Welded	0.025	0.024	0.026	0.024	0.024
ASTM G 48	CRAD	0.021	0.025	0.023	0.023	0.024
Practice B[f]	Welded	0.021	0.024	0.023	0.025	0.023

[a] Samples were exposed for one 120 h period in a boiling ferric sulfate-sulfuric acid solution.

[b] Samples were exposed for five 48 h periods in a boiling 65 wt% nitric acid solution. Cited rates are total average for the five periods.

[c] Test was stopped after four 48 h periods due to high corrosion rates. The solution was boiling.

[d] Samples were exposed for one 100 h period at 30°C (80°F).

[e] Samples were exposed for one 72 h period at room temperature. Practice B involves the use of teflon blocks held on the sample surface by two rubber bands.

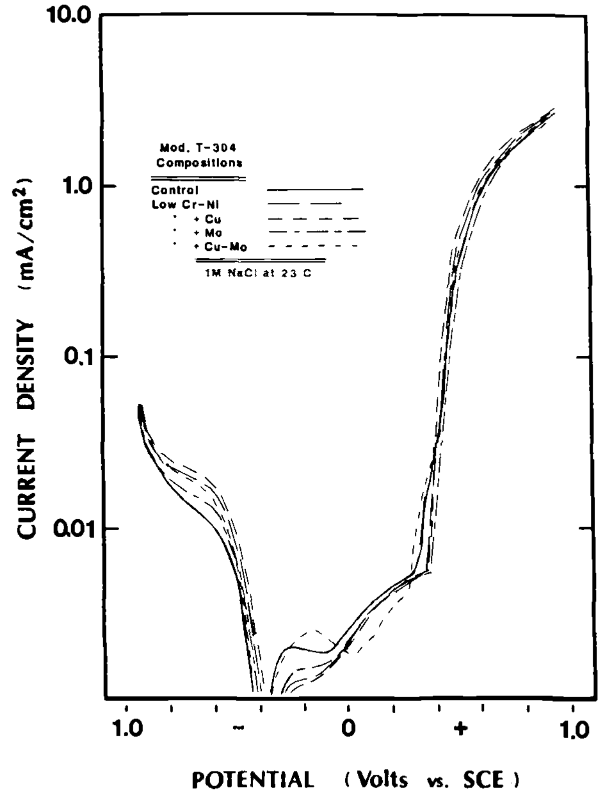

FIG. 2—*Potentiodynamic anodic polarization curves for modified Type 304 stainless compositions in 1M sodium chloride at 23°C.*

current densities were an order of magnitude higher in the acid solutions (0.5 pH) than in the chloride solution with neutral pH. Two results were consistent in all the electrochemical tests described above: (1) all five compositional modifications had passivating characteristics that were typical of the Type 304 product, and (2) no scan for a given composition deviated from any other by more than the experimental error.

Based on the above observations, the reproducibility of the testing method was concluded to be sufficient for identifying significant differences in corrosion performance. However, such trends were not evident. For example, the control heat had the highest I_c in 1 N sulfuric acid and the low Cr-Ni + Mo cast had the lowest value, but the difference was within the observed limit of reproducibility. Therefore, this difference in corrosion behavior could not be considered significant. The rates of corrosion, both calculated and measured, for all compositions in 1N sulfuric acid varied by only 0.001 mm/y (<0.00001 ipm). Similarly, the rates for the boiling 10 wt% sulfuric acid exposures were also of the same order of magnitude with the important qualification that the environment was far too aggressive (a desirable rate would be under 0.6 mm/y or 0.002 ipm) to assess accurately the influence of minor changes in alloy content. Autogenous GTA welding did not appear to degrade the corrosion properties of any of the compositions in the solutions listed in Table 3.

The results of an ASTM A01.17 committee interlaboratory study program (twelve industrial labs testing per ASTM A 262-85a, Practice C) are plotted in Figs. 3 and 4. There was no consistent distinction in the performance of any given composition. The range of corrosion rates at any given lab for the five compositions varied by at most 0.09 mm/y (0.0003 ipm). The range of values obtained at the different labs varied by 0.31 mm/y (0.001 ipm). However, ten of the twelve labs obtained values within a range of 0.15 mm/y (0.0005 ipm). Decreasing the chromium content by 0.64 wt% and the nickel by 0.23 wt% only increased the average corrosion rate by 0.03 mm/y (0.0001 ipm): compare the lab control and the low Cr-Ni heats. Increasing the copper or molybdenum to 0.065 wt% reduced the average corrosion rate by 0.015 to 0.024 mm/y (0.00005 and 0.00008 ipm), respectively. The corrosion rates for all modified compositions were below the 0.45 mm/y (0.0015 ipm) limit specified by E. I. du Pont de Nemours and Co. [*14*] for annealed Type 304 in the Huey test. All of the cited variations are in the second and third decimal places for rates in terms of mm/y (forth and fifth for ipm). Such variations are of no practical significance since they are well within experimental error. Figure 4 compares results of three laboratories for samples in CRAD and welded conditions to a total average of all twelve laboratories for CRAD samples. The similarity in corrosion rates and the appearance after exposure of samples in both conditions indicated that there was no preferential attack at the weldment. All of the rates were below 0.45 mm/y (0.0015 ipm).

Influence of Boron on Type 304

Tests conducted per ASTM A 262-85a, Practice A (Table 4) on commercially produced strip in the hot rolled and annealed condition indicated that heats containing 0.0003, 0.0007, 0.0012, and 0.0015 wt% boron might be susceptible to intergranular corrosion attack in other ASTM A 262-85a tests. Discontinuous globular precipitates were observed on the grain boundaries of these heats (Fig. 5). The precipitates are thought to be $M_{23}(C,B)_6$ borocarbides rather than M_2B borides considering the boron contents of the examined alloys [*4,6,7,15,16*]. The size, shape,

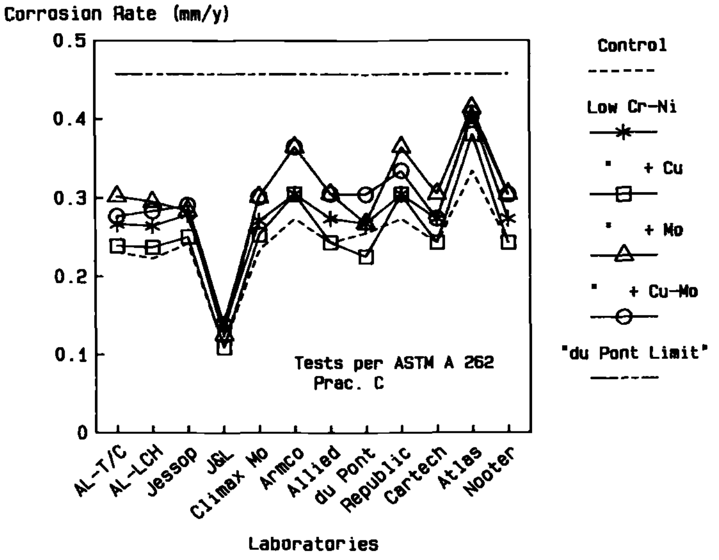

FIG. 3—*Corrosion rates for modified Type 304 chemistries as determined by twelve industrial laboratories in tests per ASTM A 262-85a, Practice C. Each value represents an average of two determinations.*

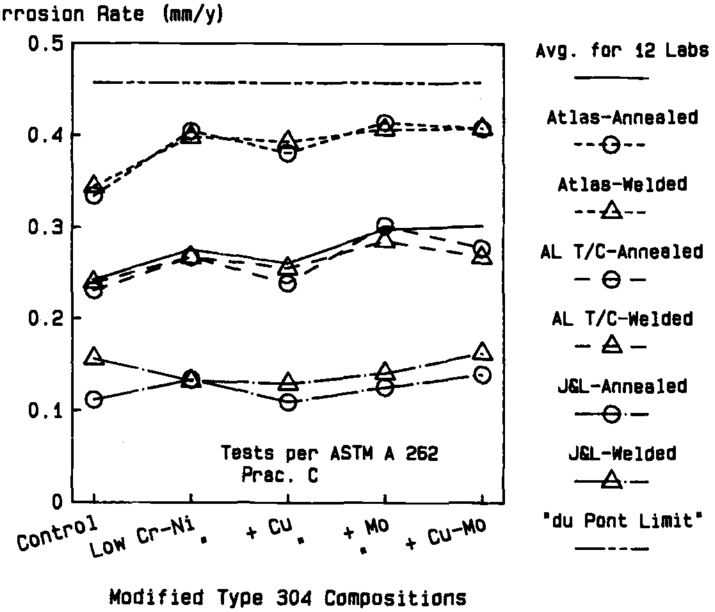

FIG. 4—*Comparison of intergranular corrosion rates for compositionally modified Type 304 samples in fully annealed (CRAD) and autogenously welded (GTAW) conditions. The averages of the rates determined by twelve industrial laboratories in tests per ASTM A 262-85a, Practice C, are also plotted.*

TABLE 4—*Corrosion test results for Type 304 with boron.*[a]

	Visual Rating of Microstructure for Cited Alloy Boron Contents (ppm)					
Test	3	5	6	7	12	15
Carbide Rating[b]	C1	C1	C1	C1	C2	C3
Carbide Rating[b,c]	C5	C5	C5	C5	C5	C5
ASTM A 262 Practice A	Dual	Step	Step	Dual	Dual	Dual

	Corrosion Rates (mmy)[d] for Cited Alloy Boron Contents (ppm)					
Test	3	5	6	7	12	15
ASTM A 262:						
Practice B	0.610	0.610	0.579	0.610	0.610	0.579
Practice C	0.244	0.335	0.244	0.244	0.244	0.305
Practice C[c]	12.68	. . .	. . .	13.81	14.36	14.33

[a] Samples were in the hot rolled and annealed condition.

[b] Ratings established relative to the visual standards shown in Fig. 6.

[c] Samples were sensitized by heat treating for one hour at 677°C (1250°F) followed by air-cooling. Sensitized samples were descaled prior to immersion testing.

[d] The cited rates are averages of two tests.

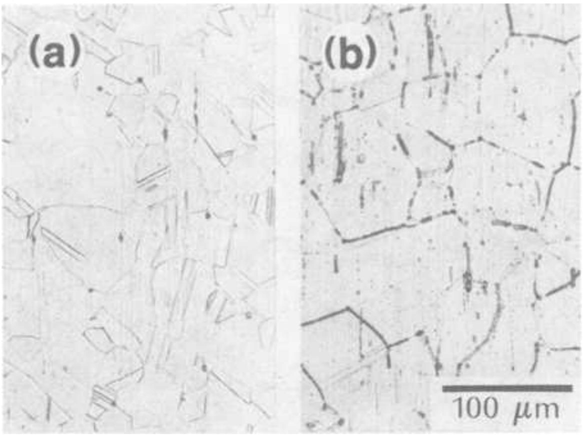

FIG. 5—*Photomicrographs of Type 304 samples containing* (a) *0.0005, and* (b) *0.0015 wt% boron after exposure in electrolytic 10 wt% oxalic acid (ASTM A 262-85a, Practice A). The etched microstructures were rated as step and dual, respectively.*

density, and distribution of particles were rated by subjective visual examination relative to the standards illustrated in Fig. 6. The ratings for all of the hot rolled annealed samples were acceptable (that is, rated as C-3 or below) for subsequent production stages. Standard mill final anneal cycles were adequate to obtain C-1 microstructure ratings and corrosion rates less than 0.45 mm/y (0.00015 ipm) in the Huey test. After exposure at 677°C for 1 h, all of the Type 304 samples had unacceptable carbide content ratings and very high corrosion rates in the Huey test (Table 4). The observed microstructure and corrosion behavior are both typical of Type 304 grades containing more than 0.03 wt% carbon when in a sensitized condition.

The rate of corrosion for samples sensitized by exposure at 815°C for 24 h declined rapidly

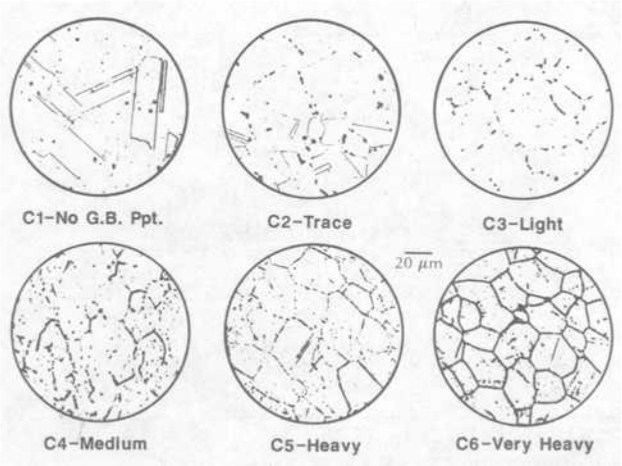

FIG. 6—*Reference standards used in rating the carbide contents of austenitic stainless steel transverse microstructures when etched and in chromic acid.*

with increasing boron contents in the range from 0.0004 to 0.0011 wt% (Fig. 7). The corrosion rates for samples containing 0.0015 to 0.0057 wt% boron and sensitized at 815°C for 24 h were constant and, on the average, 0.6 mm/y (0.002 ipm) higher than those for samples of the same composition in an as-annealed condition. All of the compositions in the as-annealed condition had rates that were below 0.6 mm/y (0.002 ipm) and only one (0.039 wt% boron) corroded at a rate exceeding 0.45 mm/y (0.0015 ipm). The increase in corrosion rates for sensitized Type 304 (2 h at either 649, 704, or 760°C) with alloy boron contents in the range of 0.0007 and 0.0037 wt% observed by Farrell and Rosenthal [*8*] was not confirmed by this study.

The sensitizing treatment at 815°C for 24 h resulted in corrosion rates in the Huey test that were lower than those for samples that had been sensitized at 677°C for 1 h. The former heat treatment results in carbide morphologies that tend toward discrete particles versus the continuous grain boundary films formed by the latter treatment [*17, 18*]. Grain boundary regions containing discrete particles are less susceptible to attack in oxidizing acids.

The previously cited corrosion rates were averages for five 48-h exposure periods. The same body of data for samples sensitized at 815°C for 24 h is presented in another format (Fig. 8) to show that the corrosion rates increased with each successive period of exposure. Continued attack of regions adjacent to grain boundary precipitates caused more grains to drop from the microstructure, which resulted in higher rates with each successive exposure period.

Many of the environments that induce the intergranular corrosion of annealed austenitic stainless steels in commercial applications do not involve strongly oxidizing solutions such as 65 wt% nitric acid. Therefore, immersion tests in three boiling organic acids were performed to supplement results discussed above. The corrosion rates ranged from: (1) <0.03 to 0.06 mm/y (<0.0001 to 0.0002 ipm) in 10% phosphoric acid, (2) 0.50 to 0.64 mm/y (0.00165 to 0.00209 ipm) in glacial acetic acid, (3) <0.03 to 7.00 mm/y (<0.0001 to 0.02298 ipm) in 10% oxalic acid, and (4) 0.03 to 29.79 mm/y (0.0001 to 0.09772 ipm) in 50% lactic acid. The changes in rates within the cited ranges did not correlate with the boron contents of the laboratory heats.

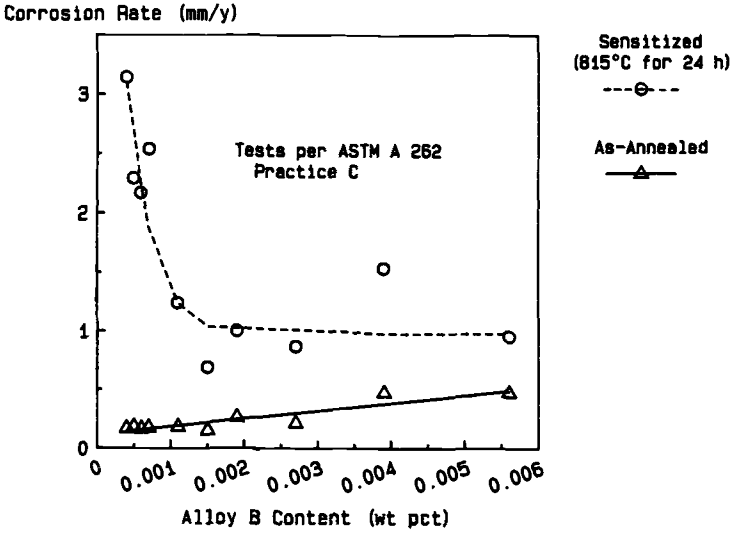

FIG. 7—*The effect of alloy boron content and sensitizing treatment on the corrosion rate of Type 304 stainless steel tested in boiling 65 wt% nitric acid (per ASTM A 262-85a, Practice C).*

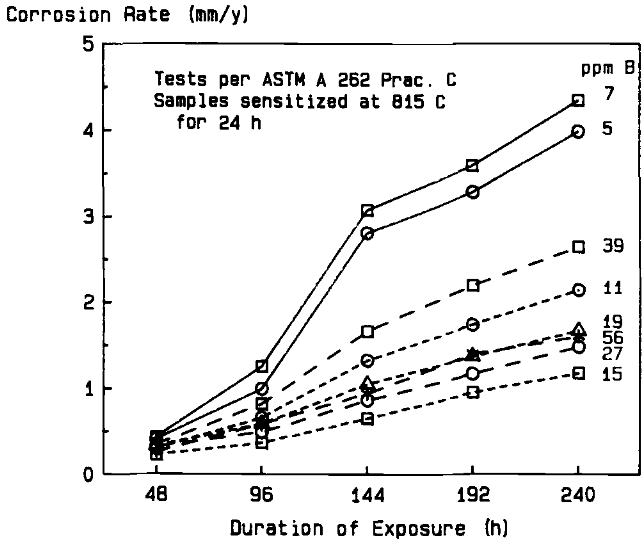

FIG. 8—*The effect of alloy B content on the corrosion rate of sensitized Type 304 stainless steel tested in boiling 65 wt% nitric acid (per ASTM A 262-85a, Practice C).*

Conclusions

1. Type 304 chemistries with chromium and nickel contents in the flat rolled product tolerance range performed as well as compositions within the specified analytical limits in acid and chloride solutions.

2. Relatively high copper or molybdenum or both residual element contents (0.6–0.7 wt%) had no detrimental effect on the corrosion resistance of Type 304 compositions with lean chromium and nickel contents.

3. The results of an ASTM sponsored interlaboratory program (twelve industrial labs testing per ASTM A 262-85a, Practice C) did not reveal any significant difference in the corrosion resistance of the five Type 304 chemistries varying in chromium, nickel, copper, and molybdenum contents.

4. Commercially acceptable levels of intergranular precipitation and corrosion resistance were obtained using standard mill annealing cycles for 304 strip containing 0.0003 to 0.0015 wt% boron.

5. Greater than normal boron contents (0.0011 to 0.0056 wt%) were found to reduce the corrosion rates of sensitized Type 304 in nitric acid.

6. The corrosion rates for annealed Type 304 in the Huey test increase slightly with boron contents in the range 0.0004 to 0.0056. Only a composition with 0.0039 wt% boron had a rate above 0.45 mm/y (0.0015 ipm).

Acknowledgments

The efforts of the Allegheny Ludlum Steel Technical Center staff in metal production, analysis, fabrication, and testing are gratefully acknowledged. Thanks are also offered to the twelve industrial laboratories that participated in the interlaboratory study.

References

[1] Scharfstein, L. R., *Effects of Residual Elements on Properties of Austenitic Stainless Steels, ASTM STP 418,* American Society for Testing and Materials, Philadelphia, 1967, pp. 90-104.

[2] Pruger, T. A., Blake, F., and Valley, J. A., *Effects of Residual Elements on Properties of Austenitic Stainless Steels, ASTM STP 418,* American Society for Testing and Materials, Philadelphia, 1967, pp. 23-36.

[3] Kiefer, G. C. and Renshaw, W. G., *Corrosion,* Vol. 6, No. 8, 1950, pp. 235-244.

[4] Goldschmidt, H. J., *Journal of the American Iron and Steel Institute,* Vol. 209, No. 11, 1971, pp. 900-909.

[5] Ziemianski, J. P. and Aggen, G., "Boron in Stainless Steels as Related to Mill Processing," Presented at American Iron and Steel Institute Meeting, Pittsburgh, Nov. 11, 1965.

[6] Robinson, F. P. A. and Scurr, W. G., *Corrosion,* Vol. 33, No. 11, 1977, pp. 408-417.

[7] Williams, T. M. and Talks, M. G., *Journal of the American Iron and Steel Institute,* Vol. 210, No. 11, 1972, pp. 870-871.

[8] Farrell, J. W. and Rosenthal, P. C., *Metal Progress,* Vol. 77, No. 2, 1960, p. 101-103.

[9] Voeltzel, J. and Henry, G., "Memoires Scientifique," *Revues Metallurgie,* Vol. 61, No. 2, (BISI translation #4493) pp. 123-128.

[10] Johnson, M. J., *Localized Corrosion—Cause of Metal Failure, ASTM STP 516,* American Society for Testing and Materials, Philadelphia, 1972, pp. 262-272.

[11] Greene, N. D. and Wilde, B. E., *Corrosion,* Vol. 25, No. 7, 1969, pp. 300-306.

[12] Greene, N. D. and Wilde, B. E., *Corrosion,* Vol. 26, No. 12, 1970, pp. 533-538.

[13] Morris, P. E. and Scarberry, R. C., *Corrosion,* Vol. 28, No. 12, 1969, pp. 444-452.

[14] Brown, M. H., *Corrosion,* Vol. 30, No. 1, 1974, pp. 1-12.

[15] Alden, M., Asplund, S., and Aronsson, B., *Journal of the American Iron and Steel Institute,* Vol. 207, 1969, p. 235.

[16] Keown, S. R., *Scandinavian Journal of Metallurgy,* Vol. 2, 1973, pp. 59-63.

[17] Aust, K. T., Armijo, J. S., and Westbrook, J. H., *Transactions of the American Society for Metals,* Vol. 59, 1966, pp. 545-556.

[18] Stickler, R. and Vinckier, A., *Transactions of the American Society for Metals,* Vol. 54, 1961, pp. 363-380.

DISCUSSION

A. A. Tavassoli,[1] *(discussion question)*—We have found that in general, Type 316LN (UNS S31603 and S31651) behaves better than Type 304 with regard to improved weldability and resistance to radiation embrittlement with reductions in boron content. What is your opinion on the behavior of Type 304 (UNS S304000) in respect to these properties?

J. R. Kearns (author's response)—Your question is beyond the scope of the present study, so we have no new data to offer. A few comments based on a cursory review of the literature are offered for the sake of discussion. In a recent paper, Otterburg and Roberts [*1*] have hypothesized that boron delays the precipitation of $M_{23}(C,B)_6$ in Type 304 relative to the low carbon grade Type 304L by blocking the diffusion of chromium and carbon to grain boundaries. Alternatively, the segregation of boron at grain boundaries was said to promote the rapid formation of the M_2B boride in the low carbon grade. Therefore, the rate of formation and quantity of borides and carboborides would tend to be greater for a low carbon grade. The removal of chromium from the matrix by either type of boride not only would degrade corrosion properties but would also increase hot cracking sensitivity by retarding the formation of ferrite. One benefit of this phenomena, particularly for a molybdenum-bearing grade such as Type 316LN, is that the formation of borides at grain boundaries occurs at the expense of inter-metallic phases,

---

[1] SRMA, Department de Technologie, CEN-Saclay, France.

such as sigma phase, and other type carbides and inter-metallic phases. Your observation of superior weldability for the Type 316LN indicates that the molybdenum and nitrogen can compensate for an unfavorable carbon/boron ratio. It has been proposed that molybdenum inhibits the diffusion of boron to grain boundaries [*2*] and it is well known that nitrogen also retards the precipitation rate of carbides and inter-metallic phases (but without depleting the matrix of chromium by precipitation).

In regard to the hot cracking aspect of weldability, Type 304 with boron contents below 0.4 wt% tend to be susceptible to heat affected zone liquation cracking due to the formation of low melting point interdendritic films. At higher boron levels (greater than 0.35 wt% boron) hot cracks are suppressed or "healed" by excess eutectic boride [*3*]. Such a Type 304 composition would be easily sensitized to intergranular corrosion and stress corrosion cracking, and would have poor impact properties. But, there are certain applications, such as containment of spent nuclear fuel, where these factors are not limiting [*3*].

Boron generally has a beneficial effect on the high temperature ductility of austenitic stainless by refining the size and distribution of carbide phases [*4*]. However, irradiation transmutes boron isotopes to helium and lithium, and the subsequent coalescence of helium bubbles at grain boundaries results in intergranular cracking. Harries and Roberts [*5*] have found the net effect to be that the radiation embrittlement of austenitic stainless appears to be independent of the alloy boron content (up to 0.01 wt% boron). The role of boron and phosphorus in relation to the radiation damage of austenitic stainless steels has been extensively studied by Hamilton et al. as presented in this volume.

W. R. Warke[2] *(discussion question)*—ASTM A 262-85a is an ASTM Practice for Detecting Susceptibility to Intergranular Attack in Austenitic Stainless Steels. Both molybdenum and copper would be predominantly in solid solution rather than at the grain boundaries in Type 304 and they would not participate significantly in the sensitization process. Why was ASTM A 262-85a practice used as the primary method to evaluate corrosion resistance in your work rather than a test for general corrosion resistance pitting and crevice corrosion?

J. R. Kearns (author's response)—We appreciate the logic of your argument, but there were compelling commercial and technical reasons for using the Huey test. The accelerated corrosion rates of sensitized samples in hot nitric acid have been attributed not only to chromium depletion associated with precipitation but also to the formation of porous Mo(VI) oxides [*6*] in localized regions. (The later point is why the test is not recommended for use in evaluating grades in the American Iron and Steel Institute 300 that contain molybdenum.) Therefore, a Type 304 bulk composition with a reduced chromium or elevated molybdenum content or both would be expected to corrode at a higher rate. Although data in the literature indicates that copper and molybdenum in the 0.5-0.7 wt% range would not be detrimental, as discussed in the paper, the behavior of Type 304 compositions containing high residuals with lean major alloying elements has not, to our knowledge, been demonstrated. In addition, the A 262-85a, Practice C, test was chosen by the ASTM A01.17 subcommittee since it is the most widely used method of evaluating Type 304 for industrial applications. Supplemental tests were also conducted in sulfuric acid since sight changes in copper and molybdenum contents have been shown to influence the dissolution of Type 304 in sulfuric acid more than in nitric acid. Potentiodynamic polarization tests in chloride-bearing solutions were also conducted to establish the effect of compositional modifications on localized corrosion resistance.

W. R. Warke (discussion question)—Have you compared the high temperature oxidation/scaling resistance of these steels?

---

[2] Amoco Corp., P.O. Box 400, Naperville, IL 60566.

J. R. Kearns (author's closure)—Evaluating the oxidation behavior of the selected Type 304 compositions was beyond the scope of this work. In considering the work of Aggen and Ziemainski [*7*] on Type 201 (UNS S20100), boron contents below 0.01 wt% would not be expected to influence the scaling of an austenitic stainless steel. The said study revealed that precipitate-free surface layers could be formed to a depth of 0.005 in by annealing at 2200°F for 7 min. The treatment was effective in reducing the boron content to below 0.001 wt% (from as much as 0.009 wt% boron) as well as producing substantial decarburization. It was thought that boron readily volatilized and, consequently, had no observable effect on the amount of scale formed during the anneal. Unfortunately, the high temperature anneal was not a practical means of controlling alloy boron content because it also produced poor surface quality and an objectionably large grain size.

References

[*1*] Otterberg, R. and Roberts, W., *Stainless Steels '84*, Institute of Metals, London, 1985, pp. 229-239.
[*2*] Elen, J. D., and Glas, A., *Journal of Nuclear Materials*, Vol. 34, 1970, pp. 182-188.
[*3*] King, K. J. and Wilkinson, J., *Stainless Steels '84*, Institute of Metals, London, 1985, pp. 368-378.
[*4*] Thomas, B. J. and Henry, G., *Boron in Steel*, Metallurgical Society of the American Institute of Mechanical Engineers, Warrendale, PA, 1980, pp. 80-105.
[5] Harries, D. R. and Roberts, A. C., *Effects of Radiation on Structural Metals, ASTM STP 426*, American Society for Testing and Materials, Philadelphia, 1967, pp. 21-47.
[*6*] Otterberg, R., *9th International Congress on Metallic Corrosion*, National Research Council of Canada, Toronto, Ont., Vol. 3, 1984, pp. 134-140.
[*7*] Ziemianski, J. P. and Aggen, G., "Boron in Stainless Steels as Related to Steel Processing," Presented at the American Iron and Steel Institute Meeting, Pittsburgh, Nov. 1965.

Welding, Preheating, and Postweld Heat Treating

David J. Abson[1]

The Influence of Current Supply Type on the Composition, Microstructure, and Mechanical Properties of C-Mn and C-Mn-Ni Shielded Metal Arc Welds

---

REFERENCE: Abson, D. J., **The Influence of Current Supply Type on the Composition, Microstructure, and Mechanical Properties of C-Mn and C-Mn-Ni Shielded Metal Arc Welds,** *Residual and Unspecified Elements in Steel, ASTM STP 1042,* A. S. Melilli and E. G. Nisbett, Eds., American Society for Testing and Materials, Philadelphia, 1989, pp. 169-191.

ABSTRACT: An American Welding Society (AWS) E7016 type C-Mn electrode and an AWS E7018 type C-Mn-Ni electrode were each used to produce a series of butt welds in 25-mm (1-in.) thick British Standard (BS) 4360 50E (C-Mn-Nb) steel plate in the flat (1G) position. For each consumable, direct current (DC) reverse polarity (electrode positive), DC straight polarity (electrode negative), and AC power supplies were each used for a complete panel. In addition, DC straight polarity was employed for vertical-up (3G) welding with the C-Mn-Ni electrode. The chemical composition, strength, microstructure, and toughness of the deposits were studied in the as-welded condition.

For the C-Mn-Ni 1G welds (and to a lesser extent for the C-Mn welds), manganese and silicon decreased in the order DC reverse polarity, AC and DC straight polarity. For both consumables, there was a concomitant increase in nitrogen content. There were no associated changes in strength or microstructure, but there was generally a progressive decrease in crack tip opening displacement (CTOD), measured at −10°C, and in Charpy toughness. As a consequence of strain aging, Charpy toughness was lower in the root than in the fill region.

The 3G DC straight polarity C-Mn-Ni deposit had higher strength in the root and higher Charpy toughness than the corresponding 1G deposit. The CTOD of the former was lower and showed much more scatter, to which locally low toughness regions (revealed by fractographic examination) contributed.

KEY WORDS: carbon-manganese steels, shielded metal arc welding, vertical-up welding, polarity, AC, DC, weld metal, composition, oxygen, nitrogen, microstructure, strength, impact toughness, fracture toughness, CTOD

The root pass or passes in a multiple-pass shielded metal arc (SMA) weld in structural steels are, in common practice, welded using straight polarity (electrode negative), and the joint is completed using reverse polarity (electrode positive). Straight polarity is chosen for the root pass because of the lesser penetration achieved and because the faster freezing of the weld pool and molten slag give easier manipulation of the electrode. An alternative that is (in principle) available for the welding engineer is to employ alternating current (AC) welding. However, in practice the deciding factor may be the type of welding equipment available. There are national differences in the usage of different types of welding sets, and these persist because of the willingness of electrode manufacturers to meet local demands. For example, AC welding is preferred in Japan and DC welding in Europe. Particularly in butt welds where high weld tough-

---

[1] Principal research metallurgist, The Welding Institute, Cambridge, England CB1 6AL.

ness is required, inquiring whether the current type and polarity have any significant influence on weld composition and mechanical properties is pertinent, especially as such procedural details have not always been included in welding procedure specifications. Little relevant information has been published relating to this aspect of SMA welding; Dawson and Judson [*1*] found minimal difference in Charpy toughness between SMA welds produced using reverse polarity and straight polarity. However, they did report that "some fabricators consider that DC positive gives fewer defects, better penetration and, ultimately, enhanced joint toughness." In unpublished work carried out at The Welding Institute, which included welds deposited with American Welding Society (AWS) A5.5 E8018-C1 (UNS W22018) and AWS A5.1 E7016-C1 electrodes, Haugh et al. [*2*] observed poorer Charpy toughness for DC straight polarity deposits compared with AC or DC reverse polarity deposits, but found that welder-to-welder toughness variations were generally of similar magnitude to those arising from the changes in power supply type.

The present study was undertaken to investigate the influence of current supply type on weld composition, microstructure, and mechanical properties. Butt welds were produced in 25-mm thick steel plate in the flat position for both C-Mn and C-Mn-Ni electrodes and also vertically-up for the latter. The welds were assessed by chemical analysis, measurement of the tensile properties, hardness, Charpy toughness, crack tip opening displacement (CTOD), and fractographic and quantitative metallographic examination.

Experimental Details

Parent Steels and Welding Electrodes

The composition of the 25-mm (1-in.) thick BS 4360 grade 50E parent steel employed in this investigation is given in Table 1. The main analysis was carried out on a remelted sample in a direct-reading optical emission vacuum spectrometer, with oxygen and nitrogen analysis being carried out by inert gas fusion in a Leco T136 analyzer.

The 4-mm diameter commercial basic-coated electrodes employed were a C-Mn, AWS E7016-G electrode, for which the manufacturer recommended AC or DC straight polarity, and a C-Mn-Ni AWS E7018-G electrode, for which the manufacturer recommended AC or DC reverse polarity.

Analysis techniques for the core wires and electrode coatings are given in the companion paper [*3*], and the results are presented here in Tables 2 and 3. Note that the core wire of the C-Mn electrode has higher nitrogen and lower oxygen contents than that of the C-Mn-Ni electrode. The coating analyses reflect the presence of nickel and iron powder in the C-Mn-Ni electrode and the higher carbon dioxide (CO_2) content of the C-Mn electrode coating. The magnesium in the C-Mn electrode coating may be present mainly (or entirely) as magnesium carbonate.

Welding

The weld preparation was a symmetrical double-V with a 70° included angle, and with a 2-mm root face and 3-mm root gap. The panel length was 500 mm and its total width 230 mm. An end restraint 25 mm thick, and 230 by 150 mm was welded to each end of the panel and in the same plane, by means of four partial penetration welds, terminating $\geq$25 mm from the weld preparation. The electrodes were given a 350°C/1 h drying treatment and were stored at 150°C before use.

For all welding, the specified welding conditions were a current of 145A and an arc energy of 1.7 kJ/mm. The same welder was employed for all welding, which was carried out without preheat, and with a maximum interpass temperature of 150°C. Duplicate panels were welded in

TABLE 1—*Chemical analysis (wt%) of the 25 mm thick BS 4360 Grade 50E parent plate (1B 345) employed.*

Plate Code Number	C	S	P	Si	Mn	Ni	Cr	Mo	V	Cu	Cb	Ti	Al	N	O	IIW CE[a]	P_{cm}[b]
1B345	0.13	0.006	0.014	0.33	1.29	0.02	0.02	0.01	0.005	0.03	0.032	<0.002	0.036	0.005	0.002	0.36	0.214
Sn, Co ≤ 0.005; B < 0.0003																	

[a] $\text{IIW CE} = C + \frac{Mn}{6} + \frac{Cr + Mo + V}{5} + \frac{Ni + Cu}{15}$

[b] $P_{cm} = C + \frac{Si}{30} + \frac{Mn}{20} + \frac{Cu}{20} + \frac{Ni}{60} + \frac{Cr}{20} + \frac{Mo}{18} + \frac{V}{10} + 5B$

TABLE 2—*Chemical analysis (wt%) of the electrode core wires.*

Electrode	C	S	P	Si	Mn	Ni	Cr	Mo	V	Cu	Cb	Ti	Al	N	O
C-Mn	0.055	0.008	0.011	<0.01	0.51	0.02	0.02	<0.005	<0.002	0.03	<0.002	<0.002	<0.003	0.008	0.018
C-Mn-Ni	0.050	0.010	0.006	<0.01	0.45	0.02	0.005	<0.005	<0.002	0.01	<0.002	<0.002	<0.003	0.004	0.028

TABLE 3—*Chemical analysis (wt%) of the electrode coatings.*

Electrode	Si	Ti	Zr	Al	Fe	Mn	Ca	Mg	Na	K	Li	F	CO_2	Ba	Ni	Cr	Mo	Cb	V	Cu
C-Mn	7.8	4.9	1.2	0.4	4.8	4.8	26.3	2.5	0.7	2.5	<0.2	8.0	19.8	<0.1	<0.1	<0.1	<0.1	<0.1	<0.1	<0.1
C-Mn-Ni	5.9	4.3	<0.1	0.4	26.0	5.4	20.2	0.9	0.4	1.5	<0.2	8.3	12.3	<0.1	1.6	0.1	<0.1	<0.1	<0.1	<0.1

all cases, in order to provide sufficient material for investigation without the risk of bowing. In the flat (1G) position, panels were welded using DC straight polarity, DC reverse polarity, and AC supplies. In addition, the C-Mn-Ni electrode was employed in the vertical-up (3G) position using DC straight polarity, which was found to give the poorest toughness in welds deposited in the flat position, in order to see if further degradation in toughness occurred, possibly related to an expected higher weld nitrogen content. It will be noted that this power supply type is contrary to the manufacturer's recommendation, but reflects possible "abuse" of the electrode, which could occur during fabrication.

The first side of each panel was completed, and in order not to remove the potentially strain age damaged region in the root, the second side was only ground to sound metal (removing typically ~2 mm of metal) before the second side was completed. In the flat position, all welds were completed in a total of 14 passes. In the vertical-up welding, in spite of the attempt to employ closely similar welding conditions, the arc energy ranged from 1.7 to 1.85 kJ/mm, and the welds were each completed in a total of only eleven passes.

Specimen Extraction and Testing

Chemical Analysis—Chemical analysis of the welds was achieved by cutting a small sample of weld down the central plane and then analyzing in a direct reading optical emission vacuum spectrometer, sparking on the central plane in the first side root region and towards the surface in the second side beads. These locations correspond approximately to the regions which were tested in the tensile and Charpy specimens, which were machined as discussed below. Oxygen and nitrogen analyses were measured on two to four small samples cut from the corresponding locations on the mating half. The latter analyses were carried out by inert gas fusion in a Leco TC136 analyzer.

Mechanical Testing—The cutting scheme for the complete welded panels is shown in Fig. 1. One longitudinal tensile specimen to BS 18, with a gauge length of 22.7 mm and a gauge diameter of 5.64 mm was extracted from the first side root regions and a further one from the second side subsurface region. These specimens were tested at ambient temperature in a Dartec Universal testing machine. Ten Charpy specimens were extracted from the first side root region and a further ten from the second side subsurface region. These specimens were notched in the through-thickness direction, that is, with the root of the notch perpendicular to the weld sur-

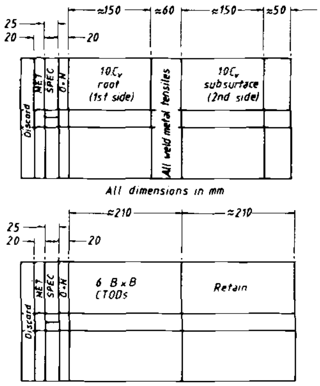

FIG. 1—*Cutting scheme for each pair of butt welds.*

face, on the central plane of the weld, and each set was tested over a range of temperatures to give a transition curve.

The duplicate panels provided samples for metallographic examination, chemical analysis, and CTOD testing. Six BS 5762 subsidiary geometry square section specimens for CTOD testing were extracted with their long direction across the weld. They were notched through the thickness on the weld central plane, and, following local compression of ~1% to induce the subsequent formation of a uniform fatigue precrack [*4*], were fatigue precracked with *a/W* ~0.25, where *a* and *W* are the depths of the precrack and the specimen, respectively. These specimens were all tested at −10°C. The testing and the subsequent measurement of crack lengths and calculation of the crack tip opening displacement (CTOD) were carried out according to BS 5762: 1979. Prior to fatigue precracking and testing, all the CTOD specimen blanks, and also the machined tensile specimens, were given a hydrogen removal treatment at 150°C for 40 h; this treatment accelerated the reduction in hydrogen that would normally occur in a fabrication before service. The CTOD tests were carried out in three point bending under displacement control at a crosshead displacement rate of 0.010 mm/s. Any specimen that did not break during the test was cooled in liquid nitrogen and then broken in the test machine.

Except for the hydrogen removal treatments mentioned above, all mechanical testing was carried out on specimens in the as-welded condition.

Metallographic and Fractographic Examination—A transverse section from each butt welded panel for metallographic examination was prepared by mechanically polishing to a 1 μm diamond finish and by etching in nital. The regions of primary interest were as-deposited beads in the first side root region and in the low dilution region on the second side. Within these regions, the beads that were examined in detail and employed for point counting (in which 1000 points were counted on a Swift point counter at ×500 magnification) were typically about the third bead deposited in the first side root region and the final bead in the capping pass on the second side. The proportion of as-deposited weld metal, in regions corresponding to those sampled by the notch in the Charpy specimens, was determined by linear intercept at a magnification of ×10 as the mean of the values on the central plane of the weld and 1 mm on each side of it. Vickers hardness measurements were made down the central plane of each weld in both first and second side regions on the transverse metallographic sections. Measurements were made in both as-deposited and reheated, that is, re-austenitized, regions.

Examination of the CTOD sample fracture faces was carried out using a scanning electron microscope (SEM).

Results

Butt Weld Chemical Analyses

The butt weld chemical analyses are presented in Table 4, together with calculated values of the International Institute of Welding (IIW) carbon equivalent and values of the inclusion volume fraction, estimated from the chemical analyses according to the procedure outlined in Ref *5*. The duplicate welds, and also subsurface and root regions of corresponding welds, were of closely similar composition. However, the manganese level was particularly high in the root region of W7 (1.74%) and in the subsurface region of weld W10A (1.95%), and was low in the root region of weld W18 (1.37%), for which a high nitrogen content was determined (0.022%). These differences are probably attributable to inadvertent variations in arc length, and thus in the efficacy of shielding, with a slightly longer arc length having been used for the beads sampled in the root region of W18, and a short arc length having been used for the beads sampled in the two regions. Surprisingly, the vertical-up C-Mn-Ni welds have slightly lower nitrogen contents than the welds deposited in the flat position with this consumable (~0.007 versus ~0.011%), and also very slightly higher silicon and lower manganese contents. The larger esti-

TABLE 4—*Weld metal chemical analysis (wt%), IIW carbon equivalent values (CE), and the volume % of nonmetallic inclusions, estimated using the procedure employed in Ref 5.*

Weld Code	Region Sampled	Electrode	Current Type or Polarity	C	S	P	Si	Mn	Ni	Cr	Mo	V	Cu	Cb	Ti	Al	N	O	IIW CE[c]	I, %
W7	SS	C-Mn[a]	DC reverse	0.06	0.007	0.016	0.41	1.62	0.02	0.03	0.01	0.002	0.03	0.005	0.018	0.003	0.010	0.026	0.34	0.19
W7	Root	C-Mn[a]	DC reverse	0.07	0.007	0.014	0.39	1.74	0.02	0.04	0.005	0.002	0.03	0.005	0.029	0.009	0.008	0.029	0.39	0.19
W17	SS	C-Mn[a]	DC reverse	0.06	0.006	0.016	0.39	1.65	0.02	0.03	0.01	0.002	0.03	0.005	0.016	<0.003	0.011	0.028	0.35	0.20
W17	Root	C-Mn[a]	DC reverse	0.09	0.006	0.016	0.37	1.61	0.02	0.03	0.005	0.005	0.03	0.012	0.018	0.004	0.010	0.027	0.38	0.19
W9	SS	C-Mn[a]	AC	0.06	0.006	0.014	0.39	1.58	0.02	0.03	0.005	0.002	0.02	<0.002	0.018	<0.003	0.011	0.027	0.33	0.19
W9	Root	C-Mn[a]	AC	0.07	0.006	0.014	0.41	1.63	0.02	0.03	0.005	0.002	0.03	0.003	0.021	<0.003	0.012	0.027	0.35	0.19
W19	SS	C-Mn[a]	AC	0.07	0.007	0.016	0.39	1.62	0.02	0.03	0.005	0.002	0.03	0.005	0.016	<0.003	0.012	0.027	0.35	0.20
W19	Root	C-Mn[a]	AC	0.08	0.007	0.016	0.41	1.55	0.05	0.03	0.005	0.002	0.03	0.010	0.023	0.005	0.011	0.027	0.35	0.19
W8	SS	C-Mn[a]	DC straight	0.07	0.007	0.015	0.38	1.64	0.02	0.03	0.005	0.002	0.03	<0.002	0.017	<0.003	0.014	0.027	0.35	0.20
W8	Root	C-Mn[a]	DC straight	0.07	0.007	0.015	0.38	1.54	0.02	0.03	0.005	0.002	0.03	0.002	0.019	0.004	0.016	0.026	0.34	0.18
W18	SS	C-Mn[a]	DC straight	0.09	0.007	0.016	0.35	1.55	0.02	0.03	0.005	0.002	0.03	0.004	0.017	<0.003	0.016	0.026	0.36	0.19
W18	Root	C-Mn[a]	DC straight	0.09	0.007	0.016	0.31	1.37	0.02	0.03	0.005	0.002	0.03	0.006	0.015	<0.003	0.022	0.026	0.33	0.19
W10A	SS	C-Mn-Ni[a]	DC reverse	0.05	0.008	0.010	0.40	1.95	0.89	0.02	0.005	0.01	0.01	<0.002	0.009	0.004	0.006	0.036	0.44	0.26
W10A	Root	C-Mn-Ni[a]	DC reverse	0.05	0.008	0.010	0.35	1.87	0.85	0.02	0.005	0.01	0.01	<0.002	0.007	0.004	0.006	0.039	0.43	0.28
W10B	SS	C-Mn-Ni[a]	DC reverse	0.05	0.008	0.010	0.31	1.85	0.83	0.02	0.005	0.01	0.01	<0.002	0.007	0.004	0.008	0.036	0.42	0.26
W10B	Root	C-Mn-Ni[a]	DC reverse	0.05	0.008	0.010	0.34	1.86	0.81	0.02	0.005	0.01	0.01	0.002	0.007	0.004	0.007	0.036	0.42	0.26
W12A	SS	C-Mn-Ni[a]	AC	0.05	0.008	0.010	0.36	1.76	0.82	0.02	0.01	0.01	0.01	<0.002	0.010	0.004	0.008	0.035	0.41	0.25
W12A	Root	C-Mn-Ni[a]	AC	0.05	0.008	0.009	0.31	1.75	0.88	0.02	0.01	0.01	0.01	<0.002	0.007	<0.003	0.006	0.035	0.41	0.26
W12B	SS	C-Mn-Ni[a]	AC	0.06	0.009	0.010	0.35	1.74	0.78	0.02	0.01	0.01	0.01	0.003	0.009	0.003	0.009	0.037	0.41	0.27
W12B	Root	C-Mn-Ni[a]	AC	0.05	0.008	0.010	0.30	1.68	0.81	0.02	0.005	0.01	0.01	<0.002	0.006	<0.003	0.009	0.032	0.39	0.24
W11A	SS	C-Mn-Ni[a]	DC straight	0.05	0.009	0.010	0.30	1.66	0.85	0.02	0.005	0.01	0.02	0.002	0.007	<0.003	0.012	0.038	0.39	0.29
W11A	Root	C-Mn-Ni[a]	DC straight	0.05	0.009	0.010	0.28	1.64	0.85	0.02	0.005	0.01	0.02	<0.002	0.007	<0.003	0.012	0.036	0.39	0.27
W11B	SS	C-Mn-Ni[a]	DC straight	0.05	0.009	0.010	0.29	1.65	0.84	0.02	<0.005	0.01	0.02	0.002	0.007	0.004	0.009	0.038	0.39	0.28
W11B	Root	C-Mn-Ni[a]	DC straight	0.05	0.009	0.010	0.31	1.67	0.85	0.02	<0.005	0.01	0.02	<0.002	0.007	<0.003	0.011	0.036	0.39	0.27
W25A	SS	C-Mn-Ni[b]	DC straight	0.05	0.008	0.010	0.31	1.61	0.85	0.02	<0.005	0.01	0.02	0.002	0.007	<0.003	0.007	0.035	0.38	0.26
W25A	Root	C-Mn-Ni[b]	DC straight	0.05	0.008	0.009	0.33	1.63	0.87	0.02	<0.005	0.01	0.02	<0.002	0.008	<0.003	0.008	0.033	0.39	0.25
W25B	SS	C-Mn-Ni[b]	DC straight	0.05	0.008	0.009	0.33	1.62	0.88	0.02	<0.005	0.01	0.02	<0.002	0.008	<0.003	0.006	0.039	0.39	0.27
W25B	Root	C-Mn-Ni[b]	DC straight	0.05	0.008	0.009	0.31	1.60	0.85	0.02	<0.005	0.01	0.02	<0.002	0.007	<0.003	0.006	0.039	0.38	0.27

Co ≤ 0.01; Sn, Pb, As, Zr ≤ 0.005; B, Ca ≤ 0.0003
SS = second side (subsurface)
Root = first side

[a] Welded in the flat position.

[b] Welded vertically-up.

[c] $$\text{IIW CE} = \text{C} + \frac{\text{Mn}}{6} + \frac{\text{Cr} + \text{Mo} + \text{V}}{5} + \frac{\text{Ni} + \text{Cu}}{15}$$

mated inclusion volume fractions of the C-Mn-Ni welds, compared with the C-Mn welds (~0.26 versus ~0.19%) is attributable to the higher oxygen contents of the former (~0.035 versus ~0.026%). Compared with the C-Mn welds, the C-Mn-Ni welds also had slightly higher levels of manganese and lower levels of carbon, silicon, and nitrogen.

The data for the C-Mn-Ni welds deposited in the flat position show small but progressive reductions in manganese and silicon, and an increase in nitrogen in going from DC reverse polarity, through AC to DC straight polarity welding. The compositional changes are associated with a progressive change in the carbon equivalent from ~0.43% (DC reverse polarity) through ~0.41% (AC) to 0.39% (DC straight polarity). For the C-Mn deposits, the progressive decrease in silicon and manganese was much less pronounced, and there was no systematic change in the carbon equivalent. However, there was a change in nitrogen content similar to that observed in the C-Mn-Ni deposits. Taken together, these results suggest that the absorption of nitrogen at the cathode occurred more readily when the cathode was the electrode tip, that is, for DC straight polarity welding, and that oxidation (which resulted in a loss of manganese and silicon with minimal change in oxygen content) also occurred more readily for DC straight polarity welding.

A comparison of the weld oxygen contents (Table 4) with those achieved in two-pass welds that were deposited with the same consumable in a companion study [*3*] provides confirmation that, at least for these C-Mn deposits, the welder employed a short arc (corresponding to an arc voltage of ~21 V, which is at the lower end of the range reported in Ref *3*) in depositing the butt welds. The corresponding information for the C-Mn-Ni deposits is not so readily interpreted, as the oxygen contents of the butt welds are consistently higher than those produced in the companion two-pass beads. However, the nitrogen content of the butt welds is consistent with an arc voltage of 21 V having been employed. The difference in the oxygen contents may be a consequence of a progressive buildup of oxygen with decreasing dilution, as the butt weld regions that were analyzed were undoubtedly higher up the weld than the first two passes, at least for the first side weld region.

Butt Weld Microstructural Observations

As noted above, the welds deposited in the flat position were all completed in a total of 14 passes. Visual inspection revealed no major differences in weld profile and in bead shape between them, although it was noted that the minimum weld width in the root was greater in Weld W18 (DC straight polarity) and was least in weld W17 (DC reverse polarity), in spite of an expected slight difference in penetration, probably as a result of slight differences in the root gap. Also as noted above, the vertical-up C-Mn-Ni welds, W25A and W25B, were completed in only eleven passes, having unintentionally a slightly larger average bead size; in these welds, part of the first side root pass had not been re-austenitized by the first bead on the second side. Macrographs of typical weld cross sections are shown in Fig. 2, and the measured proportions of as-deposited weld metal are reported in Table 5. The welds deposited in the flat position all contained similar amounts of as-deposited weld metal in the second side region (~25 to ~45%); however, for the first side root region, the range of values was different for the C-Mn welds (~20 to ~40%) from that found for the C-Mn-Ni deposits (~10 to ~30%). Comparison of the C-Mn-Ni welds produced in the flat and vertical-up positions reveals that the latter have a higher proportion of as-deposited weld metal in the first side root and, at least in comparison with Weld W11A, a lower proportion in the second side sub-surface region.

The quantitative metallographic data, determined by point counting in selected as-deposited regions, are presented in Table 6. The as-deposited microstructures consisted primarily of acicular ferrite. The proportion of this and the other microstructural constituents was similar in the C-Mn welds and the C-Mn-Ni welds deposited in the flat position. This observation suggests that the difference in inclusion volume fraction (Table 4) has not had an overriding effect on the

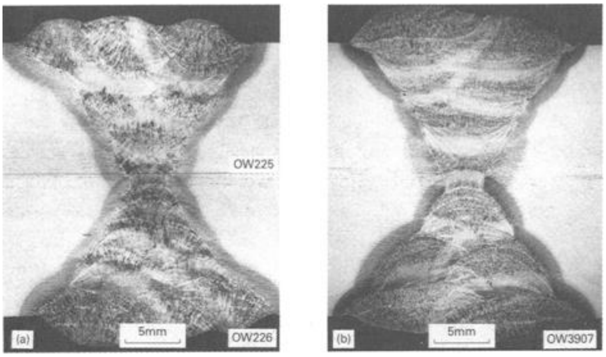

FIG. 2—*Macrographs showing typical transverse sections; etchant 2% nital.* (a) *C-Mn weld W19 (AC weld, deposited in the flat position).* (b) *C-Mn-Ni weld W25B (DC straight polarity weld, deposited vertically-up).*

TABLE 5—*Proportion of as-deposited weld metal in the metallographic sections in regions corresponding to those sampled by Charpy toughness specimens.*

			Proportion as-deposited	
Identity	Electrode	Current Type or Polarity	First Side (Root), %	Second Side (Subsurface), %
W7	C-Mn[a]	DC reverse polarity	35	40
W17	C-Mn[a]	DC reverse polarity	27	32
W9	C-Mn[a]	AC	41	44
W19	C-Mn[a]	AC	22	41
W8	C-Mn[a]	DC straight polarity	30	40
W18	C-Mn[a]	DC straight polarity	30	26
W10A	C-Mn-Ni[a]	DC reverse polarity	13	25
W10B	C-Mn-Ni[a]	DC reverse polarity	9	45
W12A	C-Mn-Ni[a]	AC	32	41
W12B	C-Mn-Ni[a]	AC	20	37
W11A	C-Mn-Ni[a]	DC straight polarity	22	49
W11B	C-Mn-Ni[a]	DC straight polarity	30	41
W25A	C-Mn-Ni[b]	DC straight polarity	28	41
W25B	C-Mn-Ni[b]	DC straight polarity	36	41

[a] Welded in the flat position.
[b] Welded vertically-up.

as-deposited microstructure. The amount of primary ferrite was generally slightly lower in the second side cap than in the first side root region for deposits produced with both electrode types (~5 versus 10%). There were no marked systematic differences resulting from the changes in current type or polarity, although the root region of the AC deposits had the lowest proportion of acicular ferrite and the highest proportion of primary ferrite for both the C-Mn and the C-Mn-Ni welds. There was, however, some variability in the quantities of the various microstructural constituents. For welds W18 and W12B, the microstructural differences between the cap and the root regions are probably attributable to the observed differences in silicon and manga-

TABLE 6—*Quantitative metallographic data determined at* ×500.

Weld Code	Region Sampled	Electrode	Current Type or Polarity	Primary Ferrite, %	Ferrite with Aligned Second Phase, %	Acicular Ferrite, %
W17	Cap	C-Mn[a]	DC reverse polarity	6	25	69
W17	Root	C-Mn[a]	DC reverse polarity	7	24	69
W19	Cap	C-Mn[a]	AC	8	26	66
W19	Root	C-Mn[a]	AC	14	26	60
W18	Cap	C-Mn[a]	DC straight polarity	6	21	73
W18	Root	C-Mn[a]	DC straight polarity	10	28	62
W10B	Cap	C-Mn-Ni[a]	DC reverse polarity	6	32	62
W10B	Root	C-Mn-Ni[a]	DC reverse polarity	9	27	64
W12B	Cap	C-Mn-Ni[a]	AC	6	23	71
W12B	Root	C-Mn-Ni[a]	AC	10	28	61
W11B	Cap	C-Mn-Ni[a]	DC straight polarity	6	29	65
W11B	Root	C-Mn-Ni[a]	DC straight polarity	5	22	73
W25B	Cap	C-Mn-Ni[b]	DC straight polarity	10	19	71
W25B	Root	C-Mn-Ni[b]	DC straight polarity	11	15	74

[a] Welded in the flat position.
[b] Welded vertically-up.

nese levels between the two regions. The proportions of the various constituents measured in the root region of weld W11B are slightly anomalous; however, the reasons for this are not known.

In the vertical-up weld, W25B, the percentage of ferrite with aligned second phase is approximately 10% less than in the other welds, with a corresponding slight increase in the proportions of primary ferrite and, at least for the weld cap, in acicular ferrite. Note that the proportions of the various microstructural constituents from the two different weld regions are closely similar, as expected from their similar compositions. Micrographs of as-deposited regions of welds W19 (C-Mn deposit welded AC in the flat position) and W25B (C-Mn-Ni welded DC straight polarity vertically-up) are shown in Fig. 3.

Butt Weld Tensile and Hardness Data

The tensile and hardness results, together with the other mechanical test data, are summarized in Tables 7 through 9. For the welds deposited in the flat position, the C-Mn and C-Mn-Ni deposits were of similar strength, ductility, and hardness, and had similar values of the yield to tensile ratio. For the C-Mn deposits, both DC reverse polarity and AC welding produced deposits that had both higher strength and a higher yield to tensile ratio in the first side root region than in the second side. However, this was not the case for the DC straight polarity deposit, probably because of the lower manganese and silicon contents of the root region; see Table 4. Similar behavior did not show in the hardness results, where no clear trends were apparent. For the C-Mn-Ni deposits, only AC welding gave a significant difference in strength between the subsurface and root regions, but the former was of higher strength and hardness. The difference in silicon content (Table 4), and probably also the higher proportion of acicular ferrite in the second side deposit (Table 6), are presumably the main factors contributing to this difference. The hardness of the as-deposited regions was frequently greater than that of the reaustenitized regions, but this situation was not always so.

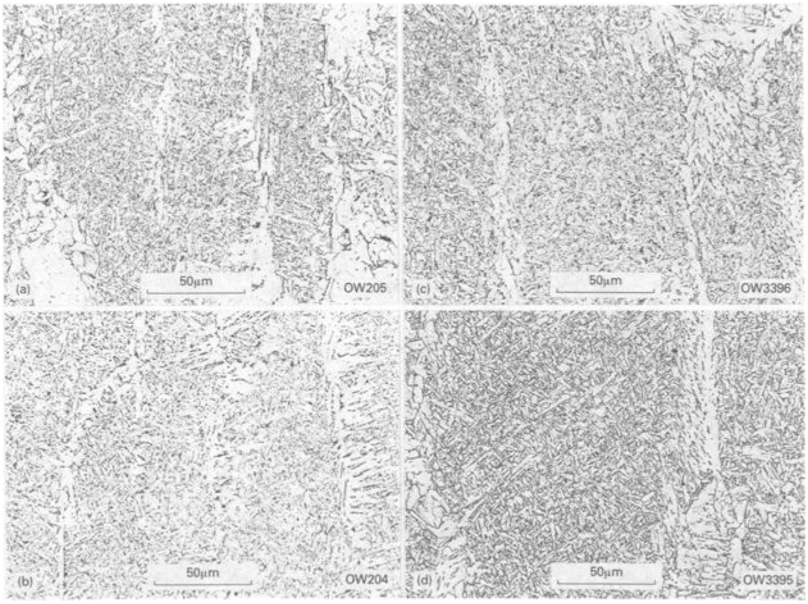

FIG. 3—*Micrographs of welds shown in the previous figure; etchant 2% nital.* (a) *Weld W19, first side root;* (b) *Weld W19, second side cap;* (c) *Weld W25B, first side root; and* (d) *Weld W25B, second side cap.*

Considering the C-Mn-Ni vertical-up welds, for the second side subsurface region, the hardness levels of the duplicate welds W25A and W25B were similar. However, in the root region, weld W25B was harder than W25A (~217 HV 2.5 compared with ~200 HV 2.5), and the root region (in weld W25B) was of higher strength than the subsurface region (in weld W25A). The hardness of the reheated region in the root of W25B was similar to that of the comparable weld deposited in the flat position, W11B, although both the yield and tensile strength in the root region of W25B were substantially higher than those of W11. Thus, with some exceptions, notably among the C-Mn-Ni welds deposited in the flat position, the root region generally had higher strength and hardness than the subsurface region. In the light of the close similarity of chemical composition and microstructure generally observed between the two regions, the strength differences are attributed to strain aging in the root.

Butt Weld Charpy Toughness Data

Pertinent toughness data derived from the Charpy transition curves are summarized in Tables 7 through 9, and the summary data for the welds deposited in the flat position are presented in Fig. 4. The overall trend of the data in Fig. 4 is quite clear in the first side root region, namely that for both types of electrode the toughness decreases progressively in the order DC reverse polarity, AC, and DC straight polarity. The C-Mn and C-Mn-Ni consumables yield welds with similar Charpy toughness, and for both of them toughness is lower in the root region, which is concluded to be a consequence of strain aging. For the 40J and 27J criteria in the subsurface regions in the AC welds, the toughness is similar to or even slightly better than that of the DC reverse polarity deposits. As the 27J and 40J criteria are essentially a measure of cleavage resistance, then the slightly higher toughness of the subsurface region (in welds W9

TABLE 7—*Mechanical property data for the C-Mn welds deposited in the flat position.*

Weld code	Region sampled[a]	Current type or polarity	Yield strength, MPa	Tensile strength, MPa	Yield: tensile ratio	Elongation, %	Reduction in area, %	Hardness expressed as min-max/mean		Charpy					CTOD at −10°C for nominally 25mm square specimens notched through the thickness, mm
										Temperature, °C			Absorbed energy, J		
								As-deposited, HV5	Reheated, HV5	27J	40J	100J	−20°C	−40°C	
W7	SS	d-c reverse polarity	530	621	0.85	21	70	214, 229	180-225 200	−65	−55	−35	155	68	
W7	Root	d-c reverse polarity	600[b]	658	0.91	15	72	199-237 223	178-221 203	−58	−52	−45	155	110	
W17	SS	d-c reverse polarity						221	208-241 220						
W17	Root	d-c reverse polarity						234, 241	216-239 226						1.68[c], 1.54[c], 1.44[c], 0.53[d], 0.50[d], 0.39[d]
W9	SS	ac	520[b]	613	0.85	17	71	237, 237	185-229 207	−70	−55	−32	155	58	
W9	Root	ac	585[b]	657	0.89	18	68	225	174-218 205	−48	−38	−8	65	38	
W19	SS	ac						232, 244	188-218 203						
W19	Root	ac						210	193-244 218						1.88[c], 1.26[c], 1.22[c], 1.00[c], 0.36[d], 0.064[d]
W8	SS	d-c straight polarity	585[b]	654	0.89	18	70	210, 212	193-216 205	−45	−38	−28	145	40	
W8	Root	d-c straight polarity	572[b]	648	0.88	17	65	202-221 212	206-244 214	−38	−30	−4	54	28	
W18	SS	d-c straight polarity						216-249 231	204-260 232						
W18	Root	d-c straight polarity						212-241 228	177-244 222						1.26[c], 1.03[d], 0.38[d], 0.18[d], 0.16[d], 0.16[d]

[a] SS = second side (subsurface)
Root = first side

[b] = 0.2% proof stress

[c] = δ_m

[d] = δ_u

TABLE 8—*Mechanical property data for the C-Mn-Ni welds deposited in the flat position.*

Weld code	Region sampled[a]	Current type or polarity	Yield strength, MPa	Tensile strength, MPa	Yield: tensile ratio	Elongation, %	Reduction in area, %	Hardness expressed as min-max mean		Charpy					CTOD at −10°C for nominally 25mm square specimens notched through the thickness, mm
										Temperature °C			Absorbed energy, J		
								As-deposited, HV5	Reheated, HV5	27J	40J	100J	−20°C	−40°C	
W10A	SS	d-c reverse polarity	544[b]	634	0.86	19	74	210	204-252 226	−72	−60	−50	150	132	
W10A	Root	d-c reverse polarity	536[b]	622	0.86	22	74	234, 214	206-249 222	−57	−50	−30	120	65	
W10B	SS	d-c reverse polarity						241, 232	221, 227						1.69[c], 1.41[c], 1.19[c], 1.15[c], 1.12[c], 0.87[c]
W10B	Root	d-c reverse polarity						212, 212	214-257 229						
W12A	SS	ac	570[b]	647	0.88	18	72	225-232 228	199-268 235	−73	−67	−35	120	88	
W12A	Root	ac	523	620	0.84	19	73	241, 227	197-227 214	−50	−35	−18	85	35	
W12B	SS	ac						239, 212	216-246 228						1.42[d], 1.16[c], 1.04[c], 0.96[c], 0.85[c]
W12B	Root	ac						237, 239	199-223 212						
W11A	SS	d-c straight polarity	532[b]	622	0.86	17	72	206-237 218	199-234 216	−47	−37	−20	100	33	
W11A	Root	d-c straight polarity	538	626	0.86	18	68	234, 223	204-212 208	−43	−27	−5	47	30	
W11B	SS	d-c straight polarity						234, 237	201-218 207						1.27[c], 1.16[c], 1.08[c], 1.07[c], 1.01[d], 0.59[c]
W11B	Root	d-c straight polarity						234, 239	195-227 216						

[a] SS = second side (subsurface)
Root = first side

[b] = 0.2% proof stress

[c] $= \delta_m$

[d] $= \delta_u$

TABLE 9—*Mechanical property data for the C-Mn-Ni welds deposited vertically-up.*

								Hardness expressed as min-max mean		Charpy					
										Temperature, °C			Absorbed energy, J		
Weld code	Region sampled[a]	Current type or polarity	Yield strength, MPa	Tensile strength, MPa	Yield: tensile ratio	Elongation, %	Reduction in area, %	As-deposited, HV2.5	Reheated, HV2.5	27J	40J	100J	−20°C	−40°C	CTOD at −10°C for nominally 25mm square specimens notched through the thickness, mm
W25A	SS	d-c straight polarity	512[b]	612	0.84	18	71	193-247 228	201-232 216	−65	−51	−9	85	55	
W25A	Root	d-c straight polarity	. . .	. . .	. . .	. . .	. . .	90, 201	168-219 199	−45	−39	−21	113	38	
W25B	SS	d-c straight polarity	. . .	. . .	. . .	. . .	. . .	206-243 227	195-251 219	. . .	. . .	. . .	. . .	. . .	
W25B	Root	d-c straight polarity	599[b]	657	0.91	16	65	200-230 213	206-230 217	. . .	. . .	. . .	. . .	. . .	0.96[c], 0.33[d], 0.099[e], 0.097[e], 0.093[e], 0.068[e]

[a] SS = second side (subsurface)
Root = first side

[b] = 0.2% proof stress

[c] = δ_m

[d] = δ_u

[e] = δ_c

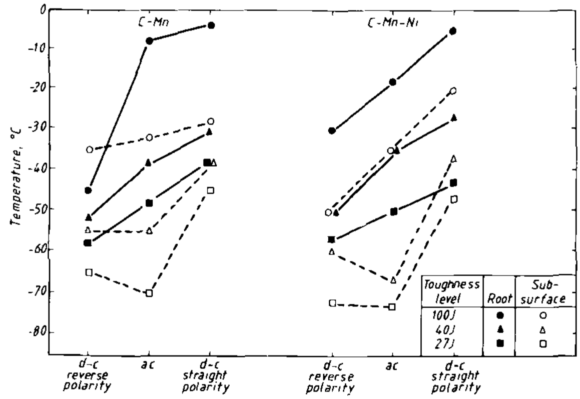

FIG. 4—*Charpy toughness of root and subsurface regions for the C-Mn and C-Mn-Ni welds deposited in the flat position.*

and W12A) is puzzling, in view of the high proportion of as-deposited microstructure (which is likely to be of lower toughness than the re-austenitized regions with their more uniform grain structure); see Table 5. One slight anomaly in the Charpy toughness results is the comparatively high toughness, with a low temperature for 100 J, in the root region of the DC reverse polarity weld produced with the C-Mn electrode. This behavior may be attributable, at least in part, to the higher manganese and lower nitrogen contents of the root region compared with the subsurface region. However, this cannot be the sole explanation, as the 27J and 40J criteria did not also indicate anomalously high toughness for the root region of this weld.

Considering now the C-Mn-Ni welds deposited vertically-up, while the subsurface and root regions generally had similar levels of toughness, the subsurface regions had a less abrupt transition from upper to lower shelf values. An examination of the Charpy transition curves for all deposits suggests that a high percentage of as-deposited regions, and thus a comparatively inhomogeneous microstructure, is generally associated with a low slope, and this appears to be true also for the vertical-up C-Mn-Ni deposit. Compared with the corresponding C-Mn-Ni weld deposited in the flat position, the vertical-up C-Mn-Ni weld had higher Charpy toughness in the subsurface regions, probably resulting from a lower nitrogen content (0.007 compared with ~0.011%). The root region of weld W25A is of higher toughness than W11A at higher temperatures; this difference is probably attributable to the higher strength of weld W25 in the root region.

Butt Weld CTOD Results

The CTOD data for the welds deposited in the flat position, obtained at −10°C, are included in Tables 7 through 9 and are presented graphically in Fig. 5. For the C-Mn-Ni deposits, the scatter is very small (only a factor of ~2) and the trend is essentially that shown by the Charpy data, namely that the toughness decreases slightly in the order DC reverse polarity, AC and DC straight polarity. The small scatter of the data suggests that, in spite of an acicular ferrite content of only ~65%, there are no regions of particularly low cleavage resistance. This phenomenon is almost certainly a consequence of both the presence of the nickel and the lower nitrogen content (0.006 to 0.11%, cf. 0.008 to 0.022% for the corresponding C-Mn deposits) having a slightly beneficial effect on the cleavage resistance of the coarser ferrite grains. Thus, the test temperature of −10°C is still in the upper shelf region for these deposits. By contrast, the

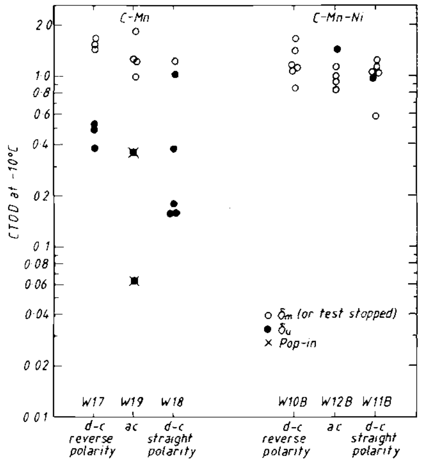

FIG. 5—*CTOD data determined at* $-10°C$ *for the C-Mn and C-Mn-Ni welds deposited in the flat position.*

CTOD data for the C-Mn deposits show very much greater scatter, varying by about a factor of ten. As for the corresponding C-Mn-Ni deposits, the toughness of the DC straight polarity weld, with three values of < 0.2 mm, was significantly worse than that of the DC reverse polarity weld. In addition to the small differences in chemical composition noted above, the C-Mn deposits had a higher proportion of as-deposited regions in the first side root, compared with the C-Mn-Ni deposits, and this proportion would be expected to influence the toughness adversely. However, the AC weld W19, which showed the greatest scatter in CTOD, had the smallest proportion of as-deposited weld metal. The behavior of the AC weld was not entirely intermediate between that of the other two deposits, as it showed both the highest and the lowest CTOD values. The increased scatter of the CTOD values for this deposit cannot be ascribed to any differences in chemical composition or in microstructure and thus may be due to statistical variation. Possibly, the reheated weld metal was controlling resistance to fracture initiation in this weld, contrary to expectation.

The CTOD data for the C-Mn-Ni vertical-up welds, also obtained at $-10°C$, are included in Tables 7 through 9. The values range from $\delta_c = 0.068$ mm to $\delta_m = 0.96$ mm, showing a range of a factor of ~ 14, which is substantially larger than that for the corresponding weld deposited in the flat position, with several of the CTOD values being considerably lower. Four of the CTOD values for the vertical-up weld are < 0.1 mm, with these and the specimen that gave a δ_u value all showing substantial abrupt load drops of 30–55% during testing; the occurrence of these load drops is considered in the next section.

Butt Weld Fractographic Examination

Fractographic examination of all CTOD specimens that had given δ_c or $\delta_u \leq 0.50$ mm revealed that, for the welds deposited in the flat position, initiation of the cleavage fracture had occurred in the first side root region; the distance of the initiation point from the fusion boundary at the base of the second side weld ranged from ~ 2 to ~ 4.5 mm. This region is the one that will have been subjected to strain aging, and which is included in the Charpy specimens taken from the first side root region.

For the C-Mn-Ni welds deposited vertically-up, examination of the fracture surfaces revealed that the regions of large arrested cleavage fracture corresponding to the large load drops were not all visible on the fracture surfaces. Examination of the band of tearing (which was typically ~2 mm wide) on all the C-Mn-Ni CTOD specimens, regardless of welding position, revealed that many of them had small patches of cleavage within this band of microvoid coalescence. Some of the traces for the specimens that had failed by unstable fracture also revealed that there had been small pop-ins ($\leq 3\%$ load drop), namely for specimens W25/4 and W25/6 ($\delta_c = 0.03$ mm and $\delta_c = 0.068$ mm, respectively). No regions of arrested cleavage fracture were found on the fracture surfaces of these specimens, probably as a consequence of the very low toughness of the welds allowing little tearing to occur before the final cleavage fracture.

As the toughness of most of the specimens from the vertical-up C-Mn-Ni weld was low, not surprisingly, initiation regions were not clearly defined. In some specimens, there appeared to be two or three poorly defined initiation regions, and which had been the first was not clear. The initiation regions were typically 0.2 to 0.5 mm below the fatigue crack tip, and were generally either in reheated weld metal in the first side root (within a few millimetres of the second side weld fusion boundary) or in the as-deposited weld metal of the first pass on the second side. This observation suggests that the toughness was similar in these regions. Large inclusions were noted to be responsible for cleavage initiation in some of the instances where initiation occurred in coarse-grained as-deposited regions, as reported by other workers [*6-10*]. Scanning electron micrographs of typical initiation regions are shown for the main initiation in reheated weld metal in Fig. 6 and for local cleavage initiation by a large inclusion (in this case an oxide inclusion ~15 μm in diameter containing iron, silicon, and magnesium), Fig. 7. Some of the isolated regions of cleavage in the specimen from weld W25 that gave a δ_m CTOD value are shown in Fig. 8.

Discussion

Deposit Nitrogen Contents

Instead of the expected higher deposit nitrogen contents for the vertical-up C-Mn-Ni welds, compared with the corresponding welds deposited in the flat position, the values were slightly lower (~0.007 versus ~0.011%). This observation suggests that for the C-Mn-Ni electrode employed, the gas shield generated by the electrode was sufficient to overcome the expected "chimney effect" in which convection currents can reduce the efficacy of the gas shield to protect the weld metal from the ingress of atmospheric nitrogen in vertical-up welding.

Weld Toughness

The Influence of Composition on Toughness—Both in this investigation and in the companion study [*3*], deposit nitrogen content increased in going from DC reverse polarity, through AC to DC straight polarity welding. In the light of this observation and the known deleterious effect of nitrogen on weld toughness, DC straight polarity SMA welding generally is expected to give deposits of lower toughness than will DC reverse polarity welding, as observed in the present study. Note that the lower Charpy toughness of the DC straight polarity deposits (compared with DC reverse polarity), corresponding to shifts in temperature of ~ +20°C for the various toughness criteria of Fig. 4, is similar to that expected for an increase in nitrogen content of ~0.0005%, according to the data reviewed by Vines [*11*]. A practical implication of this observation is that the use of DC straight polarity for the whole of a welded joint should be avoided where the procedure used is likely to be marginal with respect to toughness, although DC straight polarity might be allowed only for a small root pass that will be completely remelted by subsequent passes deposited employing DC reverse polarity welding. In this regard, electrodes

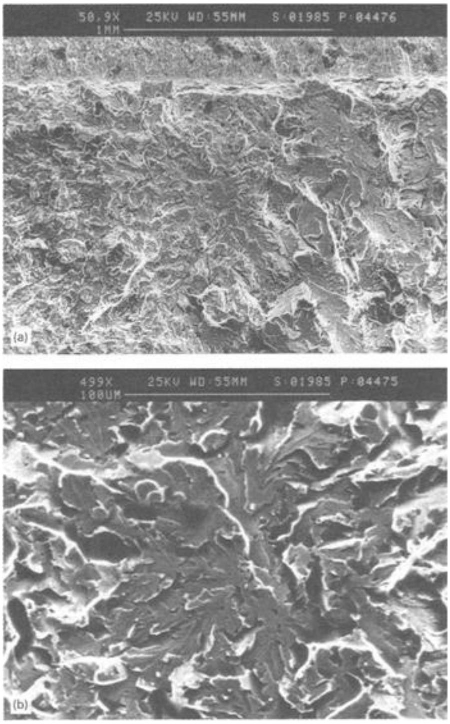

FIG. 6—*Main initiation point in reheated weld metal in the first side ~2.5 mm from the root in a vertical-up C-Mn-Ni fractured CTOD specimen.* (a) *Overall view, with the fatigue crack tip at the top,* ×*50.9; and* (b) *Detail from the center of* (a), ×*499.*

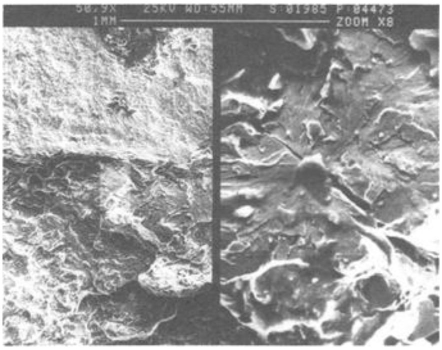

FIG. 7—*Local initiation at a large inclusion in the first side in a vertical-up C-Mn-Ni fractured CTOD specimen. The fatigue crack is in the upper half of the left side picture,* ×*50.9/*×*457.2.*

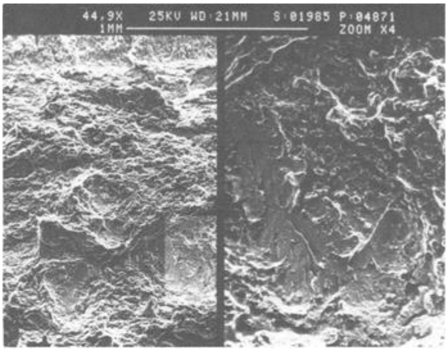

FIG. 8—*Isolated regions of cleavage within the band of tearing in specimen W25/3 (δ_m = 0.96 mm). The fatigue crack tip is at the top of the left side picture.* ×*44.9/*×*179.6.*

capable of running well on DC reverse polarity may well prove of advantage in fabrications requiring consistently high levels of weld metal toughness. In light of the increases in weld nitrogen content with increasing arc voltage, the welder's maintaining a short arc, as far as possible, is clearly vital.

Whilst the precise values of composition and toughness obtained in the present study are specific to the electrodes and welding parameters that were employed, similar trends are likely to arise with alternative consumables and welding conditions. Certainly, close attention clearly must be paid to the current type and polarity to achieve optimum weld metal properties in procedural test and production welds, and changes in current type or polarity, whether deliberate or inadvertent, could produce substantial changes in toughness.

The higher weld nitrogen content in the C-Mn butt welds (Table 4) arose largely from a higher level of nitrogen in the core wire and, for DC straight polarity operation, as a consequence of greater absorption from the atmosphere. Nickel is known to have a beneficial effect on the cleavage resistance of ferrite [*12*] and its favorable influence on the Charpy toughness of low hydrogen SMA deposits has been demonstrated [*13,14*]. However, in the present study, for the welds deposited in the flat position, the relative contributions (of the presence of ~0.8% nickel and the lower level of nitrogen) to the higher CTOD values of the C-Mn-Ni deposits compared with the C-Mn deposits cannot be determined. Their combined effect has clearly been to move the transition curve so that the C-Mn-Ni deposits display upper shelf CTOD at −10°C. Whilst the change of consumable had minimal influence on the as-deposited microstructure, the smaller proportion of as-deposited regions in the first side of the C-Mn-Ni welds probably also contributed to the improvement in toughness. By contrast, the CTOD results obtained from the C-Mn-Ni weld deposited vertically up indicate that the toughness was in the transition region; the possible reasons for this behavior are considered below.

Strain Aging—In the light of the similar chemical composition of the root and subsurface regions, the weld tensile and hardness data indicate that some strain aging has occurred in the (first side) root region in most of the welds studied. The welds were subjected to only moderate restraint during welding, and the amount of distortion that occurred was clearly sufficient to cause some strain age damage. Concerning the toughness results obtained for the vertical-up welds W25A and W25B and for the corresponding welds W11A and W11B deposited in the flat position, Charpy toughness in the root, at least at the higher temperatures, was noted earlier to be slightly higher for weld W25 than for W11. However, the CTOD results obtained for weld W25 were much lower than those for W11.

These differences in toughness occurred despite the vertical-up weld having the lower nitrogen content (~0.007 cf. ~0.011%). The differences are therefore likely to be due to microstructural differences and to the higher strength of the root region of the vertical-up weld. The most likely cause of this higher strength is considered to be a greater amount of strain aging. The vertical-up welds were intended to be duplicates of the panels welded in the flat position. However, the welds differed in two important ways. Firstly, the bead size of the vertical-up welds was slightly larger, as evidenced by the smaller number of passes required to complete the weld (11 compared with 14). This slightly larger bead size was probably associated with a slightly coarser microstructure (and with a consequent increase in fracture facet size for the coarser microstructural constituents), although detailed measurements have not been carried out to verify this. Also probable was a slight increase in the size of inclusions. At the same time, the oxygen contents and thus the estimated inclusion volume fraction for the vertical-up welds are no larger than those of the flat position welds. Secondly, and perhaps partly as a consequence of a slightly larger bead size, a larger proportion of the first bead on the first side remained unmelted or was not re-austenitized in the root. The parts of this bead which were not re-austenitized would, in view of their comparatively inhomogeneous microstructure, be more susceptible to strain age damage. Both these factors would be expected to contribute to a lower toughness in both the first and second side weld beads in the root region of the vertical-up welds than that found in the corresponding regions of the welds deposited in the flat position.

Scatter in CTOD Values—The C-Mn welds deposited in the flat position and the vertical-up C-Mn-Ni weld displayed wide scatter in CTOD results. Similar scatter has been explained *[15]* as resulting from the presence of widely spaced low toughness regions (estimated as being of the order of 1/mm^3) within a tougher matrix. This explanation is invoked to explain the present results. According to the Charpy toughness data, the impact toughness of the vertical-up C-Mn-Ni weld is comparable with that of the comparator weld W11. Moreover, the δ_m CTOD value of 0.96 mm obtained for weld W25 is comparable with the δ_m values obtained for weld W11, suggesting that the toughness of the matrix was similar in the two welds. According to the hypothesis adopted to explain the scatter, welds that show considerable scatter in CTOD contain low toughness regions, each of which is capable of initiating cleavage fracture in a CTOD test but which are sufficiently small in total volume to have minimal influence on Charpy toughness. The presence of such regions is readily apparent from examination of the band of tearing in those specimens that gave δ_m CTOD values, where small isolated patches of cleavage fracture (each of which clearly did not initiate fracture in the present tests) were observed. In light of this observation, only a slight degradation in toughness clearly would be required for such a weld to show a transition from ductile to brittle behavior, and this result appears to have occurred for the present weld W25B. The same explanation can be invoked to explain the wide scatter observed in the CTOD results for the C-Mn butt welds. The microstructure of the present welds is sufficiently inhomogeneous that in some of the tests no low toughness regions were sampled by the advancing crack tip and δ_m CTOD values were recorded, whilst in other tests low toughness regions were encountered, giving rise to δ_u CTOD values. In light of the wide scatter observed in the CTOD results for the C-Mn deposits, removing the first side root region by back-gouging (in order to remove the low toughness regions) would clearly be necessary if consistently high CTOD values were required, and this removal would be true also for the C-Mn-Ni electrode employed for vertical-up welding, if a closely similar sequence of beads to that produced in the present study were to be produced. By contrast, for the particular plate thickness, joint preparation, and welding procedure, and the C-Mn-Ni consumable used in the present study, consistently high levels of CTOD at −10°C (>0.5mm) were achieved in welds deposited in the flat position without resorting to back-gouging, with marginally higher levels of CTOD (>0.8 mm) having been obtained by employing either DC reverse polarity or AC welding as recommended by the consumable manufacturer.

The occurrence of small pop-ins during some of the CTOD tests each is assumed to be due to the initiation and arrest of a small cleavage crack. Willoughby [*16*] has discussed the significance of pop-ins recently. His conclusion was essentially that where the maximum increase in crack length is less than 4% of the test piece ligament, arrest of the crack depends on microstructural features rather than on either the geometry of the test piece or features of the loading system. Whilst the maximum increases in crack length could not be established by fractographic examination of the present specimens, the small size of the load drops suggests that they were only a few percent. Therefore, the present pop-ins are concluded to be in compliance with Willoughby's criterion for pop-ins to be regarded as insignificant events, as their arrest depended on the microstructure rather than on the specimen geometry or the characteristics of the loading system, as might be the case for substantially larger pop-ins. However, Willoughby cautioned against ignoring small pop-ins in inhomogeneous microstructural regions such as weldments, since arrest would not have occurred if the region surrounding the arrested crack had itself been a low toughness region. Whilst these small pop-ins may be regarded as structurally insignificant, and the subsequent CTOD value (δ_c = 0.23 mm rather than δ_c = 0.093 mm for specimen W25/4, and δ_u = 0.46 mm rather than δ_c = 0.068 mm for specimen W25/6) employed for design purposes, in the context of the present research program, the pop-ins have not been ignored, but are interpreted as indicating the presence of low toughness microstructural regions situated close to the fatigue crack tip, with crack arrest having been fortuitous.

Conclusions

Two series of butt welds have been produced in the flat position in 25-mm thick C-Mn-Nb steel plate using a C-Mn and a C-Mn-Ni basic-coated low hydrogen electrode and employing DC reverse polarity, DC straight polarity, and AC power supplies. In addition, the C-Mn-Ni electrode was employed to produce a vertical-up weld with a DC straight polarity power supply. From this study, the following conclusions have been drawn.

1. The power supply type influenced the composition by producing a greater pickup of nitrogen for DC straight polarity, which had a deleterious effect on weld toughness. There was also an associated decrease in the manganese and silicon contents that was more pronounced for the C-Mn-Ni welds.
2. Changes in the power supply type had a minimal influence on microstructure for both the C-Mn and the C-Mn-Ni welds.
3. For the C-Mn welds deposited in the flat position, Charpy toughness generally decreased in the order DC reverse polarity, AC and DC straight polarity. The CTOD at −10°C was lower for DC straight polarity than for DC reverse polarity, although AC welding, which gave increased scatter, yielded the lowest CTOD values.
4. The Charpy toughness of the C-Mn-Ni welds was generally similar to that of the C-Mn welds. However, the C-Mn-Ni welds that were deposited in the flat position showed higher levels of CTOD with comparatively little scatter. This higher toughness was attributed largely to the small beneficial effects of the lower weld nitrogen levels and of the ~0.8% nickel on the cleavage resistance of the coarser regions of ferrite, with a contribution also from the lower proportion of as-deposited regions in the first side root of the C-Mn-Ni welds.
5. For the C-Mn-Ni vertical-up weld, strength was higher in the root region, probably as a consequence of a greater amount of strain aging compared with the corresponding weld produced in the flat position, in spite of the lower nitrogen content of the former.
6. Crack tip opening displacement values at −10°C for the vertical-up weld were generally low, with only one δ_m value being recorded and with wide scatter (δ_c = 0.068 mm to δ_m = 0.96 mm). Low toughness regions, which initiated the cleavage fractures, occurred in both the second side as-deposited weld metal in the root (where weld beads slightly larger than those in the flat position welds probably contributed to a lower toughness) and also in the first side root

region, where part of the first pass had been neither remelted nor re-austenitized by subsequent passes.

7. In the light of the influence of current supply type on weld toughness, care must be taken in deciding upon this aspect of weld procedure specifications for C-Mn steel fabrications.

Acknowledgments

The assistance of staff of The Welding Institute with the experimental work, particularly Mrs. W. Martin, Messrs M. D. Tiplady, J. Haugh, G. M. Courtman, J. C. Ford, J. J. Rickard, K. J. Tiplady, G. T. Hall, N. J. Tebbit, W. Hedley, and P. T. Bennett, is gratefully acknowledged, as are helpful discussions with colleagues, particularly from the Materials Department.

The work was jointly funded by Research Members of The Welding Institute and the Minerals and Metals Division of the UK Department of Trade and Industry.

References

[1] Dawson, G. W. and Judson, P. "Procedural Guidelines for the Achievement of Tough Welds in Structural Steels for Offshore Applications," *Offshore Welded Structures*, The Welding Institute, 1982.
[2] Haugh, J., Pisarski, H. G., and Salter, G. R. Unpublished research, The Welding Institute, Cambridge, England, 1981.
[3] Abson, D. J., "The Influence of Current Supply Type and Arc Length on C-Mn, C-Mn-Ni and C-Mn-Ti-B Shielded Metal Arc Deposit Nitrogen and Oxygen Contents," *Residual and Unspecified Elements in Steel, ASTM STP 1042*, A. S. Melilli and E. G. Nisbett, Eds., American Society for Testing and Materials, Philadelphia, 1989.
[4] Pisarski, H. G. and Dawes, M. G., "Measurement of Crack Opening Displacement with Particular Reference to Offshore Structures," Research Report 111/1980, The Welding Institute, Cambridge, England, June 1980.
[5] Bailey, N. and Pargeter, R. J., "The Influence of Flux Type on the Strength and Fracture Toughness of Mild Steel Weld Metal, Part 1: Two-Pass Welds," Research Report 70/1978/M, The Welding Institute, Cambridge, England, July 1978.
[6] Baryshev, V. M., Shebaron, A., Birbrover, A., and Malov, V. V., "Increasing the Cold Resistance of Weld Metal in the Multipass Submerged-Arc Welding of a Low Alloy Steel of Type 16GZAF," *Welding Production*, Vol. 25, No. 7, 1978, pp. 43-45.
[7] Tweed, H. and Knott, J. F., "Effect of Reheating on Microstructure and Toughness of C-Mn Weld Metal," *Metal Science*, Vol. 17, No. 2, 1983, pp. 45-54.
[8] Tweed, J. H. and Knott, J. F., "Microstructure-Toughness Relationships in a C-Mn Weld Metal," *Proceedings of the 4th European Conference on Fracture*," K. L. Maurer and F. E. Matzer, Eds., Materials Advisory Services Ltd., Warley, England, 1982, pp. 127-133.
[9] Terlinde, G., Muller, L., Beaven, P. A., and Schwalbe, K-H., "Microstructure Effects on the Toughness of FCAW-Ferritic Weld Metal," *Proceedings of the 5th European Conference on 'Fracture'* (ECF-5), Sociedade Portuguesa de Materiais, Seccao Tecnica Fractura, Lisbon, Portugal, 1984, pp. 257-268.
[10] Shiliang, W., Weiping, H., and Bogang, T., "Improving the Toughness of Weld Metal by Adding Rare Earth Elements," *Welding International*, Vol. 1, No. 3, 1987, pp. 284-287. (Translated from *Transactions of the China Welding Institute*, Vol. 7, No. 2, 1986, pp. 56-63).
[11] Vines, M. J., "Nitrogen in C-Mn Weld Metal—A Review," Unpublished research, The Welding Institute, Cambridge, England, 1982.
[12] Jolley, W., "Influence of 3.28 Percent Nickel Addition on the Yield and Fracture Behavior of Alpha Iron," *Transactions of the American Institute of Mechanical Engineers*, Vol. 242, 1968, pp. 306-314.
[13] Taylor, D. S. and Evans, G. M., "Development of MMA Electrodes for Offshore Fabrication," *Met. Con.* Vol. 15, No. 8, 1983, pp. 438-443.
[14] Mentink, H., "Introduction of Philips 76S, A New Coated Electrode (E7018-G) for Offshore Structures," *Scandinavian Offshore Symposium*, Philips, Eindhoven, June 1983.
[15] Abson, D. J., "The Influence of Manganese and Coating Basicity on the Microstructure and Mechanical Properties of Vertical-Up MMA Welds in 38 mm Thick C-Mn-Nb Steel Plate: Final Report," Research Report 309/1986, The Welding Institute, Cambridge, Eng., August 1986.
[16] Willoughby, A. A., "Significance of Pop-Ins in Fracture Toughness Testing," *International Journal of Fracture*, Vol. 30, No. 1, 1986, pp. R3-R6.

Phillippe Bourges,[1] *Regis Blondeau,*[2] *and Lucien Cadiou*[3]

Influence of Low and Ultra Low Sulfur Contents on Weldability of Ferritic Steels

REFERENCE: Bourges, P., Blondeau, R., and Cadiou, L., **"Influence of Low and Ultra Low Sulfur Contents on Weldability of Ferritic Steels,"** *Residual and Unspecified Elements in Steel, ASTM STP 1042,* A. S. Melilli and E. G. Nisbett, Eds., American Society for Testing and Materials, Philadelphia, 1989, pp. 192-201.

ABSTRACT: The existing possibilities of steelmaking imply that ultra low sulfur contents can be obtained. The weldability of these steels had not yet been clearly defined as good or not. In this study the welding behavior has been determined both for normalized steels, and quenched and tempered steels. Results concern underbead hardness in the heat affected zone (HAZ) and critical preheat temperature determined by the implant test. Ultra low sulfur steels appear to present a significant improvement in weldability. The underbead hardness is not affected by a sulfur content decrease. The preheat temperature is the same for different stress directions (that is, longitudinal and short transverse) only for steels with a sulfur content lower than about 15/20 ppm. The influence of the weld metal's hydrogen content on cold cracking prevention is reduced with ultra low sulfur steels.

KEY WORDS: Steel, welding, hydrogen, sulfur, inclusions, steelmaking

During the last years, the cleanliness of steels has been greatly improved. The decrease of sulfur and oxygen content contributes to a lower quantity of nonmetallic inclusions and to differences in the shape of these inclusions, particularly for sulfides. Recent papers have presented results concerning the behavior of low sulfur content steels. These papers conclude that the lack of sulfur contributes to an increase in cold cracking sensitivity [*1*] and to an increase in underbead hardness in the heat affected zone (HAZ) [*2*]. Some other papers seem to have a different view, seeing no effect of the sulfur content [*3*]. This problem is particularly important as some specifications require a minimum value for the sulfur content (that is, 4.10^{-3} %) despite the important increase in properties such as toughness and SCC behavior. Clarifying some ideas appears necessary for this particular point: sulfur content and weldability.

Materials

The materials to be investigated are supplied as thick plates. Steel is produced in an electric furnace where dephosphorization and oxygen blowing take place. Then, heating ladle refining permits desulfurization, deoxidation, degassing, and alloy adjustments. Afterwards, the steel is

---

[1] Head, welding group, Materials Research Center, Creusot-Loire Industrie, Le Creusot F.71202, France.

[2] Head, Materials Research Center, Creusot-Loire Industrie, Le Creusot F.71202, France.

[3] Product manager, Creusot-Marrel Division, Creusot-Loire Industrie, Le Creusot F.71202, France.

poured in ingots. This process can produce very clean steels with an excellent reproducibility of the chemistry, which is very close to the aim composition. Some of the steels studied in this work were not produced in these conditions, low quality steels (higher sulfur) having to be introduced for comparison.

Tested materials are presented in Table 1. The results of chemical analyses presented here are obtained on the plates in the zone to be tested. Two types are considered: normalized steels without subsequent tempering or postweld heat treated (PWHT) (C Mn, C Mn Ni V) or quenched and tempered steels (Ni Cr Mo). As previously remarked, different qualities have been studied, with various sulfur contents, but with only slight variations of the alloying elements. Thus, the hardenability properties inside the different families are very close.

The inclusion contents of the different steels studied were determined using a quantitative microscope Cambridge QTM 720 and compared to usual charts such as ASTM Practice for Determining the Inclusion Content of Steel (E45-76) A or DIN 50602. Unfortunately, these standardized quotations cannot be used for very clean steels. To compare the steels used in this study, we prefer to consider the morphology (generally quantified by the radio between length L and thickness T for sulfides observed on longitudinal cuts), number, and location of the inclusions. These examinations have been performed on through thickness samples in the zone to be tested during welding (generally mid-thickness).

Welding Tests

The aim of the research program is to determine the sulfur content's influence both on underbead hardness and on cold cracking sensitivity characterized by the critical preheat temperature. All these aspects have been determined by use of the implant test [*4*]. This test is illustrated in Fig. 1. The sample is a small cylinder smoothly inserted in a 20-mm thick plate. A weld is performed to join plate to implant and to produce a heat affected zone. A preliminary observation determines the depth of the fused and heat affected zones. A circular notch is machined on the implant, which will be in the coarse grain zone after welding. After performing the weld, the load is applied to the implant when the temperature goes down to T_p + 50°C (T_p is the preheat temperature), or at least 150°C. The load is left for at least 16 h. During this maintaining time, the implant may or may not break. If the implant is broken, the test result is clear—the welding conditions are not usable. If the implant is not broken, it is extracted and observed microscopically in five sections to determine the evidence of a crack at the notch tip. The implant is defined as cracked or not. The limits between usable and unusable conditions are defined by cracking conditions and not only by rupture conditions.

The implant test cannot define real post heating conditions (due to the geometry of the sample), but can define accurately the critical preheat and interpass temperature. This one is defined by using a test where the implant is maintained for 1 h at the preheat temperature after welding. Critical temperature T_o is defined where cracking occurs as $T_p < T_o$ and where no cracking occurs as $T_p \geq T_o$.

This test is used to determine welding conditions even for very thick plates. The effect of thickness is taken into account through the stress level. The 20-mm thickness is considered to be representative of thick plates for the cooling cycle in the welding conditions used.

Concerning the welds performed for this study, they were realized both by shielded metal arc welding (SMAW) and gas metal arc welding (GMAW). In this last case, small amounts of hydrogen can be added in the protective gas to increase the hydrogen content of the weld. Table 2 summarizes the welding parameters and the hydrogen content of weld deposits. Deposits for hydrogen determination are performed as described in ISO 3690, but the samples are put in a vacuum degassing unit at 650°C to measure the total hydrogen content. The hydrogen level is read after palladium filtering to be sure to have only hydrogen, and nothing else. Such values are always higher than those obtained by degassing at room temperature.

TABLE 1—*Chemical analyses of normalized and quenched and tempered steels.*

Type	C	S	P	Si	Mn	Ni	Cr	Mo	V	Al	O_2	N_2
Normalized	190	1.5	8	395	1490	100	149	20	...	24	1.6	8
	190	10	15	266	1500	165	106	36	...	29	1.7	10.5
YS > 350 MPa	218	1.2	7.7	304	1430	136	131	33	...	18	1.7	7.2
A 516 Gr 70	197	1.3	8.9	344	1410	142	125	30	...	25	2.0	6.7
	187	1.5	11.1	291	1340	206	130	50	...	23	1.8	6.9
	214	2.3	8.2	332	1420	150	129	30	...	23	1.5	10.4
	183	3.8	7.7	406	1390	154	113	30	...	21	2.1	8.1
	199	7.2	11	372	1360	224	111	61	...	23	1.4	9.6
	185	6.6	12	322	1330	162	151	40	...	34	1.7	11.3
	190	1.2	7.6	327	1380	134	120	28	...	27	1.1	7.0
Normalized	161	1.0	9.5	264	1230	450	268	88	96	11	2.5	13.8
YS[a] > 420 MPa	163	2.7	11	271	1240	425	247	72	82	9	2.5	13.7
Normalized	180	0.5	9.3	293	1400	429	238	67	95	9	4	13.6
YS > 470 MPa	152	1.3	7.5	276	1330	432	245	85	78	10	3.7	13.8
	167	3.8	8.9	290	1410	443	220	66	71	8	3.9	13.9
	169	6.3	9.7	266	1380	413	249	66	92	10	2.6	16.6
Normalized	165	7.0	11.4	270	1420	421	257	71	94	7	3.5	17.5
YS > 470 MPa	183	1.4	9.6	292	1430	440	245	81	84	9	1.6	15.0
	190	4.1	12.2	272	1440	461	259	72	82	12	1.8	17.2
Quenched and tempered	170	0.5	8.0	381	1110	969	1020	352	2	21	1.3	9.1
YS > 690 MPa	161	0.9	8.9	369	1140	928	1050	367	5	32	0.9	6.7
	176	2.0	7.7	362	1160	978	1100	403	7	28	0.9	7.3
	168	11	10	329	1420	789	817	244	...	25	2.3	12.4

[a] YS is yield strength.

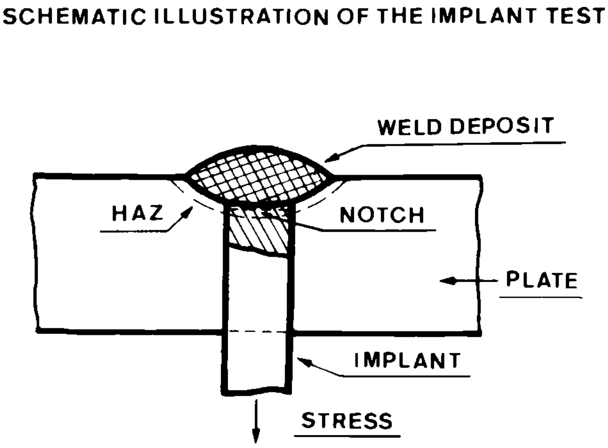

FIG. 1—*Schematic illustration of the implant test.*

TABLE 2—*Welding parameters and weld deposit hydrogen content.*

Condition	Process	Heat Input, kJ/cm	Protection Gas	Hydrogen Content, cm^3/100 g
1	SMAW	10	...	8
2	GMAW	10	Ar + 15% + CO$_2$	4
3	GMAW	10	Ar + 15% CO$_2$ + 2% H$_2$	12

Underbead Hardness

Measurements

Underbead hardness is determined as described in the French standard AFNOR NF A 81460. Five Vickers indentations under 50 N are performed in the coarse grain area of the HAZ. The underbead hardness is defined as the mean value of the three higher results if their range is lower than 25 HV 50.

Results

Figure 2 shows the underbead hardness values observed on normalized steels for an energy input of 10 kJ/cm. Results are plotted against sulfur content. The range (±15 HV) seems only due to cast to cast variations and not to the sulfur content. Notice that models predicting [5-7] the underbead hardness do not take into account the sulfur content. This means that the effect is not statistically significant as observed during the reported tests.

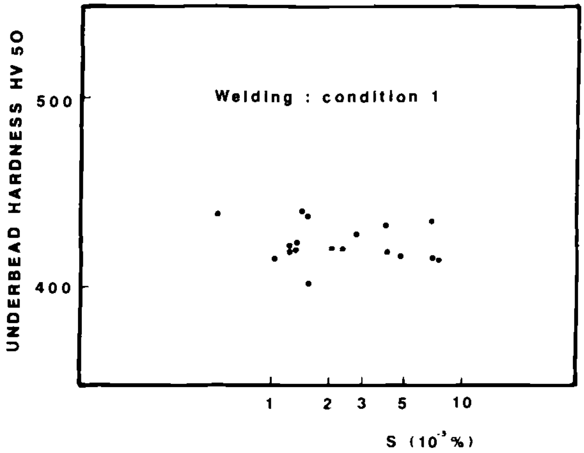

FIG. 2—*Underbead hardness as a function of sulfur content.*

Welding Conditions

Some authors [2] have shown that the preheating temperature must be increased for "new" steels with a low sulfur content. Different tests have been performed in this study to determine the real facts. The influences of hydrogen content in weld metal and of stress direction (longitudinal or short transverse) have been studied.

Influence of Hydrogen Content in Weldments

Tests were performed with GMAW and various protective gases to obtain different hydrogen levels in weldments. The material to be tested was ASTM Specification for Pressure Vessel Plates, Carbon Steel, for Moderate- and Lower-Temperature Service (A 516/A 516M-84), Gr70 (UNS K02700), a C Mn steel. The applied stress was 300 MPa. Figure 3 plots the critical preheating temperature (To) as a function of sulfur content. The lower sulfur content apparently contributes to a slightly independent behavior versus hydrogen content and the higher sulfur content increases sensitivity to hydrogen. For the lower hydrogen content, the high sulfur is favorable, but the increase of the preheating temperature with hydrogen is quite dramatic. Lower sulfur steels seem safer due to this lower sensitivity to hydrogen content variations.

Effect of Stress Direction

Samples were taken for different plates both in the longitudinal direction at mid-thickness and the short transverse direction. In this last case the notch was located at mid-thickness. All the implants were welded with SMAW, conducting to an hydrogen content around 8 cm^3/100 g of weld metal.

Normalized Steels—The implant tests were performed with respectively 350 (A 516/A 516M-84, Gr 70), 400, and 470 MPa. The results are presented in Fig. 4 with the critical preheating temperature plotted against the sulfur content. Clearly, the effects of steel grade do not appear. The transverse axis is significantly worse than the longitudinal axis. The difference reaches 75°C between the two critical preheating temperatures (and at least 25°C), significantly depending on the sulfur content. Thus, the sensitivity to hydrogen cracking appears to be very

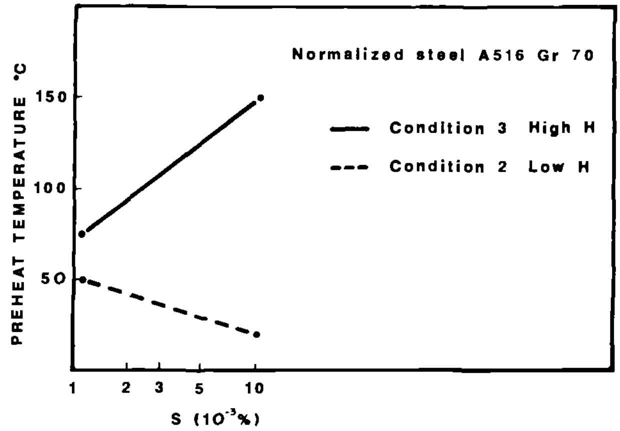

FIG. 3—*Effect of hydrogen content on the critical preheat temperature of steels having different sulfur contents.*

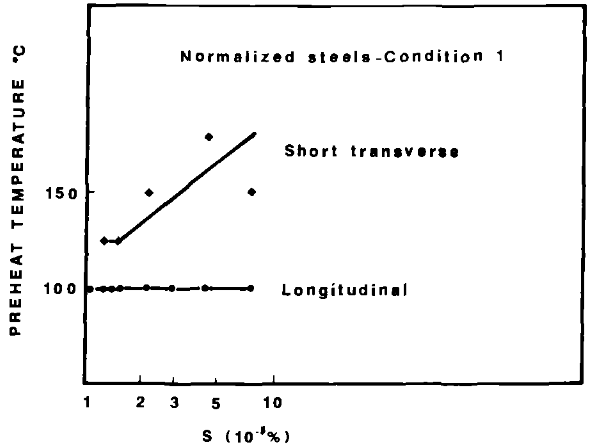

FIG. 4—*Effect of the sulfur content on the critical preheat temperature for two different stress orientations and for normalized steels.*

high in the short transverse direction, much higher than classical observations on lamellar tearing.

Quenched and Tempered Steels—The implant tests are performed with an applied stress of 550 MPa in accordance with the high mechanical characteristics of these steels. As on normalized steels, the critical preheating temperature is plotted versus the sulfur content as shown in Fig. 5. As previously observed, no difference is observed for the longitudinal axis (and for sufficiently low sulfur contents), but significant differences appear as soon as for 2.10^{-3}% in the short transverse axis.

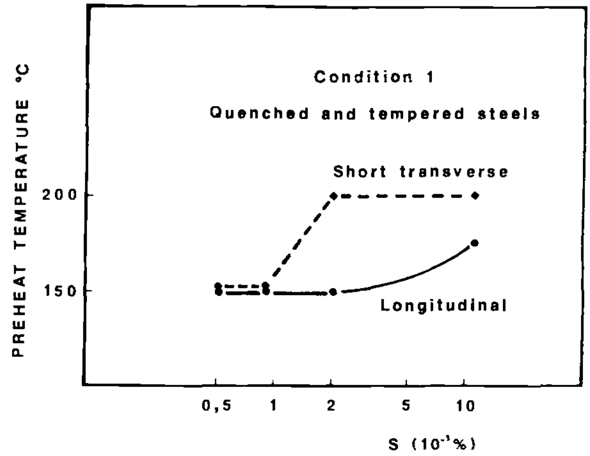

FIG. 5—*Effect of the sulfur content on the critical preheat temperature for two different stress orientations and for quenched and tempered steels.*

Discussion

The different tests performed in this study lead to the following observations:

(1) Underbead hardness seems to be independent from the sulfur content;
(2) Ultra low sulfur steels are less sensitive to hydrogen content in weldments; and
(3) Cold cracking of ultra low sulfur steels is insensitive to the stress direction.

Underbead Hardness

The influence of sulfur content on underbead hardness is a sensitive problem. Generally, the differences observed appear between steels without microalloying additions and "new" steels with low carbon content and microalloying additions such as niobium. A significant fact is that self-tempering of martensite is considerably lower in microalloyed steels. This point can explain numerous distortions observed on steels with similar carbon equivalent values. The results obtained here on C Mn or C Mn Ni V steels show no clear effect as statistically observed elsewhere.

Hydrogen Sensitivity

Different theories have been developed concerning the hydrogen embrittlement of steels. Considering the problem of sulfur's influence, the trap theory seems to be interesting to apply to these results [*8*]. Sulfides are hydrogen traps. This capability explains steel's behavior when it has a low hydrogen content. As the total amount of hydrogen is higher than the sulfide trapping capacity of low sulfur steel, sulfides are saturated and cracks occur. On the other hand, the sulfide trapping capacity of high sulfur steel is above the hydrogen content, so the sulfides are not saturated and no cracks occur. At higher hydrogen levels, both low and high sulfur steels have a sulfide trapping capacity lower than the hydrogen content. Cracks appear in both cases. But the shape of sulfides in the case of high sulfur content increases the risk of crack initiation. This part will be particularly developed in the next section.

Influence of Stress Direction

The influence of the stress direction has been observed before in pipe steels [9], but rarely in construction steels. The worst behavior of steels in the short transverse direction has always been associated only with lamellar tearing, this last phenomena being eventually increased by cold cracking. Results presented before show clearly that sulfur contents leading to worse results in cold cracking are significantly lower than those generally admitted as sufficient in regard to lamellar tearing.

Figures 6 and 7 show the critical preheating conditions versus the L/T parameter describing the shape of sulfides. Clearly, some small distortions observed previously when plotted with the only sulfur content are corrected. The shape of sulfides is the main parameter as shown in Fig. 8. The ratio between the short transverse and the longitudinal critical preheat temperatures

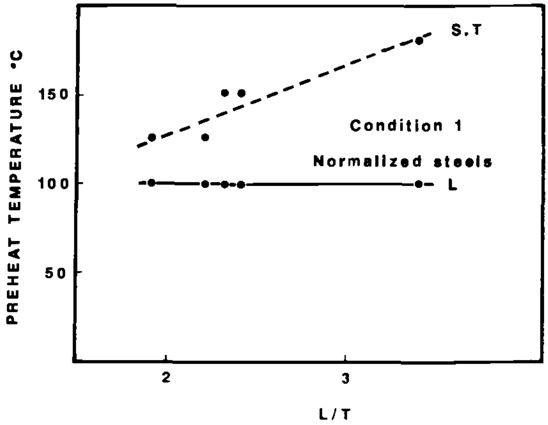

FIG. 6—*Effect of the sulfide shape on the critical preheat temperature for two different stress orientations and for normalized steels.*

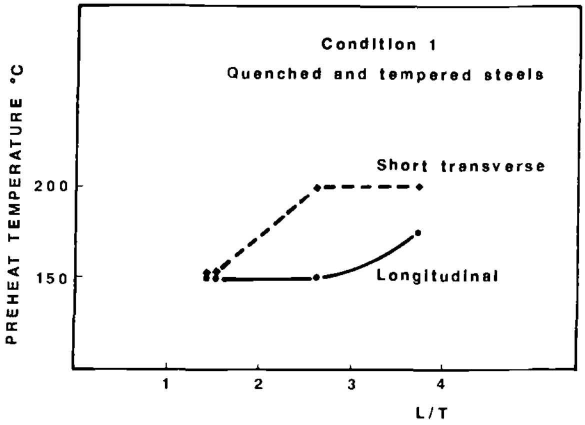

FIG. 7—*Effect of the sulfide shape on the critical preheat temperature for two different stress orientations and for quenched and tempered steels.*

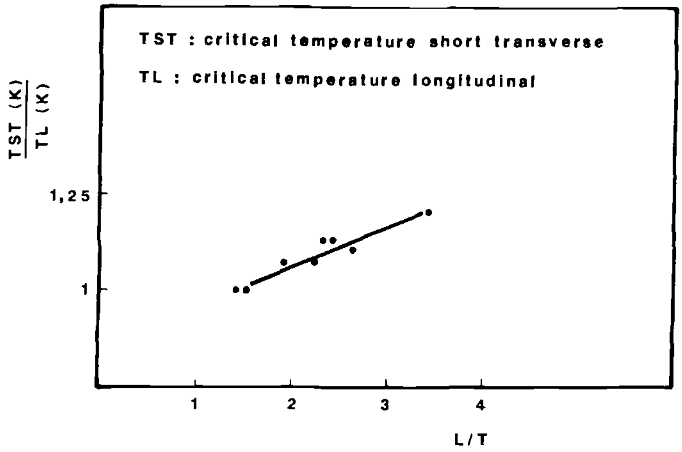

FIG. 8—*Effect of the sulfide shape on the ratio between the critical preheat temperatures obtained for two different orientations.*

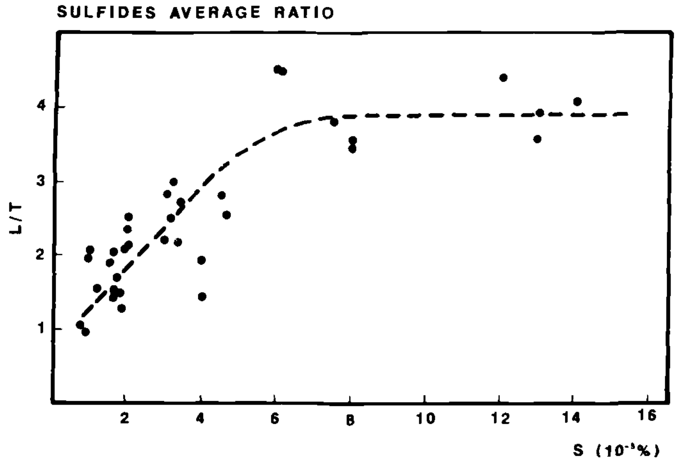

FIG. 9—*Effect of the sulfur content on the sulfides' shape.*

(values in Kelvins) varies quite linearly with the shape factor. From this variation, ensuring a shape factor of sulfides L/T under a critical value, which is around 1.7-1.8, appears necessary to eliminate completely the short transverse sensitivity to cold cracking.

Weldability and Sulfur Content

From the previous examinations and remarks, low sulfur contents seem not as detrimental as can be said. Rather, maintaining the shape factor L/T as low as possible appears to be extremely important. Figure 9 shows the correlation between shape factor and sulfur content. The curve shape explains the choice of linear rules for L/T curves (Figs. 6, 7, 8) and of logarithmic rules for sulfur content curves (Figs. 3, 4, 5). Despite the results from Fig. 9, neglecting other effects such as the reduction ratio on the sulfide shape is impossible. Nevertheless, a sulfur content limited at a maximum value of $2.10^{-3}\%$ in base metal should be required to ensure a really safe weld in the HAZ. For such values, it is also important to control other inclusion formers such as oxygen, oxides being also hydrogen traps.

Conclusion

Welding tests have shown that low sulfur contents are not detrimental to cold cracking behavior of ferritic steels. Instead, requiring ultra low sulfur contents (or an accurate control of sulfides' shape factor) to obtain less sensitivity to hydrogen and homogenous results in the various stress directions appears to be necessary.

References

[*1*] Hart, P. H. M., "Trends in steels and consumables for welding" The Welding Institute, 1978, pp. 21-53.
[*2*] McKeown, D., Judson, P., Apps, R. L., and Pumphrey, W. I., *Metals Construction*. Nov. 1983, pp. 667-673.
[*3*] Bourges, Ph., *Soudage et Techniques Connexes*, Vol. 37, No. 11/12, 1983, pp. 375-385.
[*4*] Granjon, H. and Gaillard, R., *Soudage et Techniques Connexes*, Vol. 18, No. 9/10, 1964.
[*5*] Vallon, B., Bourges, Ph., Maynier, Ph., and Blondeau, R., International Institute of Welding, Doc. IIW IX B, 137-87.
[*6*] Suzuki, H., International Institute of Welding, Doc. IIW IX 1418-86.
[*7*] Duren, C., International Institute of Welding, Doc. IIW IX 1437-86.
[*8*] Pressouyre, G. M., *Acta Metallurgica*. Vol. 28, pp. 895-911.
[*9*] Gondoh, H. and Nakasugi, H., "Processing and Properties of Low Carbon Steel," American Institute of Mechanical Engineers, New York, 1973, pp. 133-143.

Richard L. Bodnar,[1] *Bruce L. Bramfitt,*[1] *and*
Raymond F. Cappellini[2]

The Influence of Residual Copper in Annealed and Postweld Heat Treated 2-1/4Cr-1Mo Steel

REFERENCE: Bodnar, R. L., Bramfitt, B. L., and Cappellini, R. F., "**The Influence of Residual Copper in Annealed and Postweld Heat Treated 2-1/4Cr-1Mo Steel,**" *Residual and Unspecified Elements in Steel, ASTM STP 1042,* A. S. Melilli and E. G. Nisbett, Eds., American Society for Testing and Materials, Philadelphia, 1989, pp. 202–231.

ABSTRACT: Vacuum arc remelted (VAR) and electroslag remelted (ESR) 2-1/4Cr-1Mo tubesheet forgings were produced for the steam generators of the now terminated Clinch River breeder reactor project. The forgings were produced to American Society of Mechanical Engineers (ASME) SA336 Grade F22a, and test metal in the annealed and simulated postweld heat treated (PWHT) condition had to meet the minimum yield strength requirement of 207 MPa. All of the VAR forgings passed the yield strength requirement, while all of the ESR forgings marginally failed the yield strength requirement. The main difference between the two steels was the lower copper content of the ESR forgings (for example, 0.046 versus 0.13%). The yield strength increment in the annealed condition was accounted for by solid-solution strengthening due to copper, whereas in the PWHT condition, precipitation strengthening due to ϵ-copper accounted for the difference. This additional strengthening increment would have been sufficient to ensure that all of the ESR forgings met the minimum yield strength requirement. Both strengthening increments were confirmed with laboratory-produced and heat treated 2-1/4Cr-1Mo steels with copper levels of 0, 0.16, and 0.32%, and were found to be compatible with the most recent iron-copper phase equilibria. Yield strength was also found to increase by increasing the cooling rate from the PWHT. This strengthening increment is attributed to solid-solution strengthening due to carbon, nitrogen, molybdenum, and chromium, and precipitation strengthening due to (M_2X) carbides. The data presented in this paper provide an example of residual copper affecting the mechanical properties of a 2-1/4Cr-1Mo steel. Furthermore, much of the data base used to establish the mechanical property capabilities of 2-1/4Cr-1Mo steel was developed using steels that had relatively high copper levels (or were not analyzed for copper), and were air-cooled from the PWHT, thus producing a data base of yield strength values that are higher than can be achieved under the constraints of the specification.

KEY WORDS: 2-1/4Cr-1Mo steel, residual copper, full annealing, iron-copper phase diagram, postweld heat treatment, precipitation strengthening, solid-solution strengthening, carbide strengthening, steam generator, tubesheet forgings

Residual or incidental elements in steel, like copper, are usually not considered as a factor in the design of component properties as long as they are held below the specified limits. In the specific case of copper, supplementary requirement S1 of ASTM Specification for Steel Forgings, General Requirements (A 788), limits the residual level to 0.35%. This percentage is a common limit for copper in most alloy steels. The exceptions include steels that are exposed to

---

[1] Senior research engineer and research fellow, respectively, Research Department, Bethlehem Steel Corporation, Bethlehem, PA 18016.

[2] Director of technology and new product development, BethForge Division, Bethlehem Steel Corporation, Bethlehem, PA 18016.

nuclear radiation where copper is specifically restricted to 0.10% maximum to prevent irradiation embrittlement. The maximum limit for copper was established over 50 years ago and remains in effect today because it is thought that copper does not strongly influence mechanical properties or have a harmful effect. However, as the present study will show, a copper level below the specified limit can influence strength depending upon the processing, particularly the heat treatment and postweld heat treatment (PWHT) of the steel. The study involves tubesheet forgings of 2-1/4Cr-1Mo steel for the Clinch River demonstration liquid-metal fast breeder reactor that was terminated by the U.S. Senate in October 1983, just before the planned start of major construction.

Tubesheet forgings measuring approximately 1230 mm in diameter by 380 mm in thickness were required for the Clinch River steam generators. The tubesheet forgings hold 739 tubes that are exposed to water/steam mixtures on the inside of the tubes (peak temperature of 500°C) and to liquid sodium on the outside. Figure 1 shows the location of two tubesheet forgings in the Clinch River steam generator. Figure 2 is a schematic drawing of a machined tubesheet forging without the tubes. After forging and heat treatment, the tubesheet forgings are machined to the

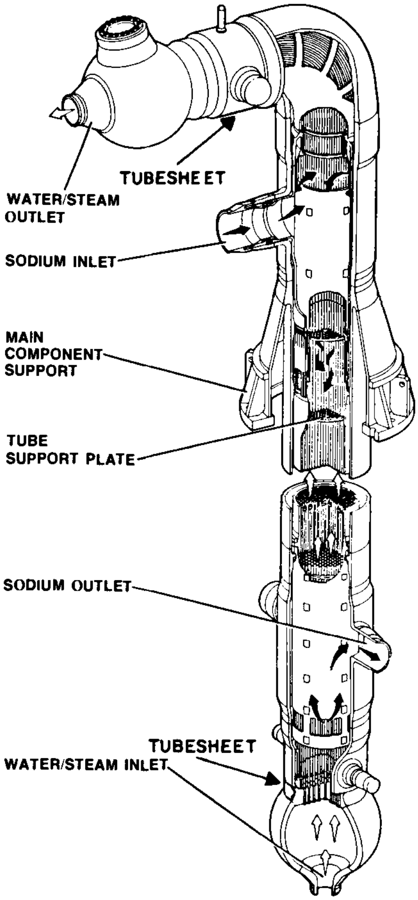

FIG. 1—*Diagram of a steam generator for the Clinch River breeder reactor showing the location of two tubesheet forgings.*

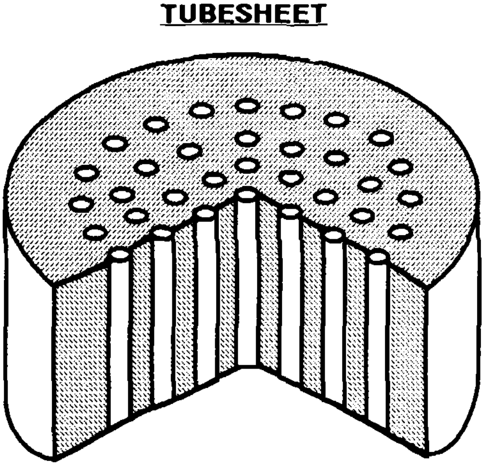

FIG. 2—*Schematic cross section of a machined tubesheet forging without the tubes.*

required size and then drilled. The tubes are inserted into the drilled holes and welded to the tubesheet forging. Each weld is given a postweld heat treatment to relieve residual stresses that develop during welding.

The alloy chosen for the tubesheet forgings was 2-1/4Cr-1Mo steel, based on its proven fabricability and resistance to severe environmentally induced failures, namely, stress corrosion cracking, water and sodium corrosion, decarburization from flowing sodium, oxidation (scaling), temper embrittlement, creep embrittlement, and stress relief embrittlement. The 2-1/4Cr-1Mo steel was specified as American Society of Mechanical Engineers (ASME) SA336 Class F22a as modified by Nuclear Standard M2-19T. The chemistry requirements of these specifications are listed in Table 1.

Normally, 2-1/4Cr-1Mo heavy forgings are either normalized and tempered or water quenched and tempered to provide a bainitic microstructure for the best combination of strength, toughness, and creep properties. However, for long-term creep stability and due to the large data base developed for annealed 2-1/4Cr-1Mo steel from extensive research conducted for this specific application [*1-31*], tubesheet forgings for the Clinch River breeder reactor program were specified to be supplied in the fully annealed heat treated condition. In addition, test material from each forging was required to meet a minimum 0.2% yield strength of 207 MPa in a simulated postweld heat treated condition. These two heat treatment cycles are shown graphically in Fig. 3.

Twenty vacuum arc remelted (VAR) and twenty electroslag remelted (ESR) tubesheet forgings were produced by two independent suppliers. Both melting processes produced ingots of sound quality. All of the VAR forgings passed the yield strength requirement (207 MPa minimum) after simulated PWHT with values in the range of 223 to 272 MPa. Conversely, all of the ESR forgings failed the yield strength requirement after PWHT with values in the range of 186 to 203 MPa. A histogram of the actual yield strength data for each process is shown in Fig. 4. In an effort to enhance the yield strength of the ESR forgings, numerous laboratory heat treatments were conducted. The main findings from these experimental heat treatments were that yield strength could be increased by lowering the PWHT temperature to the minimum level allowed by the specification, namely, 708°C, and increasing the cooling rate from the PWHT temperature. A lower PWHT temperature allowed a few of the ESR forgings just to meet the

TABLE 1—*Chemistry specification and production test material analyses.*

	C	Mn	P	S	Si	Ni	Cr	Mo	Cu	V	Ti
SA336-F22A and M2-19T	$\frac{0.07}{0.11}$	$\frac{0.30}{0.60}$	<0.015	<0.015	$\frac{0.20}{0.40}$	<0.25	$\frac{2.00}{2.50}$	$\frac{.90}{1.10}$	<0.35	<0.03	<0.03
ESR	0.09	0.45	0.010	0.004	0.27	0.19	2.28	0.98	0.046	<0.01	<0.002
VAR	0.09	0.45	0.006	0.006	0.29	0.20	2.24	0.95	0.130	<0.01	<0.002
	Al_T	N_T	Mobile N	B	Cb	Zr	W	Sb	As	Sn	O
ESR	0.009	0.0120	<0.0005	<0.001	<0.005	<0.01	<0.03	0.0011	0.0058	<0.002	<0.0040
VAR	0.004	0.0060	<0.0005	<0.001	<0.005	<0.01	<0.03	0.0025	0.0083	<0.002	0.0030

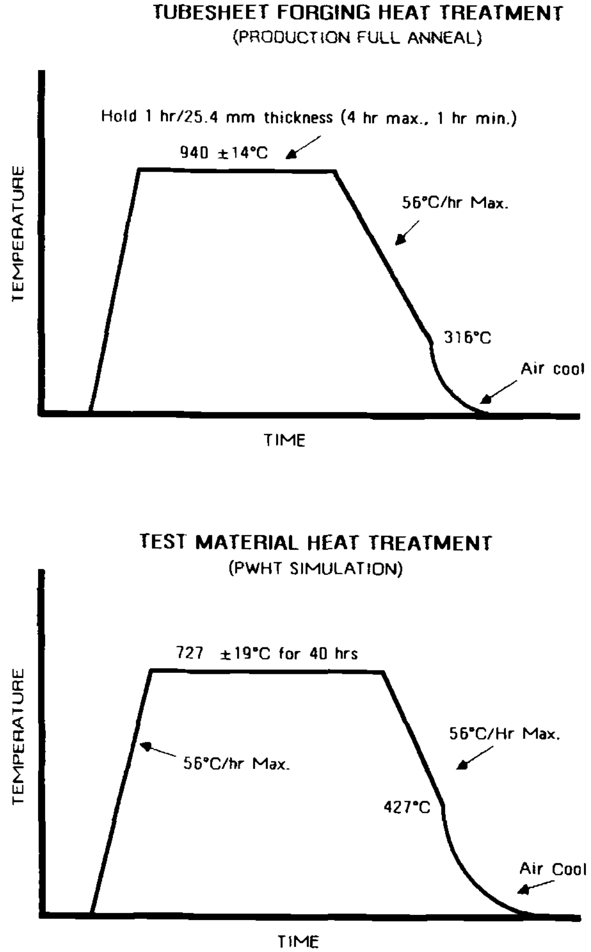

FIG. 3—*Schematic diagram illustrating the specified heat treatment cycles for both the tubesheet forgings and the test material.*

minimum yield strength requirement. With a sufficiently fast cooling rate from the PWHT temperature, all of the ESR forgings passed the yield strength requirement, however, this exceeded the cooling rate allowed by the specification.

As will be shown later, the primary difference between the two groups of forgings is their copper content. The VAR steels contained 0.08 to 0.15% copper while the ESR steels contained 0.03 to 0.05% copper. This difference in copper content is not related to the remelting process but to the composition of the scrap used in the electric furnace steelmaking for the casting of the consumable electrodes. One of the attributes of copper is that it is considered non-oxidizable during steelmaking. The ESR electrodes were made from a controlled supply of low residual element scrap (including low copper), while the scrap source for the VAR electrodes was higher in residual elements. The ESR practice involved the use of selective scrap to attain low copper levels to minimize forging surface problems and loss in high temperature ductility in forgings for high temperature applications [*32*]. The use of a selective scrap practice was not utilized for

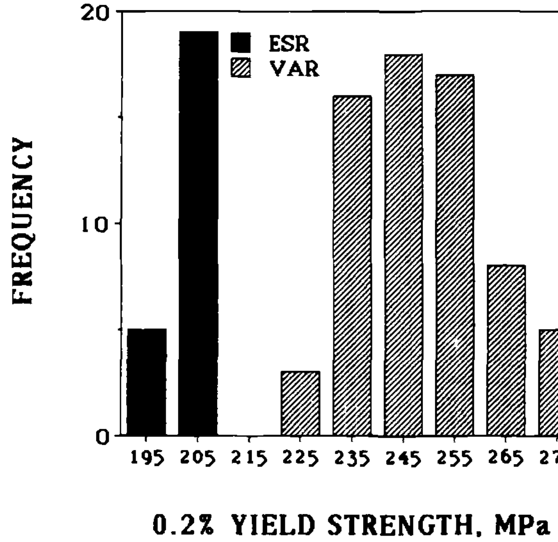

FIG. 4—*A histogram of the actual yield strength data for both ESR and VAR tubesheet forgings.*

the VAR electrodes. In order to assess further the influence of copper in annealed and PWHT 2-1/4Cr-1Mo steel, laboratory-produced steels with varying levels of copper were studied; these results are also included in this paper.

Before presenting the experimental procedures and results of our studies, some general background on the effects of copper additions to steel is provided in the next section.

Copper in Steel

The most reliable iron-copper phase diagram is that of Kubaschewski [*33*], which is reproduced in Fig. 5. From this diagram one can see that copper is quite soluble in austenite and much less soluble in ferrite. While several investigators have studied the solubility of copper in ferrite [*34–38*], there is still disagreement on the specific limits. The maximum solubility of copper in ferrite is 2.10 wt. % (1.8 at. %) at 850°C. Below 850°C the solubility decreases rapidly. Unfortunately, solubility data are not available below about 600°C. The iron-rich end of the iron-copper binary phase diagram is shown in Fig. 6. The extension of the solvus line below 600°C (dashed line) was calculated from the free energy functions for body-centered cubic and face-centered cubic solid solutions as given by Kubaschewski et al. [*37*]. In view of the limited solubility of copper in ferrite, any copper remaining in solution during quenching precipitates as pure copper (ϵ-phase) upon aging. Copper steels are well known for their ability to age harden [*39–42*], and commercial steels have been designed to take advantage of the precipitation strengthening potential of copper [*43,44*].

Copper in amounts up to 0.5% in low carbon steels have also been reported to provide a modest degree of solid-solution strengthening in ferrite [*45–49*]. The solid-solution strengthening effect of copper in ferrite is reported to be between 38 and 70 MPa per 1% copper. The effect is linear up to about 1.1% copper [*45*]. The solid-solution strengthening, coupled with the precipitation strengthening, accounts for a modest increase in yield strength in those steels containing substantial amounts of copper. For example, the maximum level of 0.35% copper

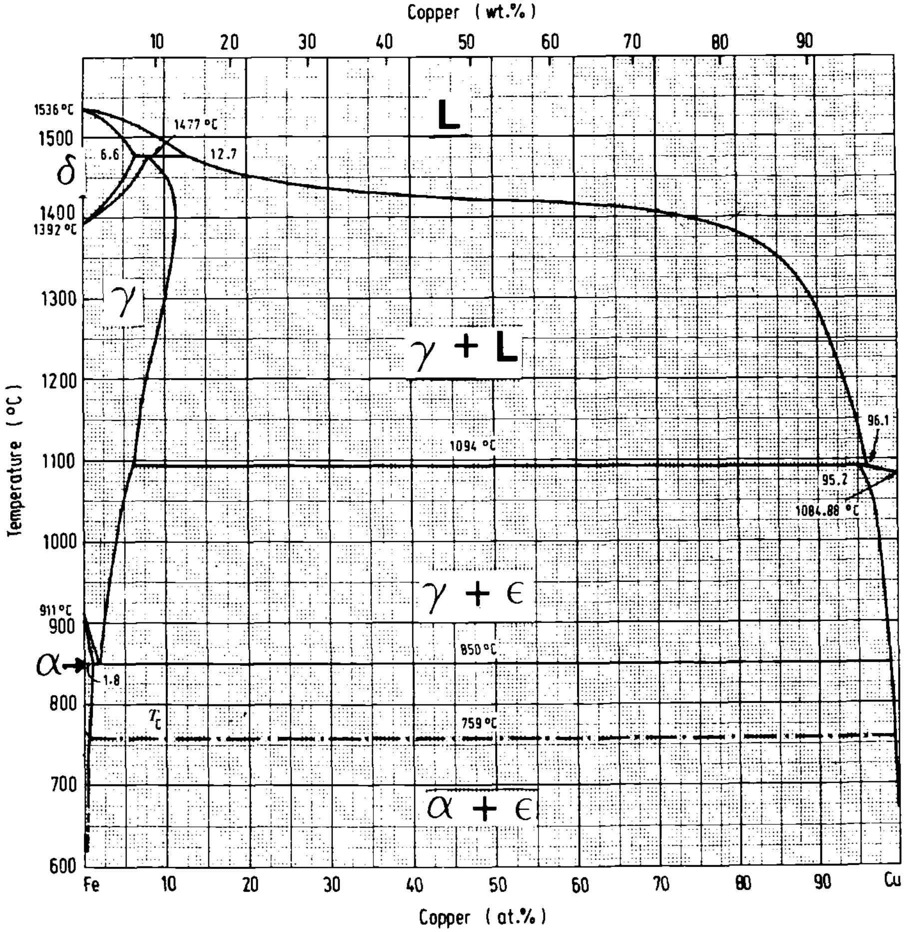

FIG. 5—*Iron-copper binary phase diagram* [33].

allowed in most construction steels can account for about 13 to 25 MPa, due to solid-solution strengthening.

The copper level designated for the tubesheet forgings is interpreted to have been set to control the content of this residual element. Copper cannot be considered an alloying element in this case since none of the literature that discusses the physical metallurgy of annealed and PWHT 2-1/4Cr-1Mo steel for the Clinch River breeder reactor [*1-6,8-16,19-22,24,25*] addresses the influence of copper in this steel, and most of the references do not even include the level of copper in the steels discussed [*1-6,8-10,16,19-21,25*]. Furthermore, the American Iron and Steel Institute (AISI) products manual for carbon, alloy, and HSLA steels [*50*], and ASTM specification A 788 consider copper levels up to 0.35% as incidental when not specified or required because of their modest solid-solution strengthening effect and alleged innocuousness.

In addition to strengthening steel, copper also increases the fluidity of molten steel and provides atmospheric corrosion resistance. Reports also show that copper can retard austenite recrystallization [*51*], which can influence microstructure upon thermomechanical treatment. In addition, copper increases the hardenability of steel [*52*]. On the negative side, copper pro-

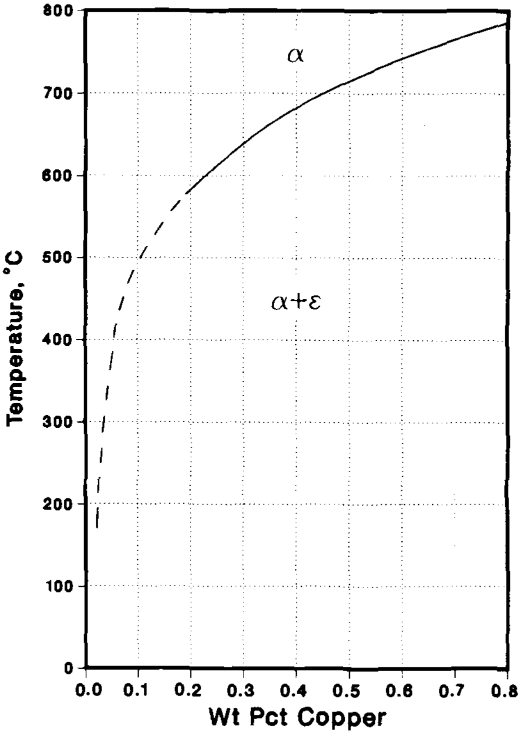

FIG. 6—*Enlarged portion of the ferritic region of the iron-copper binary phase diagram.*

motes hot shortness, which is often associated with surface cracking during mechanical working [*53*]. In fact, even levels as low as 0.2% copper in the presence of tin and antimony have caused hot shortness in mild steel [*54-56*]. Copper also promotes the formation of an adherent scale during hot deformation, which can contribute to poor surface quality [*57*]. As with most precipitation strengthened steels, the yield and tensile strength enhancement from copper also leads to a reduction in ductility and notch toughness. Depending on the particular application, steels with a high residual copper content may be susceptible to other problems, for example, irradiation embrittlement [*58*], stress relief embrittlement [*59,60*], reduction in hot tensile and creep rupture ductility [*61-63*] and temper embrittlement [*64*]. As a result of these negative factors, copper is not intentionally added to heavy forging steels. In fact, as in the case of the ESR tubesheet forgings, selective scrap was used to keep residual copper at a low level.

Experimental Procedure

Mid-radius, tangential blanks measuring 25-mm square by 130-mm long were removed from the respective prolongs of representative production annealed ESR and VAR tubesheet forgings. The chemical analyses of these blanks in the PWHT condition are compared with the specified chemistry in Table 1. While both steels met the specification requirements, the ESR steel is higher in aluminum and nitrogen, but lower in copper in comparison to the VAR steel. All of the other minor differences in chemistry between the ESR and VAR steels were considered insignificant.

Heat Treatment

Blanks representing both forgings were given a simulated PWHT. The blanks were either cooled according to the specification at a maximum rate of 56°C/h or still air cooled (3000°C/h). The exact heat treatment cycles are summarized in Table 2. The cycles are slightly different since the heat treatments were conducted by different suppliers. In addition, three 68-kg vacuum induction melted ingots were produced in the laboratory from the same master heat of 2-1/4Cr-1Mo steel with copper levels (ingot additions) of 0, 0.16, and 0.32%, respectively. The ingots were hot rolled to 25- by 102-mm plate, cut into 127-mm lengths, and heat treated in the laboratory to the following conditions: fully annealed, PWHT/FC, and PWHT/AC. The heat treatment cycles are listed below (Table 3). The chemical analyses of the laboratory melted and heat treated plates, all within the specified ranges, are included in Table 4.

TABLE 2—*Comparison of ESR and VAR tubesheet forgings.*

ESR	VAR
Production Full Anneal	
Annealed at 940°C, 4 h Cooled 28°C/h to 316°C Air cooled to room temperature	Annealed at 927°C, 4 h Cooled 56°C/h to 316°C Air-cooled to room temperature
PWHT/FC[a]	
Heated 56°C/h to 710°C Held 40 h Cooled 56°C/h to 427°C Air cooled to room temperature	Heated 56°C/h to 727°C Held 40 h Cooled 56°C/h to 427°C Air cooled to room temperature
PWHT/AC[b]	
Heated 56°C/h to 710°C Held 40 h Air cooled to room temperature	Heated 56°C/h to 727°C Held 40 h Air cooled to room temperature

[a] PWHT/FC means control furnace cooled from the post-weld heat treatment temperature.

[b] PWHT/AC means air cooled from the post-weld heat treatment temperature.

TABLE 3—*Heat treatment cycles.*

Full Anneal	PWHT/FC[a] or PWHT/AC[b]	
Annealed at 940°C, 4 h	heated 56°C/h to 727°C	
Cooled 56°C/h to 316°C	held 40 h, and	
Air cooled to room temperature	(a) Cooled 56°C/h to 427°C	(PWHT/FC)
	Air cooled to room temperature	
	or	
	(b) Air cooled to room temperature	(PWHT/AC)

[a] PWHT/FC means control furnace cooled from the post-weld heat treatment temperature.

[b] PWHT/AC means air cooled from the post-weld heat treatment temperature.

TABLE 4—*Chemical analyses of the laboratory produced steels.*

	C	Mn	P	S	Si	Ni	Cr	Mo	Cu	V	Ti	Al_T	N_T	Mobile N	B	O
Base	0.08	0.49	0.003	0.004	0.33	0.21	2.23	1.03	<0.005	<0.003	0.002	0.006	0.0019	<0.0002	<0.0005	0.0021
Base + 0.16Cu	0.08	0.49	0.003	0.004	0.34	0.21	2.27	1.03	0.16	<0.003	0.002	0.005	0.0022	<0.0002	<0.0005	0.0025
Base + 0.32Cu	0.08	0.48	0.003	0.004	0.33	0.21	2.23	1.01	0.32	<0.003	0.002	0.005	0.0023	<0.0002	<0.0005	0.0032

Dilatometry

Dilatometer pins measuring 2.5 mm in diameter and 50 mm in length were machined from both the ESR and VAR test material in the annealed condition. Critical temperatures were determined using the PWHT heating rate of 56°C/h.

Tensile/Impact Testing

Standard 12.8-mm diameter tensile specimens were machined from blanks heat treated to the various conditions. Longitudinal tensile specimens were removed from the laboratory produced steels. All tensile testing was performed in accordance with ASTM Methods of Tension Testing of Metallic Materials (E 8) at room temperature. Twelve full-size Charpy V-notch specimens were machined in the L-T orientation for each heat treated condition from the laboratory produced steels to evaluate the influence of the three levels of copper on toughness. The Charpy testing was conducted according to ASTM Methods for Notched Bar Impact Testing of Metallic Materials (E 23).

Light and Electron Microscopy

Specimens cut from the threaded ends of tensile specimens representing each condition were polished and etched using standard metallographic procedures. The specimens were first etched with picral, which contained a few drops of hydrochloric acid, and examined in the light microscope. The percentage of each microconstituent was determined by point counting. Ferrite grain size was determined by the three circle method of ASTM Methods for Determining Average Grain Size (E 112).

Analytical electron microscopy (AEM) was used to define differences in the fine scale microstructures of the ESR and VAR steels. Both two stage carbon extraction replicas and thin foils were made using the same tensile ends employed for the light microscopy examination. In preparing the replicas, the specimens were repolished and etched in 2% nital for 1 min. After etching, a cellulose acetate tape, softened on one side with a few drops of acetone, was pressed firmly onto the etched surface, allowed to dry for 30 min, and then stripped from the specimen. The stripped tape (replica) was then mounted on a glass slide and coated with a thin film of carbon in a vacuum evaporator. Subsequent to carbon deposition, the replica was cut into two 4-mm pieces, mounted on beryllium grids, and immersed in a covered dish of acetone for several hours until the cellulose acetate tape was completely dissolved, leaving the extracted particles (carbides, copper particles, etc.) in the carbon film.

In the case of the thin foils, sections about 1-mm thick were cut from the tensile ends and mechanically and chemically thinned to 0.1 mm. Discs measuring 3 mm in diameter were punched from the sections and thinned electrochemically to electron transparency in a twin jet apparatus at an applied potential of 25 V in a solution of 15% perchloric acid/85% methanol maintained at about −60°C.

The replicas and thin foils were examined in both a Philips EM-400T transmission electron microscope/scanning transmission electron microscope (TEM/STEM) operating at 120 kV and a VG Scientific Model HB501 dedicated STEM operating at 100 kV. These microscopes are also equipped with energy dispersive spectrometers (EDS), which allow for X-ray microanalysis. Images of various carbides and precipitate structures were obtained over a range of magnifications (2,800 to 280,000x) in the TEM mode, whereas in the STEM/EDS mode, 20- to 40-nm and 1-nm diameter focused electron beams were employed in the Philips and VG microscopes, respectively, to analyze precipitate composition. Both microscopes were equipped with computer based X-ray analyzer systems and suitable standards were used to convert the emitted X-ray intensities into weight percentages of elements present in the precipitates.

Results

Production Forgings

Dilatometry—The Ac_1 and Ac_3 temperatures for both the ESR and VAR steels are listed in Table 5. The critical temperatures are similar for the two forgings. The Ac_1 temperature is well above the PWHT temperature of 727 ±19°C, thus no reaustenitization is expected during PWHT.

TABLE 5—*Critical temperatures for 2-1/4Cr-1Mo steel.*

Forging	Ac_1(°C)	Ac_3(°C)
ESR	784	912
VAR	783	914

Tensile Properties/Light Microscopy—Tensile properties and quantitative metallographic data are summarized in Table 6. Each of the conditions met the tensile requirements of SA336-F22a with the exception of the ESR steel in the PWHT/FC condition, which typifies the 20 ESR tubesheet forgings. Samples in the annealed condition exhibited continuous yielding (no yield point) behavior while samples in the PWHT/FC and PWHT/AC conditions displayed discontinuous yielding (yield point) behavior. Figure 7 shows a comparison of the load-elongation curves for the ESR steel in the three conditions. The shapes of the load-elongation curves for the VAR steel were similar.

Figure 8 provides a comparison between the ESR and VAR as-annealed microstructures. Minor differences in average grain size, percent bainite and percent eutectoid were observed. The term eutectoid is used since this steel does not contain normal pearlite as found in plain carbon and lower alloyed steels. However, as explained later in this paper, these microstructural differences do not account for the observed differences in yield strength between the ESR and VAR steels.

Electron Microscopy

Annealed—In the as-annealed condition, the ESR and VAR samples displayed similar microstructures. Both of these structures contain the eutectoid phase, consisting of ferrite and molybdenum-rich carbide, Figs. 9a and b. Both samples also contain a large amount of needlelike (Type 1) and coarse (Type 2) carbides in the ferrite matrix, as shown in Figs. 10a and b. These carbides have been identified as M_2X type where M is predominately molybdenum with lesser amounts of chromium and iron, and X is carbon with or without nitrogen. In addition to these carbides, 20- to 30-nm copper particles were also observed along ferrite grain boundaries of the VAR steel. An example of grain boundary copper precipitation is shown in Fig. 11; an arrow locates one of the copper particles. In the ESR sample, a few copper precipitates were also observed throughout the matrix with very little grain boundary precipitation.

PWHT/FC—In the PWHT/FC condition, the ESR and VAR samples exhibited similar carbide microstructures consisting of Type 1 needlelike and Type 2 coarse M_2X carbides, Figs. 12a and b. More Type 2 carbides were present in the PWHT/FC condition compared to the annealed condition, presumably due to spheroidization of many of the Type 1 carbides during PWHT. EDS microanalysis of the M_2X carbides showed that their average molybdenum/chromium ratio was 3.3 for the coarse carbides compared to 1.9 for the needlelike carbides. Al-

TABLE 6—*Summary of tensile properties and quantitative metallographic data for the production steels.*

Condition	Yield Strength 0.2% Offset, MPa	Tensile Strength, MPa	% Total Elongation	% Reduction in Area	Average Grain Size, μm	% Bainite	% Eutectoid
ESR Annealed	224	486	34.0	75.0	24	2	11
EST PWHT/FC[a]	200	452	35.0	76.0	24	2	11
ESR PWHT/AC[b]	262	445	34.0	72.0	32	2	11
VAR Annealed	231	480	30.5	72.3	36	5	12
VAR PWHT/FC	219	441	34.0	76.0	36	5	12
VAR PWHT/AC	257	448	33.5	75.0	36	5	12
SA336-F22A	207 min	414/586	20.0 min	45.0 min			

[a] PWHT/FC means control furnace cooled from the post-weld heat treatment temperature.

[b] PWHT/AC means air cooled from the post-weld heat treatment temperature.

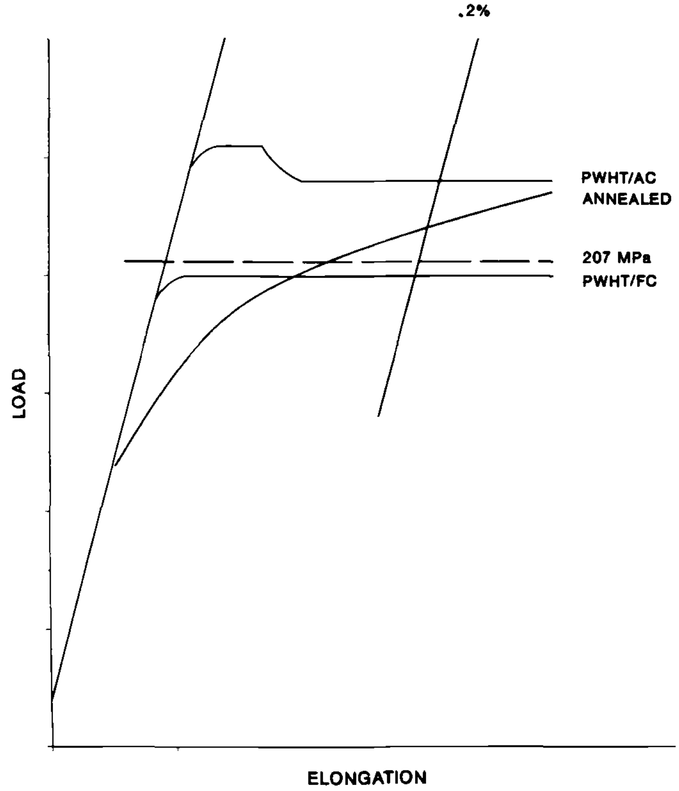

FIG. 7—*Comparison of the tensile load-elongation curves for the ESR steel in the annealed, PWHT/FC, and PWHT/AC conditions.*

though the molybdenum/chromium ratios of the two types were significantly different, their iron/chromium ratios are nearly the same with an average value of 0.12. A few grain boundary carbides of the M_7C_3 type were also observed. These particles were found to be chromium-rich and to have average molybdenum/chromium and iron/chromium ratios of 0.1 and 0.7, respectively.

The bainitic regions of these samples also contained carbides that were identified as $M_{23}C_6$ type carbides. These carbides exhibit well-defined crystallographic facets as shown in Fig. 13. The average molybdenum/chromium and iron/chromium ratios are 0.5 and 1.6, respectively.

Although the carbide precipitation reactions in the ESR and VAR samples are quite similar, the precipitation and chemistry of the non-carbide forming elements are significantly different. The VAR sample, which has more copper than the ESR sample, contains more copper particles (presumably ϵ-copper). An example of these copper particles and the associated EDS X-ray spectrum are presented in Figs. 14a and b. As shown by the arrow in Fig. 14b, some of the copper particles appear as 50-nm clusters, presumably due to electrostatic attractive forces, during the replicating process between particles, originally located at various depths within the steel.[3] Many individual copper particles were also observed in the VAR steel and measured to be

[3] Work aimed at eliminating this particle clustering artifact is under way at our laboratory.

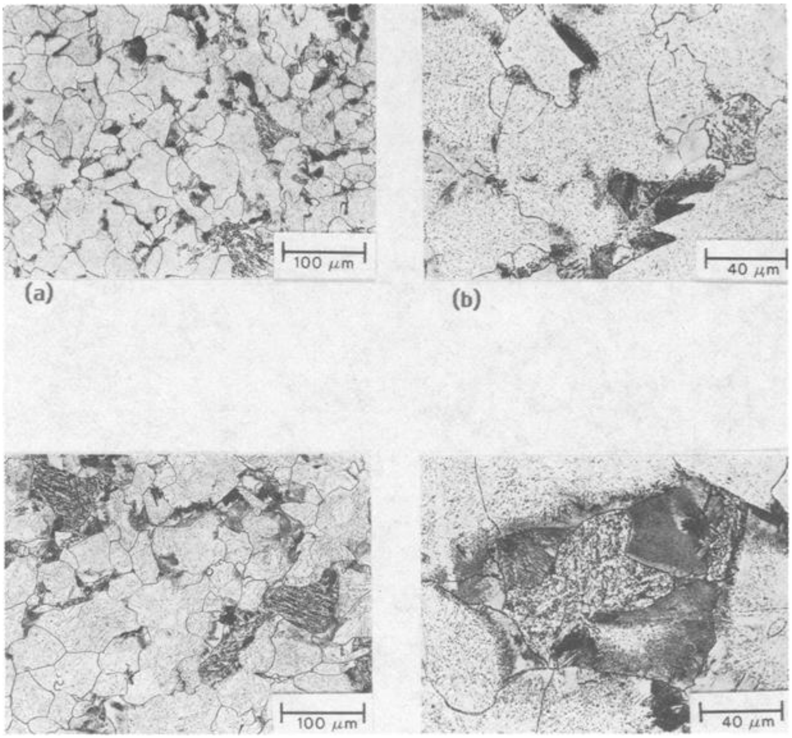

FIG. 8—*Light micrographs comparing (a,b) ESR and (c,d) VAR steels in the fully annealed condition (Picral + HCl).*

between 5 and 50 nm in diameter.[4] The copper particles were finely dispersed throughout the matrix. Copper particles could only be detected at the thinnest edges of the thin foils due to the lack of precipitate contrast when embedded in the steel matrix. This phenomenon may be attributed to the similarity of the electron scattering factors of iron and copper and the negligible strains produced by the precipitates because of the small difference in the atomic radii of the two elements. Others have experienced similar difficulties in imaging fine copper particles in thin foils of iron-copper alloys [*65*].

In contrast, the ESR steel with higher aluminum and nitrogen contents shows a modest dispersion of approximately 100-nm diameter polygonal aluminum nitrogen (AlN) particles and very few copper precipitates. The particles are too large to contribute significantly to precipitation strengthening. The 5- to 50-nm copper particles, as found in the VAR steel, were observed to a much less extent in the ESR steel because of its lower copper content. Also, numerous observations of copper being associated with AlN particles in the ESR steel, Fig. 15, suggests that some of the copper nucleates on AlN particles and thus becomes ineffective as a precipitation strengthener.

PWHT/AC—Both the ESR and VAR samples in the PWHT/AC condition contained a large number of needlelike carbides designated as Type 1 and relatively few coarse carbides designated as Type 2 in the ferrite matrix, Figs. 16a and b. The volume fraction of the fine Type 1

---

[4] These copper particles are considered to be real and not artifacts since, as will be shown later, no copper particles were observed in either of the ESR or VAR steels in the PWHT/AC condition using the same replicating technique.

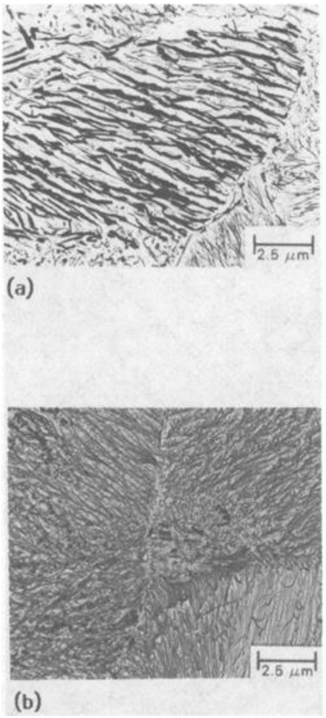

FIG. 9—*Electron micrographs of eutectoid phase consisting of ferrite and molybdenum-rich carbide in the fully annealed condition:* (a) *ESR steel and* (b) *VAR steel (extraction replicas).*

carbides appeared greater than in the PWHT/FC condition.[5] The ferritic carbides are M_2X type with average molybdenum/chromium and iron/chromium ratios of 2.1 and 0.12, respectively. $M_{23}C_6$ type carbides found in bainitic regions and the M_7C_3 type carbides observed in the grain boundaries were similar in size, shape, and chemistry to those of the ESR and VAR samples in the PWHT/FC condition. No copper precipitates were observed in either of the steels in this condition, thus indicating that the copper was in solid solution.

In summary, the size, structure, and chemistries of the carbide particles were similar for the ESR and VAR steels for a given heat treatment condition. The main difference between the two steels was the copper precipitation behavior. In the annealed condition, the VAR steel exhibited some grain boundary copper precipitates, while the ESR steel displayed a few copper precipitates throughout the matrix and on the ferrite grain boundaries. In the PWHT/FC condition, copper particles in the range of 5 to 50 nm were finely dispersed throughout the matrix of the VAR steel. The ESR steel contained very few 5- to 50-nm copper precipitates, which were sometimes associated with coarse 100-nm AlN particles, thus rendering them ineffective for precipitation strengthening. In the PWHT/AC condition, no copper particles were evident indicating that the copper remained in solid solution.

[5] M_2X carbides may dissolve during PWHT, and, upon air cooling from the PWHT temperature, some of the dissolved carbon and nitrogen presumably precipitates as fine Type 1 carbides.

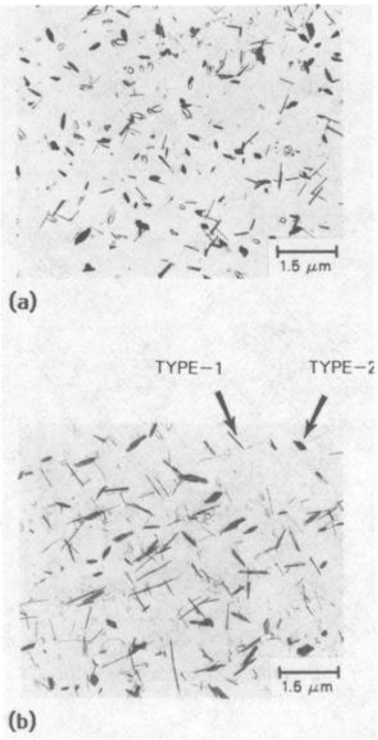

FIG. 10—*Electron micrographs of M_2X carbides in the ferrite matrix of fully annealed 2-1/4Cr-1Mo steel:* (a) *ESR and* (b) *VAR samples (extraction replicas).*

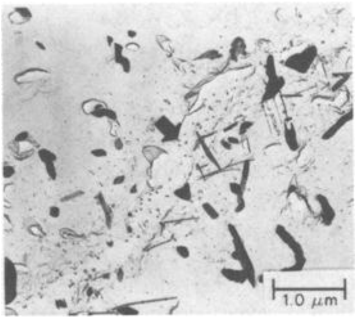

FIG. 11—*Electron micrograph of fully annealed VAR 2-1/4Cr-1Mo steel showing 20-nm copper precipitates along a ferrite grain boundary (extraction replica).*

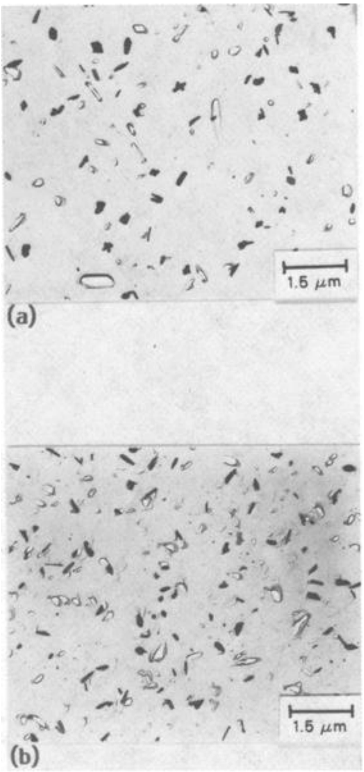

FIG. 12—*Electron micrographs of M_2X carbonitrides formed in the ferrite matrix of 2-1/4Cr-1Mo steel in the PWHT/FC condition:* (a) *ESR and* (b) *VAR samples (extraction replicas).*

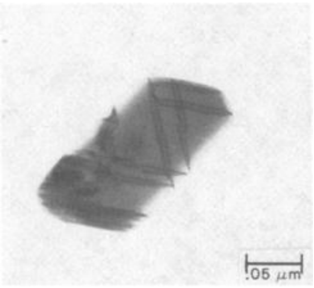

FIG. 13—*Electron micrograph of a $M_{23}C_6$ bainitic carbide in the ESR steel in the PWHT/FC condition (extraction replica).*

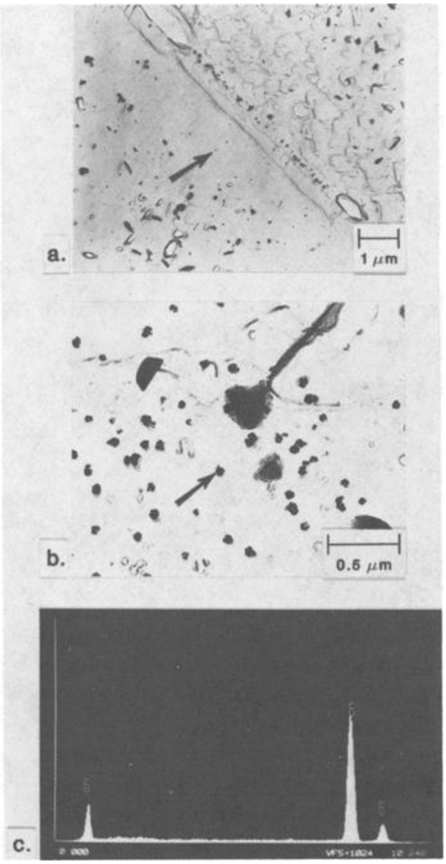

FIG. 14—*Electron micrographs* (a) and (b) *show copper particles extracted from a ferrite matrix in VAR 2-1/4Cr-1Mo steel in the PWHT/FC condition (extraction replicas). Arrows locate copper particles and* (c) *displays the EDS x-ray spectrum from one of the copper particles.*

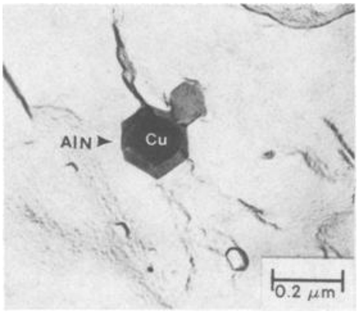

FIG. 15—*Electron micrograph of the ferrite matrix in the ESR steel in the PWHT/FC condition showing the association of copper and AlN (extraction replica).*

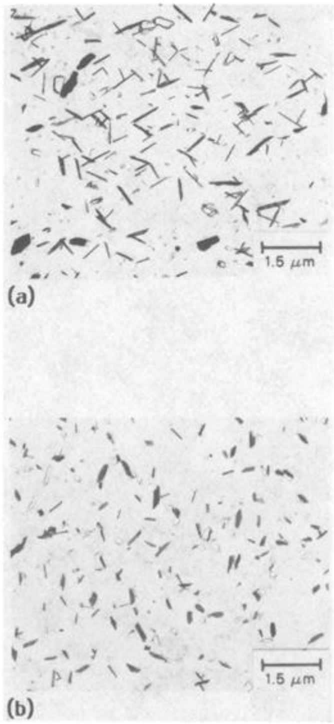

FIG. 16—*Electron micrographs of ferritic M_2X carbonitrides in:* (a) *ESR and* (b) *VAR steels in the PWHT/AC condition (extraction replicas).*

Laboratory-Produced Steels

Light Microscopy—The quantitative light microscopy data for the laboratory produced steels are summarized in Table 7. These steels exhibit a coarser ferrite grain size in comparison to the production steels, for example, about 60 versus 30 μm. Presumably, this coarser ferrite grain size is indicative of a coarser austenite grain size. A coarser austenite grain size provides enhanced hardenability for these steels, and leads to higher bainite and lower eutectoid volume fractions than observed in the production steels.

Tensile Properties—The tensile properties for the various heat treatment conditions are summarized in Table 7. Tensile and yield strengths are plotted versus copper content for the various heat treatment conditions in Fig. 17. Each data point represents the average of two tensile tests. As shown in this figure, the yield strength requirement can be easily met for all copper levels between 0 and 0.32% in the fully annealed and PWHT/AC conditions. However, in the annealed and PWHT/FC conditions, the data suggest that yield strength peaks at a copper level of approximately 0.16%. At this copper level, the average yield strength just meets the 207 MPa requirement in the PWHT/FC condition. In contrast, the yield strength requirement is not met at the 0 and 0.32% copper levels for the PWHT/FC condition. Bush and Lindsay [*66*] found a similar peak with a copper bearing, annealed 1008 steel.

Once again, yield strength was found to increase dramatically as the cooling rate from the PWHT temperature was increased (PWHT/AC versus PWHT/FC). Furthermore, continuous

TABLE 7—*Summary of mechanical properties and quantitative metallographic data for the laboratory produced steels.*

Cu Level	Condition	Yield Strength 0.2% Offset MPa	Tensile Strength MPa	% Total Elongation	% Reduction in Area	50% FATT (°C)	Upper Shelf Energy (J)	Average Grain Size (μm)	% Bainite	% Eutectoid
0.0%	Annealed	231	528	27.3	51.8	+60	137	58	27	<1.0
	PWHT/FC	197	431	35.8	78.3	−4	>358	"	"	"
	PWHT/AC	250	420	36.0	77.5	+18	>358	"	"	"
0.16%	Annealed	249	555	25.8	48.9	+54	130	62	27	<1.0
	PWHT/FC	208	438	35.0	78.0	−1	>358	"	"	"
	PWHT/AC	252	419	37.0	76.7	+18	>358	"	"	"
0.32%	Annealed	234	516	27.0	50.8	+57	163	64	25	<1.0
	PWHT/FC	201	435	36.0	78.3	+10	>358	"	"	"
	PWHT/AC	255	420	37.3	76.4	+21	>358	"	"	"

[a] PWHT/FC means control furnace cooled from the post-weld heat treatment temperature.

[b] PWHT/AC means air cooled from the post-weld heat treatment temperature.

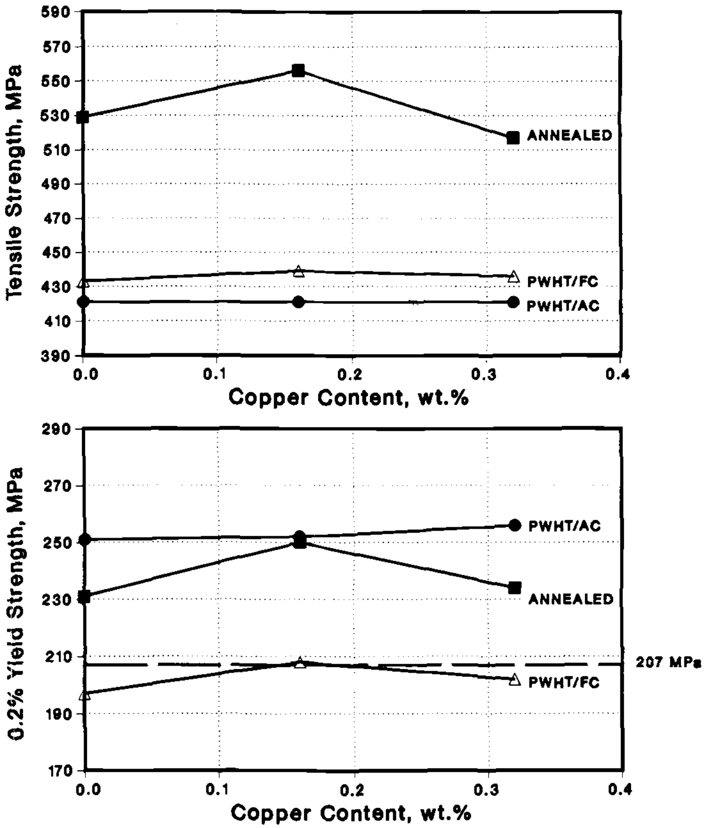

FIG. 17—*Graph of room temperature 0.2% yield and tensile strengths versus copper content for the laboratory produced 2-1/4Cr-1Mo steels.*

yielding behavior was again observed for the annealed condition and discontinuous yielding behavior was observed for the PWHT/FC and PWHT/AC conditions.

In all cases, the corresponding tensile strengths and ductilities shown in Table 7 are above the minimum levels required by the specification. As expected, the tensile ductilities (% elongation and % reduction in area) are inversely related to tensile strength.

Impact Properties—50% fracture appearance transition temperature (50% FATT) and upper shelf Charpy V-notch energy for each of the heat treatment conditions are also compared in Table 7. The PWHT/FC condition provided the best combination of 50% FATT and upper shelf energy. As expected, this condition also has the lowest yield strength level. Copper content does not appear to influence significantly 50% FATT or upper shelf energy within any of the heat treatment conditions with the exception of the PWHT/FC condition, where 50% FATT increases slightly with copper content.

Discussion

In general, the chemical analyses of the ESR and VAR steels were similar with the exceptions of the higher aluminum and nitrogen content, but lower copper content of the ESR steel. In addition, dilatometry work indicated that both the ESR and VAR steels exhibited similar Ac_1 and Ac_3 critical temperatures. However, the ESR and VAR steels had differences in yield strength levels that changed depending on heat treatment. This discussion will focus on the strengthening mechanisms responsible for these differences. The specific focus will be the role of copper in these mechanisms.

Yielding Behavior

The shape of the load-elongation curve (stress-strain curve) plays a role in defining yield strength. In the ESR and VAR steels, the yielding behavior is either continuous or discontinuous depending on heat treatment. The bainite is responsible for the continuous yielding behavior shown in Fig. 7 for the annealed condition. The freshly formed bainite provides the source of dislocations for continuous yielding. The other curves representing the two PWHT conditions display discontinuous yielding because the bainite is tempered during the PWHT at 710°C for 40 h. Thus for the PWHT condition, yielding is controlled by the nucleation and growth of Luders bands during tensile testing. Interstitial carbon and nitrogen play an important role in this discontinuous yielding process. There may be differences in the carbon and nitrogen interstitial levels in the two PWHT conditions that explain the different shapes in the tensile curves. Although the yielding behavior changes from continuous to discontinuous, it does so in both the ESR and VAR steels, and is not thought to be responsible for the yield strength difference between the two steels.

Differences in Strength Levels with Heat Treatment

Annealed Condition—Both the ESR and VAR steels passed the 207 MPa minimum yield strength requirement with respective values of 224 and 231 MPa. These steels displayed similar average ferrite grain sizes and carbide microstructures. Precipitation strengthening by copper particles is considered to be insignificant since the copper particles that reside on the ferrite grain boundaries are not effective for precipitation strengthening and there are too few copper particles in the matrix for significant precipitation strengthening. Grain boundary precipitation of copper is expected since the annealed steels went through the austenite to ferrite transformation (the PWHT steels did not). Since the solubility of copper in ferrite is far less than in austenite, the copper is presumably rejected to the ferrite grain boundaries (the last place to transform). The 7 MPa difference in yield strength between the two steels can, however, be attributed to solid-solution strengthening with the higher copper level in the VAR steel. This difference is real as seen earlier (Fig. 4) in the distribution of strength for the ESR and VAR steels. For example, if one calculates the solid-solution strengthening increment (ΔYield Strength) between the ESR and VAR steels using the 38-70 MPa per %copper relationships for air cooled iron-copper alloys [*45–49*] and assumes that all of the copper is in solution, one obtains values of 3-6 MPa. If we were to use our laboratory data for the annealed condition (Fig. 17), the solid-solution strengthening increment is higher than that shown above. The slope of the line for the annealed 2-1/4Cr-1Mo steel is 125 MPa per %copper. This slope implies that the yield strength increment between ESR and VAR is 10 MPa, which is higher but of the same order of magnitude of that predicted by others.

PWHT/FC Condition—In the PWHT/FC condition, although both the ESR and VAR steels possessed similar carbide microstructures, the ESR steel failed and the VAR steel passed the yield strength requirement with respective values of 200 and 219 MPa. In this condition, the additional 3% tempered bainite is considered insignificant to account for the difference in yield strength between the two steels. This assumption is supported by the laboratory produced steel with 0% copper that failed the yield strength requirement with 27% tempered bainite in the microstructure.

The main contributor to the difference in PWHT/FC yield strength between the ESR and VAR steels is the difference in copper levels. Upon heating to the PWHT temperature, copper dissolves in the ferrite matrix. This is illustrated in Fig. 18, which is the same enlarged portion of the iron-copper binary phase diagram shown in Fig. 6 but with the ESR and VAR compositions superimposed. Other alloying elements such as those in the 2-1/4Cr-1Mo grade affect the location of the solvus. For example, it is known that carbon and chromium reduce the solubility of copper in iron [*67*]. Thus for this system the solvus moves toward the left in Fig. 18. However, for illustration purposes we will use the binary iron-copper diagram. During furnace cooling of both steels there is ample time for copper to precipitate from the ferrite. Because there is more copper in the VAR steel compared to the ESR steel (0.13 versus 0.046%), the VAR steel has more precipitated particles. One can use the Ashby-Orowan equation [*68*] to calculate the increment in strengthening due to precipitates

$$\Delta\text{yield strength (MPa)} = \frac{5900\sqrt{f}}{d} \times \ln\,[4d] \qquad (1)$$

where

f = volume fraction of precipitated copper and
d = diameter of copper precipitates, nm.

This equation assumes that the particles are hard and incoherent. Our assumption that the 5- to 50-nm copper particles are incoherent is consistent with the field ion microscopy results on a iron-copper alloy of Goodman et al. [*69*], who found that particles above 5 nm in diameter were

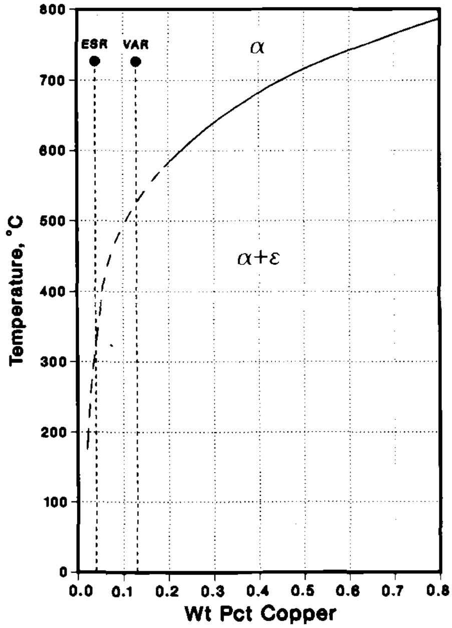

FIG. 18—*Enlarged portion of the iron-copper binary phase diagram with the ESR and VAR compositions superimposed.*

incoherent. The volume fractions used in equation 1 were 0.0011 for the VAR steel and 0.00045 for the ESR steel based on the atomic weight of copper.

At the low end of the distribution, that is, 5 nm, Eq 1 predicts yield strength increments of 75 and 117 MPa, respectively, for the ESR and VAR steels due to the precipitation of copper. At the high end of the distribution, that is, 50-nm particles, Eq 1 predicts yield strength increments of 13 and 20 MPa, respectively, for the ESR and VAR steels due to the precipitation of copper. Therefore, a difference of 7 to 42 MPa can be attributed to the different copper levels in the two steels. This strengthening increment range coincides with the actual 19 MPa difference in yield strength observed between the ESR and VAR steels.

Thus it appears that one way to meet the specified minimum yield strength in the PWHT/FC condition would have been to intentionally add copper to the steel, possibly as much as 0.20%. In fact, work by General Electric [*11-13,20,23*] confirms this contention. For example, Offer, Krankota, and Ring [*11*] present data that show that low copper (0.04%) 2-1/4Cr-1Mo steel produced by either ESR or VAR methods fails to meet the yield strength requirement in the PWHT/FC condition. In contrast, work of Offer and Ring [*12*] and the data from the VAR tubesheet forgings, both of which contain data for higher copper (0.08-0.15%) 2-1/4Cr-1Mo steels, show that the yield strength in the PWHT/FC condition can be met. As was pointed out earlier, copper was not intentionally added to any of the tubesheet forging ingots. This is a case where the use of special scrap selection practices to control copper adversely affected the ESR steel's ability to develop the required mechanical properties after the specified PWHT/FC heat treatment.

PWHT/AC Condition—In the PWHT/AC condition, the ESR and VAR steels displayed similar yield strengths (262 versus 257 MPa). During air cooling from the PWHT, which is about 50 times faster than furnace cooling, all of the copper is retained in solid solution in the ferrite. Based on the data from the laboratory produced steels shown in Fig. 17, copper appears to have a small solid-solution strengthening effect in this condition (16 MPa/%copper).

However, the question still remains as to why the PWHT/AC condition has higher strength than the PWHT/FC condition. This same effect has been observed by others [*70-72*]. For example, in the ESR steel, which has very little copper (0.046%), strengthening mechanisms other than those relating to copper must be responsible for the differences in yield strength between the PWHT/AC and PWHT/FC conditions. The difference in strength can be explained on the basis of three strengthening mechanisms: (1) solid-solution strengthening due to interstitial carbon and nitrogen, (2) solid-solution strengthening due to substitutional molybdenum and chromium, and (3) precipitation strengthening due to fine needlelike M_2X carbides. Much more work is required to establish the magnitude for each of these strengthening mechanisms, which is outside the scope of our discussion on the influence of residual copper in 2-1/4Cr-1Mo steel. Nevertheless, supporting evidence for the proposed strengthening mechanisms is presented below.

1. Interstitial carbon and nitrogen—Wada and Biss [*70*] suggest that M_2X carbides might dissolve during PWHT and upon air cooling from the PWHT temperature some of the dissolved carbon and nitrogen is trapped in solution, thus contributing to solid-solution strengthening. This is consistent with our results where the more pronounced yield point, attributed to the greater interstitial content, was observed for the steels in the PWHT/AC condition. In the PWHT/FC condition, the M_2X carbides dissolve during PWHT, but reprecipitate during furnace cooling, rendering much of the interstitial carbon and nitrogen ineffective for solid-solution strengthening.

2. *Substitutional molybdenum and chromium*—Our AEM results showed that the molybdenum/chromium ratios of the predominant M_2X carbides in the PWHT/AC and PWHT/FC samples were 2.1 and 3.3, respectively. Assuming a constant volume fraction of carbides in both

conditions, the steels in the PWHT/AC condition are expected to have more molybdenum and less chromium available for solid-solution strengthening. Since molybdenum and chromium have positive (14 MPa/%) and negative (−31 MPa/%) influences on solid-solution strengthening, respectively [*47*], these elements also partially account for the strengthening increment between the PWHT/AC and PWHT/FC conditions.

3. M_2X Carbides—The effect of carbide strengthening is well known [*73*]. In 2-1/4Cr-1Mo steel, the needlelike M_2X type 1 carbides have the greatest effect on strengthening because of their small thickness, around 10 nm. The PWHT/AC condition having a higher volume fraction of M_2X Type 1 carbides than the PWHT/FC condition (see Figs. 12 and 16), would be expected to have a higher strength level.

Therefore, by increasing the cooling rate from the PWHT temperature, the yield strength of 2-1/4Cr-1Mo tubesheet steel can be substantially improved. Our data alone indicates a 38 MPa improvement in the VAR steel and a 62 MPa improvement in the ESR steel. Much of the development work on the Clinch River breeder reactor tubesheet forgings was performed on material that had been cooled at a faster rate than the specified 56°C/h maximum from the PWHT temperature [*8,11,12,19,23*], thus producing yield strength results that are higher than can be achieved under the constraints of the specification.

Conclusions

The key results of this paper on the influence of residual copper in annealed and postweld heat treated 2-1/4Cr-1Mo steel can be summarized as follows:

- The main difference between the ESR and VAR steels was their residual copper content. This difference in copper content (0.046 and 0.13%) allowed the VAR tubesheet forgings to pass the specified minimum yield strength requirement in the PWHT/FC condition while the ESR tubesheet forgings marginally failed this same requirement. The strengthening increment between the two steels is attributed to precipitation strengthening due to ϵ-copper.
- The difference in yield strength between the ESR and VAR steels in the annealed condition is attributed to solid-solution strengthening due to copper.
- In both the PWHT/FC and annealed cases, the strengthening increments were confirmed using laboratory produced and heat treated 2-1/4Cr-1Mo steels. In addition, the behavior of copper in both of these conditions was found to be consistent with the most recent iron-copper phase equilibria data.
- Yield strength was found to increase by 38 to 62 MPa by increasing the cooling rate from the PWHT from 56 to 3000°C/h. This strengthening increment is attributed to solid-solution strengthening due to carbon, nitrogen, molybdenum, and chromium and precipitation strengthening due to fine needlelike M_2X carbides.

Summary

The data presented in this paper provides an example of where residual copper affected the ability of 2-1/4Cr-1Mo steel to meet the required mechanical properties. Furthermore, much of the data base used to establish the mechanical property capabilities of both annealed and PWHT/FC 2-1/4Cr-1Mo steel for the Clinch River breeder reactor project was developed using steels that had relatively high copper levels (or were not analyzed for copper) and were air cooled from the PWHT, thus producing a data base of yield strength values that are higher than can be achieved under the constraints of the specification.

Acknowledgments

The authors would like to thank the Bethlehem Steel Corporation and its BethForge Division for permission to publish this paper. Special thanks goes to K. A. Taylor for his technical input and his help in calculating the solvus curve for the iron-copper phase diagram. In addition, the authors would like to thank S. S. Hansen for his many helpful discussions, J. R. Michael for his technical input and conducting a portion of the electron microscopy, S. Mehta for conducting the balance of the electron microscopy, L. L. Hahn and L. R. Salvage for preparing the electron microscopy specimens, R. E. Steigerwalt for rolling the laboratory steels and expediting the testing, and R. A. Sauers for conducting many of the heat treatments.

References

[*1*] Licina, G. J. and Copeland, J. F., "A Review of 2-1/4Cr-1Mo Steel for Steam Generator Applications in the Clinch River Breeder Reactor," General Electric Report GEAP-20589, UC-79a, San Jose, CA, Oct. 1974.

[*2*] Klueh, R. L., "The Effect of Carbon on 2-1/4Cr-1Mo Steel (I): Microstructure and Tensile Properties," *Journal of Nuclear Materials*. Vol. 54, 1974, pp. 41–54.

[*3*] Leitnaker, J. M., Klueh, R. L., and Laing, W. R., "The Composition of Eta Carbide Phase in 2-1/4Cr-1Mo Steel," *Metallurgical Transactions*, Vol. 6A, October 1975, pp. 1949–1955.

[*4*] Klueh, R. L. and Leitnaker, J. M., "An Analysis of the Decarburization and Aging Processes in 2-1/4Cr-1Mo Steel," *Metallurgical Transactions*, Vol. 6A, November 1975, pp. 2089–2093.

[*5*] Shields, J. A. and Longua, K. J., "The Effects of Ten Years Experimental Breeder Reactor II Service on 2-1/4Cr-1Mo," *Nuclear Technology*, Vol. 28, March 1976, pp. 471–481.

[*6*] Klueh, R. L. and Canonico, D. A., "Microstructure and Tensile Properties of 2-1/4Cr-1Mo Steel Weldments with Varying Carbon Contents," *Welding Journal Research Supplement*, Vol. 55, September 1976, pp. 253s-259s.

[*7*] Klueh, R. L. and Oakes, R. E. Jr., "High Strain Rate Tensile Properties of Annealed 2-1/4Cr-1Mo Steel," *Trans ASME, Journal of Engineering Materials and Technology*, Vol. 98, October 1976, pp. 361-368.

[*8*] Fetterolf, F. P. and Hurtt, J. H., "An Evaluation of the Material Capabilities of Low Carbon 2-1/4Cr-1Mo Steel Forgings," *Transactions of ASME, Journal of Pressure Vessel Technology*, Vol. 98, November 1976, pp. 316–322.

[*9*] Klueh, R. L., "Creep and Rupture Behavior of Annealed 2-1/4Cr-1Mo Steel," ORNL Report 5219, Oak Ridge, TN, December 1976.

[*10*] Klueh, R. L., "Heat Treatment Effects on the Tensile Properties of Annealed 2-1/4Cr-1Mo," *Journal of Nuclear Materials*, Vol. 68, 1977, pp. 294-307.

[*11*] Offer, H. P., Krankota, J. L., and Ring, P. J., "Properties of Remelted 2-1/4Cr-1Mo Steel for Nuclear Steam Generators," in *Ferritic Steels for Fast Reactor Steam Generators*, British Nuclear Energy Society, Thomas Telford Ltd., London, 1978, pp. 24.1–24.5.

[*12*] Offer, H. P. and Ring, P. J., "An Evaluation of Vacuum Arc Remelted Tubesheet Forging Properties for CRBRP Steam Generators," General Electric Report GEFR-00245(L), San Jose, CA, Sept. 1977.

[*13*] Offer, H. P., et al., "The Effects of Remelting and Heat Treatment on 2-1/4Cr-1Mo Steel Elevated Temperature Tensile Properties," in *Effects of Melting and Processing Variables on the Mechanical Properties of Steel*, G. V. Smith, Ed., ASME Winter Annual Meeting, Atlanta, November 1977, pp. 195–220.

[*14*] Klueh, R. L., "Thermal Aging Effects on the Mechanical Properties of Annealed 2-1/4Cr-1Mo," ORNL Report 5324, Oak Ridge, TN, November 1977.

[*15*] Klueh, R. L. and Griffith, J. L., "Mechanical Properties of Tubesheet Forgings for LMFBR Steam Generators," ORNL Report 5378, Oak Ridge, TN, April 1978.

[*16*] Klueh, R. L., "Interaction Solid-Solution Hardening in 2-1/4Cr-1Mo Steel," *Materials Science and Engineering*, Vol. 35, 1978, pp. 239-253.

[*17*] Offer, H. P., Roit, W. J., and Ring, P. J., "LMFBR Steam Generator Tube/Tubesheet Weld Evaluation," General Electric Report GEFR-00472 Rev 1, UC-79H, K, August 1979.

[*18*] Offer, H. P. and Ring, P. J., "Failure Susceptibility of Tube to Tubesheet Welds," General Electric Report GEFR-00539, UC-79H, K, San Jose, CA, Sept. 1980.

[*19*] Klueh, R. L., "Thermal Aging Behavior of 2-1/4Cr-1Mo Steel," ORNL Report 5686, Oak Ridge, TN, October 1980.

[*20*] Pizzo, P. P. and Mandurrago, G. L., "Age Softening Characteristics of Annealed 2-1/4Cr-1Mo Steel in the Temperature Range 424 to 704°C," *Transactions of ASME. Journal of Engineering Materials and Technology*, Vol. 103, January 1981, pp. 62-70.

[*21*] Klueh, R. L., "Effect of Postweld Heat Treatment on Creep and Creep Rupture Properties of 2-1/4Cr-1Mo Steel," ORNL Report 5751, Oak Ridge, TN, June 1981.

[*22*] Klueh, R. L. and Griffith, J. L., "Mechanical Properties of a 2-1/4Cr-1Mo Steel Tubesheet Forging," *Journal of Materials for Energy Systems*, Vol. 3, No. 3, December 1981, pp. 26-38.

[*23*] Ring, P. J., et al., "Some Considerations in the Specification of 2-1/4Cr-1Mo for LMFBR Service," General Electric Report GEFR-SP-263, San Jose, CA, January 1982.

[*24*] Klueh, R. L., "Heat Treatment of 2-1/4Cr-1Mo Steel for Breeder Reactor Steam Generators," *Nuclear Technology*, Vol. 57, April 1982, pp. 114-124.

[*25*] Licina, G. J. and Roy, P., "Effects of Thermal Aging and Decarburization on the Mechanical Properties of 2-1/4Cr-1Mo Steel," General Electric Report GEFR-00627, San Jose, CA, Aug. 1982.

[*26*] Patriarca, P., "The Selection of Tube-to-Tubesheet Joints for Sodium-Cooled Fast Reactors," in *Shell and Tube Heat Exchangers*, W. R. Apblett, Jr., Ed., ASM, Metals Park, OH, 1982, pp. 115-121.

[*27*] Hebbar, M. A. and Sessions, C. E., "LMFBR Steam Generator Materials Development at Westinghouse," *Journal of Engineering for Power*, Vol. 105, October 1983, pp. 719-725.

[*28*] Challenger, K. D. and Vining, P. G., "The Effects of Hold Period on the Fatigue Crack Growth Rate of 2-1/4Cr-1Mo Steel at Elevated Temperatures," *Trans. ASME, Journal of Engineering Materials and Technology*, Vol. 105, October 1983, pp. 280-285.

[*29*] Klueh, R. L., "Heat-to-Heat Variations in Creep-Rupture Properties of Annealed 2-1/4Cr-1Mo Steel," *Transactions of ASME, Journal of Pressure Vessel Technology*, Vol. 105, November 1983, pp. 320-328.

[*30*] Viri, D. P. and Iceland, W. F., "Clinch River Modular Steam Generator Tube-to-Tubesheet and Shell Closure Welding," *Welding Journal*, Vol. 63, July 1984, pp. 18-21.

[*31*] Klueh, R. L., "Creep-Rupture Strength of Annealed 2-1/4Cr-1Mo Steel," *Scripta Metallurgical*, Vol. 19, 1985, pp. 789-793.

[*32*] Bodnar, R. L. and Cappellini, R. F., "Effects of Residual Elements in Heavy Forgings—Past, Present and Future," *MiCon 86: Optimization of Processing, Properties, and Service Performance Through Microstructural Control. ASTM STP 979*, 1988, pp. 47-82.

[*33*] Kubaschewski, C., *Iron-Binary Phase Diagram*. Springer-Verlog, New York, 1982, p. 35.

[*34*] Speich, G. R., Gula, J. A., and Fisher, R. M., "Diffusivity and Solubility Limit of Copper in Alpha and Gamma Iron," in *The Electron Microprobe*, T. D. McKinley, K. F. J. Heinrich, and D. B. Witty, Eds., Wiley, 1966, pp. 525-542.

[*35*] Wriedt, H. A. and Darken, L. S., "The Solubility of Copper in Ferrite," *Trans. AIME*, Vol. 218, 1960, pp. 30-36.

[*36*] Qureshi, A. H., "Experimentelle Untersuchungen uber magnetische Eigenschaften und die Ausscheidungskinetik von Eisen-Kupfer-Legierungen," *Zeitschriff für Metallkunde*, Vol. 52, December 1961, pp. 799-813.

[*37*] Kubaschewski, O., Smith, J. F., and Bailey, D. M., "A Thermodynamic Analysis of Phase Relationships in the Iron-Copper System," *Zitschiff für Metallkunde*, Vol. 68, 1977, pp. 495-499.

[*38*] Harvig, H., Kirchner, G., and Hillert, M., "On the Ferrite-Austenite Equilibrium in the Fe-Cu System," *Metallurgical Transactions*, Vol. 3A, January 1972, pp. 329-332.

[*39*] Irani, J. J., Dulieu, D., and Tither, G., "Role of Copper in Low Alloy Steels," in *Low Alloy Steels*, ISI Publication 114, 1968, pp. 75-89.

[*40*] Greg, J. L. and Daniloff, B. N., in *Alloys of Iron and Copper*, McGraw-Hill, Chapter VI, 1934, pp. 144-166.

[*41*] Pattanaik, S., Tromans, D., and Lund, J. A., "The Strengthening of Ferrite by an Incoherent Dispersion of Copper," *Transactions of JIM*, Vol. 9, 1968, pp. 381-387.

[*42*] Hornbogen, E. and Glenn, R. C., "A Metallographic Study of Precipitation of Copper from Alpha Iron," *Transactions of the AIME*, Vol. 218, December 1960, pp. 1064-1070.

[*43*] LeMay, I. and Krishnadev, M. R., "On the Aging of Copper-Bearing Steel," *Proceedings of ICSTIS, Supplementary Transactions of ISIJ*, Vol. 11, 1971, pp. 1005-1009.

[*44*] Krishnadev, M. R. and LeMay, I., "Microstructure and Mechanical Properties of a Commercial Low-Carbon Copper-Bearing Steel," *JISI*, Vol. 208, May 1970, pp. 458-462.

[*45*] Wada, H., Houbaert, Y., Penning, J., and Dilewijns, J., "Strengthening Effects of Copper in Steel," in *Proceedings of Copper in Steel*, Luxembourg, Vol. 23, No. 3, 1983, pp. 3.1-3.31.

[*46*] DeSy, A. L., "Optimization of Composition and Rolling Variables of Tough, Ductile and Readily Weldable Medium Strength Low Copper-Niobium Steels," *Trans. ISIJ*, Vol. 14, 1974, pp. 139-154.

[*47*] Irvine, K. J. and Pickering, F. B., "Low-Carbon Steels with Ferrite-Pearlite Structures," *JISI*, Vol. 201, 1963, pp. 944-959.

[*48*] Baird, J. D. and Preston, R. R., "Relationships Between Processing, Structure and Properties in Low

Carbon Steels," in *Processing and Properties of Low Carbon Steels*. J. M. Gray, Ed., AIME, 1973, pp. 1-46.

[*49*] *Metals Handbook, Properties and Selection: Irons and Steels*, Vol. 1, 9th Edition, ASM, Metals Park, OH, 1978, p. 162.

[*50*] *Steel Product Manual for Alloy, Carbon, and HSLA Steels: Semifinished for Forging; Hot-Rolled Bars. Cold Finished Bars, Hot-Rolled Deformed and Plain Concrete Reinforcing Bars*, AISI, August 1977, p. 7.

[*51*] Abe, T., et al., "Effect of Thermomechanical Processing on Mechanical Properties of Copper Bearing Age Hardenable Steel Plates," *Transactions of ISIJ*, Vol. 27, 1987, pp. 478-484.

[*52*] Grange, R. A., Lambert, V. E., and Harrington, J. J., "Effect of Copper on the Heat Treating Characteristics of Medium-Carbon Steel," *Transactions of ASM*, Vol. 51, 1959, pp. 377-393.

[*53*] Pursian, G., Zeise, F., and Weber, K. H., "Hot Shortness Behavior of Forging Ingots on the Commencement of Forging, Caused by Copper and Other Tramp Elements," *Neue Hutte*, Vol. 21, July 1976, pp. 394-397, Henry Brutcher translation 9861.

[*54*] Melford, M. A., "Surface Hot Shortness in Mild Steel," *JISI*, April 1962, pp. 290-299.

[*55*] Nicholson, A. and Murray, J. D., "Surface Hot Shortness in Low-Carbon Steel," *JISI*, October 1965, pp. 1007-1018.

[*56*] Melford, D. A., "Influence of Antimony and Arsenic on Surface Hot Shortness in Copper-Containing Mild Steels," *JISI*, May 1966, pp. 495-496.

[*57*] Okada, H., et al., "Copper-Containing Structural Steels," in *Copper in Iron and Steel*, I. LeMay and L. M. Schetky, Eds., Wiley, New York, 1982, pp. 83-133.

[*58*] Hawthorne, J. R., "Demonstration of Improved Radiation Embrittlement Resistance of A533B Steel Through Control of Selected Residual Elements," in *Irradiation Effects on Structural Alloys for Nuclear Reactor Applications, ASTM STP 484*, ASTM, 1970, pp. 96-127.

[*59*] Ito, Y. and Nakanishi, M., "Study of Stress Relief Cracking in Welded Low Alloy Steels," *Sumitomo Search*, No. 7, May 1972, pp. 27-36.

[*60*] Lundin, C. D. and Menon, R., "Postweld Heat Treatment Cracking in HSLA Steels," presented at the 68th Annual AWS Convention, Chicago, March 1987.

[*61*] Jackson, W. J. and Southall, D. M., "Effect of Copper and Tin in Residual Amounts on the Mechanical Properties of 1.5Mn-Mo Cast Steel," *Metals Technology*, Vol. 5, November 1978, pp. 381-390.

[*62*] King, B. L., "Intergranular Embrittlement in CrMoV Steels: An Assessment of the Effects of Residual Impurity Elements on High Temperature Ductility and Crack Growth," *Phil. Trans. R. Soc. Lond.*, Vol. A295, 1980, pp. 235-251.

[*63*] Seah, M. P., "Impurities, Segregation and Creep Embrittlement," *Phil. Trans. R. Soc. Lond.*, Vol. A295, 1980, pp. 265-278.

[*64*] Hasegawa, M., et al., "Effects of Copper and Phosphorus on Temper Embrittlement on Mn-Mo-Ni Low Alloy Steel (ASTM A533-B)," *Trans. JIM*, Vol. 16, 1975, pp. 641-646.

[*65*] Hornbogen, E., "Aging and Plastic Deformation of an Fe-0.9%Cu Alloy," *Transactions of ASM*, Vol. 57, 1964, pp. 120-132.

[*66*] Bush, G. W. and Lindsay, R. W., "Tensile Properties of Copper-Bearing Low Carbon Steel," *Transactions of ASM*, Vol. 52, 1960, pp. 422-433.

[*67*] LeMay, I. and Krishnadev, M. R., in *Copper in Iron and Steel*, I. LeMay and L. M. Schetky, Eds., Wiley, Chapter 2, 1982, pp. 5-43.

[*68*] Gladman, T., Dulieu, D., and McIvor, I., "Structure-Property Relationships in High-Strength Microalloyed Steels," in *Micro Alloying 75 Proceedings*, Union Carbide, New York, 1977, pp. 32-54.

[*69*] Goodman, S. R., Brenner, S. S., and Low, J. R., Jr., "An FIM—Atom Probe Study of the Precipitation of Copper from Iron—1.4 At. Pct. Copper. Part II: Atom Probe Analyses," *Metallurgical Transactions*, Vol. 4, Oct. 1973, pp. 2371-2378.

[*70*] Wada, T. and Biss, V. A., "Restoration of Elevated Temperature Tensile Strength in 2-1/4Cr-1Mo Steel," *Metall. Trans.*, Vol. 14A, May 1983, pp. 845-855.

[*71*] Sato, K., Okubo, Y., and Watanabe, T., "Deterioration of 2-1/4Cr-1Mo Steel after Long-term Service at Elevated Temperature (Part 2)," *Journal of Japan Petroleum Institute*, Vol. 22, No. 1, 1979, pp. 21-31.

[*72*] Watanabe, T. and Sato, K., "Mechanical Properties of CrMo Steels After Elevated Temperature Service," IIW Document IX-1116-79-WG, 1979, pp. 1-13.

[*73*] Pickering, F. B., "Precipitation Processes During the Tempering of Martensitic Alloy Steels," in *Precipitation Process in Steel*, Special Report No. 64, The Iron and Steel Institute, London, 1959, pp. 23-43.

DISCUSSION

G. S. Hartman[1] *(discussion question)*—What were the nitrogen levels in the two production tubesheet forgings?

R. L. Bodnar (author's response)—The nitrogen levels were as shown in Table 1.

In the annealed and PWHT/FC conditions, the nitrogen is tied up as AlN or M_2X (<5 ppm mobile nitrogen were detected). As we discussed in the paper, some of the M_2X carbonitrides dissolve at the PWHT temperature of 727°C, and some of the carbon and nitrogen are trapped interstitially upon air cooling (PWHT/AC). As a result, there is probably more interstitial nitrogen for solid-solution strengthening in the ESR steel in the PWHT/AC condition due to its higher total nitrogen content. This may be the reason for the slightly higher yield strength of the ESR steel compared to the VAR steel in the PWHT/AC condition.

TABLE 1—*Nitrogen levels in production tubesheet forgings.*

Steel	Total N
ESR	120 ppm
VAR	60 ppm

G. S. Hartman (discussion question)—Why did the VAR steel have a slightly coarser ferrite grain size and more bainite compared to the ESR steel?

R. L. Bodnar (author's response)—This is presumably due to the slightly coarser austenite grain size of the VAR. The austenite grain size is controlled by the precipitation of AlN. Since the VAR steel has less total aluminum than the ESR steel (0.004 vs. 0.009%), the VAR steel is expected to have less AlN precipitates, which are less effective for the pinning of austenite grain boundaries. The slightly coarser austenite grain size of the VAR steel enhances hardenability (more bainite) and is responsible for the slightly coarser ferrite grain size of the VAR steel (36 μm versus 24 μm).

G. S. Hartman (discussion question)—Did you attempt to coarsen the austenite grain size of the ESR steel to enhance hardenability, which would hopefully result in a higher yield strength in the PWHT/FC condition?

R. L. Bodnar (author's response)—Yes, although this work is not included in our paper since it is not consistent with our general theme of residual copper in steel. We have found that the yield strength requirement can be met with the ESR steel if it is step-annealed at 1120°C, cooled to 940°C and annealed according to specification. At 1120°C, the AlN precipitates dissolve and the austenite grains can coarsen. Upon cooling from the 940°C annealing temperature at a maximum cooling rate of 56°C/h, up to 48% bainite can form. This additional bainite in the microstructure raises the yield strength to approximately 242 MPa in the PWHT/FC condition. Unfortunately, such a heat treatment was not allowed by the specification.

---

[1] A. Finkl and Sons Company, 2011 Southport Ave., Chicago, IL 60614.

Robert J. Christoffel[1] *and Alan J. Silvia*[2]

Embrittlement of a Copper Containing Weld Metal

REFERENCE: Christoffel, R. J. and Silvia, A. J., **"Embrittlement of a Copper Containing Weld Metal,"** *Residual and Unspecified Elements in Steel, ASTM STP 1042,* A. S. Melilli and E. G. Nisbett, Eds., American Society for Testing and Materials, Philadelphia, 1989, pp. 232-242.

ABSTRACT: Elevated temperature isothermal exposure of a "weathering" steel weld containing approximately 0.5% copper, in the as-welded condition, embrittled the weld as characterized by an increase in strength and a decrease in toughness and tensile ductility. A similar embrittlement was not encountered for material exposed in the postweld stress relieved condition. The embrittlement was attributed to the precipitation of an iron-copper intermetallic compound. Control of copper content below the solubility limit or the use of a postweld stress relief heat treatment should prevent the occurrence of any significant embrittlement.

KEY WORDS: weld metal, weathering steel, copper content, embrittlement, elevated temperature exposure, tensile strength, notch toughness, postweld heat treatment, precipitation hardening

Copper is present in most carbon and low alloy steels, generally as a residual element, but in some cases it is intentionally added to provide corrosion or oxidation resistance.[3] In most cases the copper is innocuous and, in some cases, even beneficial. However, studies have shown that when copper containing low alloy steels are used at elevated temperatures, the possibility exists for an embrittling reaction to occur [*1-3*].

Welds contain copper levels similiar to those in the base metal and hence should also be susceptible to embrittlement if used for elevated temperature service. In fact, welds could have a greater potential for embrittlement because they are generally put in service in a less structurally stable condition than are base metals. The weld metal, when produced, experiences a very rapid cooling rate from the austenite region. The weld metal then may be used in this condition, that is, the as-welded condition, or after receiving only a sub-critical stress relief heat treatment. Shackleton [*4*] has shown that welds containing 1% to about 1.5% copper do in fact embrittle when exposed to elevated temperatures.

This relatively high copper content is probably the exception, but a significant usage does exist with copper in the range of 0.5%, which is not significantly above the solubility limit of copper in iron of 0.3%. The sources of this copper are residual levels in the steel, copper coating applied to the welding electrode to prevent rusting, and that intentionally added to provide

---

[1] Senior engineer, Materials and Processes Engineering, Turbine Technology Department, General Electric Company, Schenectady, NY 12309.

[2] Senior engineer, Northeast Utilities, Meriden. CT. At the time this work was performed, he was welding engineer, Materials and Processes Laboratory, General Electric Company, Schenectady, NY 12309.

[3] When this paper was written, the authors included information and expressed opinions believed to be correct and reliable. Because of the constant advance of technical knowledge, the widely differing conditions of possible specific application, and the possibility of misapplication, any application of the contents of this paper must be at the sole discretion and responsibility of the user. The observations and conclusions drawn are considered appropriate for the exposure conditions tested. However, it is cautioned that other exposure conditions may produce other embrittlement phenomena, even in the stress relieved condition.

"weathering" qualities. Therefore, determining if carbon and low alloy steels at this copper level are susceptible to embrittlement if used at elevated temperatures is considered important. The evaluation of the embrittling tendencies of low alloy steel weld metal containing approximately 0.5% copper when exposed to elevated temperatures is the subject of this paper.

Procedure

To obtain test material, two welds were deposited by the submerged arc process using nominally "weathering" materials for both the base metal and the electrode. The base metal, which was 1¼ in. thick, was SA 516 Gr 70 plus copper material, and the electrode was American Welding Society (AWS) EW classification. The details of the welding procedure used are given in Table 1. The chemical composition of the base metal, the electrode, and the resultant weld metal are given in Table 2. On completion of welding, one weldment was left in the as-welded condition, and the other was given a postweld heat treatment of 8 h at 1100°F (593°C) with a heating and cooling rate of 100°F (55°C)/h. Both welds were radiographed and found to have acceptable quality.

Each plate was then sectioned into segments, and each segment was used for one test condition that represented a specific thermal exposure. The test conditions evaluated were:

(1) Initial condition,
(2) 3000 h exposure at 329°C (625°F),
(3) 10 000 h exposure at 329°C (625°F),
(4) 10 000 h exposure at 329°C (625°F) plus a de-embrittling heat treatment,
(5) 3000 h exposure at 371°C (700°F),
(6) 10 000 h exposure at 371°C (700°F), and
(7) 10 000 h exposure at 371°C (700°F) plus a de-embrittling heat treatment.

The de-embrittling heat treatment was intended to identify any reversible embrittlement and consisted of 1 h at 1100°F followed by a water quench.

The effects of the thermal treatments were measured with respect to the weld metal tensile and impact properties. Two longitudinal all weld metal tensile specimens and ten cross weld Charpy V-notch specimens were removed from material exposed to each condition. The orientation of the test specimens is shown in Fig. 1.

One tensile specimen was tested at room temperature and the other was tested at 316°C (600°F). For consistency, the specimen removed from the top of the weld was tested at room

TABLE 1—*Welding procedure details.*

Base metal	SA516 Gr 70 + Cu
Base metal thickness	31 mm (1¼ in.)
Joint design	Vee groove (60° included-12 mm root)
Electrode	AWS A5.23 Class EW
Electrode diameter	2.38 mm (3/32 in.)
Flux	AWS A5.23 Class F8A/P-EW-W (L-860)
Process	Submerged Arc
Type power	Direct Current
Polarity	Electrode Positive (Reverse)
Preheat temperature	21°C (70°F) Minimum
Interpass temperature	204°C (400°F) Maximum
Electrode extension	19 mm (¾ in.)
Current	550 to 580 A
Voltage	36 to 37 V
Travel speed	40.6 to 45.7 cm/min. (16-18 in./min)

TABLE 2—*Chemical composition of materials.*

Material	C	Mn	Si	P	S	Ni	Cr	Mo	Cu	O[a]	N[a]
				Composition (wt. %)							
Base Metal	0.240	1.14	0.28	0.012	0.013	0.14	0.18	0.04	0.27	—	—
Electrode	0.081	0.51	0.25	0.010	0.014	0.48	0.59	0.05	0.73[b]	223	156
Weld #1	0.056	1.04	0.34	0.014	0.015	0.40	0.54	0.01	0.53	710	140
Weld #2	0.047	1.01	0.33	0.013	0.015	0.047	0.48	0.05	0.54	910	145

[a] Oxygen and Nitrogen contents are in ppm.

[b] Copper content includes electrode coating; Copper content without coating = 0.43%.

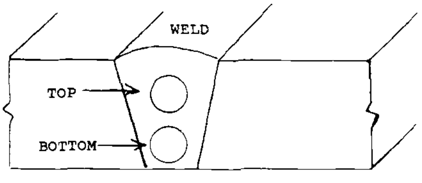

ORIENTATION & LOCATION of TENSILE SPECIMENS

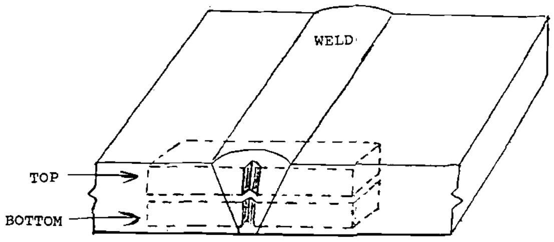

ORIENTATION & LOCATION of CHARPY SPECIMENS

FIG. 1—*Location of mechanical test specimens.*

temperature and the specimen from the bottom of the weld at 316°C (600°F). The Charpy V-notch specimens were tested at −40°C (−40°F) −12°C (+10°F), +21°C (+70°F), +38°C (+100°F), and +100°C (+212°F) with a specimen removed from the top and bottom of the weld tested at each temperature.

Results

The tensile test results are listed in Tables 3 and 4. To aid in the interpretation of these data, the tensile strength results at room temperature and at 316°C (600°F) are plotted in Figs. 2 and 3, respectively. The 0.02% yield strength results are plotted in Figs. 4 and 5.

The impact test results were averaged and plotted. From these results, average toughness values at −12°C (+10°F), +38°C (+100°F), and +100°C (+212°F) were determined as well as the 50% fracture appearance transition temperature (FATT) and the change in FATT from the initial condition. These results are listed in Table 5. To aid in the interpretation of the data, the 50% FATT results are plotted in Fig. 6 and the energy absorbed at +100°C (+212°F)

TABLE 3—*All weld metal tensile test results at room temperature.*

Condition	Tensile Strength, MPa	0.2% Yield Strength, MPa	0.02% Yield Strength, MPa	Elongation in 50.8 mm %	Reduction in Area %
		As-Welded Condition			
Initial (As-welded)	613.6	524.0	510.2	28.0	60.5
3000 h @ 329°C	677.1	601.2	589.5	24.0	58.0
10 000 h @ 329°C	706.7	631.6	622.6	25.0	58.1
10 000 h @ 329°C +De-emb.	631.6	547.4	554.3	26.0	62.7
3000 h @ 371°C	775.0	710.8	721.9	24.0	53.4
10 000 h @ 371°C	715.7	646.0	646.0	25.0	56.0
10 000 h @ 371°C +De-emb.	677.8	618.5	573.6	25.0	55.0
		Stress Relieved Condition			
Initial (Stress relieved)	577.4	496.4	468.8	32.0	65.2
3000 h @ 329°C	589.5	502.6	477.1	28.0	62.7
10 000 h @ 329°C	601.9	516.4	481.3	28.0	59.1
10 000 h @ 329°C +De-emb.	564.7	477.1	477.1	29.0	69.0
3000 h @ 371°C	587.4	497.1	484.0	31.0	68.4
10 000 h @ 371°C	617.8	523.2	523.3	31.0	64.9
10 000 h @ 371°C +De-emb.	578.5	494.4	463.3	30.0	67.8

TABLE 4—*All weld metal tensile test results at 316°C (600°F).*

Condition	Tensile Strength, MPa	0.2% Yield Strength, MPa	0.02% Yield Strength, MPa	Elongation in 50.8 mm %	Reduction in Area %
		As-Welded Condition			
Initial (as-welded)	675.7	462.6	364.7	23.0	38.6
3000 h @ 329°C	737.0	539.2	449.5	20.0	29.5
10 000 h @ 329°C	723.3	547.4	477.1	20.0	34.8
10 000 h @ 329°C +De-emb.	625.4	477.1	417.8	24.0	42.6
3000 h @ 371°C	686.7	533.7	484.7	24.0	40.3
10 000 h @ 371°C	671.5	550.2	491.6	20.0	33.4
10 000 h @ 371°C +De-emb.	604.0	456.4	379.2	26.0	50.5
		Stress Relieved Condition			
Initial (Stress relieved)	527.4	415.8	364.0	24.0	61.8
3000 h @ 329°C	533.7	407.5	337.2	24.0	49.9
10 000 h @ 329°C	522.6	398.5	350.9	24.0	56.4
10 000 h @ 329°C +De-emb.	548.8	400.6	334.4	27.0	54.1
3000 h @ 371°C	530.9	399.9	348.9	26.0	59.5
10 000 h @ 371°C	547.4	442.0	399.9	23.0	59.1
10 000 h @ 371°C +De-emb.	526.8	379.2	294.4	28.0	58.0

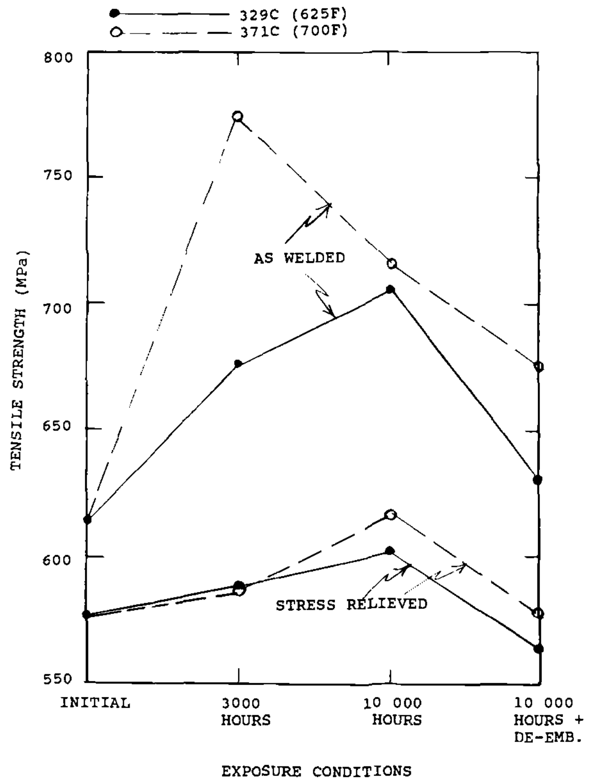

FIG. 2—*Tensile test results at room temperature.*

results are plotted in Fig. 7. The energy results at +100°C (+212°F) are considered to represent the upper shelf energy and this figure is so labeled.

Discussion

Examination of the room temperature tensile strength results for material exposed in the initial as-welded condition shows that increased exposure at 329°C (625°F) produced a continual increase in strength. Exposure for 3000 h at 371°C (700°F) produced a very significant increase in strength. Further exposure at this temperature produced a decrease in strength compared to that after 3000 h, but it was still greater than it was initially. On the other hand, material in the initial stress relieved condition had somewhat lower initial strength, and exposure at 329°C (625°F) and 371°C (700°F) produced only a slight increase in strength. Note that the de-embrittling heat treatment essentially restored the initial condition strength, except that the material exposed at 371°C (700°F) was still somewhat higher than the initial strength level.

The yield strength values paralleled those of the tensile strength, and the ductility values were generally the inverse. However, the reduction in ductility was not as significant as the increase in strength.

The phenomenon responsible for these results is a classic case of precipitation hardening. The precipitating phase is probably the iron-copper intermetallic compound. In the initial as-welded condition, the excess copper beyond the solubility limit is held in solid solution due to

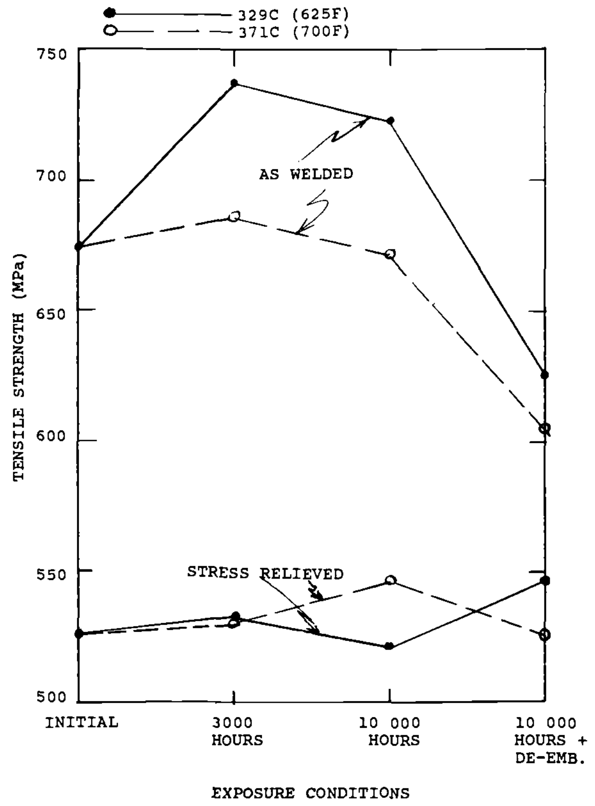

FIG. 3—*Tensile test results at 316°C (600°F).*

the fast cooling rate associated with the weld thermal cycle. Exposure at 329°C (625°F) causes the excess copper to precipitate with increasing exposure, causing increased precipitation. Exposure at 371°C (700°F) causes the maximum precipitation apparently to occur in the vicinity of 3000 h, and further exposure produces overaging with a decrease in strength. The de-embrittling heat treatment is undoubtedly a total overaging treatment reducing the strength to a relatively low level.

The postweld stress relief heat treatment was also very likely a complete overage treatment. This heat treatment could precipitate all the excess copper, so exposure at 329°C (625°F) or 371°C (700°F) would have little or no effect. Actually, some slight effect is possible as represented by the difference in solid solubility at 621°C (1150°F) compared to that at 329°C (625°F) and 371°C (700°F). This difference, of course, is very slight so the effect would be slight, which was the case.

The 316°C (600°F) tensile test results for material tested in the as-welded condition produced some interesting results. In the initial condition, the 0.02% yield strength was less at 316°C (600°F) than at room temperature, as expected. However, the tensile strength in the initial condition was greater at 316°C (600°F) than it was at room temperature. This higher tensile strength at 316°C (600°F), compared to that at room temperature, persisted for exposure at 329°C (625°F), although not for material exposed at 371°C (700°F). Also, considering just the

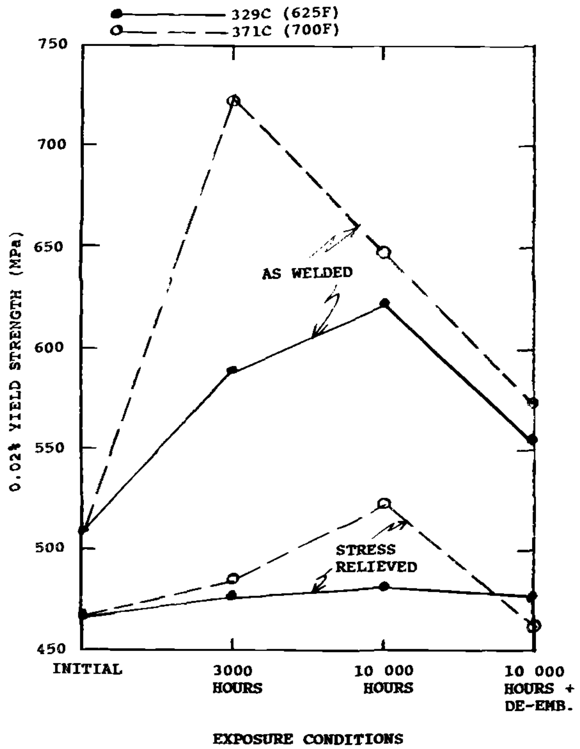

FIG. 4—*0.02% yield strength results at room temperature.*

316°C (600°F) tensile strength results, exposure at 329°C (625°F) caused an increase in strength while exposure at 371°C (700°F) had no effect on tensile strength.

Examination of the 0.02% yield strength results after exposure at 329°C (625°F) and 371°C (700°F) shows values always below those for comparable exposures and tested at room temperature. However, the 0.02% yield strength did continue to increase with increased exposure at 329°C (625°F) and 371°C (700°F) when compared to the initial condition.

This series of tests appears to exhibit the combined effect of precipitation hardening and dynamic strain hardening phenomena. The 0.02% yield strength results are as expected if influenced only by precipitation hardening. However, the significant increase in tensile strength can only be accounted for by a strain hardening effect in addition to a precipitation hardening effect. A review of the 0.2% yield strength results shows that the 316°C (600°F) results are less than those at room temperature but not as much as for the 0.02% yield strength. Thus, as plastic strain increased, the precipitation of the strengthening compound—probably the iron-copper intermetallic compound—accelerated in the elevated temperature test. The absence of any tensile strength increase on exposure at 371°C (700°F) is probably due to the fact that overaging had already occurred after exposure for 3000 h, coupled with the strain aging effect.

This strain aging effect is completely absent, as is any precipitation hardening effect, for material tested in the stress relieved condition. The precipitation and overaging produced by the stress relief heat treatment would remove any available copper from contributing to any subsequent precipitation.

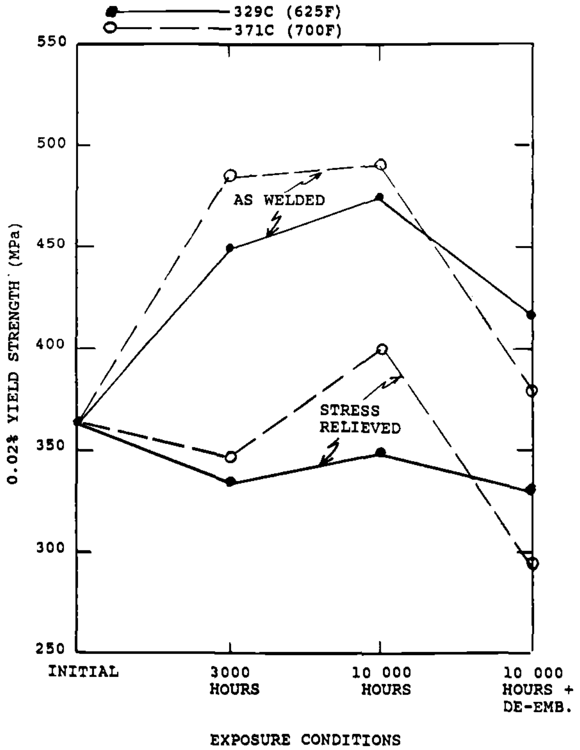

FIG. 5—*0.02% yield strength results at 316°C (600°F).*

TABLE 5—*Summary of weld metal charpy impact test results.*

	Impact Strength (Joules)			50% FATT C	Change in 50% FATT C
Condition	−12C	+38C	+100C		
	As-Welded Condition				
Initial (As-welded)	45.8	86.1	93.9	−29	—
3000 h @ 329°C	40.0	74.6	99.7	−12	+17
10 000 h @ 329°C	8.8	49.2	67.1	+27	+56
10 000 h @ 329°C +De-emb.	56.3	86.5	94.2	−40	−11
3000 h @ 371°C	16.3	44.1	53.6	+24	+53
10 000 h @ 371°C	22.4	58.3	69.2	+4	+33
10 000 h @ 371°C +De-emb.	62.4	100.1	91.5	−23	+6
	Stress Relieved Condition				
Initial (Stress relieved)	78.1	148.5	150.2	−29	—
3000 h @ 329°C	100.3	141.7	145.1	−26	+3
10 000 h @ 329°C	70.9	126.8	141.0	−29	0
10 000 h @ 329°C +De-emb.	79.7	106.4	149.2	−40	−11
3000 h @ 371°C	47.5	130.2	139.7	−12	+17
10 000 h @ 371°C	59.7	115.3	113.9	−12	+17
10 000 h @ 371°C +De-emb.	92.2	151.2	143.7	−18	+11

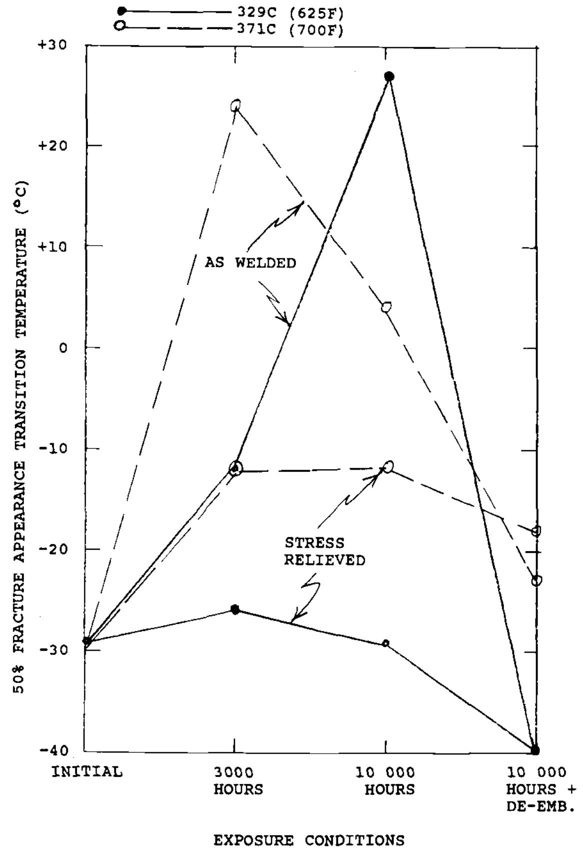

FIG. 6—*50% FATT test results.*

The results produced by the Charpy impact tests showed behavior similiar to that exhibited by the tensile tests. For material exposed in the as-welded conditions, the 50% FATT was higher than the initial value for all exposures. The increase was continuous for increasing times at 329°C (625°F) while exposure at 371°C (700°F) produced a peak after 3000 h exposure and then a reduction after 10 000 h exposure. The upper shelf energy showed the same type behavior for the material exposed in the as-welded condition, except the change was a decrease in energy. The de-embrittling heat treatment eliminated any effect produced by the isothermal exposure.

For material in the stress relieved condition and exposed at 329°C (625°F), no change in either 50% FATT or upper shelf energy occurred. Only a slight increase in 50% FATT and decrease in upper shelf energy for material exposed at 371°C (700°F) happened. Note that material initially stress relieved had the same 50% FATT as the as-welded material but a higher upper shelf energy.

A review of the overall results clearly demonstrates that welds containing approximately 0.5% copper will embrittle when exposed, in the as-welded condition, to elevated temperatures at least in the range of 329°C (625°F) to 371°C (700°F). The embrittlement is characterized by an increase in 50% FATT, a decrease in upper shelf energy, an increase in tensile and yield strength, and a decrease in tensile ductility. On the other hand, such embrittlement was not

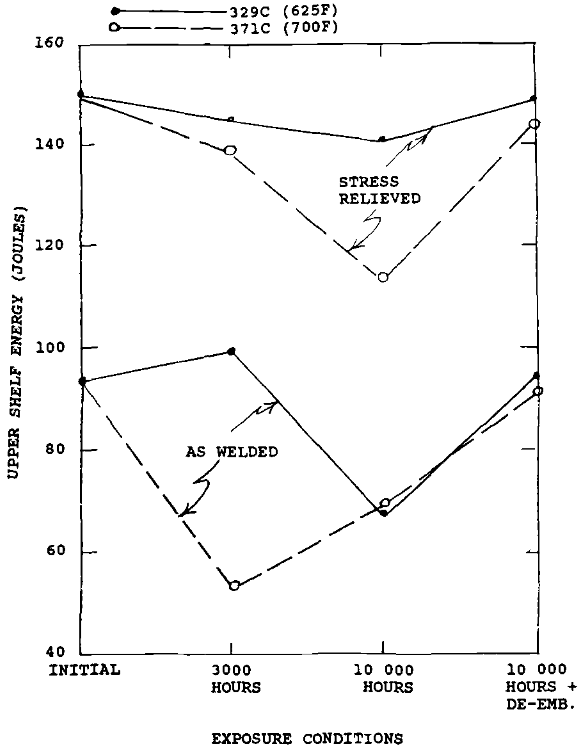

FIG. 7—*Upper shelf energy test results.*

encountered in material that had been exposed after receiving a postweld stress relief heat treatment.

Although the embrittling constituent was not specifically identified, the phenomenon observed did not appear to be classic temper embrittlement. The temper embrittlement phenomenon is characterized by an increase in 50% FATT but without the associated increase in tensile strength and decrease in upper shelf energy encountered in these results. The behavior observed may reasonably be attributed to the precipitation of an iron-copper intermetallic compound as was previously stated.

The practical implications of these results are obvious. If a carbon or low alloy steel weld is to be used at an elevated temperature, either the copper content should be controlled through specification limits to less than the solubility limit or the weld should be put in service in the stress relieved, or fully overaged condition.

Conclusions

The following conclusions can be drawn.

1. Isothermal exposure of a low alloy "weathering" steel containing approximately 0.5% copper in the as-welded condition at temperatures in the range of 329°C (625°F) to 371°C (700°F) produced an increase in tensile strength, yield strength, 50% FATT, and a decrease in upper shelf energy and tensile ductility.

2. Isothermal exposure of the same material in the postweld stress relieved condition had little or no effect on the weld metal properties.

3. The property changes observed are attributed to the precipitation of an iron-copper intermetallic compound rather than temper embrittlement.

References

[1] Smith, C. S. and Palmer, E. W., *Transactions of the American Institute of Mining and Metallurgical Engineers*, Vol. 105, 1933, p. 133.
[2] Rickett, R. L. and Leslie, W. C., *Transactions of the American Society for Metals*, Vol. 51, 1959, pp. 310-333.
[3] Grange, R. A., Lambert, V. E., and Harrington, J. J., *Transactions of the American Society for Metals*, Vol. 51, 1959, pp. 377-392.
[4] Shackleton, D., *British Welding Journal*, Vol. 14, Nov. 1967, pp. 592-597.

DISCUSSION

B. M. Kapadra[1] *(discussion question)*—Did the elevated temperature tests show serrated stress-strain behavior in view of the dynamic strain-aging effert observed?

A. J. Silva (author's response)—Yes, the elevated temperature tensile tests did show a serrated stress-strain behavior.

B. M. Kapadra (discussion question)—Would similar effects be observed also for base metal properties at these upper levels?

A. J. Silva (author's response)—Similar embrittling results should be encountered in base metals if the copper content exceeds the solubility limit and the thermal processing produces a non-equilibrium condition. Embrittlement was not noted in this investigation even in the heat affected zone in the as-welded condition, which is a nonequilibrium situation, probably because of the low copper content in the base metal.

R. L. Bodnar[2] *(written discussion)*—I would like to congratulate the authors for preparing an excellent paper. I have one comment and one question. I do not consider the loss in toughness that you observed as an embrittlement, but rather a simple strength/toughness trade-off. In my opinion, embrittlement is synonymous with intergranular failure. The question is, what microstructural evidence do you have for precipitation strengthening due to copper?

A. J. Silva (author's response)—No microstructural studies were done that would relate the precipitation strengthening to copper.

---

[1] U.S.S. Technical Center, 1000 Tech Center Drive, Monroeville, PA 15146.

[2] Bethlehem Steel Corporation, Building G, Homer Research Laboratories, Bethlehem, PA 18016.

David J. Abson[1]

The Influence of Current Supply Type and Arc Length on C-Mn, C-Mn-Ni, and C-Mn-Ti-B Shielded Metal Arc Deposit Nitrogen and Oxygen Contents

---

REFERENCE: Abson, D. J., "**The Influence of Current Supply Type and Arc Length on C-Mn, C-Mn-Ni, and C-Mn-Ti-B Shielded Metal Arc Deposit Nitrogen and Oxygen Contents,**" *Residual and Unspecified Elements in Steel, ASTM STP 1042,* A. S. Melilli, and E. G. Nisbett, Eds., American Society for Testing and Materials, Philadelphia, 1989, pp. 243-260.

ABSTRACT: Nitrogen and oxygen contents have been determined for welds simulating root and hot passes, and deposited with progressively longer arc lengths to give arc voltages in the range 18 to 28 V. Commercial basic-coated C-Mn, C-Mn-Ni, and C-Mn-Ti-B shielded metal arc electrodes were employed in the flat (1G) position with DC straight polarity (electrode negative), DC reverse polarity (electrode positive), and alternating current (AC) supplies.

In all deposits, nitrogen content increased with increasing arc length, with the C-Mn-Ti-B deposits showing the most rapid rise. The highest low voltage nitrogen levels and the most rapid increases always occurred for DC straight polarity welding, which gave >0.06% nitrogen at the highest arc voltage for each of the consumables. Deposit nitrogen content always exceeded the level in the core wire, but approached it at the lowest voltage for DC reverse polarity welds, with two of the C-Mn-Ti-B deposits showing the lowest nitrogen contents.

Deposit oxygen contents were not related to core wire levels. For DC straight polarity deposits, oxygen increased progressively over the voltage range studied. For DC reverse polarity deposits, oxygen decreased progressively for AWS E7016 type electrodes, and showed an initial decrease and a subsequent increase for AWS E7018 type electrodes. The AC deposits showed either a small increase or decrease at low arc voltages and an increase at higher arc voltages.

The findings reflect the incomplete shielding provided by the gas shield and slag layer at high arc voltages, particularly for DC straight polarity welding. They suggest that reactions involving the molten droplets emanating from the electrode tip are important in influencing deposit nitrogen content, and that those occurring in the slag layer at the surface of the weld pool are important in influencing deposit oxygen content.

KEY WORDS: carbon-manganese steels, shielded metal arc welding, process parameters, polarity, alternating current (AC), direct current (DC), voltage, weld metals, composition, oxygen, nitrogen

While general guidance can be given regarding welding procedures to give optimum mechanical properties from shielded metal arc (SMA) weld metal, limited quantitative data are available on the influence of a number of procedural variables. One aspect of welding procedure in SMA welding that can influence deposit composition and mechanical properties, but which is generally an unintentional variable, is the arc length and therefore the arc voltage. Longer arc lengths are known to give greater pick-up of oxygen and nitrogen from the atmosphere [*1-4*]. Boniszewski [*2*] also comments on the consequent lower recovery of deoxidants, such as manganese and silicon, and notes that changes in arc length caused by different weave widths and

---

[1] Principal research metallurgist, The Welding Institute, Cambridge CB1 6AL, England.

weave motions can be important. The pick-up of nitrogen during welding has been reviewed by Blake [*5*] and by Vines [*6*]; these authors also discussed the deleterious effect of nitrogen on weld toughness. Vines concluded that the shift in the Charpy curve to higher temperatures was typically ~0.5°C/1 ppm increase in total weld nitrogen. For SMA welding, the deleterious effect of nitrogen on Charpy toughness has been documented for C-Mn-Ni deposits [*3*] and on crack tip opening displacement (CTOD) for C-Mn-Ti-B deposits [*4*].

In addition to the data on current type and polarity generated for SMA welding, a considerable amount of work has been carried out on gas-shielded deposits, including work on gas-shielded [*7*] and self-shielded [*8–10*] flux-cored welds. Research in which solid wires have been employed includes studies of welds deposited in a chamber with a controlled atmosphere [*11,12*], as well as those with gas supplied from a nozzle or pipe [*7,13*]. Investigations of metal droplets that were deliberately prevented from entering the weld pool have shown that the droplets have a higher nitrogen content in DC straight polarity than in DC reverse polarity welding [*8,11,13*]; this is attributed to nitrogen ions or atoms being absorbed readily by the cathode [*8*]. For alternating current (AC) welding, the droplets were reported to have an intermediate level of nitrogen [*9,11*], although the weld nitrogen contents were found to increase in the order reverse polarity, straight polarity, and AC in Refs *9* and *11*. The deposit nitrogen content has been observed to decrease with increasing electrode diameter for solid wires [*13*], but the opposite behavior was reported for self-shielded flux-cored wires [*10*]. Deposit nitrogen content generally increases with increasing nitrogen level of the shielding gas [*11–13*] and with higher arc voltage [*12,13*], and is decreased with increasing current [*7,12,13*]. However, the relationships are not simple ones, as deposit nitrogen content depends on the nature and content of other gases present in the gas shield [*12*], on the character of the flux core [*7*], and has even been found to decrease with increasing carbon content in the welding wire [*13*].

In the light of this information, there are clearly many questions that remain unanswered in relation to SMA welding, for which the gas-shield is produced by the electrode coating. The present study was intended to determine the influence on deposit oxygen and nitrogen content of progressively increasing the arc length for reverse polarity, straight polarity, and AC deposits.

The consumables chosen for the study were all commercial basic-coated low hydrogen types employed for C-Mn steel fabrications, in view of the industrial importance of such materials, especially for offshore and allied applications. They comprised two C-Mn, one C-Mn-Ni, and three C-Mn-Ti-B electrodes. The C-Mn-Ti-B electrodes were included in the light of qualitative information supplied by at least one manufacturer of such electrodes, which showed higher levels of nitrogen in deposits produced with longer arcs [*14*].

With each consumable in turn, two weld passes were deposited in the root from one side of a double-V preparation in 25-mm-thick steel plate; the arc length was varied for the different current conditions and appropriate deposit analyses carried out.

Experimental Details

Parent Steels and Welding Electrodes

The compositions of the parent steels employed are given in Table 1. The steels are closely similar in composition, except for a difference in niobium content; however, for the present experiments, this was of no consequence, and no distinction was made between the two plates in production of the welds.

Basic-coated SMA electrodes were employed, which were all 4 mm (5/32 in.) diameter. Two C-Mn electrodes, coded P and Q, one C-Mn-Ni electrode, coded R, and three C-Mn-Ti-B electrodes, coded S, T, and U, were selected. The AWS classification and the recommended current supply type for all electrodes are given in Table 2.

TABLE 1—*Chemical analysis (wt%) of the pair of 25-mm-thick experimental steels.*

Plate Code Number	C	S	P	Si	Mn	Ni	Cr	Mo	V	Cu	Cb	Ti	Al	N	O	IIW CE	P_{cm}
195	0.15	0.012	0.009	0.29	1.45	0.04	<0.01	0.01	0.09	0.04	<0.005	<0.01	0.047	0.011	0.006	0.42	0.245
197	0.14	0.010	0.008	0.26	1.46	0.03	<0.01	0.01	0.10	0.03	0.060	0.01	0.032	0.012	0.019	0.41	0.234

TABLE 2—*Details of the consumables employed.*

Electrode Code	AWS A5.1 or A5.5 Classification	Recommended Type of Current Supply	Current, A	Arc Energy, kJ/mm
P	E7016-G	AC or DC straight polarity[a]	~145	~1.7
Q	E7016-1	AC or DC straight polarity	~145	~1.7
R	E7018-G	AC or DC reverse polarity	~145	~1.7
S	E7016-G	AC	~130	~1.7
T	E7018-G	DC reverse polarity[a]	~130	~1.7
U	E7018-1	DC	~130	~1.7

NOTE: Arc voltage values were as follows: short arc, and aim values of 22, 24, and 26 V.
[a] Straight polarity recommended for root pass.

Analyses of remelted samples of the electrode core wires, obtained on a direct-reading optical emission vacuum spectrometer (ARL Quantovac 34000), are given in Table 3. The main differences in chemical composition are the higher carbon levels in S, T, and particularly in U, the presence of trace levels of aluminum in Q and U, and the lower sulfur, nitrogen, and oxygen of the latter; electrode P had the highest nitrogen content (0.008%) and an intermediate level of oxygen (0.018%).

The principal analysis of the coatings was achieved by fusing 1 g of sample with 2 g of lanthanum oxide and 9 g of lithium tetraborate at 1200°C, and analyzing the resulting bead by X-ray fluorescence. The fluorine content was determined by pyrohydrolysis; carbon dioxide was determined by a combustion infrared method. The coating analyses (Table 4) confirm the presence of nickel in electrode R and of iron powder in electrodes, R, T, and U, and reveal the substantially higher carbonate content of electrodes P, S, and T. Differences in aluminum and magnesium suggest that there may have been differences in the metallic deoxidants employed. In addition, the presence of barium in electrodes S and T constitutes a potential health hazard, requiring careful attention to fume extraction and the collection and safe disposal of both fume and slag. An experimental technique has not been devised to measure the B, which is present in the coatings of electrodes S, T, and U.

Welding

The weld preparation was a symmetrical double-V with a 70° included angle, and with a 2-mm root face and 3-mm root gap. Short lengths (~60 mm) of two-pass welds were deposited in the root, using DC straight polarity, DC reverse polarity, and AC welding. The welding current was ~145 A for the C-Mn and C-Mn-Ni electrodes, with slightly lower values (~130 A) being employed inadvertently during the subsequent welding with the C-Mn-Ti-B electrodes (Table 2). The lowest arc voltage was a "convenient short arc," which was expected to correspond to an arc voltage of approximately 20 V; aim values for the higher voltages, achieved by holding artificially long arcs, were 22, 24, and 26 V. Travel speeds were adjusted to give approximately constant values of arc energy of ~1.7 kJ/mm. Before use, the electrodes were dried for 1 h at 350°C and were stored at 150°C. All welding was carried out in the flat position without preheat, and the panels were allowed to cool to room temperature before deposition of the second pass.

For the convenient short arc condition, both passes were deposited manually; for the other voltage conditions, the first pass was deposited manually, and the second by means of a machine [*15*] in which the burn-off rate was pre-selected, but for which continual small manual adjustments were necessary in order to maintain the aim voltage. This approach was adopted because of the difficulty of maintaining constant values of the arc voltage in manual welding

TABLE 3—*Chemical analysis (wt%) of the electrode core wires.*

Electrode Code	C	S	P	Si	Mn	Ni	Cr	Mo	V	Cu	Cb	Ti	Al	N	O
P	0.055	0.008	0.011	<0.01	0.51	0.02	0.02	<0.005	<0.002	0.03	<0.002	<0.002	<0.003	0.008	0.018
Q	0.043	0.008	0.007	<0.01	0.35	0.02	0.01	<0.005	<0.002	0.02	<0.002	<0.002	0.003	0.003	0.035
R	0.050	0.010	0.006	<0.01	0.45	0.02	0.005	<0.005	<0.002	0.01	<0.002	<0.002	<0.003	0.004	0.028
S	0.07	0.010	0.011	<0.01	0.45	0.02	0.01	<0.005	<0.002	0.02	<0.002	<0.002	<0.002	0.002	0.042
T	0.07	0.010	0.009	<0.01	0.50	0.02	0.01	0.005	<0.002	0.02	<0.002	<0.002	<0.002	0.002	0.046
U	0.09	<0.002	0.003	0.02	0.49	0.01	<0.005	<0.005	<0.002	<0.005	<0.002	<0.002	0.004	0.0005	0.002

with unusually long arc lengths. (A modification to the machine before the welding with the C-Mn-Ti-B electrodes prevented use of the machine for AC welding, which was therefore all carried out manually with these electrodes.) The same welder was employed for all the manual welding.

The current and voltage (root mean square) for the manual welding were monitored on overdamped moving coil galvanometers with a response time (for the current and voltage employed) of ~1 s; the voltage measurements were made between the electrode holder and the clamp, which attached the return lead to the work-piece. In addition, a print-out of the current and voltage (mean values) was obtained, for the AC welding, on the printer of a portable arc monitoring device (PAMs II, designed by The Welding Institute). For the automated welding, the DC voltage and current were monitored with digital displays, which had a sampling frequency of 0.5 s.

Largely to verify the presence of titanium and boron in electrodes S, T, and U, a two-layer pad, for spectrographic analysis, was produced in the flat position with each of the three electrodes, operating with a normal short arc.

Specimen Extraction and Testing

For the arc voltage studies, specimens for oxygen and nitrogen analysis were cut from the short lengths of weld, and these were analyzed, usually in triplicate, by inert gas fusion in a Leco TC136 analyzer. Both passes were included in each of these specimens. Any measurement errors were negligible compared with the wide scatter of the data, particularly that which occurred at the higher arc voltages.

The two-layer test pad, which was produced to check the presence of titanium and boron in electrodes S, T, and U, was ground flat and analyzed on a direct-reading optical emission vacuum spectrometer. (The detection limits for titanium and boron were 0.002% and 0.0003%, respectively, with the accuracy of measurement being of similar magnitude.)

Results

Electrode Handling Characteristics

It proved possible to maintain an arc and to deposit sound weld metal (as revealed during subsequent sectioning) for all the welding conditions employed, although electrodes S, T, and U each gave unstable arcs during welding at the highest voltage. Also, restarting with electrodes S and U sometimes gave porosity. Control of the weld pool was improved, for electrodes S, T, and U, when using the automatic deposition machine, by employing a leading angle of 10 to 15°. No pronounced effect of changing the power supply type was reported by the welder for any of these three electrodes. By contrast, electrode P gave a more stable arc when DC straight polarity was employed than for DC reverse polarity or AC. For DC straight polarity welding with electrode R, restarting and slag removal were more difficult, and the electrode did not run as smoothly, compared with DC reverse polarity or AC welding; these observations for electrode R are consistent with the manufacturer's recommendations.

Weld Pad Chemical Analyses

Spectrographic analyses of the two-layer weld pads produced with electrodes S, T, and U are presented in Table 5. The deposit compositions are broadly similar, with the largest differences occurring for Si, Mn, Ti, and Al electrode U giving the highest Si and lowest Mn, Ti, and Al levels; the boron levels were ~0.004% (electrode T) to ~0.006% (electrode S). Nominal com-

TABLE 4—*Chemical analysis (wt%) of the electrode coatings and coating factors.*

Electrode Code	Si	Ti	Zr	Al	Fe	Mn	Ca	Mg	Na	K	Li	F	CO_2	Ba	Ni	Cr	Mo	Cb	V	Cu	Coating Factor[a]	
																					D/d	$(D^2-d^2)/d^2$
P	7.8	4.9	1.2	0.4	4.8	4.8	26.3	2.5	0.7	2.5	<0.2	8.0	19.8	<0.1	<0.1	<0.1	<0.1	<0.1	<0.1	<0.1	1.55	1.42
Q	6.6	5.3	<0.1	0.3	4.8	4.2	28.1	3.9	0.4	1.7	<0.2	8.2	12.5	<0.1	<0.1	<0.1	<0.1	<0.1	<0.1	<0.1	1.56	1.43
R	5.9	4.3	<0.1	0.4	26.0	5.4	20.2	0.9	0.4	1.5	<0.2	8.3	12.3	<0.1	1.6	0.1	<0.1	<0.1	<0.1	<0.1	1.83	2.33
S	5.3	3.4	<0.1	1.9	3.3	5.3	28.8	1.4	1.3	0.8	NA[b]	8.0	23.2	2.5	<0.1	<0.1	<0.1	<0.1	<0.1	<0.1	1.62	1.61
T	4.5	4.3	<0.1	1.8	23.5	3.7	21.1	1.1	0.8	1.1	NA	6.0	17.1	1.5	<0.1	0.1	<0.1	<0.1	<0.1	<0.1	1.61	1.58
U	4.9	3.0	<0.1	0.6	32.7	3.5	20.7	0.7	1.0	0.6	NA	9.1	12.5	<0.1	<0.1	0.1	<0.1	<0.1	<0.1	<0.1	1.65	1.72

[a] D = overall electrode diameter. d = core wire diameter.

[b] NA = not analyzed.

TABLE 5—*Chemical analysis (wt%) of two layer weld pads.*

Electrode Code	Weld Code	C	S	P	Si	Mn	Ni	Cr	Mo	V	Cu	Cb	Ti	Al	B
S	W40	0.07	0.003	0.013	0.21	1.85	0.02	0.02	<0.005	0.005	0.04	<0.002	0.028	0.007	0.0057
T	W41	0.08	0.004	0.011	0.29	1.53	0.03	0.02	0.01	0.005	0.02	0.002	0.044	0.011	0.0041
U	W42	0.09	<0.002	0.008	0.40	1.51	0.005	0.01	<0.005	0.005	0.01	0.002	0.016	0.004	0.0042

Sn, Co, As, Pb, Zr < 0.005; Ca < 0.0003.

positions of deposits produced with electrodes P and R are 0.07%C-0.38%Si-1.6%Mn and 0.05%C-0.35%Si-1.75%Mn-0.85%Ni, respectively. Full chemical analyses of the root and sub-surface regions of butt welds produced with these two electrodes are given in a companion paper.[2]

Influence of Arc Voltage and Current Type and Polarity on Deposit Nitrogen and Oxygen Levels

The results of this study are presented graphically in Figs. 1 to 6, where the mean values and the range of measurements of deposit nitrogen and oxygen contents are plotted as a function of arc voltage. The arrows indicate the typical operating voltage range for welding in the flat position, and core wire nitrogen and oxygen values are also shown. For all the electrodes, the most rapid increase in deposit nitrogen and oxygen with increasing arc voltage occurred in DC straight polarity welding. The lowest rate of increase in nitrogen content and the lowest level at the lowest arc voltage was generally achieved with DC reverse polarity welding, with AC showing

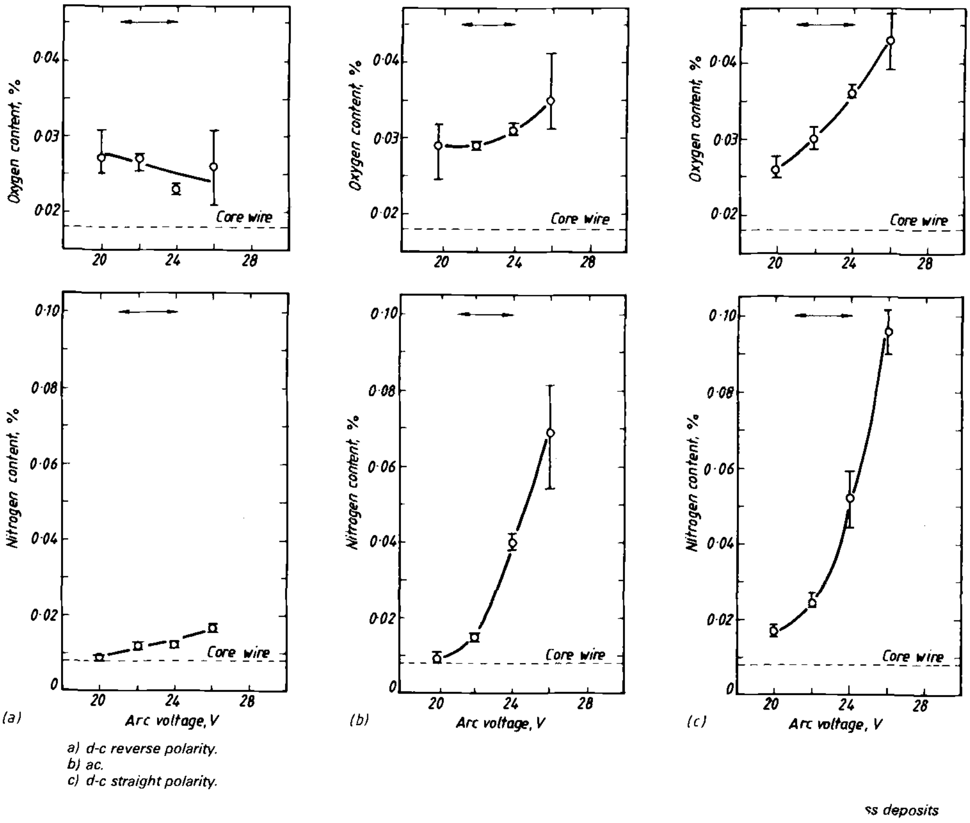

FIG. 1—*The influence of arc voltage and current type and polarity on deposit oxygen and nitrogen contents for two-pass deposits (C-Mn AWS E7016-G electrode coded P):* (a) *DC reverse polarity,* (b) *AC, and* (c) *DC straight polarity.*

---

[2] Abson, D., in this publication.

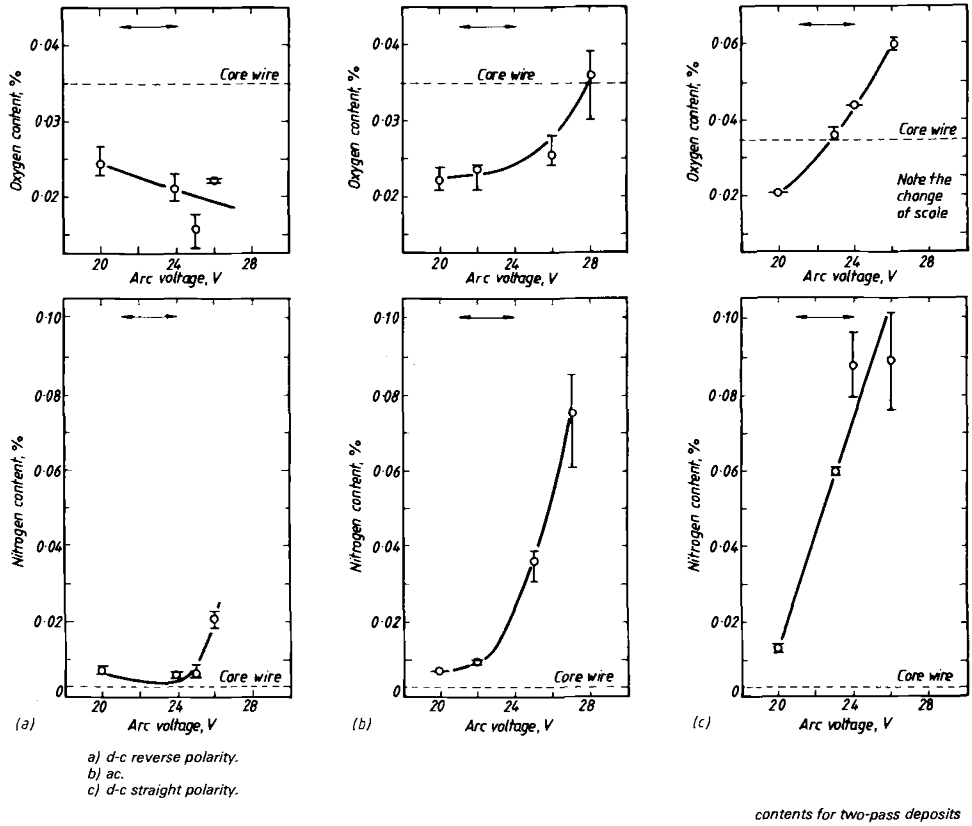

FIG. 2—*The influence of arc voltage and current type and polarity on deposit oxygen and nitrogen contents for two-pass deposits (C-Mn AWS E7016-1 electrode coded Q):* (a) *DC reverse polarity,* (b) *AC,* (c) *DC straight polarity.*

an intermediate value; however, for electrode R (Fig. 3) AC welding gave a slightly lower minimum nitrogen content than DC reverse polarity, and a slightly lower rate of increase. In all cases, the lowest deposit nitrogen level was slightly above that of the core wire. For DC straight polarity welds, even the lowest deposit nitrogen levels were >0.01% for electrodes P and Q, and >0.02% for electrodes S and U; at the highest arc voltages, deposit nitrogen levels were all >0.06%, with both electrode T and U showing maximum nitrogen contents of ~0.1%. At the lowest arc voltages, the three C-Mn-Ti-B electrodes gave the lowest deposit nitrogen contents of ≤0.005%, largely as a consequence of their lower core wire nitrogen levels.

The deposit oxygen levels bear no relation to the oxygen levels in the core wire. The trend for the AWS E7016 type electrodes (P, Q, and S, Figs. 1, 2, and 4) was for a progressive decrease in deposit oxygen content for the DC reverse polarity deposits, although the highest arc voltages achieved were only 25 or 26 V. The DC straight polarity deposits all showed a rapid increase in deposit oxygen content with increasing arc voltage, and the changes for AC welding were again intermediate, generally showing little change at the lowest voltages and then an increase. For DC reverse polarity deposits produced with AWS E7018 type electrodes (R, T, and U, Figs. 3, 5, and 6), oxygen levels decreased initially with increasing voltage and then increased from

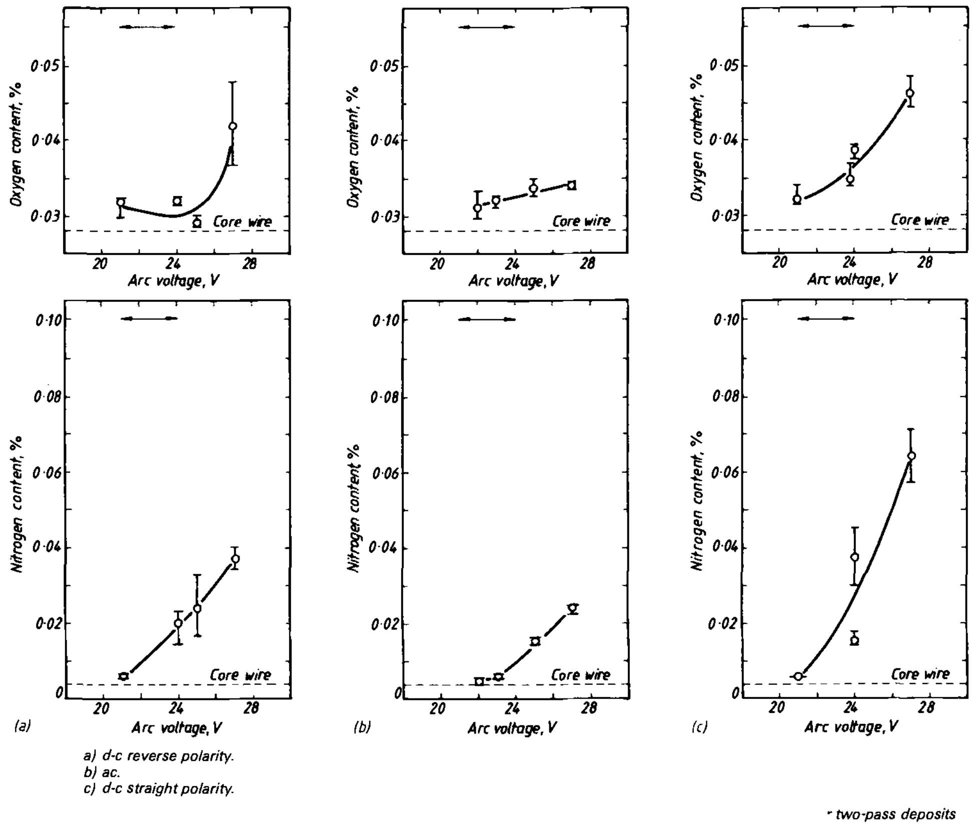

FIG. 3—*The influence of arc voltage and current type and polarity on deposit oxygen and nitrogen contents for two-pass deposits (C-Mn-Ni AWS E7018-G electrode coded R):* (a) *DC reverse polarity,* (b) *AC,* and (c) *DC straight polarity.*

~24 V up to the highest voltages of between 27 and 28 V, that is, beyond the voltage range in which they would normally be used. The DC straight polarity deposits produced with these electrodes all showed a steep increase in deposit oxygen content, while the AC deposits again showed intermediate behavior.

It will be noted that the arc voltage levels achieved with the convenient short arc condition are slightly below the normal voltage ranges for C-Mn electrodes marked in the figures. Such low voltage levels could be achieved by a welder who has been trained to employ a short arc, but otherwise would not normally be achieved in production welds.

Discussion

In the studies of the influence of increasing arc voltage on deposit oxygen and nitrogen content, the range of voltages studied was deliberately extended beyond that which would normally be achieved consistently during welding. Nonetheless, occasional increases in arc length are inevitable in a manual welding process. The study has therefore given some indication of the local variations in deposit oxygen and nitrogen that could arise in a weld bead, and how these

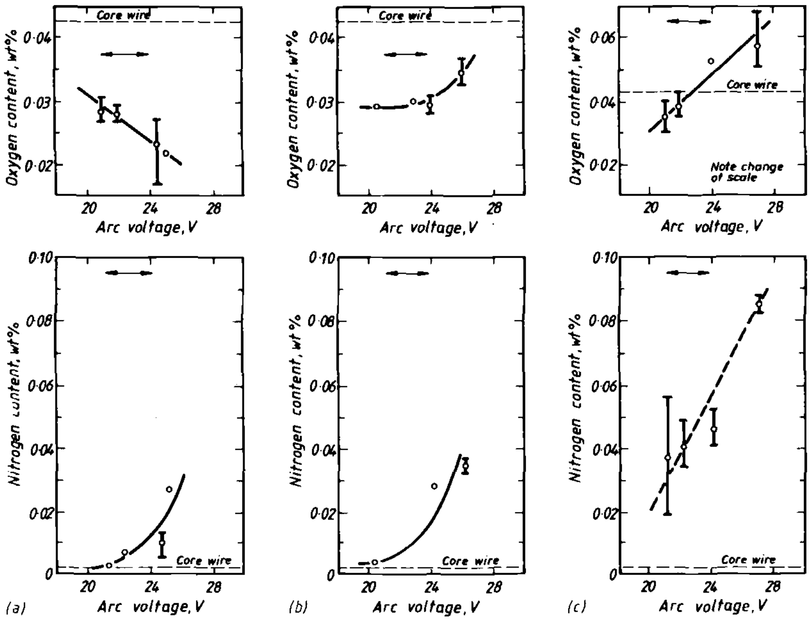

a) d-c reverse polarity.
b) ac.
c) d-c straight polarity.

FIG. 4—*The influence of arc voltage and of current type and polarity on deposit oxygen and nitrogen contents for two-pass deposits (C-Mn-Ti-B AWS E7016-G electrode coded S):* (a) *DC reverse polarity,* (b) *AC, and* (c) *DC straight polarity.*

may be influenced by current type and polarity. The datum for deposit nitrogen contents was the level in the core wire, thereby illustrating the important influence of core wire nitrogen content. The deposit oxygen contents did not show similar behavior; they are influenced more strongly by the coating formulation, as reported by Vines and Bailey [*16*].

Deposit Oxygen Contents

For basic-coated electrodes, metal transfer during normal welding occurs predominantly by short-circuiting, but also by the transfer of large droplets. The growing droplets are presumably coated with a layer of slag, as observed in flux-cored wire welding by Voropai et al. [*17*]. For 4-mm-diameter electrodes and an arc voltage of 20 V, Wegrzyn [*18*] reports the arc lengths as 4 mm. As arc voltage (and thus arc length) is increased, it is probable that free flight transfer will occur, resulting in the production of droplets with a progressively larger surface to volume ratio and thus with a thinner slag layer; the temperature of the electrode tip probably increases, thereby reducing the equilibrium oxygen content. While negatively charged oxygen ions in the arc plasma will migrate towards the anode, it appears that (with the exception of the AWS E7018 electrodes at high arc voltages) these ions do not influence the weld metal oxygen content when the anode is the electrode tip (DC reverse polarity welding), probably being prevented from doing so by the slag layer. When the anode is the weld pool (DC straight polarity welding), the ingress of oxygen increases as the arc voltage increases. Thus, it appears that migration of (negatively charged) oxygen ions in the slag layer on the weld pool overrides any effects occurring in the arc or at the electrode tip. The reason for the increase in deposit oxygen content at

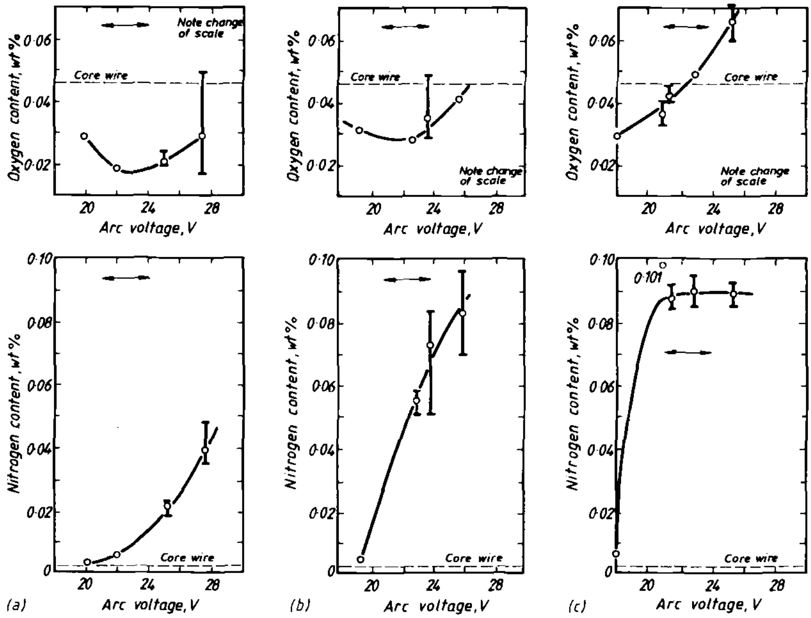

FIG. 5—*The influence of arc voltage and of current type and polarity on deposit oxygen and nitrogen contents for two-pass deposits (C-Mn-Ti-B AWS E7018-G electrode coded T):* (a) *DC reverse polarity,* (b) *AC, and* (c) *DC straight polarity.*

the higher arc voltages in the AWS E7018 reverse polarity deposits is not known. The changes in oxygen content for AC welding are intermediate between those for DC reverse polarity and for DC straight polarity (with the exception of the anomalously high deposit oxygen content at 27 V DC reverse polarity in Fig. 3). As long as the coatings of basic-coated electrodes do not contain significant proportions of easily dissociated fluorides, such as $Na_2SiF_6Na_3AlF_6$ and AlF_3, which hinder arc restriking on the DC reverse polarity cycle [*18*], such behavior is to be expected.

Deposit Nitrogen Contents

Concerning the nitrogen pick-up of the AWS E7016 type electrodes, the best behavior in this respect for electrodes P and Q was obtained for DC reverse polarity welding, in spite of the manufacturer's recommendation, in each case, that AC or DC straight polarity should be employed. At least for electrode P, this recommendation is consistent with the welder's report of a more stable arc during DC straight polarity welding with this electrode; thus, arc stability alone does not necessarily lead to low nitrogen deposits. For electrode S, AC welding was recommended and, while such welding gave lower nitrogen levels than the corresponding values obtained with electrodes P and Q, the behavior was still not as good as for DC reverse polarity welding with this electrode. The reason for the wide scatter in nitrogen levels for DC reverse polarity welding with electrode S is not known; it may reflect poor arc stability, although the welder did not report this.

The lowest deposit nitrogen contents, which were only slightly above the core wire levels, were achieved for DC reverse polarity welding with a short arc with electrodes S (AWS E7016 type) and T (AWS E7018 type). This behavior is probably partly a result of scavenging by titanium

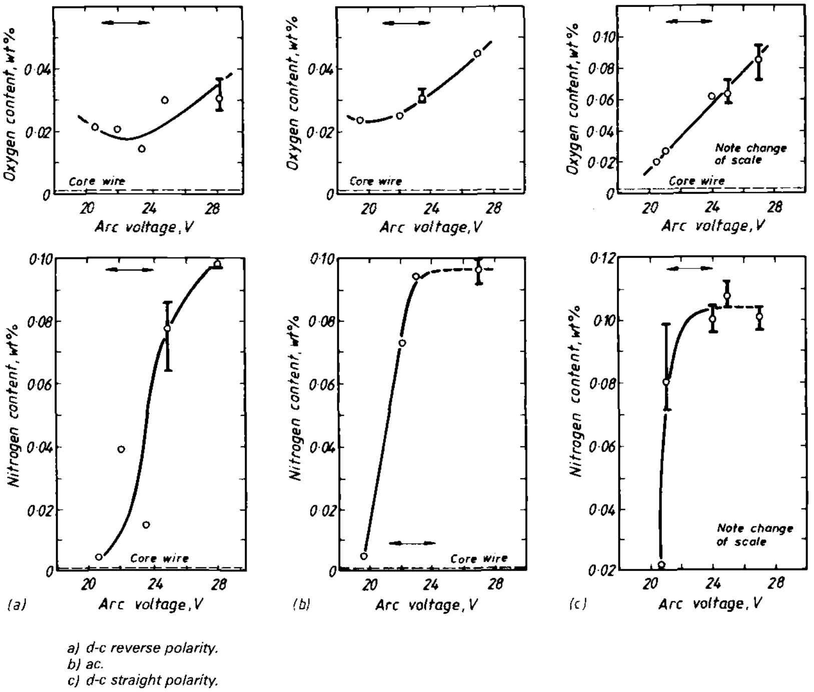

FIG. 6—*The influence of arc voltage and of current type and polarity on deposit oxygen and nitrogen contents for two-pass deposits (C-Mn-Ti-B AWS E7018-1 electrode coded U):* (a) *DC reverse polarity,* (b) *AC, and* (c) *DC straight polarity.*

and boron; however, an effective gas shield is also required, and this appears not to have been achieved with electrode U. (Effective shielding was, however, achieved for DC reverse polarity welding with a short arc with electrode P, as the deposit nitrogen content was again only slightly above the core wire level.) It will be recalled that a lower welding current was employed for the C-Mn-Ti-B electrodes, and this probably assisted slightly in giving low deposit nitrogen levels. However, with such electrodes, the increase in deposit nitrogen with increasing arc voltage was generally greater than with the C-Mn and C-Mn-Ni electrodes, at least for reverse polarity welding.

Comparing the nitrogen pick-up of the AWS E7016 and AWS E7018 type electrodes, and considering particularly the behavior at the higher arc voltages for DC straight polarity welding, it will be noted that electrode R (AWS E7018 type) performed better than the AWS E7016 type electrodes. By contrast, electrodes T and U (both AWS E7018 type) were both worse than the AWS E7016 types. Consideration of the product of the coating factor $(D^2 - d^2)/d^2$ and of both the carbon dioxide (CO_2) and the fluorine contents, which gives an indication of the volumes of these gases produced per unit length of electrode, suggests that the gas shield produced by decomposition of the coatings should be greatest for electrodes S and R and least for electrodes T and Q. In the light of the observed deposit nitrogen contents, it appears that this gas shield is important in excluding atmospheric nitrogen, although the line of reasoning does not explain the poor performance of electrode U.

As discussed in the Introduction, it is well-established for gas-shielded welding that nitrogen pick-up during arc welding occurs primarily at the cathode. The results of the present work show that such pick-up occurs more readily when the cathode is the electrode tip (DC straight polarity welding). This is probably because the electrode tip is hotter than the weld pool [*18*], and the probable consequences are that this not only gives more complete dissociation of nitrogen (to N^+ ions) in the plasma when the electrode is DC negative, but also increases the reaction rates for the processes involved in the transfer of nitrogen across the plasma/slag and slag/metal interfaces, compared with DC reverse polarity welding, where the ingress of N^+ ions will occur at the surface of the weld pool. The effect is small for the convenient short arc condition, but gives a dramatic change in deposit nitrogen level (for DC straight polarity welding) as the arc voltage is increased (Figs. 1 to 6). As noted above, increasing arc voltage is probably associated with a change from predominantly short-circuit metal transfer to free flight transfer with the consequent increase in surface to volume ratio of the metal droplets and thinning of the slag layer. Also, the effectiveness of the gas shield, in preventing the ingress of nitrogen is likely to diminish as the time of flight of the droplets is increased. As a consequence, the deposit nitrogen content increases with increasing arc voltage; the effect is less pronounced for DC reverse polarity than for DC straight polarity welding, although there is still some increase for the former. In gas-shielded welding, both Kobayashi et al. [*12*] and den Ouden [*19*] have reported results obtained when employing oxygen plus nitrogen and carbon dioxide plus nitrogen as shielding gases. They observed that, for a given nitrogen content in the shielding gas mixture, the weld nitrogen content was always higher in welds deposited under the oxygen plus nitrogen shielding gas. The same phenomenon may contribute to an increase in weld nitrogen in SMA welding, regardless of polarity, if longer arc lengths render the gas shield less effective in excluding air. One small anomaly will be noted for the AC C-Mn-Ni deposits in Fig. 3, where the pick-up of nitrogen is not intermediate between those for DC reverse polarity and DC straight polarity welding, but is even lower than the former. A possible explanation is that the electrode may have operated more smoothly on AC than on DC reverse polarity, although the welder did not report any noticeable difference.

Practical Implications

In view of the known deleterious effect of nitrogen on weld toughness in C-Mn steels, it is clearly important, when welding with SMA electrodes in applications where high deposit toughness is required, to employ a short arc. For the consumables employed in the present study, it is evident that employing the C-Mn-Ti-B electrodes for DC straight polarity welding gives a risk of producing deposits with unacceptably high levels of nitrogen. Considerable care would have to be exercised to weld with a short arc if DC straight polarity were employed in the root; it would then probably be desirable to back-gouge the first two passes, in order to remove weld metal which is likely to contain high levels of nitrogen. (Such back-gouging is commonly carried out for multiple-pass welds in structural applications where high toughness is required. In addition to a higher level of nitrogen, the root pass may contain higher carbon, diluted into the weld from the parent steel, and the early passes are likely to have suffered strain age damage [*20*]; all of these factors are likely to reduce weld toughness.) It is recommended by manufacturers of C-Mn-Ti-B electrodes to employ a short arc; the need to do so, even for DC reverse polarity operation, appears to be greater than it is for C-Mn and C-Mn-Ni electrodes. This suggests that, except for welding with very short arcs, the gas shields produced by SMA electrodes are not fully effective in excluding air, and that titanium and boron draw in additional nitrogen from the atmosphere. However, it is clearly desirable to employ a short arc for all welding with SMA electrodes. It will be noted that electrode S, for which AC welding was recommended, performed well when operated on AC, and this electrode and electrode T, for which DC reverse polarity welding was recommended, both performed well for DC reverse polarity welding. In the light of the findings of the present study, it is clear that, in applications requiring high weld toughness, care should be exercised in choosing, and in ensuring the use of, the appropriate current supply type.

A further implication of the present work is that electrodes that are formulated for AC or DC reverse polarity welding, and particularly the latter, are likely to give the lowest deposit nitrogen contents, and thus have the potential, when welded with a short-arc, of giving the highest deposit toughness.

Conclusions

A series of deposits has been produced with two C-Mn, one C-Mn-Ni, and three C-Mn-Ti-B basic-coated low hydrogen electrodes, covering both AWS E7016 and E7018 types. The deposit oxygen and nitrogen contents were investigated, as a function of arc voltage, for DC reverse polarity, DC straight polarity, and AC power supplies. The following conclusions have been drawn from this work:

1. Deposit nitrogen content increased with increasing arc voltage, as expected; however, markedly different behavior was generally observed as the power supply type was changed, and this was true of deposit oxygen content also.
2. The rate of increase of oxygen and nitrogen with increasing arc voltage was highest for DC straight polarity welding. The lowest initial rate of increase in deposit nitrogen content was obtained for DC reverse polarity welding with the two C-Mn and the three C-Mn-Ti-B electrodes, and for AC welding with the C-Mn-Ni electrode. The highest initial rate of increase in nitrogen content was obtained for DC straight polarity welding with two of the C-Mn-Ti-B electrodes.
3. The lowest deposit nitrogen levels achieved with the shortest arc lengths (lowest arc voltages) were higher than the core wire nitrogen levels but, for DC reverse polarity welding, they approached the core wire levels. The three C-Mn-Ti-B electrodes gave the lowest deposit nitrogen contents.
4. Deposit oxygen levels depended on the electrode coating, rather than the oxygen content of the core wire. For DC straight polarity welding, the oxygen content increased progressively as the arc voltage was increased. For DC reverse polarity welding, depending on coating type, there was either a small but progressive decrease or an initial decrease followed by a slight increase; for AC welding, there was little or no change initially, but the oxygen content increased at higher arc voltages.
5. The findings have not only demonstrated the desirability of maintaining a short arc length, but they also suggest that caution must be exercised in selecting the power supply type, or in making changes to this aspect of a welding procedure, where high levels of weld toughness are required. For the consumables employed in the present study, it would be desirable to avoid the use of DC straight polarity in such applications.

Acknowledgments

The assistance of staff of The Welding Institute with the experimental work, particularly Mrs. W. Martin and Messrs. M. D. Tiplady, J. Haugh, G. M. Courtman, J. C. Ford, J. J. Rickard, K. J. Tiplady, G. T. Hall, N. J. Tebbit, W. Hedley, and P. T. Bennett is gratefully acknowledged, as are helpful discussions with colleagues, particularly from the Materials Department.

The work was jointly funded by Research Members of The Welding Institute and the Minerals and Metals Division of the United Kingdom Department of Trade and Industry.

References

[*1*] Houldcroft, P. T., *Welding Process Technology,* Cambridge University Press, Cambridge, 1977.

[*2*] Boniszewski, T., "Manual Metal Arc Welding—Old Process, New Developments," *The Metallurgist and Materials Technologist,* Vol. 11, No. 10, 1979, pp. 567-574, Vol. 11, No. 11, pp. 640-643, Vol. 11, No. 12, pp. 697-705.

[*3*] Morigaki, O., Tanigaki, T., Kuwabara, M., Fujibayashi, K., and Otawa, M., "Development of a Covered Electrode for Steel Structures in Low Temperature Service," IIW Document II-746-75, April 1975.

[*4*] Nippon Steel Welding Products and Engineering Company Limited, "Properties of Nittetsu N-100 Covered Electrode for Offshore Structures," April 1981.

[*5*] Blake, P. D., "Oxygen and Nitrogen in Weld Metal," *Welding Research International,* Vol. 9, No. 1, 1979, pp. 23-57.

[*6*] Vines, M. J., "Nitrogen in C-Mn Weld Metal—A Review," unpublished research, The Welding Institute, 1982.

[*7*] Verhagen, J. G., den Ouden, G., Liefkens, A., and Tichelaar, G. W., "Nitrogen Absorption by Ferritic Weld Metal During Arc Welding," *Metal Construction and British Welding Journal.* Vol. 2, No. 4, 1970, pp. 135-143; and *Phillips Welding Reporter,* Vol. 8, No. 3, 1972/3, pp. 5-15.

[*8*] Morigaki, O., Matsumoto, T., and Takemoto, Y., "Some Improvements in Self-Shielded Flux-Cored Electrodes for Arc Welding," *Welding Journal Research Supplement,* Vol. 55, No. 8, 1976, pp. 241s-248s.

[*9*] Morigaki, O., Matsumoto, T., Makita, M., and Deyama, I., "Application Studies of the DC Power Source to Self-Shielded Arc Welding (Report 1), Effects of Polarity on Welding Phenomena," Preprints of the National Meetings of the Japan Welding Society, Autumn 1969, pp. 265-266 (quoted by Ref *8*).

[*10*] Morigaki, O., Matsumoto, T., and Noda, T., "Application Studies of d.c. Power Source to Self-Shielded Arc Welding (Report 3), Effects of Wire Size on Welding Characteristics," Preprints of the National Meeting of the Japan Welding Society, Autumn 1969, pp. 269-270 (quoted by Ref *8*).

[*11*] Podgaetskii, V. V. and Galinich, V. I., "The Effects of the Type and Polarity of the Current on the Absorption of Nitrogen and Hydrogen by the Weld Pool," *Automatic Welding,* Vol. 15, No. 11, 1963, pp. 23-28.

[*12*] Kobayashi, T., Kuwana, T., and Kikuchi, Y., "Arc Atmosphere and Nitrogen Content of Weld Metal," *Welding in the World,* Vol. 5, No. 2, 1967, pp. 58-73.

[*13*] Miller, J. W., "Nitrogen in Metallic Arc Weld Metal," *Welding Journal,* Vol. 15, No. 2, 1936, pp. 5-10.

[*14*] Koshio, T., Ootawa, M., Tanigaki, T., Takino, T., Horii, Y., Tsunetomi, E., and Imai, K., "Development of the High COD Titanium-Boron-Bearing Covered Electrode," IIW Doc II-955-81, June 1981.

[*15*] Pedder, C. and Watkinson, F., "Automatic Deposition of Manual Metal Arc Covered Electrodes," *Welding Institute Research Bulletin,* Vol. 12, No. 9, 1971, pp. 253-254.

[*16*] Vines, M. J. and Bailey, N., "The Influence of Arc Wire Deoxidation Practice on Manual Metal Arc Welding—A Preliminary Appraisal," *The Effects of Residual, Impurity and Microalloying Elements on Weldability and Weld Properties,* The Welding Institute, 1984, Paper 28.

[*17*] Voropai, N. M., Alimov, A. N., and Rogatyouk, V. I., "The Composition of the Metal and Slag in the Droplet and Pool Stages during CO_2 Welding with an Activated Wire," *Welding International,* Vol. 1, No. 3, 1987, pp. 216-218.

[*18*] Wegrzyn, J., "The Covered Electrode Arc," *Weld Pool Chemistry and Metallurgy,* The Welding Institute, 1980, pp. 241-251.

[*19*] den Ouden, G., "The Role of Nitrogen in Electric Arc Welding," *Phillips Welding Reporter,* Vol. 13, No. 1, 1977, pp. 1-6.

[*20*] Robinson, J. L., "Factors Controlling Root Run Toughness in Multipass Manual Metal Arc Welds in C-Mn Steels," *Welding Research International,* Vol. 8, No. 6, 1978, pp. 425-509.

DISCUSSION

G. S. Hartman[1] *(discussion question)*—It seems as though the oxygen level in the weld deposit is independent of the O_2 content of the core wire as the core wire varied oxygen content, varied from 20 to 450 ppm. It appeared from your slides that it reached an equilibrium with the slag. Is that your conclusion?

D. J. Abson (author's response)—Clearly, the deposit oxygen content is influenced strongly by the electrode coating, which has its effect primarily through the slag. I agree that it appears to approach an equilibrium level, but this level is clearly influenced by arc voltage, particularly for DC straight polarity welding.

G. S. Hartman (discussion question)—Since the O_2 and N_2 contents have increased, have you investigated what the increase in H_2 was?

D. J. Abson (author's response)—I did not investigate deposit hydrogen contents in the study, but I was aware of earlier work [*1*] in which only a small influence of current supply type on deposit hydrogen content was observed in shielded metal arc deposits.

Reference

[*1*] Hart, P. H. M., "Weld Hydrogen Levels—The Influence of Welding Parameters," *The Welding Institute Research Bulletin*, Vol. 20, No. 4, 1979, pp. 106-108.

---

[1] A. Finkl & Sons Co., Chicago, IL 60614.

R. H. Biron,[1] *C. H. Kreischer,*[2] *and A. S. Melilli*[1]

A Method for Developing Postweld Heat Treatments and Evaluating Effects of Residual Elements on Heat-Affected Zone Tempering Resistance

REFERENCE: Biron, R. H., Kreischer, C. H., and Melilli, A. S., "**A Method for Developing Postweld Heat Treatments and Evaluating Effects of Residual Elements on Heat-Affected Zone Tempering Resistance,**" *Residual and Unspecified Elements in Steel, ASTM STP 1042,* A. S. Melilli and E. G. Nisbett, Eds., American Society for Testing and Materials, Philadelphia, 1989, pp. 261-265.

ABSTRACT: A method was developed to define a postweld subcritical heat treatment to provide optimum ductility of the heat-affected zone. The results have been used to define the post-weld heat treatment included as part of welding procedure qualification tests. By themselves, required qualification tests, which involve tensile, bend, and sometimes impact, can be misleading because they are not primarily designed to evaluate heat-affected zone ductility. The test method involved generating a heat-affected zone (HAZ), extracting a series of as-welded cross sections, heat treating each section at varying times and temperatures, measuring the peak heat-affected zone hardness, and defining the heat-affected zone ductility by correlating the peak HAZ hardness with the Hollomon-Jaffe parameter associated with each time and temperature. Several heats of CrMo and CrMoV turbine alloys were studied in this manner to define their weld HAZ tempering response and to evaluate specific tempering effects of residual alloy element content.

KEY WORDS: tempering response, heat-affected zone (HAZ), optimum ductility, post-weld heat treatment, Hollomon-Jaffe parameter, hardness

Temperatures for post-weld heat treatments are normally specified as minimum values, and sometimes the times at temperature are also specified as minimum requirements. Such minimum requirements permit considerable latitude in selected tempering temperatures and times by various fabricators, even for identical alloy steels, provided the normally required tests for welding procedure qualification are satisfactorily met.

Reduced section tension tests, bend tests, and sometimes notched impact tests are the traditional methods for procedure qualification. Satisfying the minimum tensile strength of the base material is the normal criterion for the tension test whether the fracture occurs in the base, weld, or fusion zone. In the bend tests, the maximum strain is designed to take place in the center section of the weld metal with a minimum strain occurring in the fusion and heat affected zone (HAZ). Impact tests of the weld metal, and sometimes the HAZ, may also be required. It is possible to satisfy all the criteria for procedure qualification testing using a variety of temperatures and times for the postweld heat treatments, none of which may achieve optimum HAZ ductility.

---

[1] Welding engineer and manager of Materials and Processes Engineering, respectively, General Electric Company, Lynn, MA 26442.

[2] Welding engineer, General Electric Company, Schenectady, NY 12345.

When one is interested in developing a post-weld heat treatment for optimum mechanical properties, the ductility of the HAZ becomes increasingly important. Whereas the traditional tests for procedure qualification are not primarily designed for evaluating the HAZ ductility, development of another method was studied.

To evaluate the tempering resistance of the heat-affected zone, tempering parameter data were developed utilizing Vickers DPH and Knoop microhardness traverse measurements across the base metal, HAZ, and weld metal. As-welded specimens were tested followed by additional tests of specimens subjected to various post-weld heat treating temperatures. Hardness data were correlated with the Hollomon-Jaffe parameter for temperature and time [*1*]. Several alloy steels were studied in this manner. In addition, the tempering resistance of the HAZ of base metals with various amounts of residual elements was also studied using this method.

Application of this method for measuring the maximum as-welded HAZ hardness can also be used for identifying the severity and need for special welding procedure parameters and controls to prevent HAZ cracking during fabrication.

Procedure and Results

Development of an optimum critical post-weld heat treatment was based on correlation of HAZ hardness as a function of the Hollomon-Jaffe time-temperature tempering parameter defined by $P = T(C + \log t)$ where $T =$ degrees Rankine, $t =$ time in hours, and $C =$ a constant. A constant of 20 is usually used for low alloy steels, but actual calculation may provide more precise values.

A weld HAZ was generated using a single bead-on-plate weld deposited at a fixed heat input and preheat. As-welded transverse cross sections were removed along the length of the weld. One cross section was set aside to represent the as-welded condition, and the others were individually tempered at varying temperatures and times. Alternatively, longitudinal sections were tempered in a gradient furnace that exposed the length of the section to a known, continuous thermal gradient of several hundred degrees encompassing the possible tempering temperature range. Such specimens were tempered for varying times. Selection of subcritical temperatures and times was aimed to be within the parameter range of $P = 31\,000$ to $38\,000$, $C = 20$. Typical times and temperatures used for the CrMo and CrMoV alloys examined are presented in Table 1.

Upon completion of the thermal cycle, each specimen cross section was ground with parallel faces; sufficient material was removed to eliminate any potential decarburized surface condition. The specimens were then polished and etched to reveal the weld, HAZ, and unaffected base metal. Macrohardness measurements were made at a fixed distance from the fusion line on each specimen, and the results were plotted as a function of the associated tempering parameter P. The results of a typical series of measurements is shown in Fig. 1 [*2*].

TABLE 1—*Typical temperature-time relationships.*

Parameter, $P_{x10^{-3}}$ $C = 20$	Temperature, °F	Time, h
33	1200	0.75
34	1250	0.75
35	1250	3
36	1250	10
36	1275	6
37	1275	20
38	1275	75

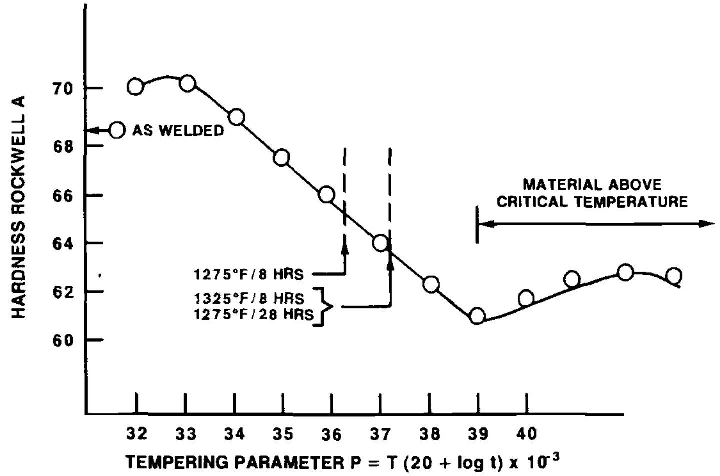

FIG. 1—*Typical heat affected zone tempering response.*

Variations of the method for measuring hardness have also been used to characterize the weld and the complete HAZ. Microhardness traverses, normal to the weld fusion line with measurements made at intervals of 0.005- and 0.010-in. (0.127 and 0.254 mm) traversing from the weld and across the complete HAZ, have been used to characterize the tempering response of the weld metal as well as the maximum and minimum (overtempered) hardness within the HAZ. Such traverses reveal that hardness of both as-welded and tempered heat affected zones varies from a maximum value typically located within about 0.03 in. (0.762 mm) of the weld fusion line, to a minimum value located at the far extremity of the structurally altered HAZ where the peak temperature reached during welding was close to the lower critical temperature (Acl). In alloy steels, the maximum as-welded HAZ hardness is typically much greater than the unaffected base metal hardness while the minimum hardness at the far extremity of the HAZ is often less than that of the unaffected base metal. Correlation of the HAZ maximum hardness as a function of the tempering parameter *P* was used to define the tempering response of the least ductile area of the HAZ. Selection of a post-weld heat treatment on the basis of such data has been applied for steam turbine service conditions requiring optimum ductility of the weldment.

This method has also been used to characterize HAZ tempering response of CrMo and CrMoV alloys with varying levels of deoxidizing elements, intentional alloying and residual elements, and the interaction of such elements. Figure 2 summarizes the results of selected tests involving these factors [*3*]. A calculated parameter constant of 17.5 provided the best fit for these data and was thus used for plotting them. Table 2 shows equivalent parameter values for several time-temperature combinations calculated with the 17.5 constant used for these data and the more commonly used constant of 20. Curves A and B show the temper-resisting effect of titanium on a CrMo alloy. Curves A and C compare a CrMo and CrMoV alloy at the same titanium level. Curves C, D, and E show the temper-resisting effect of increasing titanium in a CrMoV alloy, and Curves E and F show no change in the temper-resisting effect at titanium levels above 0.061%.

Discussion

The method of characterizing the HAZ tempering response using maximum hardness is seemingly conservative but justified for steam turbine applications. From the data provided, the

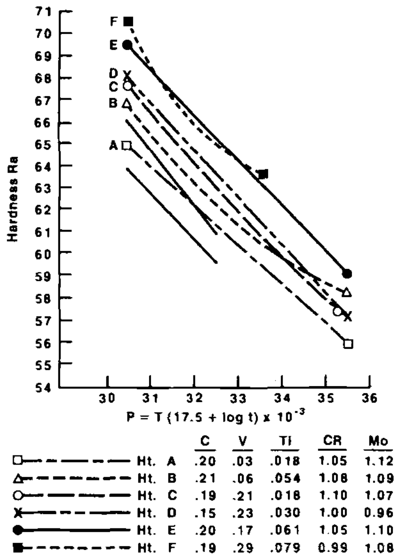

FIG. 2—*Heat affected zone tempering characteristics of CrMo and CrMoV steels with varying titanium contents.*

TABLE 2—*Equivalent parameter values for constants of 17.5 and 20,* P = T(C + *log* t).

Temperature			Parameter Value	
Fahrenheit	Rankine	Time, h	$C = 17.5$	$C = 20$
1250	1710	2	30 400	34 700
1250	1710	8	31 500	35 700
1250	1710	16	32 000	36 300
1300	1760	2	31 300	35 700
1300	1760	8	32 400	36 800
1300	1760	16	32 900	37 300
1350	1810	2	32 200	36 700
1350	1810	8	33 300	37 800
1350	1810	16	33 900	38 400

parameter value is selected that results in a tempered-HAZ-hardness value as close as possible to that of the base material without tempering the base material below the specification limits. The parameter in turn defines the appropriate post-weld temperature-time thermal cycle to use.

The data in Fig. 2 showing the effects of titanium clearly define the temper-resisting effects of titanium as a residual element in a CrMoV alloy. If one selects a hardness of 62 Rockwell A to define the optimum HAZ hardness, the appropriate parameter value is 33 for alloy C with a titanium content of 0.018%. If given the same post-weld treatment, the same nominal alloy composition with a titanium level of 0.061%, shown as alloy E, will only temper to a 64.5 Rockwell A level. For the latter alloy to temper to 62 Rockwell A, the post-weld thermal cycle would have to correspond to a temperature and time equivalent to a parameter of 34. At that parameter, alloy C would be expected to temper to a value of 59.5 Rockwell A. Such data provide the basis for arriving at a "best balance" for optimum HAZ ductility, practical postweld heat treating cycles, and severity of residual element control required in steel melting.

References

[1] Hollomon, J. H. and Jaffe, L. D., "Time-Tempering Relations in Tempering Steels," *Transactions, American Institute of Mining and Metallurgical Engineers,* Vol. 162, 1945, p. 223.

[2] Berry, T. F., "Determination of Tempering Response of the Heat Affected Zone in High Titanium B50A224B," General Electric Report AG-63-3, March 1963.

[3] Kreischer, C. H., "Tempering Characteristics of the Weld Heat Affected Zone in Titanium Deoxidized CrMo and CrMoV," General Electric Report DF57SL517, June 1957.

Koichi Yamamoto,[1] *Shouichi Matsuda,*[2] *Toshiaki Haze,*[1]
Rikio Chijiiwa,[3] *and Hiroshi Mimura*[1]

A Newly Developed Ti-Oxide Bearing Steel Having High HAZ Toughness

---

REFERENCE: Yamamoto, K., Matsuda, S., Haze, T., Chijiiwa, R., and Mimura, H., **"A Newly Developed Ti-Oxide Bearing Steel Having High HAZ Toughness,"** *Residual and Unspecified Elements in Steel, ASTM STP 1042,* A. S. Melilli and E. G. Nisbett, Eds., American Society for Testing and Materials, Philadelphia, 1989, pp. 266-284.

ABSTRACT: A study was carried out on the transformation characteristic of a newly developed Ti-O steel in comparison with that of ordinary steels. The microstructure of the weld heat affected zone (HAZ) in the Ti-O steel is characterized by the formation of intragranular ferrite plate (IFP), or so-called acicular ferrite, which was found to start from titanium sesquioxide (Ti_2O_3) particles dispersed in the matrix of the steel. The welding thermal cycle simulation test on the Ti-O steel showed that IFP development takes place over a wide range of conditions such as heating temperature and chemical composition. The high stability of Ti_2O_3 particles at high temperature explains the effect of the former condition. The effect of the latter can be well understood from the distribution of Ti_2O_3 particles, which is irrelevant to the microsegregation of alloying elements such as manganese and niobium. IFP formation restricts development of ferrite side plate, refines the effective grain size, and improves HAZ toughness. Various experimental results suggested that the Ti_2O_3 particle has an IFP formation function through the manganese sulfide (MnS) attached on it.

KEY WORDS: high strength alloy steel, low carbon steel, steel for low temperature service, phase transformation, toughness, weldability, inclusion, grain size

Nomenclature

vTrs	Charpy V notch fracture appearance transition temperature
$\Delta t_{8/5}$	Cooling time from 800 to 500°C in seconds during welding thermal cycle
FATT	Fracture appearance transition temperature
HAZ	Weld heat affected zone
CMA	Computer aided X-ray micro-analyzer
EDX	Energy dispersion X-ray analysis
SPEED	Selective potentiostatic etching by electrolytic dissolution
F_p	Grain boundary allotriomorph ferrite
F_I	Idiomorph ferrite
F_S	Ferrite side plate
IFP I, IFP II	Intragranular ferrite plate, Types I and II
P	Pearlite

---

[1] Researcher, senior researcher, and executive counsellor, respectively, Research and Development Laboratories—II, Nippon Steel Corporation, Sagamihara, Kanagawa, Japan.

[2] Senior researcher, Research and Development Laboratories—I, Nippon Steel Corporation, Kawasaki, Kanagawa, Japan.

[3] Researcher Kimitsu Works, Nippon Steel Corporation, Kimitsu, Chiba, Japan.

PL	Degenerated pearlite
B	Bainite
M*	High carbon martensite island
M	Martensite
Ti-O, Ti-N, LN, Ti-B, Ti-LN	Names of specimen used in this research (See Table 1 as to its chemical compositions)

Introduction

Platforms for oil production have been and will continue to be constructed in colder, rougher, and deeper seas than ever before. Accordingly, steels used for these platforms are required to have high strength, good toughness, good weldability, and heavy cross section. Steels that can be welded with a large heat input are often desired for the cost savings in construction. However, obtaining toughness in the weld heat affected zone (HAZ) becomes more difficult as strength and cross section increase, because an increase in the carbon equation or the addition of a microalloy such as niobium, vanadium, or molybdenum[4] usually results in deterioration of the HAZ toughness. Every effort has been made so far to develop steels with good HAZ toughness. Ti-N steel [1] is a typical one and is characterized by precipitation of fine TiN, which prevents coarsening of austenite grain and produces refined ferrite grain in the HAZ. Ti-B steel [2], developed recently, has a refined HAZ microstructure that is obtained through formation of intragranular ferrite plate (IFP)[5] by a complex precipitate, TiN + MnS + $Fe_{23}(CB)_6$. Nevertheless, the HAZ toughness of these steels is not necessarily enough when high strength and heavy section are required. In addition, on application of large heat input welding, TiN and manganese sulfide are apt to decompose and to lose the controlling function of microstructure near the fusion line, which results in the formation of ferrite side plate (F_S) and deterioration of toughness. A new steel, Ti-O steel, maintains good HAZ toughness even if strength is increased up to 60 kg/mm^2, for instance, or if large heat input welding is applied or both. These superior properties of Ti-O steel can be attributed to its transformation characteristics, which will be explained in this paper.

Experimental Method

Preparation of Specimen

Specimens were prepared by vacuum melting, casting 60 kg ingots, heating at 1150°C for 1 h and hot rolling to 13 mm thick plate. Their chemical compositions are shown in Table 1. Ti-O steel was made by deoxidization with titanium. Strong deoxidizing elements such as aluminum, calcium, or rare earth metals (REM) were not used. Oxygen content in molten steel was 40 ~ 60 ppm, and Ti content 0.01 ~ 0.015%. Titanium oxide particles were dispersed. Specimens having the best known optimum chemical compositions for good HAZ toughness and not from Ti-O steel were prepared as reference steels.

Test for HAZ Toughness

Specimens were machined into 12 by 12 by 55 mm square rods, given a simulated welding thermal cycle (simulated HAZ) consisting of heating up to 1350 ~ 1450°C and cooling from 800 to 500°C ($\Delta t_{8/5}$) in 161 s, and were tested by Charpy impact tests with the standard size test specimen.

---

[4] In this paper, molybdenum is used as a kind of microalloy in the sense that it is added in a small amount to increase resistance to tempering and to widen the nonrecrystallization region in hot rolling temperature.

[5] This microstructure is often called acicular ferrite.

TABLE 1—*Chemical compositions of steel (wt%).*

Steels	C	Si	Mn	P	S	Al	Ti	B	N	O	Nb	Ni	Cu
Ti-O	0.079	0.20	1.39	0.0007	0.0007	0.002	0.012	. . .	0.0015	0.0017	. . .	. . .	. . .
LN	0.092	0.20	1.42	0.0010	0.0008	0.020	. . .	. . .	0.0015	0.0020	. . .	. . .	. . .
Ti-B	0.090	0.26	1.41	0.0090	0.0040	0.038	0.008	0.0015	0.0028	. . .	. . .	. . .	. . .
Ti-N	0.085	0.21	1.46	0.0006	0.0011	0.018	0.019	. . .	0.0050	. . .	. . .	. . .	. . .
Ti-LN	0.084	0.20	1.43	0.0040	0.0040	0.054	0.006	. . .	0.0017	. . .	. . .	. . .	. . .
Ti-O1	0.049	0.10	1.39	0.0005	0.0009	0.001	0.011	. . .	0.0014	0.0021	0.016	0.29	0.30
Ti-O2	0.084	0.10	1.39	0.0007	0.0008	0.001	0.010	. . .	0.0014	0.0020	0.014	0.30	0.30
Ti-O3	0.120	0.10	1.40	0.0009	0.0008	0.001	0.011	. . .	0.0014	0.0021	0.015	0.31	0.31
LN1	0.038	0.09	1.40	0.0036	0.0069	0.066	. . .	. . .	0.0022	. . .	0.010	0.33	0.31
LN2	0.090	0.11	1.43	0.0070	0.0060	0.010	. . .	. . .	0.0027	. . .	0.019	0.34	0.33
LN3	0.110	0.10	1.40	0.0060	0.0050	0.016	. . .	. . .	0.0022	. . .	0.019	0.32	0.32
Ti-LN1	0.051	0.09	1.34	0.0005	0.0049	0.062	0.009	. . .	0.0016	. . .	0.008	0.31	0.29
Ti-LN2	0.085	0.10	1.40	0.0050	0.0050	0.057	0.011	. . .	0.0020	. . .	0.013	0.33	0.30
Ti-LN3	0.120	0.10	1.39	0.0050	0.0060	0.055	0.009	. . .	0.0026	. . .	0.011	0.32	0.29
Ti-O4	0.085	0.19	1.43	0.0009	0.0009	0.001	0.009	. . .	0.0016	0.0020	0.005	. . .	. . .
Ti-O5	0.082	0.19	1.42	0.0008	0.0008	0.001	0.008	. . .	0.0016	0.0020	0.009	. . .	
Ti-LN4	0.079	0.20	1.42	0.0040	0.0040	0.060	0.006	. . .	0.0017	. . .	0.005	. . .	. . .
Ti-LN5	0.080	0.20	1.40	0.0040	0.0040	0.059	0.005	. . .	0.0017	. . .	0.009	. . .	. . .
Ti-LN6	0.079	0.20	1.42	0.0005	0.0005	0.062	0.007	. . .	0.0013	. . .	. . .	. . .	. . .
Ti-LN7	0.080	0.20	1.43	0.0005	0.0013	0.064	0.007	. . .	0.0013	. . .	. . .	. . .	. . .
Ti-LN8	0.082	0.20	1.43	0.0005	0.0034	0.064	0.007	. . .	0.0013	. . .	. . .	. . .	. . .

Transformation Characteristics from γ to α

Transformation characteristics were studied with a continuous cooling transformation (CCT) diagram for welding, which was obtained by heating a specimen of 3 mmϕ by 10 mm at 1400°C for 1 s and cooling at a rate of 280 ~ 0.5°C/s. To determine definitively the transformation temperature range for a particular microstructure, the relevant microstructure was examined for the specimen quenched from various temperatures between 750 ~ 450°C on cooling with a time of $\Delta_{8/5} = 41$ s, or 161 s from 1400°C.

Analysis of Microstructure, Nucleus of IFP, and Microsegregation

Under an optical microscope, the microstructures of simulated HAZ specimens, which were polished and etched with saturated picral + 0.1% HNO_3 were studied. The martensite-austenite constituent, or high carbon martensite island M*, was relieved as a white region by etching with a modified Lepera etchant [*3*], and quantified using an image analyzer. The IFP nucleus was analyzed using an extraction replica prepared by the so-called "SPEED" method [*4*] under an electron microscope with energy dispersion X-ray analysis (EDX). Correspondence between the position of inclusions such as titanium sesquioxide (Ti_2O_3) and manganese sulfide (MnS) and microsegregation area of elements such as manganese and niobium was studied by comparing the concentration distribution map of each element obtained by computer aided X-ray micro-analyzer (CMA).

Test Results

Analysis of IFP Nucleus in Ti-O Steel

The IFP nucleated and grew radially from a titanium oxide particle of 0.5 ~ 3 μm in simulated HAZ of Ti-O steel, as shown in Fig. 1. The particle was identified as titanium sesquioxide with a hexagonal structure ($a = 5.14$Å, $c = 13.7$Å) by means of the electron diffraction method. Through EDX analysis, the particle was found to contain about 10% manganese.

Effect of Heating Temperature on the Toughness of Simulated HAZ

As shown in Fig. 2, the welding thermal cycle of 1450°C heating temperature caused serious deterioration in Ti-B steel and Ti-N steel but no recognizable damage to Ti-O steel.[6] Microscopic examination showed that the former steels had coarsened microstructures consisting of mainly F_S and coarsened cleavage facets, while the latter steel maintained a refined microstructure consisting of mainly IFP and refined cleavage facets. Naturally, one supposes that this superior property of Ti-O steel is due to the high stability of Ti_2O_3 particles at high temperature. In fact, CMA examination showed that in Ti-B steel the density of the nucleus[7] (mainly MnS particles) was 190 and 35/mm^2 for heating temperature of 1400 and 1450°C, respectively, while in Ti-O steel the density of nucleus was 50/mm^2 irrespective of heating temperature.

Effect of Carbon or Niobium Content on Toughness of Simulated HAZ

The effect of carbon content on simulated HAZ toughness was examined by using 0.3%Ni-0.3%Cu-0.01%Nb steels with a wide range of carbon contents (the second group of specimens in Table 1). As shown in Fig. 3, in LN and Ti-LN steels, the Charpy V notch impact

---

[6] This excellent simulated HAZ toughness is realized also in the actual weld joint [*7*].

[7] The density of the IFP nucleus particle was evaluated by counting the number of particles found on a unit area of polished surface.

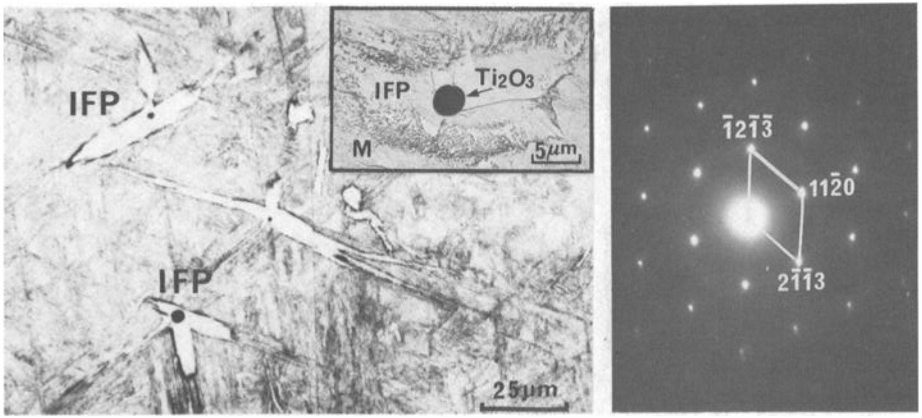

(hkil)	d (Measurement)	d Ti_2O_3 (ASTM)
$(\bar{1}2\bar{1}\bar{3})$	2.21	2.238
$(2\bar{1}\bar{1}3)$	2.23	2.238
$(11\bar{2}0)$	2.56	2.570

FIG. 1—*IFP initiated from Ti_2O_3. Specimen was quenched from 600°C on the cooling stage of the thermal cycle.*

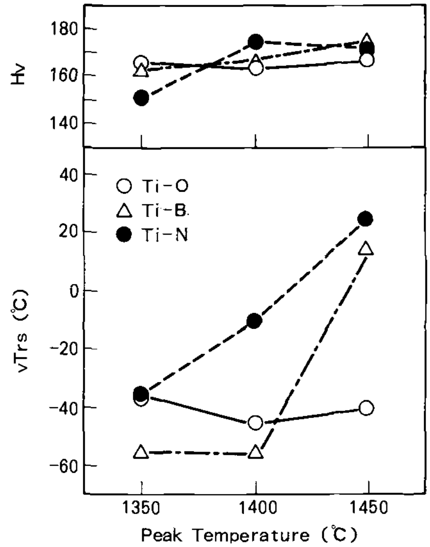

FIG. 2—*FATT of Charpy impact test* vTrs *and hardness* Hv *as a function of peak temperature in simulated HAZ of Ti-O, Ti-N, and Ti-B steels.*

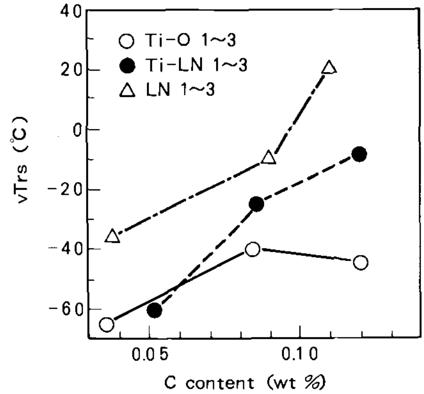

FIG. 3—*Effect of carbon content on* vTrs *in specimens subjected to simulated thermal cycle of HAZ (PT = 1400°C,* $\Delta t_{8/5}$ *= 161 s).*

fracture appearance transition temperature (vTrs) of the simulated HAZ was raised by about 50°C due to the increase in carbon content from 0.04% to 0.12%. On the other hand, the corresponding rise of vTrs in Ti-O steels was only about 20°C. Therefore, Ti-O steel can maintain good HAZ toughness even with a high carbon content. When compared with 0.12% carbon steel for example, the vTrs was −45, −10, and 20°C for Ti-O steel, Ti-LN steel, and LN steel, respectively. The effect of adding niobium was examined using a third group in Table 1, as shown in Fig. 4. In Ti-N steel, vTrs of the simulated HAZ rose in proportion to the amount of niobium with a rate of 40°C/0.01%Nb. In Ti-O steel, vTrs was nearly independent of, or rather improved by, an addition of niobium. The corresponding microstructures are shown in Fig. 5.

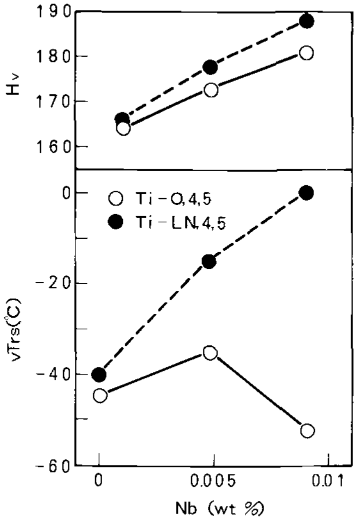

FIG. 4—*Effect of niobium content on* vTrs *in specimens subjected to simulated thermal cycle of HAZ. (PT = 1400°C,* $\Delta t_{8/5}$ *= 161 s).*

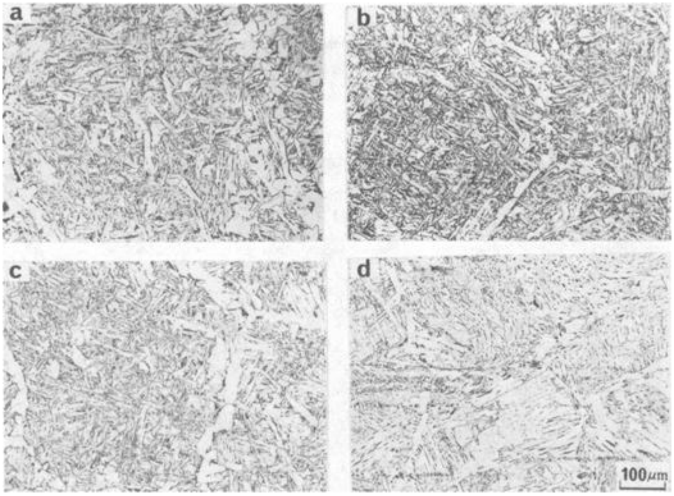

FIG. 5—*Effect of niobium content on the microstructure of the simulated HAZ:* (a) *Ti-O steel,* (b) *Ti-O5 (0.01%Nb),* (c) *Ti-LN steel,* (d) *Ti-LN5 (0.01%Nb).*

A niobium addition of 0.01% to Ti-O steel did not prevent IFP formation at all and decreased grain boundary ferrite, while an addition of the same amount of niobium to Ti-LN steel prohibited almost all IFP formation and induced a coarsened structure consisting mainly of F_S. The cause of toughness variation can be attributed to IFP formation. To clarify the reason why Ti-O steel has IFP formation ability over a wide compositional range, the correlation between the position of IFP nucleus and the microsegregation area was studied. Fig. 6a shows an overlap-

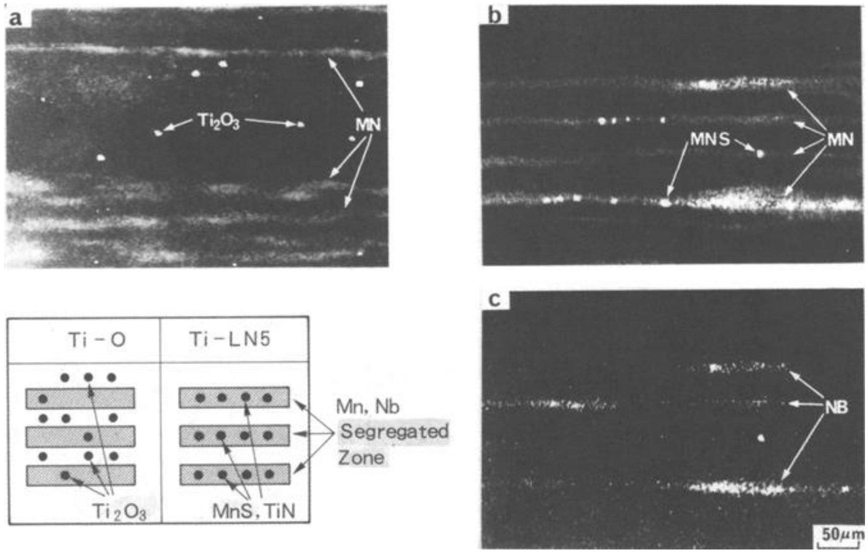

FIG. 6—*CMA patterns of Ti-O steel* (a), *and Ti-LN5 steel* (b, c).

ping CMA pattern for the distribution of titanium and manganese in Ti-O steel. The white bands express a segregating area of manganese, and the white spot shows Ti_2O_3 particles. One should note that Ti_2O_3 particles exist outside of dendrite microsegregation. Figs. 6b and c show the CMA patterns in Ti-LN-0.01Nb steel. In Fig. 6b, the distribution of manganese and sulfur are overlapped. The white band shows manganese segregation and the white spots show MnS particles. In Fig. 6c, the distribution of niobium is shown. The microsegregation zone of manganese clearly coincides with that of niobium. The IFP nucleus, which is a TiN particle surrounded by MnS, exists in the microsegregation region of manganese and niobium. The maximum segregation concentration increased with carbon content and attained 2.3% for manganese, and 0.08% for niobium. In brief, the IFP nucleus of Ti-LN steel is situated in the microsegregated area where hardenability is enhanced by niobium and manganese segregation and IFP formation is prevented. On the other hand, the IFP nucleus of Ti-O steel is distributed regardless of the microsegregation area. Then the IFP formation function is hardly affected by microsegregation.

Continuous Cooling Transformation Diagram

The CCT diagrams of Ti-O steel and LN steel are shown in Figs. 7 and 8, respectively. Typical microstructures are shown in Fig. 9. In these illustrations, austenite is denoted by A, grain boundary allotriomorph by F_p, idiomorph ferrite by F_I, ferrite side plate by F_S, intragranular ferrite plate Type I by IFP I, intragranular ferrite plate Type II by IFP II, pearlite by P, degenerated pearlite by PL, bainite by B, martensite island by M*, and martensite by M. IFP I has a wide ferrite plate shape similar to allotriomorph ferrite and is formed at relatively high temperature. IFP II has a narrow ferrite plate shape similar to F_S and is formed at relatively low temperature. LN steel transforms into a coarse structure consisting of mainly F_S over a wide range of cooling rates. In Ti-O steel, IFP II forms at a cooling rate lower than 54°C/s. Formation of IFP II attains the maximum amount at a cooling rate of 10°C/s, where overall microstructure is

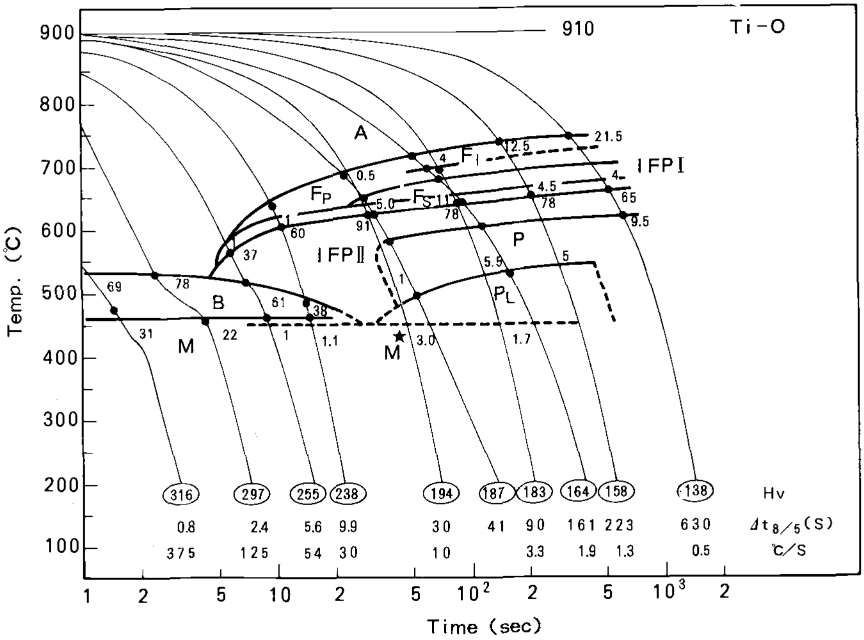

FIG. 7—*CCT diagram of Ti-O steel (heating temperature: 1400°C).*

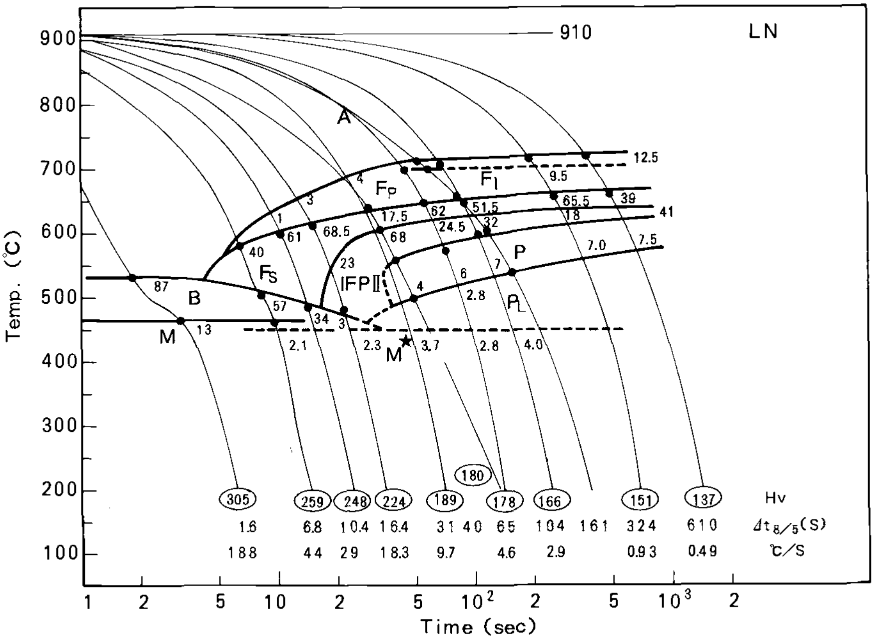

FIG. 8—*CCT diagram of LN steel (heating temperature: 1400°C).*

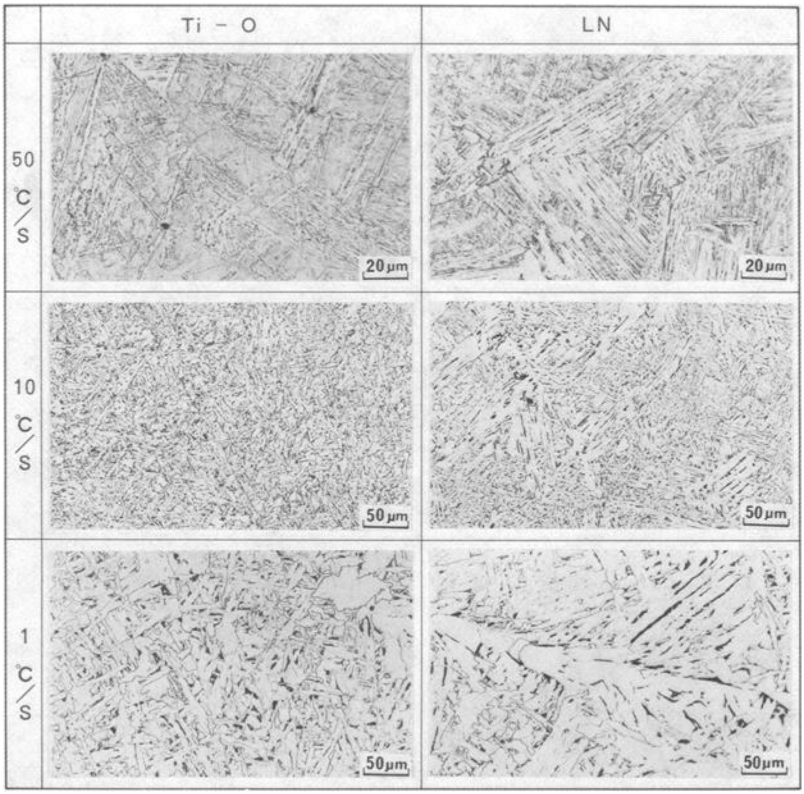

FIG. 9—*Typical microstructure produced by CCT in Ti-O and LN steel.*

controlled by IFP II. The transformation feature can be clearer by observing the microstructure obtained by quenching from various temperatures in the midst of transformation on cooling. Figure 10 shows microstructures obtained by quenching on cooling of $\Delta_{8/5}$ = 161 s. At a quenching temperature of 650°C, Fp forms along grain boundary in both Ti-O steel and LN steel. IFP I forms in Ti-O steel, and F_S develops from Fp in LN steel. At a quenching temperature of 630°C, IFP II forms in both steels. IFP II in Ti-O steel grows radially from a nucleus of Ti_2O_3, intersects each other, branches, and forms an IFP network. IFP II in LN steel develops from the plate tip of F_S in a smaller amount and at a temperature a little lower than that of Ti-O steel. The area ratio of each various microstructure is plotted as a function of quenching temperature in Fig. 11, from which it is clearly seen that IFP II in Ti-O steel forms in place of F_S. In LN steel, F_S prevails, as is the case for usual steels.

Effect of Cooling Time on Nucleation of IFP II and Growth of F_S

The number and length of ferrite plates constructing IFP were counted from a micrograph of the CCT diagrams and plotted as a function of cooling time in Fig. 12, which shows that Ti-O steel has a larger number and shorter growth length of IFP plate than LN steel. The number of IFP plate takes the maximum at a cooling time $\Delta t_{8/5}$ of 30 s in both steels. The maximum

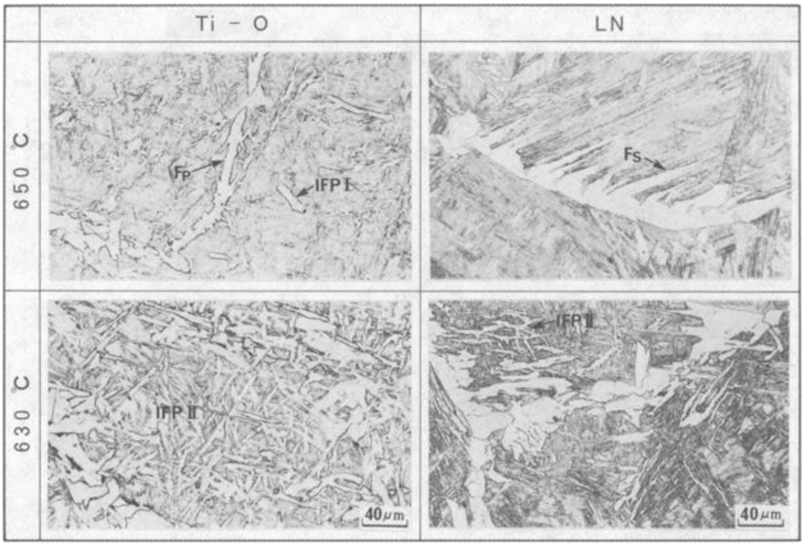

FIG. 10—*Microstructure obtained by quenching from various temperatures on cooling stage of simulated thermal cycle in Ti-O and LN steel.*

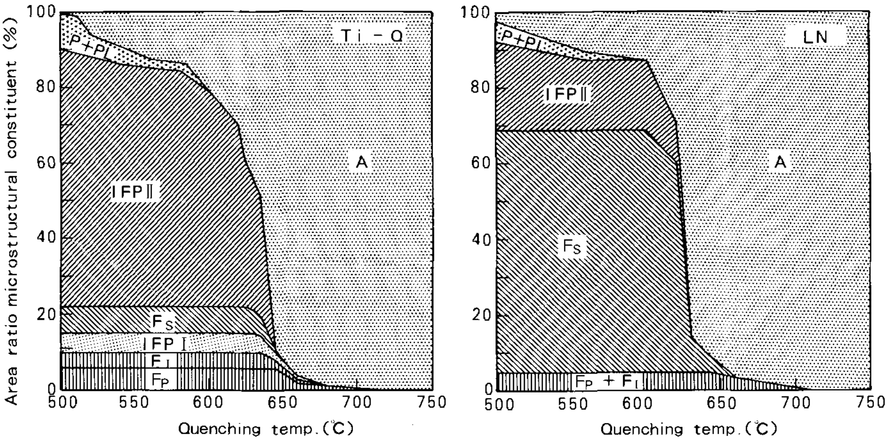

FIG. 11—*Diagram showing area ratio of microstructural constituents in Ti-O steel and LN steel (*$\Delta t_{8/5}$ = *161 s).*

number of IFP plate of Ti-O steel is three times that of LN steel. Ferrite plate length of F_S was measured and plotted in Fig. 13 in a method similar to that of IFP. The ferrite plate length of F_S increases monotonically with an increase in cooling time below the specified cooling time peculiar to the steels, and takes nearly a constant value above the specified cooling time. The specified cooling time in $\Delta t_{8/5}$ and the constant ferrite length are 200 s and 300 μm for LN steel, and 30 s and 130 μm for Ti-O steel. The specified cooling time of 30 s corresponds to that of the

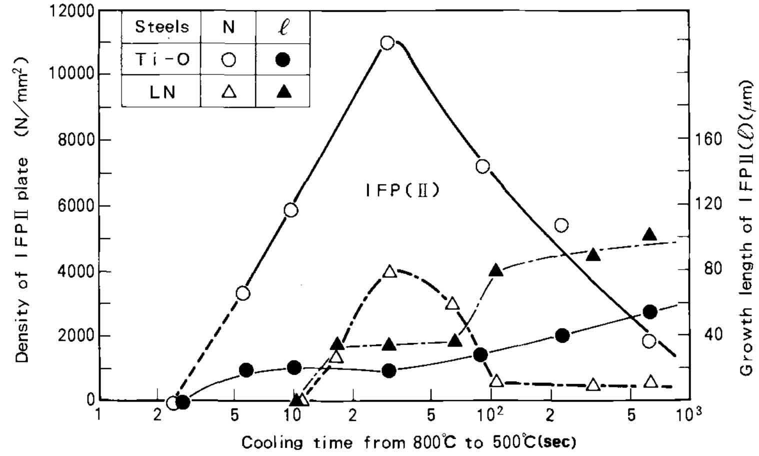

FIG. 12—*Effect of cooling time on density* N *and growth length* l *of IFP II.*

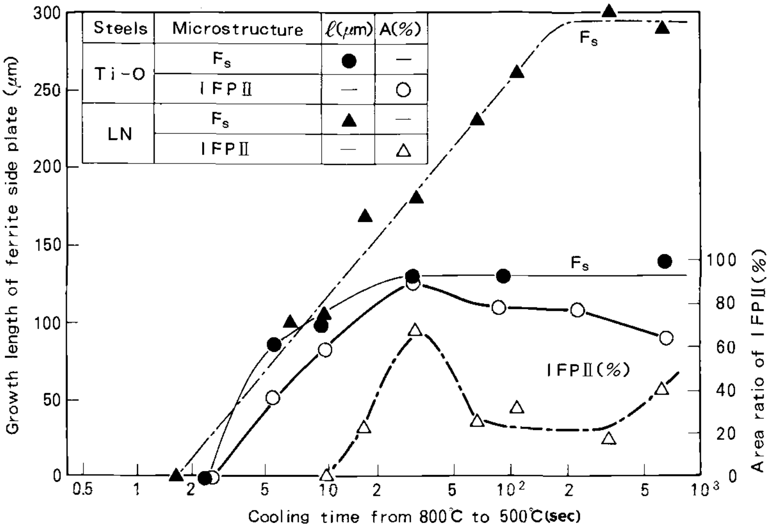

FIG. 13—*Effect of cooling time on growth length of ferrite side plate and area ratio of IFP II.*

maximum formation of IFP II. Therefore, development of F_S is interrupted by the formation of IFP II, which has a transformation initiation temperature lower than that of F_S by nearly 15°C.

*Effect of Cooling Time on the Formation of M**

The area ratio of M* varies with cooling time and takes its maximum value nearly at $\Delta t_{8/5} =$ 30 s, which corresponds to the cooling time of the maximum formation of IFP II as shown in Fig. 14. In LN steel, the area ratio of M* is high, such as 3 ~ 4% over a wide cooling time range

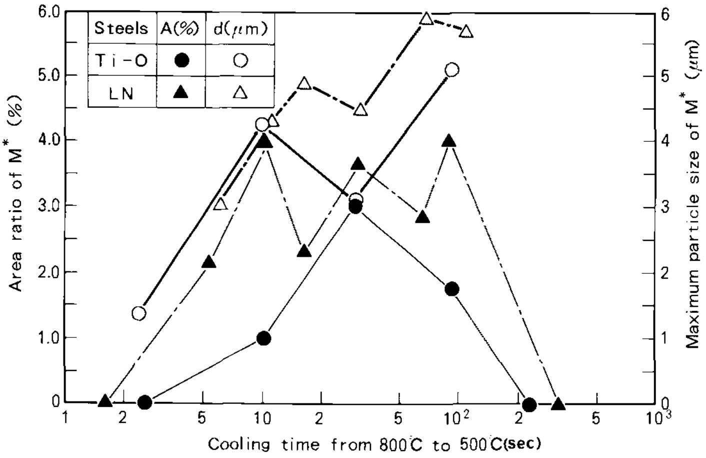

FIG. 14—*Effect of cooling time on* M* *area ratio and maximum particle size.*

($\Delta t_{8/5}$ = 10 ~ 100 s). The area ratio of M* in Ti-O steel is lower than that of LN steel by 1 ~ 2%. In both steels, the size of M* increases with an increase in cooling time as shown in Fig. 15. The shape of M* is controlled by the preceding transformation products. M* between F_S ferrite plate takes on a needle-like shape, and between IFP, is polygonal. The maximum particle size of M*[8] is shown in Fig. 14. In the range of cooling time corresponding to IFP formation, Ti-O steel has a maximum M* particle size of smaller than that of LN steel by about 1 μm.

Nucleus for IFP Formation

Dependence of Nucleus Component on Thermal History—The change of nucleus component was studied by quenching Ti-O steel from temperatures in the midst of cooling from 1400°C. In a specimen quenched from 1400°C, only bare Ti_2O_3 particles were observed. Manganese of 9 ~ 11% was dissolved in the particles. In a specimen quenched from 600°C, MnS of about 0.1 μm precipitated on the periphery of a Ti_2O_3 particle (Fig. 16). The manganese content in the Ti_2O_3 particle was nearly 7% in the latter specimen.

Effect of Thermal History in Austenite Region on IFP Transformation—The effect of holding Ti-O steel at a constant temperature in the midst of rapid cooling from 1400°C was studied as shown in Fig. 17. In the case of holding at 600°C for 40 s, Fig. 17a, the amount of IFP was small. In the case of holding at 900°C for 1000 s, Fig. 17b, IFP II formed in a larger amount. The number of IFP ferrite plates is about 3000 and 9000/mm^2 for Figs. 17a and b respectively, as shown. The specimen for Fig. 17b was etched by the SPEED method and the extraction replica of IFP nucleus was analyzed. FineTi(CN) particles of 0.1 μm were found as well as manganese sulfide particle on the periphery of the Ti_2O_3 particle.

Effect of MnS on IFP Transformation—As shown in the above, MnS necessarily attached to the IFP nucleus in Ti-O steel. The role of MnS on the IFP transformation property was examined by using Ti-LN steels containing sulfur of 0.0005 ~ 0.0034% (the fourth group in Table 1). The results are shown in Fig. 18. The toughness of the simulated HAZ was improved and the amount of IFP II increased as sulfur content increased. Manganese sulfide was not found

---

[8] The size of M* is distributed over some range. The maximum particle size of M* is defined as the maximum intercept length among arbitrary intercepts of all M* observed.

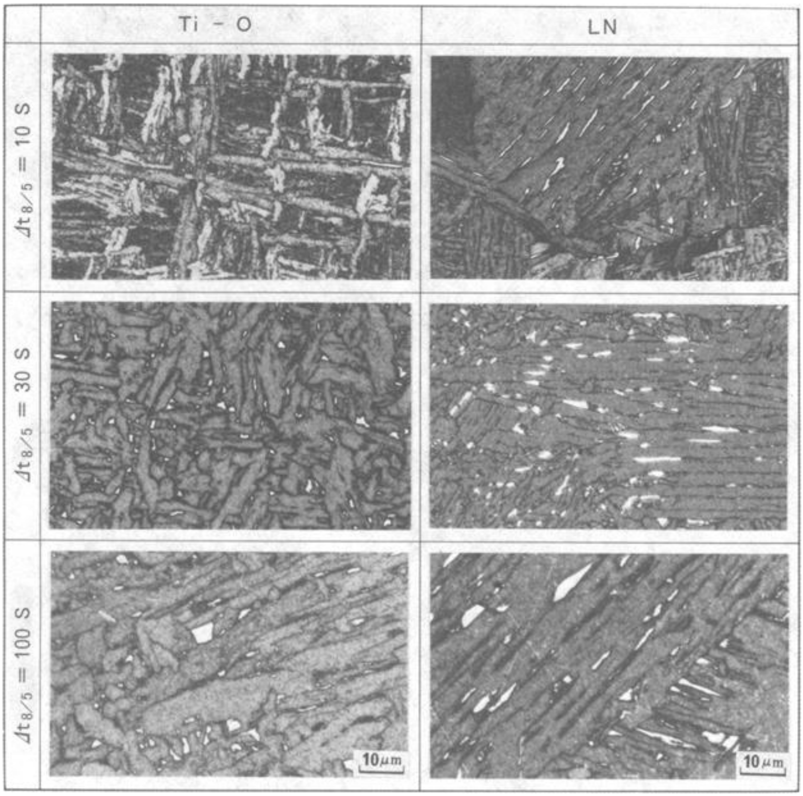

FIG. 15—*Effect of cooling time on size and distribution of martensite-austenite constituent.*

around TiN particles for specimens of low sulfur content. In Ti-O steel, a sulfur content of 0.001% gave the best HAZ toughness, such as vTrs of −45°C. Increasing the sulfur content to 0.0038% did not improve vTrs.

Discussion

Effect of IFP Formation on Toughness

That acicular ferrite (IFP) formation makes weld metal tough, which is well known. IFP itself may be tough, but does not cover all space within prior austenite grain in the HAZ of Ti-O steel, because F_S was always found near the grain boundary. Brittle fracture initiation took place in the F_S region, which was confirmed by the following method. By tracing the path of cleavage fracture named river pattern, a fracture initiation point was identified on the fracture surface of a Charpy test specimen (Fig. 19a). By polishing the fracture surface slightly and etching, the cleavage facet at the fracture initiation point was shown to be made by cracking of F_S (Fig. 19b). The cleavage facet size of the fracture initiation region is considered to be the effective grain size, that is, a factor controlling toughness. In fact, vTrs of the simulated HAZ can be well explained by the effective grain size so defined (Fig. 20). Therefore, HAZ toughness is controlled by F_S and not directly by IFP. The latter's good toughness can be safely assumed from its

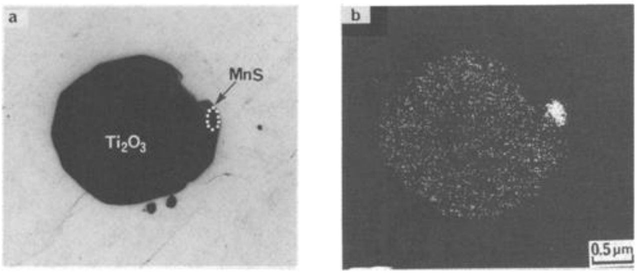

FIG. 16—*Electronmicrograph of extracting replica for a* Ti_2O_3 *particle* (a) *and its EDX pattern of Mn* (b).

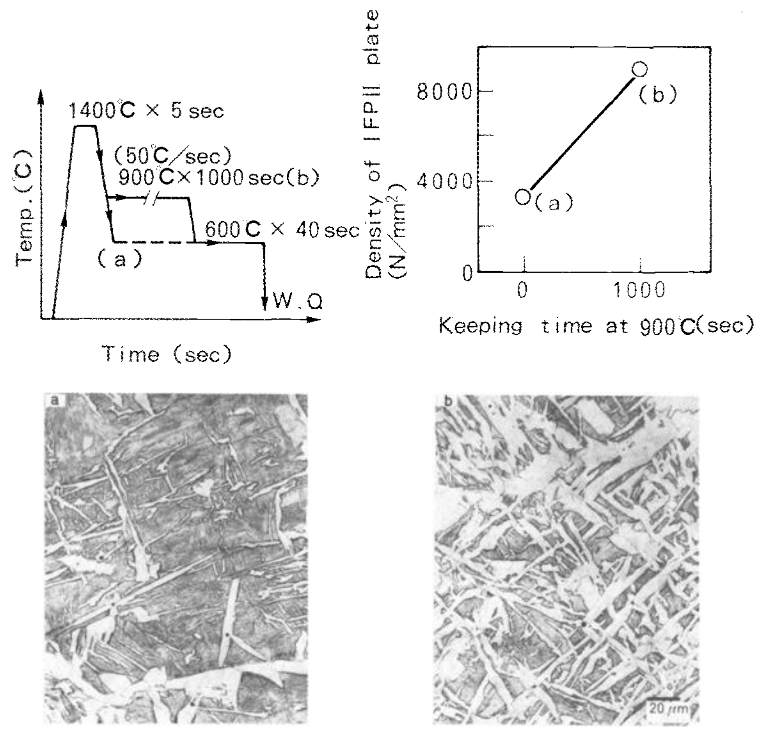

FIG. 17—*Schematic representation of thermal treatment (upper left); dependence of IFP number (upper right); and IFP configuration (lower half) on thermal treatment.* (a) *was obtained by thermal treatment without keeping constant temperature on stable region, and* (b) *by that with keeping.*

fine grain size and the decreased size of M* contained. Figure 13 shows clearly how the development of IFP restricts the growth of F_S. In a rapid cooling range (short cooling time) IFP does not develop, and the growth length of F_S is not so different between Ti-O steel and LN steel. As IFP develops in Ti-O steel, it prevents free development of F_S. At this stage, good correlation is found between F_S plate length and IFP area ratio (Fig. 21). Then the conclusion can be made

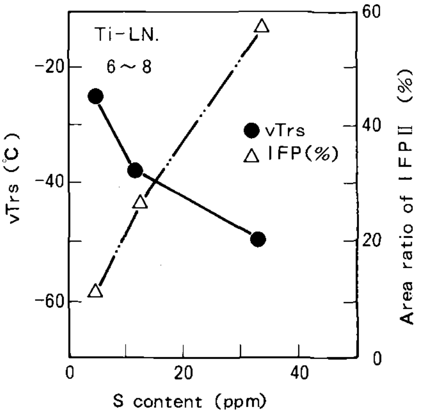

FIG. 18—*Dependence of FATT on sulfur content in Ti-LN steel.*

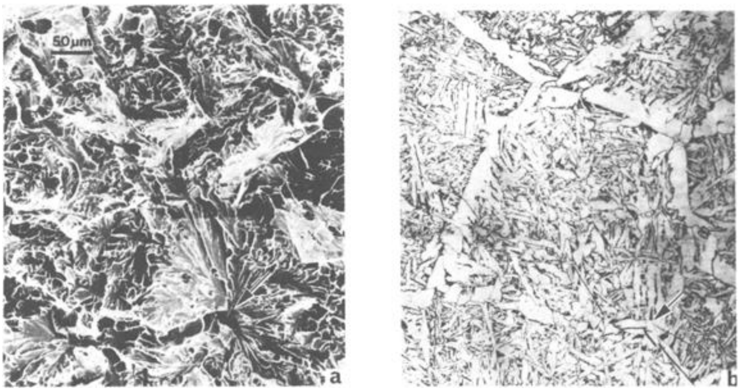

FIG. 19—*Correspondence between fracture surface* (a) *and microstructure just below it* (b); *black arrow shows a fracture initiation point.*

that IFP contributes toughness by restricting the development of F_S and refining the effective grain size.

Nucleus of IFP

The mechanism of IFP nucleation by Ti_2O_3 particle is now controversial. Three models were proposed [5].

1. The boundary between matrix and oxide is effective for reducing IFP nucleation energy, especially when two phases, matrix and oxide, have mutual lattice coherence.
2. Compositional variation in the steel matrix around the oxide favors γ/α transformation.
3. The difference of thermal expansion between inclusion and matrix causes strain around the oxide, by which IFP transformation is assisted.

More of those mechanisms can in principle be denied as effective for IFP formation to some

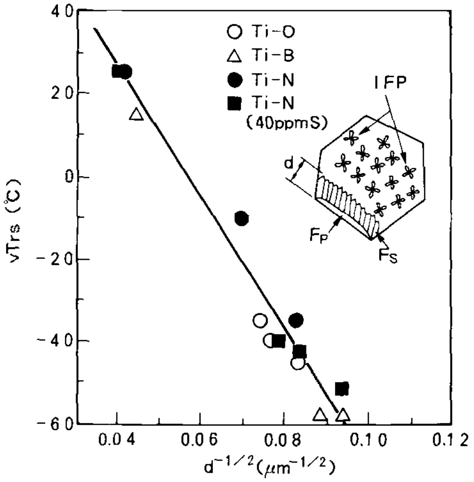

FIG. 20—*Relation between* vTrs *and effective grain size, which was cleavage facet size at fracture initiation point. All samples were free from* M* *(PT = 1350, 1400, 1450°C, $\Delta t_{8/5}$ = 161 s).*

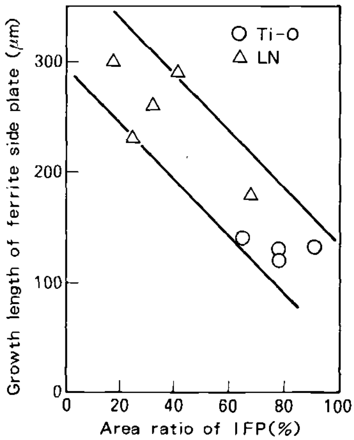

FIG. 21—*Effect of IFP area ratio on growth length of ferrite side plate ($\Delta t_{8/5}$ = 30 ~ 600 s).*

degree. An oxide such as Ti_2O_3 for itself cannot have IFP formation ability through the above mechanisms, as discussed below.

1. IFP has a crystal orientation relationship with the austenite matrix, as predicted from K-S relation [*6*]. On the other hand, Ti_2O_3 particles must have no particular crystal orientation regarding that of the matrix, because they precipitate in molten metal. Therefore, the coherent lattice relation between them cannot be expected.

2. Compositional variation in the steel matrix around the Ti_2O_3 particles can be neglected, because their precipitation is completed within molten metal, and there is enough time for the compositional variation to vanish due to their precipitation.

3. There are quite large differences of IFP formation ability between various oxides, while differences of thermal expansion coefficient between oxides is relatively small compared with those between steel and oxide. For example, aluminum oxide (Al_2O_3) and zirconium dioxide (ZrO_2) have similar thermal expansion coefficients, but different abilities for IFP formation. In addition, thermal stress due to the difference of thermal expansion coefficients on cooling is compressive around oxides, so that they are not favorable for γ/α transformation, which is accompanied by expansion.

From experimental results, one reasonably can consider that MnS deposited on Ti_2O_3 or TiN particles plays an essential role in IFP nucleation. The experimental results are as follows.

1. Ti_2O_3 particles are always accompanied by MnS.
2. As sulfur content is decreased in Ti-B steel, MnS on TiN particles vanishes and IFP disappears.
3. Holding in a γ region gives Ti_2O_3 particles some deposits on it, including MnS, and increases IFP formation in comparison with the case of no holding.

Ferrite nucleation is generally known to be often observed around MnS particles. Therefore, the IFP formation function of Ti_2O_3 and TiN may be controlled by their dispersion state and affinity to MnS. Various mechanisms by which MnS contributes IFP nucleation are considered possible for the present. From a rough estimation of these mechanisms, the compositional variation mechanism is the most promising. The precipitation of MnS causes a depleted zone of manganese around it. A decrease in concentration of manganese (austenite forming element) raises γ/α transformation temperature and promotes ferrite nucleation. A rough estimation based on the diffusion coefficient of manganese and sulfur and the solubility product of MnS shows that the welding thermal cycle causes dissolution and precipitation of MnS accompanied by a manganese depleted zone of below 0.1 μm order in extension, which is the expanse for IFP nucleation process. A decrease in manganese content in the depleted zone is 0.02 ~ 0.2% manganese on average, which might effect transformation.

Conclusions

A study was carried out to clarify the reason why a new steel, Ti-O steel, has good HAZ toughness over a wide range of chemical compositions and thermal history on welding. The findings were as follows.

1. Ti_2O_3 particles dispersed in the steel bring about IFP in HAZ, which prevents development of F_S and improves HAZ toughness.
2. Ti_2O_3 particles disperse without correlation to microsegregation, which is a reason why Ti-O steel does not lose its good HAZ toughness even by an addition of niobium or by an increase in carbon content.
3. A Ti_2O_3 particle is always accompanied by MnS, which is considered to play an essential role in IFP formation.

References

[1] Kanazawa, S., Nakashima, A., Okamoto, K., and Kanaya, K., *Transactions of the Iron and Steel Institute of Japan*, Vol. 16, 1976, pp. 486-495.

[2] Itoh, K., Mimura, H., Matsuda, S., Yamamoto, K., Ohno, Y., Okamura, Y., and Kawashima, Y., *Proceedings of the International Conference on HSLA '85*, Beijing, China, November 1985, pp. 669-673.

[3] Lepera, F. S., *Journal of Metals*, March 1980, pp. 38-39.

[4] Saeki, M., Kurosawa, F., and Matsuo, M., *Transactions of the Iron and Steel Institute of Japan*, Vol. 26, 1986, pp. 1017-1035.

[5] Devillers, L., Kaplan, D., Marandet, B., Ribes, A., and Riboud, P. V., *Proceedings of the International Conference on the Effect of Residual, Impurity and Micro-Alloying Elements on Weldability and Weld Properties,* The Welding Institute, London, November 1983, pp. 1-11.

[6] Imagumbai, M., Chijiiwa, R., Aikawa, N., Magumo, M., Homma, H., Matsuda, S., and Mimura, H., "Advanced Steels for Low-Temperature Service," *Proceedings of the International Conference on HSLA '85,* Beijing, China, November 1985, pp. 557-566.

[7] Chijiiwa, R., Tamehiro, H., Hirai, M., Matsuda, H., and Mimura, H., "Extra High Toughness Titanium-Oxide Steel Plates for Offshore Structures and Line Pipe," *Proceedings of the 7th International Conference and Exhibit on Offshore Mechanics and Arctic Engineering (OMAE),* Houston, February 1988.

B. M. Kapadia[1]

The Effect of Phosphorus on the Mechanical Properties of X-70 Line Pipe Steel

REFERENCE: Kapadia, B. M., "**The Effect of Phosphorus on the Mechanical Properties of X-70 Line Pipe Steel,**" *Residual and Unspecified Elements in Steel, ASTM STP 1042,* A. S. Melilli and E. G. Nisbett, Eds., American Society for Testing and Materials, Philadelphia, 1989, pp. 285–300.

ABSTRACT: The effect of phosphorus content on the base plate properties and coarse-grained heat affected zone (HAZ) toughness of X-70 Cb-V line pipe steel has been studied. Three laboratory heats were melted with phosphorus contents of 0.001, 0.009, and 0.027%. The ingot sections were control rolled to 13-mm (0.512-in.) thick plates employing a single delay 4T rolling practice. The HAZ toughness was evaluated on specimens subjected to a weld simulation thermal cycle corresponding to 1315°C (2400°F) peak temperature in the HAZ of a submerged arc weld deposited with a heat input of 3 kJ/mm (76 kJ/in.).

The as-rolled plates showed no significant effect of phosphorus variation on their microstructure, strength, or impact properties over the range investigated. The steels exhibited similar coarse-grained HAZ microstructures and hardnesses. Although the transition temperatures of the steels were significantly raised in the simulated HAZ condition, as expected, the variation in phosphorus content appeared to have little or no significant effect on toughness. Fractographic examination of the simulated HAZ impact specimens showed similar fracture appearances with no evidence of intergranular fracture.

The conclusion is that a specification limit of 0.010% maximum on the phosphorus content in Arctic grade line pipe steels may be unduly restrictive for ensuring superior base plate and HAZ toughness properties, as well as adequate resistance to hydrogen induced cracking (HIC).

KEY WORDS: line pipe steels, microalloyed steels, phosphorus in steel, control rolled, strength, impact toughness, submerged arc weld, heat affected zone (HAZ)

In recent years, increasingly stringent strength, impact toughness, and weldability requirements have been specified for large diameter line pipe operating under extreme climatic conditions. To meet these requirements, optimum microalloyed steel compositions and thermomechanical processing techniques have been developed that result in both high impact upper shelf energy and low transition temperature [*1–9*]. The high shelf energy is achieved primarily through low carbon and sulfur contents. The low transition temperature is achieved through ferrite grain refinement obtained by the combined influence of grain-refining additions, low reheating temperature, and controlled rolling at low temperatures followed by transformation of the deformed austenite prior to recrystallization. Such grain refinement, together with precipitation- and dislocation-strengthening effects, also contributes to the development of high strength with low carbon contents essential for good weldability.

The production of such high performance line pipe steels has been made possible by improvements in modern secondary steelmaking techniques to control and minimize the levels of residual elements such as sulfur, phosphorus, oxygen, nitrogen, and hydrogen [*10–12*]. Composition

---

[1] Research consultant, Technical Center, USS Division, USX Corporation, Monroeville, PA 15146.

specifications for Arctic grade line pipe steels typically limit the maximum sulfur content to 0.005% or less, and the maximum phosphorus content to about 0.010%. Further advances in steelmaking technology in the areas of hot metal pretreatment and furnace and ladle refining practices are expected to provide the capability of consistently attaining even lower levels of residual elements on a production basis [*13–15*]. These developments are anticipated to lead to increased specification demands for ultra clean steels and more stringent control of residual elements for line pipe and similar applications.

The production costs associated with pretreatment and secondary steel treatments are recoverable to some degree by cost savings resulting from improved yield and better process control during steelmaking. The overall economics of producing steels with very low residual element contents vary accordingly, depending on raw materials availability and the particular process route adopted. Likewise, the benefits of improved product quality offered by such steels would depend on each residual element's influence on the steel's performance in a particular application. The benefits of employing very low sulfur contents (less than 30 ppm) with inclusion shape control in line pipe steels have been well documented, both with respect to their greatly improved toughness characteristics [*1–5*] and the resistance to hydrogen induced cracking (HIC) in sour gas/oil service [*10–12,16,17*]. Significant advantages of very low sulfur steels in other product applications include a reduced tendency to lamellar tearing, improved surface and internal quality, and better formability [*13,14*]. On the other hand, little information is available in the literature on any potential benefits of very low phosphorus contents in line pipe steels to justify the higher cost of specifying a low phosphorus content (even at the 100 ppm level currently specified) in the interest of improved product performance. Therefore, the present study was conducted to determine the effect of phosphorus content on the mechanical properties of Arctic grade American Petroleum Institute (API) X-70 line pipe steel.

A low carbon columbium-vanadium steel having a nominal composition 0.08C-1.45Mn-0.025Cb-0.08V and control rolled to meet X-70 strength requirements was selected as the base steel for this study. The effects of variation in phosphorus content, in the range 0.001 to 0.030% on the base steel's strength and toughness properties were investigated. Because of the importance of having adequate toughness in the coarse-grained heat affected zone (HAZ) of line pipe welds, the toughness properties were evaluated in the simulated HAZ condition as well.

Materials and Experimental Work

Materials

Three 227-kg (500-lb) heats of the base composition with aim phosphorus contents of 0.001, 0.010, and 0.030% were vacuum induction melted and cast as 178- by 305- by 610-mm (7- by 12- by 24-in.) slab ingots. The chemical compositions of the steels, designated A, B, and C, are shown in Table 1. The compositions of all three steels, including the residual alloying elements intentionally added (copper, nickel, chromium, and molybdenum), were within the desired ranges, except for the slightly higher sulfur content of Steel B.

The ingots were cut into three equal sections, and the bottom section of each ingot was drilled at mid-thickness on the side face to accommodate a thermocouple for monitoring the temperature during rolling. The 178-mm (7-in.) thick sections were then heated to 1150°C (2100°F), fitted with a sheathed thermocouple, and control rolled straightway (rolling direction parallel to ingot axis) to approximately 13-mm (0.512-in.) thick plates. A single delay 4T practice was employed consisting of ten roughing passes (each giving approximately 12% reduction) above 1100°C (2010°F) to attain a thickness of four times the final gage, holding to a release temperature of 885°C (1625°F), and finishing with 13 additional passes to an aim final pass temperature of about 730°C (1350°F). The actual pass temperatures for each of the plates are shown in Table 2. Because of fluctuations in the thermocouple output, some difficulty was encountered

TABLE 1—*Chemical composition of steels investigated in wt%.*

Steel	C	Mn	P	S	Si	Cu	Ni	Cr	Mo	V	Cb	Al	N
Base	0.070	1.40	. . .[a]	0.004	0.20	0.15	0.08	0.08	0.04	0.070	0.022	0.025	0.008
Composition	0.090	1.50		0.008	0.25	0.25	0.12	0.12	0.06	0.090	0.028	0.035	0.012
A	0.080	1.43	0.001	0.005	0.24	0.20	0.10	0.09	0.05	0.080	0.023	0.029	0.011
B	0.079	1.46	0.009	0.009	0.22	0.19	0.10	0.10	0.05	0.082	0.024	0.032	0.011
C	0.080	1.44	0.027	0.005	0.22	0.20	0.09	0.09	0.05	0.080	0.023	0.031	0.010

[a] Aim phosphorus contents for Steels A, B, and C were 0.001, 0.010, and 0.030%, respectively.

TABLE 2—*Pass temperatures during rolling 178-mm thick ingot sections.*

Pass No.	Thickness,[a] mm	Thickness Reduction, %	Pass Temperature,[b] °C Steel A	Steel B	Steel C
1	156	12.1	1127	1138	1146
2	138	11.9	1150	1138	1152
3	121	12.2	1150	1138	1154
4	106	12.2	1150	1138	1154
5	93	12.2	1150	1138	1154
6	82	12.3	1146	1135	1152
7	72	12.1	1143	1132	1149
8	63	12.4	1140	1121	1143
9	55	12.1	1132	1116	1138
10	49	11.9	1121	1104	1132
Delay	...	...	...	...	...
11	42.7	12.5	893	880	888
12	38.3	11.9	891	877	885
13	32.4	15.5	885	846	882
14	26.7	16.0	880	838	877
15	22.9	14.3	843	819	869
16	19.8	13.3	832	804	860
17	17.8	10.3	804	793	843
18	16.0	10.0	791	782	832
19	14.7	7.9	780	771	813
20	14.0	5.2	766	766	796
21	13.2	5.5	760	749	777
22	12.5	5.8	752	741	766
23	11.9	4.1	743	732	749

[a] Gage setting.
[b] Ingot sections were heated to 1150°C for rolling.

in maintaining uniformly the temperature reduction schedule during rolling. Consequently, the temperatures of the last five finishing passes (final 20% reduction) for Steel C were, on the average, about 25°C (45°F) higher than the corresponding temperatures for the other two steels. All three plates were individually air-cooled following the last rolling pass.

Mechanical Property Tests

Tension tests were conducted at room temperature on duplicate 6.4-mm (0.252-in.) diameter specimens obtained transverse to the rolling direction from the mid-thickness position of each plate. Transverse full-size Charpy V notch (CVN) impact test specimens were obtained from the mid-thickness position of each plate (notch normal to the plate surface) and tested at temperatures between −120°C (−184°F) and room temperature to determine the ductile to brittle impact transition behavior and the upper shelf energy of the steels. Transverse mechanical properties were determined because these are indicative of properties transverse to a pipe axis, and are commonly used to determine a steel's suitability for a given strength pipe.

Impact tests were also performed on specimens containing a simulated coarse-grained HAZ microstructure. Oversized CVN blanks were obtained along the transverse direction from each plate and subjected in the Gleeble 1500 unit to a weld simulation thermal cycle shown in Fig. 1. The thermal cycle employed corresponds to a peak temperature of 1315°C (2400°F) in the HAZ of a submerged arc weld (SAW) in 12.7-mm (0.5-in.) thick plate deposited with a heat input of

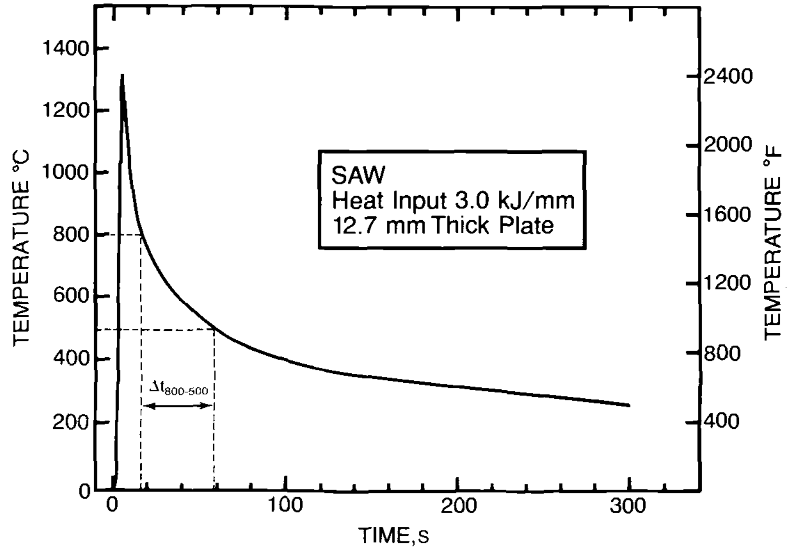

FIG. 1—*Weld thermal cycle employed for HAZ simulation.*

3.0 kJ/mm (76 kJ/in.) without preheating [*18*]. For this thermal welding cycle, the cooling time from 800° to 500°C (1472° to 932°F) $t_{800\text{-}500}$ over which temperature range most transformations occur, is approximately 40 s. These welding conditions are generally typical of longitudinal seam welds in line pipe deposited with a double pass submerged arc process, and the peak temperature selected corresponds to the coarse-grained region of lowest toughness adjacent to the weld fusion line in such welds. The thermally cycled blanks were then machined down to standard full-size CVN specimen dimensions with the notch located at the center of the simulated HAZ where the control thermocouple was attached. Fifteen specimens were tested from each plate to establish the fracture transition behavior.

Metallographic and Fractographic Studies

The microstructures of the as-rolled plates and of the simulated HAZ specimen blanks were examined by optical microscopy. Hardness measurements were also made on the latter before machining and testing. The fracture surfaces of the simulated HAZ specimens tested under impact loading were examined with a scanning electron microscope (SEM).

Results and Discussion

Microstructure

Metallographic examination showed that the as-rolled plates had a banded microstructure, consisting of polygonal ferrite and a ferrite-cementite aggregate, which ranged from nonlamellar pearlite to upper bainite, Fig. 2. All three steels exhibited a duplex ferrite grain size in the range ASTM No. 9 to 11. However, the proportion of coarser grains was noticeably greater in Steel C than in the other two steels because of its slightly higher finishing temperature. Although thermocouple recordings obtained during rolling failed to show clear indications of thermal arrest, the plates were finished somewhat below the upper critical temperature (Ar_3) for the

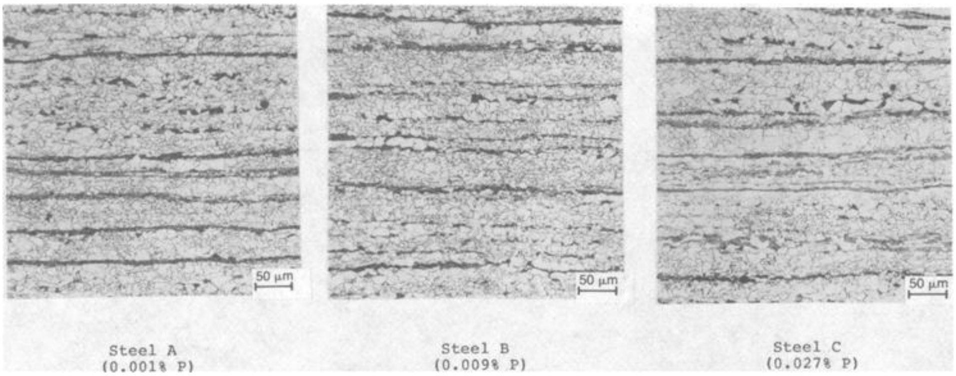

FIG. 2—*Microstructures of as-rolled plates of steels investigated. Nital etch.*

start of the austenite to ferrite transformation, which was estimated to be about 775°C (1425°F) [5] for all three compositions. Thus, the microstructures of all three plates contained some proportion of deformed ferrite although the relative amounts could not be determined with optical microscopy. The dislocation substructure in the deformed ferrite is a major component of strengthening achieved with controlled rolling.

All three steels in the simulated HAZ condition had similar coarse-grained microstructures with prior austenite grain size in the range ASTM No. 4 to 5, Fig. 3. The microstructures consisted of a mixture of upper bainite and acicular ferrite, with a small amount of proeutectoid grain boundary ferrite.

Mechanical Properties of As-Rolled Plates

The tensile properties of the as-rolled plates are summarized in Table 3. All three steels exhibited discontinuous yielding behavior as indicated by an upper yield point followed by yield point elongation. Steel C had a yield strength value about 35 MPa (5 ksi) lower than those of Steels A and B. Based on earlier studies [7–9] on control rolled steels of similar composition, this difference in yield strengths can be attributed solely to the microstructural differences re-

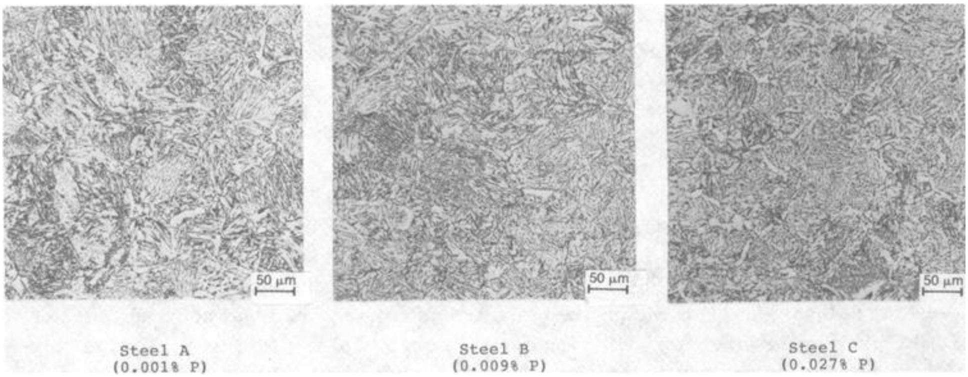

FIG. 3—*Simulated coarse-grained HAZ microstructures of steels investigated. Nital etch.*

TABLE 3—*Transverse tensile properties of as-rolled plates.*[a]

Steel	Phosphorus Content, %	Yield Strength (0.2% Offset), MPa (ksi)	Tensile Strength, MPa (ksi)	Elongation in 25 mm, %	Reduction of Area, %
A	0.001	528 (76.6)	594 (86.2)	26.5	64.4
B	0.009	520 (75.4)	590 (85.6)	25.5	60.6
C	0.027	487 (70.6)	593 (86.0)	27.0	64.8

[a] Average values from duplicate tests.

sulting from the slightly higher finishing temperature of Steel C. The tensile strengths of all three steels were very similar. Thus, the solid solution strengthening effect of phosphorus, typically about +7 MPa (1 ksi) per 0.010% P [*19,20*] in iron and low carbon steels, was not significant at the levels investigated in the present study.

The CVN impact properties of the as-rolled plates are summarized in Table 4, and the full CVN transition curves of energy absorption, percent shear fracture, and lateral expansion as a function of test temperature are shown in Fig. 4. Steels A and C had good toughness properties with nearly identical energy absorption curves, and also the same 50% shear fracture appearance transition temperature (FATT) and 0.38 mm (15 mil) lateral expansion transition temperature (LETT). Both steels had a CV 100 temperature (lowest temperature at which 100% shear fracture was obtained) of about −80°C (−112°F), with impact energy values at this temperature being substantially lower than the respective shelf values.

As controlled rolling is continued into the inter-critical temperature range (below Ar_3), the FATT generally attains a minimum value [*1,5,8*]. For this reason, the impact properties of Steels A and C were very similar despite the slightly higher finishing temperature of the latter. Moreover, the variation in phosphorus content between the two steels did not significantly influence their impact properties. This occurrence is consistent with published results [*20,21*] showing that phosphorus additions up to 0.05% to iron and hot rolled or normalized low carbon steels do not significantly affect the CVN energy absorption or fracture appearance transition temperature.

Steel B exhibited somewhat inferior impact properties as indicated by slightly higher transition temperatures [by 5 to 8°C, (10 to 15°F)] but significantly lower shelf energy, Table 4 and Fig. 4. This degradation in toughness, along with the slightly lower tensile ductility, can be attributed to its higher sulfur content of 0.009% compared with 0.005% for Steels A and C [*1-5*].

TABLE 4—*Transverse Charpy V notch impact properties of as-rolled plates.*

Steel	Phosphorus Content, %	Energy Absorbed,[a] J (ft · lb)		Transition Temperature,[a] °C (°F)	
		CV 100[b]	Shelf	50% Shear Fracture Appearance	0.38 mm (15 mil) Lateral Expansion
A	0.001	64 (47)	92 (68)	−98 (−145)	−98 (−145)
B	0.009	49 (36)	54 (40)	−93 (−135)	−90 (−130)
C	0.027	60 (44)	92 (68)	−98 (−145)	−98 (−145)

[a] Average values determined from respective transition curves for each steel.

[b] Energy absorbed at lowest temperature at which 100% shear fracture was obtained.

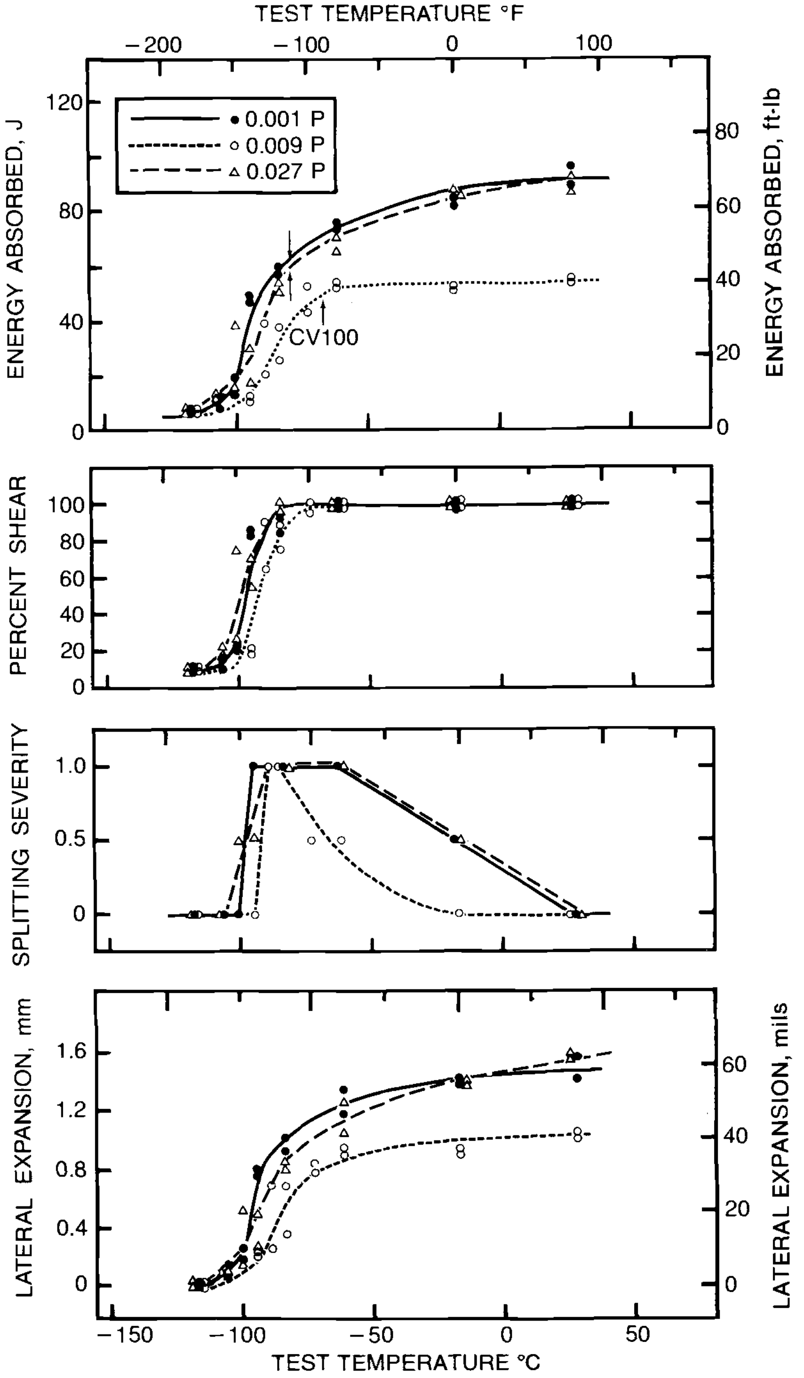

FIG. 4—*Charpy V notch transition curves for as-rolled plates of steels investigated.*

Splitting Tendency of CVN Specimens

Control rolled steels finished at subcritical (below Ar_3) temperatures, when tested under impact conditions, commonly exhibit splitting or separations on the fracture surface, which are oriented parallel to the rolling plane. Such secondary fractures generally result in a shelf energy reduction with decreasing test temperature (even though the main fracture surface exhibits 100% shear appearance) and a lowering of the transition temperature [*1,22,23*].

In the present study, Steels A and C showed a tendency toward splitting with increasing severity as the test temperature decreased below room temperature, as shown on a relative scale in Fig. 4. The severity of splitting in both steels then leveled off at temperatures corresponding to the onset of cleavage fracture, and diminished rapidly at still lower temperatures, at which the main fracture surface exhibited 50% or less shear appearance. The observed similarity in splitting behavior of Steels A and C was consistent with the accompanying decrease in shelf energy (at 100% shear) being nearly the same for both steels (Fig. 4). On the other hand, Steel B, because of its higher sulfur content, absorbed much lower shelf energy. As a consequence, splitting occurred to a much lesser degree and without any appreciable further reduction in the shelf energy, resulting in a relatively flat upper shelf region.

As one of several micromechanisms proposed to explain splitting behavior, suggestion has been made [*21,24*] that splitting occurs by intergranular fracture along planar oriented prior austenite or ferrite grain boundaries embrittled by the segregation of impurities such as phosphorus. This has been observed to occur at higher phosphorus (and manganese) levels in control rolled strip product [*21,25,26*], where cooling rates after coiling can be relatively slow. However, for the control rolled plates evaluated in the present study, the higher phosphorus content of Steel C in relation to that of Steel A did not noticeably intensify its splitting behavior.

Mechanical Properties of Simulated HAZ Specimens

As a check on the reproducibility of the thermal treatments applied, hardness measurements were made on the simulated HAZ blanks prior to machining into CVN specimens. The hardness was measured on the Rockwell B scale and subsequently converted to an equivalent HV value, as reported in Table 5. The simulated HAZ hardnesses of each of the steels were very uniform with their mean hardness values also being within a narrow range from 199 to 204 HV. Thus, the variation in phosphorus content of the steels had no noticeable effect on their hardness in the simulated HAZ condition. The hardness of the steels in the as-rolled condition were slightly lower, about 180 HV.

The literature [*27,28*] reports that very low sulfur contents can adversely affect the weldability

TABLE 5—*Mechanical properties of steels in simulated HAZ condition.*

				Charpy V Notch Impact Properties[a]		
					Transition Temperature, °C (°F)	
		Hardness, HV				
Steel	Phosphorus Content, %	Mean	Range	Self Energy, J (ft · lb)	50% Shear Fracture Appearance	0.38 mm (15 mil) Lateral Expansion
A	0.001	199	197-201	125 (92)	38 (100)	−7 (20)
B	0.009	203	200-206	66 (49)	41 (105)	18 (65)
C	0.027	204	200-208	130 (96)	43 (110)	7 (45)

[a] Average values determined from respective transition curves for each steel.

of steel plates through increased HAZ hardness and susceptibility to hydrogen induced HAZ cracking. The increase in HAZ hardness is caused by the elimination of sulfide inclusions as potential ferrite nucleation sites and a corresponding increase in the proportion of low temperature transformation products formed during cooling after welding. For the weld thermal cycle employed in the present study, the unintentional variation in the steels' sulfur contents over the range 0.005 to 0.009% had no noticeable effect on either the HAZ hardness or microstructure.

The transverse CVN impact properties of the simulated HAZ specimens are summarized in Table 5, and the full transition curves are shown in Fig. 5. In comparison with the as-rolled plate (base metal) properties, all three steels in the simulated HAZ condition showed more gradual transition behavior with significantly higher fracture transition temperatures by almost 100 to 140°C (180 to 252°F), depending on the criterion. The degradation in impact toughness was primarily related to the coarsened prior austenite grain size and to the presence of upper

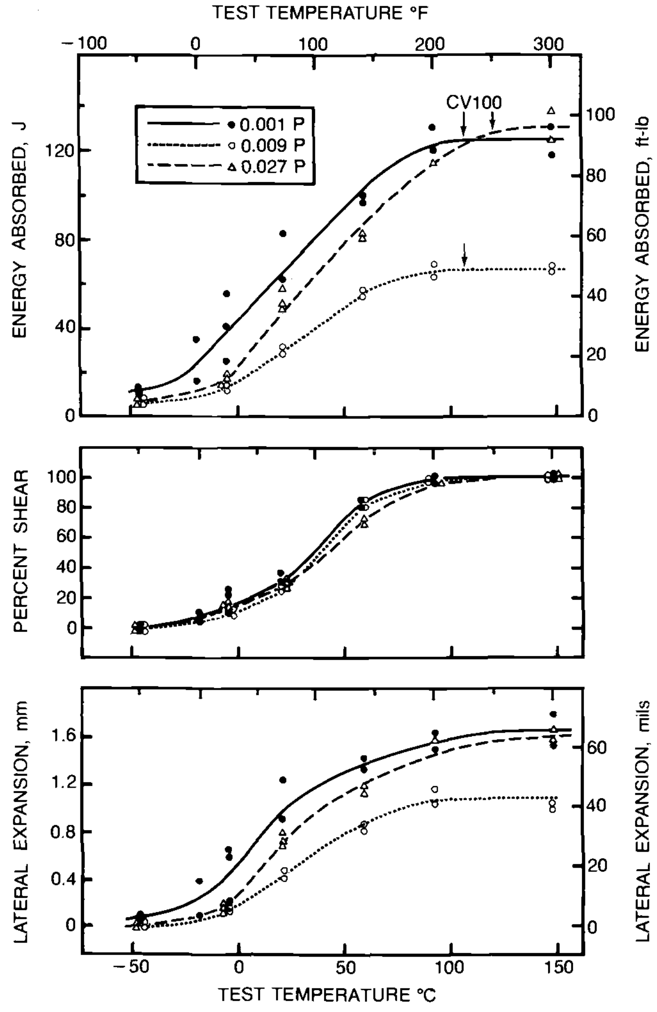

FIG. 5—*Charpy V notch transition curves for simulated HAZ specimens of steels investigated.*

bainite as the predominant microstructural constituent, Fig. 3. These microstructural changes and the accompanying loss in toughness are typically observed for coarse-grained HAZ in low carbon microalloyed steels welded with heat inputs characteristic of SAW processes [*29-31*].

The upper shelf energies absorbed in the simulated HAZ condition were generally higher than in the as-rolled condition, with Steel B having a significantly lower value than the other two steels. The size, shape, and distribution of nonmetallic inclusions remain unaffected during the weld thermal cycle, and consequently produce similar effects on base metal and HAZ toughness behavior. The fracture surfaces of the simulated HAZ impact specimens, unlike those tested from the as-rolled plates, did not exhibit splitting because of their higher transition temperatures and the elimination of microstructural effects of controlled rolling during thermal cycling. Consistent with this observation, all three steels attained their maximum shelf energies at (or about) their respective CV 100 temperatures.

Comparing the impact properties of Steels A and C, the latter had slightly higher FATT and LETT values by 5 and 14°C (10 and 25°F), respectively, but about the same upper shelf energy (Table 5). These differences in transition temperature may be attributed to the increase in phosphorus content from 0.001 to 0.027% between the two steels. On the other hand, these differences, small as they are in relation to the upward shift in transition behavior from the as-rolled to HAZ properties, may not be significant.

The fracture surfaces of the simulated HAZ impact specimens of Steels A and C were examined in the SEM and their fractographs are compared in Fig. 6. The specimens examined were tested at −46°C (−50°F) and −4°C (+25°F), and exhibited about 0 and 15% shear fracture appearance, respectively. The fractographs of both steels show almost completely transgranular

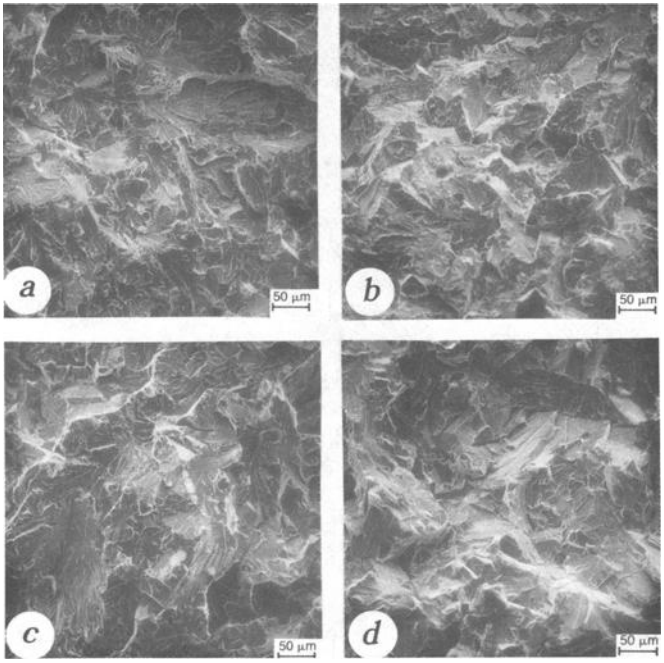

FIG. 6—*Scanning electron fractographs of simulated HAZ impact specimens of Steels A and C tested at two temperatures:* (a) *Steel A, −46°C (−50°F);* (b) *Steel C, −46°C (−50°F);* (c) *Steel A, −4°C (25°F);* (d) *Steel C, −4°C (25°F).*

cleavage mode of fracture with occasional small areas of dimpled surface characteristic of ductile tearing. The smaller facet size in some areas of the fractographs were associated with fracture through the fine-grained acicular ferrite structure. Virtually no intergranular fracture was observed on the fracture surfaces of either steel. This observation indicates that the slightly lower toughness exhibited by Steel C with the higher phosphorus content of 0.027% was not related to the intergranular embrittlement effect of phosphorus segregation at the prior austenite grain boundaries [*31-33*].

The impact results on simulated HAZ specimens reported in Fig. 5 provide a comparative assessment of the extent of HAZ embrittlement effect in the steels investigated. Previous studies [*34*] have noted that a weld thermal cycle corresponding to a given peak temperature with the same heating and cooling rates as are present in a weld HAZ will consistently produce, in a simulation specimen, a larger grain size and a correspondingly reduced toughness than expected in the weld HAZ. Moreover, because of the relatively narrow and irregular shape of the coarse-grained HAZ in submerged arc welds, its influence on the overall HAZ toughness in an actual weldment as measured by standard test methods (or performance during service) is probably not as detrimental as indicated by the results obtained on simulated specimens of uniform microstructure.

General Discussion

The results of the present investigation have shown that variation in phosphorus content from 0.001 to 0.027% in a control rolled X-70 Cb-V line pipe steel had no significant effect on the strength or impact properties of the as-rolled plates. Based on these results, limiting the phosphorus content in line pipe steels to a low level such as 0.010% max seems somewhat arbitrary. There are other applications, however, where the tendency of phosphorus to segregate to grain boundaries and affect impact transition temperatures can be detrimental and a restricted phosphorus content is necessary. This segregation tendency of phosphorus is known to be strongly enhanced by the presence of certain alloying elements and by prolonged exposure to moderately elevated temperature in the range 400 to 600°C (750 to 1110°F) either during heat treatment or service. Both these conditions are responsible for the classical temper embrittlement phenomenon observed in quenched and tempered steels [*35,36*]. Some alloy steels, notably the high nickel grades such as the 5.5% nickel and 9% nickel cryogenic steels, are more prone to such embrittlement, and for such steels, very low phosphorus contents of 0.005% maximum (together with ultra low sulfur contents) may be required for improved fracture toughness [*37,38*].

In regard to weldability considerations for line pipe fabrication, the HAZ properties of primary interest are hardness, notch toughness, and resistance to hydrogen induced cold cracking. This type of cracking is caused by a combination of tensile stress, hydrogen, and a susceptible microstructure associated with high cooling rates. Thus, HAZ cold cracking is often encountered in the field welding of girth welds made by a low energy input, multipass, manual arc process. The susceptibility to hydrogen-induced cold cracking is commonly expressed as a function of the base metal composition by various carbon equivalent (CE, P_{cm}) relationships [*39-41*], none of which consider phosphorus content to be a significant compositional variable.

Adequate toughness properties of the HAZ, on the other hand, is an important consideration for the longitudinal seam welds deposited by a high energy input SAW process. As observed in the present study, the impact toughness of the coarse-grained HAZ in such welds in line pipe steels is significantly lower than that of the base metal because of the coarsened grain structure and the presence of deleterious transformation products such as upper bainite. These microstructural effects and the resultant HAZ toughness are primarily controlled by the base metal composition and other variables, such as welding heat input and wall thickness, that determine the weld cooling rate.

An increase in phosphorus content from 0.001 to 0.027% in the steels investigated resulted in a slight apparent increase in transition temperature of the simulated HAZ with no change in the upper shelf energy. However, fractographic examination of the tested impact specimens showed no significant differences and particularly no evidence of intergranular fracture even at the higher phosphorus level. Therefore, the observed shift in transition temperature should not be directly attributed to the variation in phosphorus content. For repair welds in line pipe requiring multiple passes that involve reheating (for relatively short times) into the temper embrittlement range, some degree of HAZ embrittlement might be expected at the higher phosphorus level, depending on the susceptibility of the base metal composition. The effect of such thermal cycles in repair welds can be minimized by employing fewer weld passes, lower preheat and interpass temperature, and/or lower energy input. On the other hand, higher local concentrations of phosphorus and other elements related to chemical segregation in the base metal would intensify HAZ embrittlement.

The base metal composition, through its effect on the weld composition, exerts a significant influence on weld solidification cracking. In SAW of line pipe steels, the composition of the root passes (which are the most likely sites for such cracking) is typically derived about 70% from the parent plate and only 30% from the welding wire. The relative importance of compositional factors affecting solidification cracking have been quantified for SAW. A formula has been developed [*42*] that confirms the known deleterious effects of carbon, sulfur, and phosphorus, in decreasing order of importance, and the beneficial effects of manganese and silicon. In addition to compositional factors, the occurrence of solidification cracking is influenced by the weld pool shape and solidification pattern. Because of the relatively low carbon and sulfur contents of line pipe steels, solidification cracking is usually not a problem in welding line pipe steels, provided the welding wire and flux compositions are properly controlled. This is particularly true for girth welds because of the relatively low levels of dilution observed in them.

In addition to the requirements of high strength, toughness, and weldability, line pipes for sour gas/oil service must exhibit high resistance to HIC. Improved steel cleanliness is of primary importance in this regard, and very low sulfur contents of less than 20 or 30 ppm with effective inclusion shape control by calcium or rare earth metals (REM) treatment are generally recommended [*10-12,16,17,43,44*]. An equally important preventive measure for HIC is to minimize microstructural banding resulting from chemical segregation and the associated presence of low temperature transformation products, such as martensite or bainite [*16,17,43,44*]. This minimization is achieved within practical limits by a proper balance of carbon and manganese contents of the steel, usually with some restriction on the maximum content of the latter. While phosphorus, by virtue of its high segregation coefficient, is commonly recognized as promoting banding, its influence on HIC susceptibility at the levels found in modern line pipe steels is probably relatively small based on the results reported by various studies [*16,43,44*]. Accordingly, most guidelines for the selection of line pipe steels for sour gas/oil service recommend maximum phosphorus contents ranging from 0.010 to 0.020% [*11,12,16,43*].

Summary and Conclusions

The results of the present investigation on laboratory processed plates of an Arctic grade X-70 Cb-V line pipe steel has shown that variation in phosphorus content from 0.001 to 0.027% had no significant effect on the microstructure, strength, or impact properties of the as-rolled plates. Impact properties determined on simulated coarse-grained HAZ specimens showed that the variation in phosphorus content had little or no significant effect on toughness. Based on these results and other observations, one concludes that a specification limit of 0.010% maximum on the phosphorus content in Arctic grade line pipe steels may be unduly restrictive for ensuring superior base plate and HAZ toughness properties, as well as adequate resistance to HIC.

Disclaimer

The material in this paper is intended for general information only. Any use of this material in relation to any specific application should be based on independent examination and verification of its unrestricted availability for such use, and a determination of suitability for the application by professionally qualified personnel. No license under any USX Corporation patents or other proprietary interest is implied by the publication of this paper. Those making use of or relying upon the material assume all risks and liability arising from such use or reliance.

References

[*1*] Gondoh, H., Yamamoto, S., Nakayama, M., Nakasugi, H., and Matsuda, H., *"Microalloying '75" Proceedings,* Union Carbide Corporation, New York, 1977, pp. 435-440.

[*2*] Mihelich, J. L., *Proceedings of the Conference on Materials Engineering in the Arctic,* American Society for Metals, Metals Park, Ohio, 1977, pp. 175-182.

[*3*] Matsubara, H., Sakai, B., and Itaoka, T., *Proceedings of the Conference on Materials Engineering in the Arctic,* American Society for Metals, Metals Park, Ohio, 1977, pp. 190-200.

[*4*] Boyd, J. D., *Proceedings of the Conference on Materials Engineering in the Arctic,* American Society for Metals, Metals Park, Ohio, 1977, pp. 200-209.

[*5*] Shiga, C., Hatomura, T., Kudoh, J., Kamada, A., Hirose, K., and Sekine, T., "Kawasaki Steel Technical Report," No. 4, Kawasaki Steel Corporation, Tokyo, 1981, pp. 97-109.

[*6*] Jones, B. L., and Johnson, D. L., *Proceedings of the Conference on Steels for Line Pipe and Pipeline Fittings,* The Metals Society, London, 1983, pp. 14-21.

[*7*] Lander, H. N., Morrow, J. W., and Caldren, A. P., *Proceedings of the Conference on Steels for Line Pipe and Pipeline Fittings,* The Metals Society, London, 1983, pp. 136-146.

[*8*] Repas, P. E., *"Microalloying '75" Proceedings,* Union Carbide Corporation, New York, 1977, pp. 387-396.

[*9*] Bridoux, D., Perdrix, Ch., and Poupon, M., *Proceedings of the Conference on HSLA Steels: Metallurgy and Applications,* ASM International, Metals Park, Ohio, 1986, pp. 517-520.

[*10*] Yoshii, Y., Habu, Y., Nozaki, T., Itoyama, S. Nishikawa, H., and Imai, T., *Proceedings of the Conference on Technology and Applications of HSLA Steels,* American Society for Metals, Metals Park, Ohio, 1984, pp. 377-388.

[*11*] Hammer, R., and Simon, R. W., *Proceedings of the Conference on Technology and Applications of HSLA Steels,* American Society for Metals, Metals Park, Ohio, 1984, pp. 359-376.

[*12*] Obinata, T., *Proceedings of the Conference on Steels for Line Pipe and Pipeline Fittings,* The Metals Society, London, 1983, pp. 185-191.

[*13*] Fitzgerald, F., *Proceedings of the Third International Conference on Clean Steel,* The Institute of Metals, London, 1987, pp. 1-11.

[*14*] MacKenzie, J., and Barr, R. R., *Proceedings of the Conference on Secondary Steelmaking for Product Improvement,* The Institute of Metals, London, 1985, pp. 7-18.

[*15*] Baker, R., *Proceedings of the Conference on Secondary Steelmaking for Product Improvement,* The Institute of Metals, London, 1985, pp. 45-60.

[*16*] Bufalini, P., Buzzichelli, G., Pontremoli, M., Aprile, A., Jannone, C., and Pozzi, A., *Proceedings of the Conference on HSLA Steels: Metallurgy and Applications,* ASM International, Metals Park, Ohio, 1986, pp. 457-466.

[*17*] Hulka, K., Heisterkamp, F., and Jones, B., *Proceedings of the Conference on HSLA Steels: Metallurgy and Applications,* ASM International, Metals Park, Ohio, 1986, pp. 475-484.

[*18*] Nippes, E. F., Savage, W. F., and Allio, R. J., *Welding Journal,* Vol. 36, 1957, pp. 531s-540s.

[*19*] Pradhan, R. R., Battisti, J. J., and Melcher, E. D., *Proceedings of the 28th Mechanical Working and Steel Processing Conference,* Vol. XXIV, Pittsburgh, 1986, pp. 273-278.

[*20*] Spitzig, W. A. and Sober, R. J., *Metallurgical Transactions,* Vol. 8A, 1977, pp. 651-655.

[*21*] Kunishige, K., Fukada, M., and Sagisawa, S., *Transactions of the Iron and Steel Institute of Japan,* Vol. 19, 1979, pp. 324-331.

[*22*] Dabkowski, D. S., Konkol, P. J., and Baldy, M. F., *Metals Engineering Quarterly,* Vol. 16, No. 1, 1976, pp. 22-32.

[*23*] Tanaka, T., Tabata, N., Hatomura, T., and Shiga, C., *"Microalloying '75" Proceedings,* Union Carbide Corporation, New York, 1977, pp. 107-118.

[*24*] Baldi, G., and Buzzichelli, G., *Metal Science,* Vol. 12, 1978, pp. 459-472.

[*25*] Feldmann, U., Freier, K., Kugler, J., and Vlad, C. M., *Proceedings of the Conference on Steels for Line Pipe and Pipeline Fittings,* The Metals Society, London, 1983, pp. 115-118.

[26] Takasugi, M. and Jizaimaru, J., *Transactions of the Iron and Steel Institute of Japan,* Vol. 20, 1980, p. B-281.

[27] Hart, P. H. M., *Proceedings of the Conference on Trends in Steels and Consumables for Welding,* The Welding Institute, Cambridge, England, 1978, pp. 21-53.

[28] McKeown, D., Judson, P., Apps, R. L., and Pumphrey, W. I., *Metal Construction,* Vol. 15, 1983, pp. 667-673.

[29] McGrath, J. T., Godden, M. J., Gordine, J., and Boyd, J. D., *Canadian Metallurgical Quarterly,* Vol. 19, 1980, pp. 99-113.

[30] Collins, L. E., Godden, M. J., and Boyd, J. D., *Canadian Metallurgical Quarterly,* Vol. 22, 1983, pp. 169-179.

[31] Thaulow, C., Paauw, A. J., Gunleiksrud, A., and Naess, O. J., *Metal Construction,* Vol. 17, 1985, pp. 94-99.

[32] Ebden, J. R. and Weatherly, G. C., *Canadian Metallurgical Quarterly,* Vol. 22, 1983, pp. 149-155.

[33] Tauassoli, A. A., Bougault, A., and Bisson, A., *Proceedings of the Conference on the Effects of Residual, Impurity, and Microalloying Elements on Weldability and Weld Properties,* The Welding Institute, Cambridge, England, 1983, pp. P43-1-P43-9.

[34] Alberry, P. J., Chew, B., and Jones, W. K. C., *Metals Technology,* Vol. 4, 1977, pp. 317-325.

[35] Mulford, R. A., McMahon, C. J., Pope, D. P., and Feng, H. C., *Metallurgical Transactions,* Vol. 7A, 1976, pp. 1183-1195.

[36] Mabuchi, H., *Transactions of the Iron and Steel Institute of Japan,* Vol. 22, 1982, pp. 967-976.

[37] Murakami, M., Shibata, K., Nagai, K., and Fujita, T., *Transactions of the Iron and Steel Institute of Japan,* Vol. 23, 1983, pp. 808-814.

[38] Watanabe, I., Suzuki, M., Matsuda, Y., Tagawa, H., Matsui, K., and Shimada, S., "*Nippon Kokan Technical Report,*" Overseas No. 42, Nippon Kokan K. K., Tokyo, 1984, pp. 2-10.

[39] Suzuki, H., *Transactions of the Iron and Steel Institute of Japan,* Vol. 23, 1983, pp. 189-204.

[40] Yorioka, N., Suzuki, H., Ohshita, S., and Saito, S., *Welding Journal,* Vol. 62, 1983, pp. 147s-153s.

[41] Lorenz, K., and Duren, C., *Proceedings of the Conference on Steels for Line Pipe and Pipeline Fittings,* The Metals Society, London, 1983, pp. 322-364.

[42] Bailey, N. and Jones, S. B., *Solidification Cracking of Ferritic Steels During Submerged-Arc Welding,* The Welding Institute, Cambridge, England, 1977.

[43] Taira, T. and Kobayashi, Y., *Proceedings of the Conference on Steels for Line Pipe and Pipeline Fittings.* The Metals Society, London, 1983, pp. 170-180.

[44] Jones, C. L., Rodgerson, P., and Brown, A., *Proceedings of the Conference on Technology and Applications of HSLA Steels,* American Society for Metals, Metals Park, Ohio, 1984, pp. 809-825.

DISCUSSION

W. R. Warke[1] *(written discussion)*—You have tested the line pipe steel as base plate and simulated heat affected zones in welded plate. However, there is a considerable amount of plastic strain involved in forming the base plate into a pipe. Have you considered or would you care to speculate on the effect of this cold work, coupled with the various phosphorus levels, on the toughness properties of (1) the as-formed pipe, (2) formed pipe after subsequent strain aging, and (3) heat-affected zones in welded pipe?

B. M. Kapadia (author's closure)—During the U-O-E pipe-forming process, the plate undergoes a complicated strain history involving plastic strains of about 3.0% or less. The resulting embrittlement, which is generally observed in most cold worked steels, causes a slight decrease in toughness of the as-formed pipe. According to results reported by several studies [*1-3*], this decrease in toughness corresponds to an upward shift in Charpy V notch (CVN) 50% shear

---

[1] Amoco Corporation, P.O. Box 400, Naperville, IL 60566.

fracture appearance transition temperature (FATT) or dropweight tear test (DWTT) 85% shear FATT between plate and pipe values of up to 20°C (36°F). In line pipe steels investigated in these studies, phosphorus contents up to 0.02% had no noticeable influence on the magnitude of this loss in toughness from plate to pipe. With respect to any additional embrittlement caused by strain aging effects in the formed pipe and weld heat affected zones due to thermal cycles applied during or subsequent to fabrication, phosphorus contents in the normal range for line pipe steels do not induce deleterious strain aging effects under such conditions.

References

[*1*] Tanaka, T., Funakoshi, T., Ueda, M., Tsuboi, J., Yasuda, T., and Utahashi, C., *"Microalloying '75" Proceedings*, Union Carbide Corporation, New York, 1977, pp. 399-409.

[*2*] Yamaguchi, T., Osuka, T., Taira, T., and Iwasaki, N., *"Microalloying '75" Proceedings*, Union Carbide Corporation, New York, 1977, pp. 415-423.

[*3*] Abrams, H. and Roe, G. J., *MiCon 78: Optimization of Processing, Properties, and Service Performance Through Microstructural Control, ASTM STP 672*, American Society for Testing and Materials, Philadelphia, 1979, pp. 73-104.

Author Index

Subject Index

ISBN 0-8031-1259-9